

Pigment-Pigment Interactions and Protein Dynamics in Light-Harvesting Complexes: a Single-Molecule Study

Von der Universität Bayreuth
zur Erlangung des Grades eines
Doktors der Naturwissenschaften (Dr. rer. nat.)
genehmigte Abhandlung

von

Clemens Hofmann

aus Hamburg

1. Gutachter: Prof. Dr. Jürgen Köhler
 2. Gutachter: Prof. Dr. Markus Schwoerer
- Tag der Einreichung: 12. Dezember 2003
Tag des Kolloquiums: 24. Mai 2004

I certify that all material in this thesis which is not my own work has been identified and that no material is included for which a degree has previously been conferred upon me.

.....

(Clemens Hofmann)

Scientific publications of results presented in this work

- CLEMENS HOFMANN, THIJS J. AARTSMA, HARTMUT MICHEL, AND JÜRGEN KÖHLER, “Spectral Dynamics in the B800 band of LH2 from *Rhodospirillum molischianum*: A Single-Molecule Study”. *New Jour. Phys.* **6** 8 (2004).
- CLEMENS HOFMANN, THIJS J. AARTSMA, HARTMUT MICHEL, AND JÜRGEN KÖHLER, “Direct Observation of Tiers in the Energy Landscape of a Chromoprotein: A Single-Molecule Study”. *Proc. Nat. Acad. Sci. U.S.A.* **100** 15534-15538 (2004).
- CLEMENS HOFMANN, FRANCESCO FRANCA, GIOVANNI VENTUROLI, DIETER OESTERHELT, AND JÜRGEN KÖHLER, “Energy transfer in a single self-aggregated photosynthetic unit”. *FEBS Lett.* **546** 345-348 (2003).
- CLEMENS HOFMANN, MATIJJN KETELAARS, MICHIO MATSUSHITA, HARTMUT MICHEL, THIJS J. AARTSMA, AND JÜRGEN KÖHLER, “Single-Molecule study of the Electronic Couplings in a Circular Array of Molecules: Light-Harvesting 2 Complex from *Rhodospirillum molischianum*”. *Phys. Rev. Lett.* **90** 013004 (2003).
- MATIJJN KETELAARS, CLEMENS HOFMANN, JÜRGEN KÖHLER, TINA D. HOWARD, RICHARD J. COGDELL, JAN SCHMIDT, AND THIJS J. AARTSMA, “Spectroscopy on Individual Light-Harvesting 1 Complexes of *Rhodospseudomonas acidophila*”. *Biophys. J.* **83** 1701-15 (2002).
- JÜRGEN KÖHLER, ANTOINE M. VAN OIJEN, MARTIJJN KETELAARS, CLEMENS HOFMANN, MICHIO MATSUSHITA, THIJS J. AARTSMA, AND JAN SCHMIDT, “Optical Spectroscopy of Individual Photosynthetic Pigment Proteins Complexes” *Int. J. Mod. Phys. B* **15** 3633-3636 (2001).

Contributions to international conferences

- CLEMENS HOFMANN, THIJS J. AARTSMA, HARTMUT MICHEL, AND JÜRGEN KÖHLER, “Optical spectroscopy on individual photosynthetic membrane complexes from purple bacteria”. International Symposium on elucidating biomolecular networks by single-molecule technologies in Ascona (CH), October 2003.
- CLEMENS HOFMANN, MATIJJN KETELAARS, MICHIO MATSUSHITA, HARTMUT MICHEL, THIJS J. AARTSMA, AND JÜRGEN KÖHLER, “Spectroscopy on the B800 Band of Individual Light Harvesting 2 Complexes from *Rhodospirillum molischianum*”. EURESCO Conference on Bionanotechnology in Granada (E), July 2003.
- CLEMENS HOFMANN, MARTIN RICHTER, FRANCESCO FRANCA, DIETER OESTERHELT, AND JÜRGEN KÖHLER, “Bacterial Photosynthesis in purple bacteria, PufX and LH1 in *Rhodobacter sphaeroides*: a preliminary study”. Spring meeting of the “Deutsche Physikalische Gesellschaft” in Dresden (D), March 2003.
- CLEMENS HOFMANN, MATIJJN KETELAARS, MICHIO MATSUSHITA, THIJS J. AARTSMA, FRANCESCO FRANCA, DIETER OESTERHELT, AND JÜRGEN KÖHLER, “Optical Spectroscopy of Individual Pigment Protein Complexes”. VolkswagenStiftung: 3rd international Symposium on Physics, Chemistry and Biology with Single Molecules in Tutzing (D), September 2002.

ii Contributions to international conferences

- CLEMENS HOFMANN, MATIJJN KETELAARS, MICHIO MATSUSHITA, THIJS J. AARTSMA, HARTMUT MICHEL, AND JÜRGEN KÖHLER, “Spectroscopy of the B800 Band of Individual Light Harvesting 2 (LH2) Complexes from *Rhodospirillum molischianum*”. Spring school on Single Molecules in Physics, Chemistry and Biology in Hofgeismar (D), April 2002.
- CLEMENS HOFMANN, MATIJJN KETELAARS, MICHIO MATSUSHITA, THIJS J. AARTSMA, HARTMUT MICHEL, AND JÜRGEN KÖHLER, “Spectroscopy of Individual LH2 Complexes from *Rhodospirillum molischianum* — the electronic coupling of BChl *a* in the B800 ring”. Spring meeting of the “Deutsche Physikalische Gesellschaft” in Regensburg (D), March 2002.
- CLEMENS HOFMANN, MATIJJN KETELAARS, MICHIO MATSUSHITA, THIJS J. AARTSMA, JAN SCHMIDT, HARTMUT MICHEL, AND JÜRGEN KÖHLER, “Dynamic and static behaviour of the B800 band of *Rhodospirillum molischianum*”. International Workshop: Molecular Motors in Frankfurt (D), November 2001.
- CLEMENS HOFMANN, MATIJJN KETELAARS, MICHIO MATSUSHITA, THIJS J. AARTSMA, JAN SCHMIDT, HARTMUT MICHEL, AND JÜRGEN KÖHLER, “Single molecule Spectroscopy on individual light harvesting 2 complexes from *Rhodospirillum molischianum*”. Spring school: Optical Spectroscopy and Microscopy of Single Objects in Les Houches (F), May 2001.
- CLEMENS HOFMANN, MATIJJN KETELAARS, MICHIO MATSUSHITA, THIJS J. AARTSMA, JAN SCHMIDT, HARTMUT MICHEL, AND JÜRGEN KÖHLER, “Single molecule Spectroscopy on individual light harvesting 2 complexes from *Rhodospirillum molischianum*”. SFB 533: Light-induced dynamics in biopolymers in Freising (D), April 2001.
- CLEMENS HOFMANN, MATIJJN KETELAARS, MICHIO MATSUSHITA, THIJS J. AARTSMA, JAN SCHMIDT, HARTMUT MICHEL, AND JÜRGEN KÖHLER, “Single molecule Spectroscopy on individual light harvesting 2 complexes from *Rhodospirillum molischianum*”. VolkswagenStiftung: 2nd international Symposium on Physics, Chemistry and Biology with Single Molecules in Staffelstein (D), March 2001.

für Tanja

Contents

1	Introduction	1
2	Light harvesting complexes	5
2.1	Photosynthesis	5
2.1.1	Building blocks of the photosynthetic apparatus in purple bacteria . . .	6
	Pyrroles and chlorophylls	6
	Carotenoids	8
	The reaction centre and the antenna complexes	8
2.1.2	The photosynthetic unit (PSU)	10
	The peripheral light-harvesting 2 (LH2) complex	10
	The light-harvesting 1 (LH1) complex	12
	The reaction centre (RC)	13
	Cyclic electron transport inside and outside the PSU	13
2.2	Spectral properties of pigments	14
2.2.1	The intrinsic electronic properties of chlorophylls	15
	Absorption	16
	Emission	17
2.2.2	Pigment-protein interaction	17
	The homogeneous linewidth, zero-phonon line and phonon side-band .	17
	Inhomogeneous broadening and spectral diffusion	19
2.2.3	Pigment-pigment interaction	21
	Hamilton operator: disorder and types of interaction	22
	Pigment-pigment interaction, a dimer model	23
	Weak interaction, localised excitations	24
	Strong interaction, Frenkel excitons	25
	Eigenstates of the B850 pigment pool	25
3	Materials and methods	27
3.1	Line narrowing techniques at low temperatures	27
3.1.1	Spectral hole-burning	27
3.1.2	Photon-echo measurements	28
3.1.3	Single-molecule spectroscopy	29
3.2	This thesis: single molecule spectroscopy	29
3.2.1	Prerequisites for single molecule spectroscopy	30
3.2.2	Techniques in low temperature single molecule spectroscopy	31

	A short history	31
	Confocal microscopy	32
3.3	Samples	33
3.3.1	Sample preparation	33
3.3.2	List of samples	33
3.3.3	List of chemicals	34
3.3.4	Atomic coordinates	34
3.4	Experimental setup	35
	Widefield fluorescence microscopy	35
	Confocal fluorescence-excitation spectroscopy	36
	Widefield fluorescence-excitation spectroscopy	37
	Polarisation dependent spectroscopy	38
4	The B800 band of LH2 from <i>Rhodospirillum molischianum</i>	39
4.1	Structure of the B800 ring	40
4.2	Experimental results	41
4.2.1	Inter- and intra-complex heterogeneity	42
4.2.2	Spectral diffusion	43
	Spectral switching of individual absorption lines	43
	Spectral diffusion contributing to the homogeneous linewidth	46
	Simultaneous spectral diffusion of absorption lines	49
	Power dependence of spectral diffusion	51
4.2.3	Electronic couplings in a circular aggregate of molecules	52
	Mutual angles between absorption-dipole moments	53
	Simultaneous temporal fluctuations	54
4.3	Discussion	55
4.3.1	Inter- and intra-complex heterogeneity	55
	Statistical analysis	55
	Comparison between experiment and analysis	58
4.3.2	Direct observation of distinct tiers in the energy landscape of a protein	59
	Spectral switching: Chromophores probe the energy landscape	59
	Simultaneous spectral diffusion: coupling of chromophores	62
	Structural changes in the binding pocket of the BChl <i>a</i> molecules	63
4.3.3	Electronic couplings in a circular aggregate of molecules	65
	Coupling between neighbouring chromophores	65
	Temporal fluctuations of the coupling between two chromophores	67
4.4	Summary	69
5	Line shapes of the B800 absorptions	73
5.1	Multivariate statistical analysis	73
5.1.1	The MSA algorithm	73
5.1.2	Using MSA in spectroscopy	75
5.2	Pattern recognition on two example spectra	76
5.2.1	Application to simultaneous spectral diffusion	76
	Analysis	76
	Discussion	77
5.2.2	Application to spectral switching	78
	Analysis	78

Discussion	79
5.3 The shape of the absorption lines in the B800 band	81
5.3.1 Experimental	81
5.3.2 Analysis	82
5.3.3 Discussion	84
Line shapes of a multichromophoric macromolecule	85
The line shape extracted by the MSA algorithm	86
5.4 Summary	89
6 The B850 band of LH2 from <i>Rhodospseudomonas acidophila</i>	91
6.1 Geometric structure of the B850 ring	92
6.2 Electronic structure of the B850 ring	93
6.3 Experimental results	96
6.4 Discussion	98
6.5 Summary	103
7 The core complex: LH1-RC	105
7.1 Structural models for LH1	106
7.2 Simulation of the optical spectra	108
7.2.1 Methods	109
7.2.2 Structural heterogeneity	110
7.2.3 Site heterogeneity	112
7.2.4 Orientation of the complexes	113
7.2.5 Discussion of the simulations	114
7.3 LH1-RC from <i>Rhodospseudomonas acidophila</i>	115
7.3.1 Experimental results	115
7.3.2 Discussion	117
7.4 LH1-RC from <i>Rhodobacter sphaeroides</i>	120
7.4.1 Experimental results	121
7.4.2 Discussion	125
7.5 Summary of the experiments on core complexes	127
8 Self-aggregation of the photosynthetic unit (LH2-LH1-RC)	129
8.1 Experimental	130
8.1.1 LH1-RC sample with low concentration of LH2 impurities	130
8.1.2 Mixing of LH1-RC and LH2 solutions	132
8.2 Discussion	133
8.3 Summary	136
9 Summary and outlook	137
Bibliography	141
Deutsche Zusammenfassung	153
Acknowledgements	159
Curriculum Vitae	163

List of abbreviations

ADP	adenosine diphosphate
APD	avalanche photodiode
ATP	adenosine triphosphate
BChl	bacteriochlorophyll
Car	carotenoid
CCD	charge coupled device
Chl	chlorophyll
EMCCD	electron multiplying charge coupled device
FWHM	full width at half maximum
ILS	ideal line shape
LH1	light-harvesting 1 (complex)
LH2	light-harvesting 2 (complex)
LH3	light-harvesting 3 (complex)
MCMM	multichromophoric macromolecule
MSA	multivariate statistical analysis
PE	photon-echo
PMC	photosynthetic membrane complex
PSB	phonon side-band
PSU	photosynthetic unit
Rb	Rhodobacter
RC	reaction centre
Rps	Rhodospseudomonas
Rs	Rhodospirillum
SHB	spectral hole-burning
SMS	single-molecule spectroscopy
TLS	two level system
ZPL	zero-phonon line

Introduction

In 1988, Johann Deisenhofer, Robert Huber and Hartmut Michel were awarded the Nobel price in chemistry for the determination of the three-dimensional structure of a photosynthetic reaction centre from the purple bacterium *Rhodospseudomonas viridis* [1]. In 1995 Richard Cogdell and coworkers were the first to resolve the x-ray structure of the peripheral light-harvesting 2 complex from another purple bacterium called *Rhodospseudomonas acidophila* [2]. The progress made in high-resolution structural studies of the photosynthetic unit of these bacteria has strongly stimulated experimental and theoretical investigations to understand the fast and efficient energy transfer and tunability of their spectral properties [3–10].

In purple bacteria the sunlight is absorbed by a network of antenna pigment proteins and subsequently the excitation energy is efficiently transferred to the photochemical reaction centre (RC) where a charge separation takes place providing the free energy for subsequent chemical reactions. It is known that most of these bacteria contain two types of antenna complexes, the central light-harvesting complex 1 (LH1) and the peripheral light-harvesting complex 2 (LH2) [11]. LH1 and the RC are closely associated and form the so called core complex, whereas LH2 is not in direct contact with the RC but transfers the energy to the RC via the LH1 complex [12]. LH2 is known to comprise two distinct bacteriochlorophyll (BChl) a pigment pools which are labelled B800 and B850, whereas the LH1 complex presumably comprises only one

pigment pool labelled B870. The denotations of the pigment assemblies correspond to their room-temperature absorption maxima in the near infrared. Based on the homology between the LH1 and LH2 proteins together with theoretical modelling a scheme of the arrangement within a photosynthetic unit (PSU) has been proposed in which the core complex is surrounded by several LH2 complexes in a two dimensional structure [13, 14]. However, despite the tremendous progress in the field that has been achieved during the last decade important details, for example the structure of the LH1-RC complex or the precise supramolecular organisation of the PSU, are unknown and currently an issue of hot debate.

By now, it has been established that the spatial structure of photosynthetic complexes, especially the mutual orientation of the pigments, determine to a large extent their spectroscopic features and excited-state dynamics [15]. These assemblies of repeating non-covalently bound molecular units show intermediate features between an individual molecule and a crystal, which makes them suitable model systems to study different types of intermolecular interactions in great detail [16–23]. For the B870 system of LH1 and the B850 pool of LH2 the excited states can be described in terms of delocalised Frenkel excitons whereas for the B800 molecules the excitations can be treated in first approximation as being localised on an individual BChl *a* molecule [24–29].

Generally, information about the parameters that determine the description of the electronic structure of light-harvesting complexes can be obtained by optical spectroscopy. But even isolated protein-pigment complexes of photosynthetic systems are rather complex, and it has proven difficult to analyse the excited-state properties of these systems in all details. This is mainly caused by a pronounced disorder, which masks details in the steady-state optical spectra, even at low temperature. Therefore, in this thesis, the light-harvesting complexes from purple bacteria were investigated by applying single-molecule spectroscopic techniques. The intriguing feature of this technique is that it allows to elucidate information that is commonly washed out by ensemble averaging. Besides the possibility to circumvent spatial inhomogeneities it allows also the observation of dynamical processes which are usually obscured by the lack of synchronisation within an ensemble. A single molecule that undergoes a temporal development between different states is at any time in a distinct, well defined state and the whole sequence of steps can be studied. This allows in particular to identify short-lived intermediate states that might be essential for the understanding of the process under study but which would be completely masked otherwise.

Such dynamical processes can be observed in light-harvesting complexes when looking at the interaction of the chromophores with amino acid residues of proteins in their local environment. Conformational fluctuations of the backbone residues are equivalent to rearrangements of their atoms, and chromophores embedded in the protein experience those changes as fluctuations in the local interactions and react with changes of their electronic energies. This makes them suited to act as local probes for monitoring the dynamics of a protein and to test the validity of the model describing protein dynamics and folding put forward by Frauenfelder and coworkers, which proposes that the energy landscape of proteins is arranged in hierarchical tiers [30–33].

Since the beginnings of single-molecule spectroscopy in the late 1980s [34, 35] the field underwent a breathtaking progress away from its cryogenic roots and especially the application of single-molecule *detection* techniques under ambient conditions in biology and biochemistry has led to a revolution in these disciplines (see for some examples [36–42]). However, the low temperature approach allows to study single molecules over a very long observation period because photobleaching effects of the probe molecules, usually limiting the observation time to some tens of seconds under ambient conditions, are negligible. This offers the opportunity to determine the electronic eigenstates of an individual system, i.e., to perform single-molecule spectroscopy rather than merely detection and to apply many experimental techniques from the highly developed toolbox of spectroscopy also to single objects [43–48].

This thesis is organised as follows: in chapter 2 the photo-physical and biological properties of the photosynthetic apparatus of purple bacteria are introduced. In chapter 3 sample preparation and the single-molecule setup is described. In chapter 4 the B800 band of LH2 is studied, and the pigment-pigment interaction, energetic disorder within and between complexes and the dynamics in the energy landscape of the proteins in the binding pockets are discussed. In chapter 5 a pattern recognition approach is employed to gain information on spectral diffusion processes in the B800 band as well as on the line shapes of the individual B800 absorption. Chapter 6 deals with the delocalised Frenkel excitons in the B850 band and touches on the types of energetic and structural disorder within the LH2 complex. The large structural heterogeneity of the core complex (LH1-RC) is looked at in chapter 7 and possible pathways of protons leaving the RC into the lipid phase of the membrane for further biochemical processing are discussed. Finally, in chapter 8 the observation of energy transfer from LH2 to the core complex within a single PSU is presented and the affinity of its building blocks is evaluated.

Light harvesting complexes

2.1 Photosynthesis

Living organisms are commonly divided into two groups. The first one comprises the so called *autotrophic* organisms, which are capable of self-nourishment by using inorganic matter as the main source of carbon. They obtain the energy for life processes from the oxidation of inorganic elements (*chemotrophic*) or from radiant energy (*phototrophic*). The second group contains the so called *heterotrophic* organisms, which are capable of deriving energy for life processes only from the decomposition of organic compounds. They are unable to use inorganic compounds as sole sources of energy or for organic synthesis [49, 50].

The process by which phototrophic organisms can produce organic substances from pure inorganic compounds using electromagnetic radiation as energy source is called photosynthesis. Nearly all organic matter on earth is formed by these photosynthetic processes and life on earth would shortly come to a complete standstill if photosynthesis ceased to function.

In green plants carbon dioxide is reduced by water under the illumination with light finally leading to the synthesis of glucose:



Here, the water molecule acts as electron donor and the carbon dioxide functions as electron acceptor. Other electron donors (e.g., H_2S) and acceptors (e.g., NO_3^- , N_2 , H^+) also occur in nature. For more details on the photosynthetic process see references [49, 50].

The primary steps of photosynthesis comprise the absorption of a photon by a photosynthetic pigment such as a chlorophyll or carotenoid in a light-harvesting complex and the subsequent transport to a so called reaction centre in which the energy is stored by means of a long lived (>100 ms [51, 52]) charge separation which is necessary as the excited states of the pigments decay very rapidly in less than a few nanoseconds. This charge separation is ultimately used for the synthesis of even longer lived chemical storages such as the major energy source in biological systems, adenosine triphosphate (ATP) or the major electron donor in reductive biosynthesis, nicotinamide-adenine dinucleotide phosphate (NADPH) [53, 54].

Purple non-sulfur photosynthetic bacteria (i.e., *Rhodospirillaceae*) which were studied in this thesis depend on organic hydrogen donors and are therefore, strictly speaking, not autotrophic but photoorganotrophic. Following the primary steps of photosynthesis which take place in two different light-harvesting (LH) complexes and the reaction centre (RC), these purple bacteria feature a cyclic photoelectron transport leading to a proton gradient across the intracytoplasmic membrane (i.e., the membrane in which their photosynthetic membrane complexes are located) which is used for the synthesis of ATP [55].

In this section, the elements which constitute the photosynthetic membrane complexes as well as their supramolecular organisation will be discussed.

2.1.1 Building blocks of the photosynthetic apparatus in purple bacteria

Pyrroles and chlorophylls

Although n-heterocyclic pyrrole (Fig. 2.1A) is a very stable chemical molecule it does not exist naturally as mono-, di- or trimer. Linear tetrapyrroles do occur but only cyclic tetrapyrroles, e.g., porphyrines or chlorophylls whose structures are based on the macrocyclic porphine system (Fig. 2.1B) play a major role in living organisms [56]. The carbon atoms in these rings can be labelled according to two different conventions of which the Fischer labelling system [57]

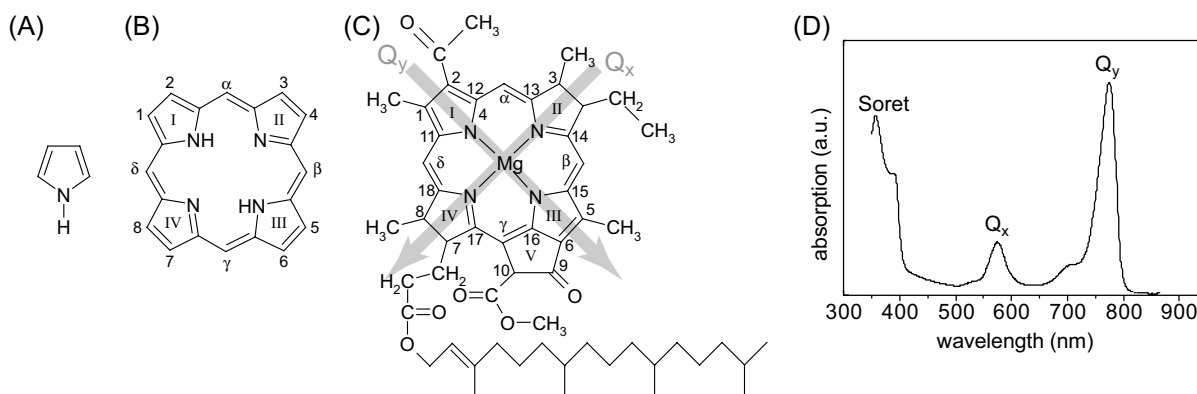


Figure 2.1: *Pyroles in Photosynthesis.* (A) *n*-heterocyclic pyrrole. (B) Porphine molecule consisting of four pyrroles connected by methine bridges. (C) Bacteriochlorophyll *a* molecule based on a phorbine skeleton with side groups and a central Mg-ion. The atoms are labelled according to the Fischer system [57]. The arrows indicate the orientations of the Q_x and Q_y transition-dipole moments. (D) Absorption spectrum of BChl *a* in diethyl ether.

will be used throughout this thesis. The structural skeleton of chlorophyll (Chl) molecules (from Greek $\chi\lambda\omega\rho\acute{o}\varsigma$, green and $\phi\acute{\upsilon}\lambda\lambda\omicron\nu$, leaf) is phorbine, which has an extra isocyclic ring (V) compared to porphine. Common features of the many existing different chlorophylls are a central Mg-ion that can be used as a ligand binding site and a phytyl group at position 7 of the ring system that serves as an anchor for the pigment in the protein environment. Chlorophylls differ by the types of further side groups that are attached to the macrocycle [49, 53, 58]. Metal-free chlorophylls are known as pheophytins. The purple bacteria which are looked at in this thesis all express the bacteriochlorophyll (BChl) *a* derivative whose structure is depicted in Fig. 2.1C. The absorption spectrum in Fig. 2.1D displays three broad bands belonging to electronically excited singlet states (S_x) which are the Soret bands (S_4 / S_3) at around 400 nm and the Q_x (S_2) and Q_y (S_1) bands in the visible and near infrared, respectively [15, 59]. The transition-dipole moments related to the latter two absorption bands are mutually orthogonal and their orientation within the plane of the phorbine molecule is given in Fig. 2.1C.

Once the pigments are embedded in a protein environment as in the light-harvesting complexes, their absorption maxima can be altered by more than 100 nm due to interactions with the proteins as well as with neighbouring pigment molecules [15, 60]. In this way nature has the possibility to fine-tune the absorption characteristics of the different organisms to match the environment in which they live. Chlorophylls in green plants, for instance, will not absorb at wavelengths longer than 680 nm, which corresponds to the amount of energy needed for water oxidation. Purple bacteria do not need these high energies and their large red-shifted absorption

allows them to live at the bottom of ponds, providing them with a niche that is not taken up by plants or algae

Carotenoids

Another important class of photosynthetic pigments is formed by the carotenoids (Car) which are basically linear molecules. They consist of a polyene chain with alternating single and double bonds, the number of which can vary typically from eight to eleven between different species of carotenoids [61]. In Fig. 2.2 lycopene is shown which is the major carotenoid in LH2 from *Rhodospirillum molischanum*. Carotenoids generally absorb in the visible around 350-570 nm where chlorophylls do not absorb and transfer their excitation energy to neighbouring chlorophylls thus increasing the spectral absorption cross section of the overall system. They are responsible for the bright variety of colours in flowers and all other plants.

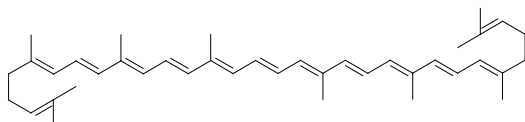


Figure 2.2: Structure of lycopene which is the major carotenoid molecule in LH2 from *Rhodospirillum molischanum*.

Apart from light-harvesting they fulfil the more important role of protection against photo-damage [62]. Excited chlorophyll has a small probability of inter-system crossing to triplet states. Then, the triplet state can transfer its energy to oxygen, producing singlet excited oxygen (${}^3\text{Chl}^* + {}^3\text{O}_2 \rightarrow {}^1\text{Chl} + {}^1\text{O}_2^*$) which is a highly reactive free radical that can damage the organism. The carotenoids provide a solution for this problem as they quench the chlorophyll triplet (${}^3\text{Chl}^* + {}^1\text{Car} \rightarrow {}^1\text{Chl} + {}^3\text{Car}^*$). The generated triplet excited state of the carotenoids is lower in energy than that of singlet oxygen so that the danger is banned [63].

Carotenoids are also necessary to assure a correct assembly of the photosynthetic pigment-protein complexes, as some pigments will not be properly incorporated in their absence [64].

The reaction centre and the antenna complexes

The photosynthetic apparatus in purple bacteria comprises several transmembrane protein and pigment-protein complexes and is located in the intracytoplasmic membrane.

In bacterial photosynthesis the radiation energy is commonly absorbed by bacteriochlorophyll or carotenoid molecules but only few BChl molecules in the so called reaction centre of the photosynthetic apparatus are photochemically active. The others, together with most of the carotenoids, form pigment-protein complexes, so called light-harvesting antennas whose function is to capture the sunlight and to funnel the electronic excitation towards the RC.

Chlorophyll molecules absorb at a rate of about 10 Hz when they are exposed to bright sunlight and about 0.1 Hz in dim light conditions. In contrast, the reaction centre has a “turn over” rate of about 1000 Hz [49, 65, 66]. Therefore, the light-harvesting antenna help to increase the efficiency of energy utilisation by about 2 orders of magnitude. In most purple bacteria the photosynthetic membranes contain two different photosynthetic membrane complexes (PMC): the light-harvesting 1 (LH1) complex and the peripheral light-harvesting 2 (LH2) complex [11, 55]. Depending on the growth conditions of the bacterium some species express another peripheral complex, LH3 [5], which is a spectroscopic variant of LH2. LH1 and the RC are closely associated and form the so called core complex (LH1-RC), whereas LH2 is not in direct contact with the RC but transfers the energy via the LH1 complex to the RC [12, 49, 67, 68].

It was found that all light-harvesting complexes are constructed in a remarkably similar fashion [58, 69]. The basic building block is a trans-membrane protein heterodimer (α - and β -apoprotein) which non-covalently binds two (LH1) or three (LH2) BChl *a* pigments and one or two carotenoid molecules. Several heterodimers form larger circular aggregates that constitute the light-harvesting complexes. The size of the complexes differs for LH1 and LH2 and is species dependent as will be discussed in more detail in the following section.

From this knowledge together with theoretical modelling a scheme of the arrangement of the pigment-protein complexes has been proposed in which the core complex is surrounded by several LH2 complexes in a two dimensional structure [11, 51, 67, 70]. A sketch of the supramolecular arrangement of the photosynthetic unit (PSU) comprising the RC and both PMCs LH1 and LH2 is shown in Fig. 2.3. Depending on the light intensity at which the cells are grown, the size of the PSU varies from about 30 BChl molecules per RC (high-light) to 200-250 BChl molecules per RC (low light) in *Rhodobacter sphaeroides*. As a fixed stoichiometry exists between the RC and LH1, only the number of LH2 and LH3 complexes is varied. Doing so, purple bacteria are able to adjust their capacity for photon capture ensuring that each RC is kept well supplied with excitation energy [11].

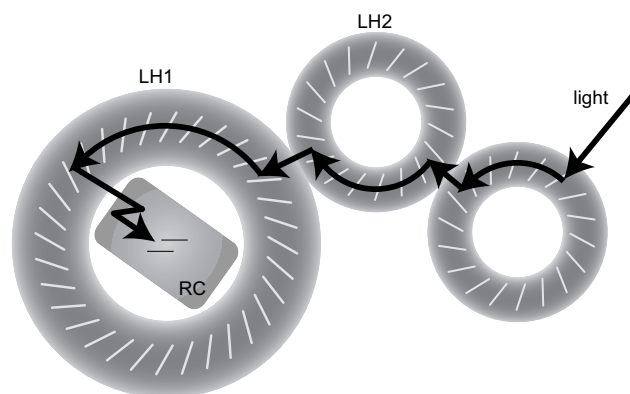


Figure 2.3: Sketch of the photosynthetic unit (PSU) of purple bacteria. It comprises the reaction centre (RC) and two types of photosynthetic membrane complexes (PMCs): the light-harvesting 1 (LH1) and the peripheral light-harvesting 2 (LH2) complex. LH1 and the RC are closely associated forming the core complex, whereas LH2 transfers the excitation energy to the RC via the LH1 complex as indicated by the arrows. The light bars indicate the BChl *a* molecules which are held in place by the grey protein scaffold. Adapted from [70].

Interestingly, the pigments show a hierarchical arrangement where pigments absorbing at higher energies are placed further away from the RC. It seems that the whole structure is highly optimised to capture light energy and, depending on the illumination conditions, either to funnel the excitation energy to the RC or to act as a reservoir to store the energy in order to avoid overexposure and damage of the RC. The different absorption energies of the accessory chromophores also lead to the utilisation of a broader spectral range of the incident light. However, despite the tremendous progress in the field that has been achieved during the last decade important details, for example the structure of the LH1-RC complex or the supramolecular organisation of the PSU, are unknown and currently an issue of hot debate [71].

2.1.2 The photosynthetic unit (PSU)

The peripheral light-harvesting 2 (LH2) complex

The structures of the LH2 complexes from *Rhodospseudomonas (Rps.) acidophila* [2, 4] and *Rhodospirillum (Rs.) molischianum* [3] were determined by x-ray crystallography and that from *Rhodobacter (Rb.) sphaeroides* by electron-microscopy [7]. Remarkably, all peripheral LH complexes form circular oligomers of the two hydrophobic α - and β - apoproteins that non-covalently bind three BChl *a* molecules and one or two carotenoids, featuring a nonameric (*Rps. acidophila*, *Rb. sphaeroides*) or octameric (*Rs. molischianum*) quaternary protein structure.

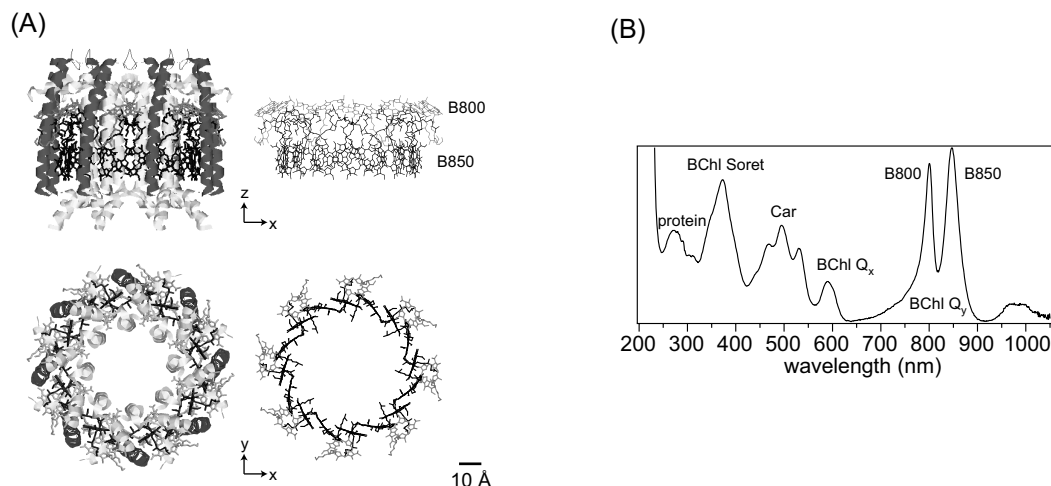


Figure 2.4: X-ray structure and absorption spectrum of the LH2 complex from *Rs. molischianum*. (A) The left part displays the whole pigment-protein complex whereas in the right part only the BChl *a* molecules are drawn. The upper part shows a side view, the lower part a top view. The pigments are arranged in two concentric rings commonly termed B800 (light-grey) and B850 (black). The atomic coordinates were taken from the Protein Data Bank, identification code 1LGH. (B) Absorption spectrum clearly featuring the B800 and B850 absorption bands in the near infrared.

In the left part of Fig. 2.4A the structure of the LH2 pigment-protein complex of *Rs. molischianum* derived from x-ray crystallography with a resolution of 2.4 Å is shown as a whole whereas in the right part only the BChl *a* molecules are depicted. Two rings of BChl *a* molecules can be distinguished. One ring consists of eight repeating pairs of one α - and one β -bound pigment which are oriented like the blades of a turbine. Due to its absorption in the near infrared at around 850 nm this pool is termed B850 ring. The other ring consists of eight well-separated pigments — each bound by a heterodimer — arranged in a C_8 symmetry that have their molecular planes perpendicular to the symmetry axis. It is labelled B800 ring as its maximum absorption occurs around 800 nm. In Fig. 2.4B the room temperature absorption spectrum is shown in which the B800 and the B850 bands are clearly distinguishable. Upon excitation, energy is transferred from the B800 to the B850 pigments in 1 to 2 ps [72–75] while energy transfer among the B850 molecules is an order of magnitude faster [76–78]. The lowest excited state of the B850 pigment pool has a relative long fluorescence lifetime of approximately 1 ns [79].

The light-harvesting 1 (LH1) complex

For LH1 it has not been possible yet to obtain high-quality crystals and therefore the three-dimensional arrangement of its subunits remains to be ascertained. Based on the homology between the LH1 and LH2 proteins, the basic LH1 subunit is believed to contain only two closely coupled BChl *a* molecules contributing to its absorption around 870 nm and presumably one carotenoid [80]. In analogy to its absorption maximum the pigment pool is termed B875 band.

Analysing the number of pigments per RC showed that this number varies between 23 and 33 for different strains of purple bacteria [81–83]. These values are higher than the 16 or 18 pigments that are present in the B850 rings of LH2 suggesting that the main difference between LH2 and LH1 is the size of the ring. This assumption is strengthened by two different 2-D projection maps from electron-microscopy experiments on LH1 from *Rb. sphaeroides* [7] and LH1 reconstituted from $\alpha\beta$ -dimers obtained by detergent treatment of native LH1 complexes from *Rs. rubrum* [6], the latter is depicted in Fig. 2.5A. These experiments revealed a closed-ring structure featuring C_{16} symmetry of the $\alpha\beta$ -subunits which would be just large enough to incorporate a reaction centre [6, 11]. However, also non-circular structures of the LH1 complexes were observed as can be seen from the electron density map of a special type of LH1 from *Rb. sphaeroides* in Fig. 2.5B [8].

The room temperature absorption spectrum of LH1-RC complexes from *Rb. sphaeroides* is shown in Fig. 2.5C.

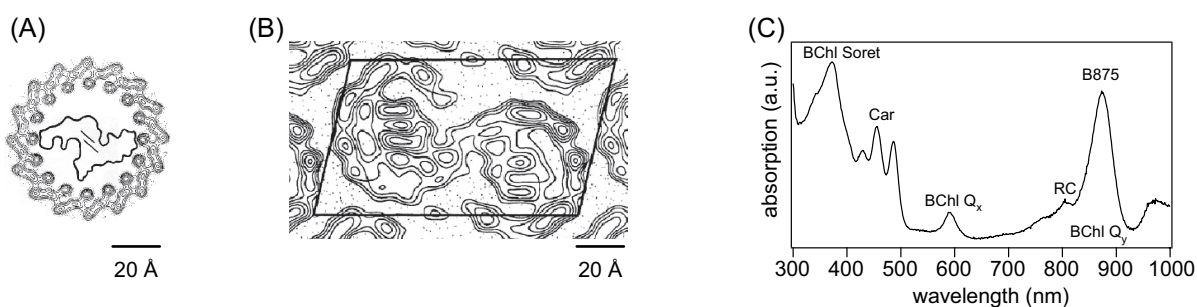


Figure 2.5: Structures of two LH1 complexes and typical absorption spectrum. (A) Projection map at 8.5 Å resolution of reconstituted LH1 complexes from *Rs. rubrum* derived by electron microscopy, from [6]. A reaction centre is schematically drawn inside the ring. (B) Projection map at 20 Å resolution of LH1-RC complexes from *Rb. sphaeroides*, from [8]. (C) Absorption spectrum of LH1-RC complexes from *Rb. sphaeroides*.

The reaction centre (RC)

The structures of the reaction centre from *Rps. viridis* [1] and *Rb. sphaeroides* [84] (the latter is depicted in Fig. 2.6) are known at atomic resolution. The RC of *Rb. sphaeroides* comprises four bacteriochlorophyll (BChl) *a* and two bacteriopheophytin (BPheo) *a* molecules, a carotenoid, a menaquinone (Q_A), an ubiquinone (Q_B) and a non heme-iron all held in place by a protein scaffold (not shown).

Cyclic electron transport inside and outside the PSU

The final goal of photosynthesis is the conversion of solar into chemical energy. This is achieved by a cyclic electron transport which sets in after the light-harvesting and transport of excitation energy to the reaction centre. The whole process of excitation and charge separation starting from light absorption and finishing with an ATP molecule will be described briefly in the following (see also [29, 49, 51, 56, 85, 86]).

- ① Upon the absorption of a photon by a BChl *a* or a carotenoid molecule in one of the peripheral antenna complexes the excitation energy is transferred within about 50 ps (B800 $\xrightarrow{0.7\text{ ps}}$ B850 $\xrightarrow{100\text{ fs}}$ B850 $\xrightarrow{3\text{ ps}}$ B875 $\xrightarrow{80\text{ fs}}$ B875 $\xrightarrow{35\text{ ps}}$ RC) [12, 49, 54, 67, 68, 87] via neighbouring complexes to the reaction centre, more precisely to the special pair (P) in the RC

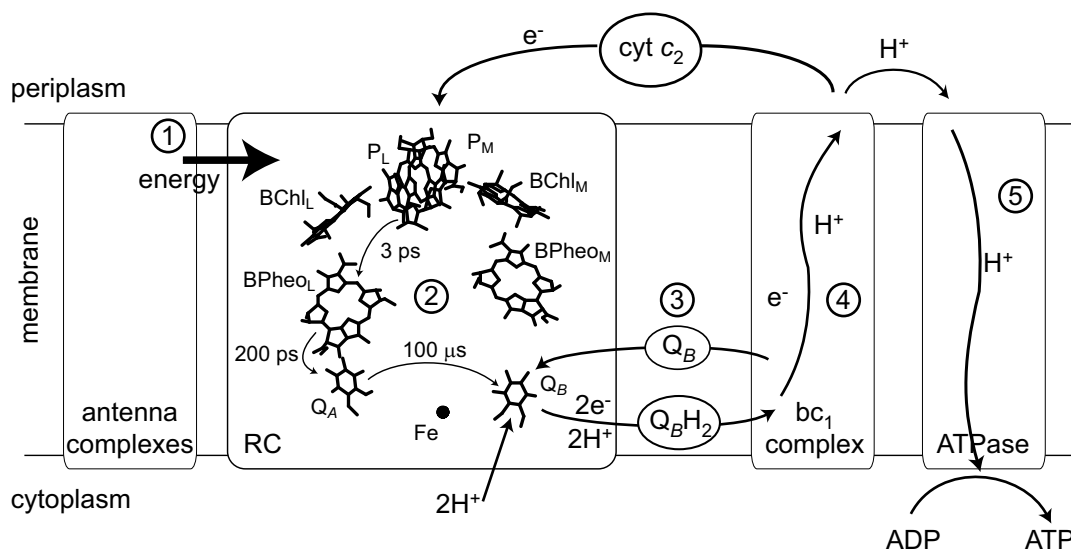


Figure 2.6: First steps in photosynthesis and subsequent cyclic electron transport [49, 51]. The atomic coordinates of the RC from *Rb. sphaeroides* were taken from the Protein Data Bank, identifier 1PSS. For more details see text.

which comprises two BChl *a* molecules, P_L and P_M. This process occurs with a quantum efficiency of about 95%.

- ② The relaxation of the excited P, which occurs in about 3 ps initiates a *charge* transfer to the BPheo_L resulting in an electron-hole pair P⁺BPheo_L⁻. The role of the BChl_L in this step is not completely clear. From here the electron is transferred to the menaquinone Q_A in 200 ps and in the final step in about 100 μs to the ubiquinone Q_B which picks up a proton from the cytoplasmic side to become Q_BH. This stepwise electron transfer leads to a stable charge separation across the membrane as the back reaction leading to RC relaxation is at least a factor of 10⁴ slower than the forward reactions.
- ③ After two electron transfer steps, the reduced hydroquinone (Q_BH₂) which is only loosely bound to the RC leaves into the lipid phase of the membrane towards the ubiquinone-cytochrome *bc*₁ complex.
- ④ The *bc*₁ complex oxidises the hydroquinone with help of the cytochrome *c*₂ complex and uses the exothermic reaction to establish a proton gradient across the membrane by pumping the protons to the periplasmic side. The electrons are shuttled back to the special pair in the RC by the cytochrome *c*₂ complex and the quinone Q_B returns to the RC.
- ⑤ The proton gradient is needed to drive the synthesis of ATP from ADP by the ATPase complex. With this last step, the conversion of solar energy into chemical energy that can be used by the metabolic processes of the organism is finished.

2.2 Spectral properties of pigments

In general, the spectroscopic properties of pigment molecules depend strongly on their interaction with the local environment, i.e., the solvent or the protein scaffold as well as on their interaction with neighbouring pigments. For bacteriochlorophyll *a*, for instance, the main absorption peak at room temperature is at 771 nm in diethyl ether but is shifted by up to 20 nm in other solvents [88]. In a solvent each pigment experiences on average the same environment whereas pigment-protein complexes feature various binding sites. Pigments in different sites experience different interactions with their specific protein environment and thus exhibit varying spectral properties.

But proteins are by no means rigid molecules and are better described as dynamic structures [89, 90]. Consequently, pigments located in identical binding sites in different proteins do not necessarily experience identical environments and even the environment of an individual pigment will change in time due to motions of the surrounding proteins. This results in a static and dynamic distribution of transition energies in an ensemble of pigment-protein complexes leading to broad emission and absorption bands compared to single pigments.

In this section, the intrinsic electronic properties of Chl molecules, the interactions with their protein environment as well as the coupling to neighbouring chlorophylls will be discussed.

2.2.1 The intrinsic electronic properties of chlorophylls

The electronic properties of (bacterio)chlorophylls are mainly determined by the conjugated π -electron system in the bacteriochlorin ring and consist of three absorption bands all belonging to singlet excited states (Fig. 2.1D). In Fig. 2.7 a schematic representation of the electronic energy-level structure of a chlorophyll molecule is shown.

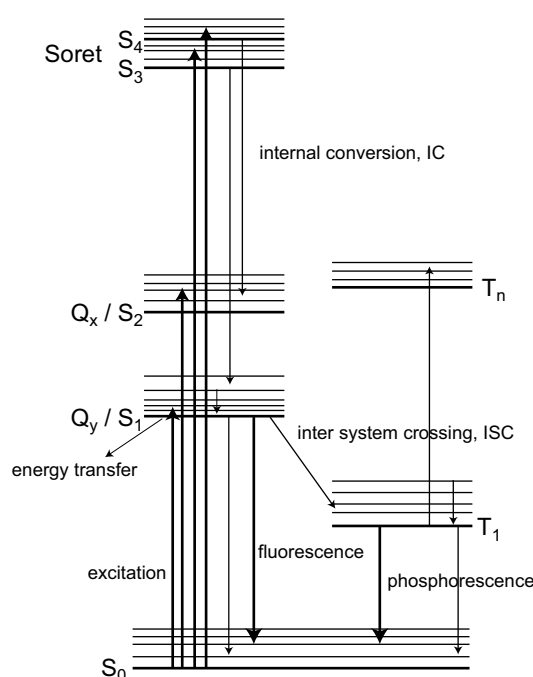


Figure 2.7: Jablonsky diagram of a chlorophyll molecule. S_0 , S_{1-4} and $T_{1,n}$ denote the ground state, the singlet excited states and the triplet states, respectively. For each state several vibronic states (thin lines) are shown. The thick arrows indicate transitions which involve the absorption or emission of a photon whereas the transitions marked by the thin arrows occur non-radiatively.

Absorption

If the laser is in resonance with an optically allowed transition, the molecule absorbs a photon and will be excited from the ground state (S_0) to an excited singlet state (S_{1-4}). Both the Q_x and the Soret states are very short-lived with internal conversion (IC) to the Q_y taking place in about 100 fs [91, 92]. On the other hand, the Q_y has a fluorescence lifetime of several nanoseconds after which the molecule relaxes to its ground state, under the emission of a fluorescence photon. The behaviour, that the emission of light only takes place from the lowest electronic excited state independent of the excitation process is called Kasha's Rule [56, 93]. Some of the emitted photons will undergo a so called Stokes-Shift and emit at longer wavelengths caused by the decay of the molecule into vibrational and/or phonon modes of the electronic ground state. Owing to the long lifetime of Q_y almost all excitation transfer between Chls occurs via interaction between Q_y transition dipoles.

Apart from the singlet excited states, Chls also have a triplet system in which the lowest state T_1 lies well below Q_y . From the excited Q_y state the Chl can convert with a small probability to T_1 via inter system crossing (ISC). The triplet lifetime is on the order of micro- to milliseconds during which the molecule can not absorb another photon. Thus the triplet state may act as a bottleneck in the excitation-relaxation cycle. From the triplet state the molecule can either emit a photon (phosphorescence) or decay non-radiatively to the ground state.

The probability for a molecule to absorb a photon is proportional to the absorption cross section σ divided by the cross-sectional area of the focused laser beam A . For σ the following relations holds [94]:

$$\sigma(T) = C_{\text{FC}} C_{\text{DW}}(T) \frac{\tau_2(T)}{2\tau_{\text{rad}}} \frac{\lambda_0^2}{2\pi} \beta(\theta) \quad (2.2)$$

where λ_0 is the wavelength at the maximum of the absorption, τ_2 the total dephasing time, T the temperature, $\beta(\theta)$ a geometrical factor which accounts for the mutual orientation of the transition-dipole moment and the exciting field and $\tau_{\text{rad}} = \tau_1/\phi_f$ the radiative lifetime with τ_1 the excited-state lifetime and ϕ_f the fluorescence yield. C_{FC} stands for the Franck-Condon factor of the 0–0 transition, i.e., a pure electronic transition from the vibronic ground state of the electronically excited state to the vibronic ground state of the electronic ground state. Within the Born-Oppenheimer approximation in which it is assumed that only the electrons and not the

nucleus are moving during a transition, the Franck-Condon factor denotes the effects of vibronic coupling and describes the distribution of oscillator strength over the vibrational sidebands of the transitions. C_{DW} denotes the Debye-Waller factor which gives the ratio of the intensity of the emission from a pure electronic excited state and the intensity of all vibrational bands connected to this state.

Emission

Using the Jablonsky diagram, rate equations can be derived and the emission rate $R(I)$ of the fluorescence of a molecule can be described by [95]

$$R(I) = R_{\infty} \left(\frac{I/I_S}{1 + I/I_S} \right), \quad \text{with} \quad R_{\infty} = \frac{(\phi_f + \phi_T)k_f}{2 + \left(\frac{k_{\text{ISC}}}{k_T}\right)} = \frac{\phi_f}{\tau_1 \left(2 + \frac{\tau_T \phi_T}{\tau_1}\right)} \quad (2.3)$$

where $k_f = \phi_f/\tau_1$ denotes the fluorescence rate with ϕ_f the fluorescence quantum yield and τ_1 the excited-state lifetime. $k_{\text{ISC}} = \phi_T/\tau_1$ stands for the inter system crossing rate with $\phi_T = k_{\text{ISC}}/(k_f + k_{\text{ISC}})$ the triplet yield and $k_T = 1/\tau_T$ for the triplet rate with the triplet lifetime τ_T . The emission saturates at high excitation intensities and ultimately becomes R_{∞} . For BChl *a* in light-harvesting complexes a rapid energy transfer with close to 100% efficiency occurs from the triplet excited BChl *a* to the carotenoid molecules which reduces the lifetime of the BChl *a* triplet state by two orders of magnitude [96, 97] thereby protecting it against photodamage. However, as the carotenoid triplet state is known to be a very efficient trap for singlet excitations in LH complexes [77, 98] the triplet lifetime of the carotenoids has to be taken into account in Eq. 2.3. For LH2 at low temperature with a fluorescence lifetime (τ_1) of about 1.25 ns [79], a fluorescence yield (ϕ_f) of 10–14% [79], a triplet yield (ϕ_T) of 2–15% [99] and a carotenoid triplet lifetime (τ_T) of 3–15 μs [100] this gives a maximum emission rate (R_{∞}) of several 100 000 counts per second [24, 101, 102].

2.2.2 Pigment-protein interaction

The homogeneous linewidth, zero-phonon line and phonon side-band

Without any interaction the absorption line shape of a pure electronic transition (e.g., $S_1 \rightarrow S_0$) would be Lorentzian and its width ($\Gamma_{\text{hom}} = 1/2\pi\tau_1$) would be completely determined by its

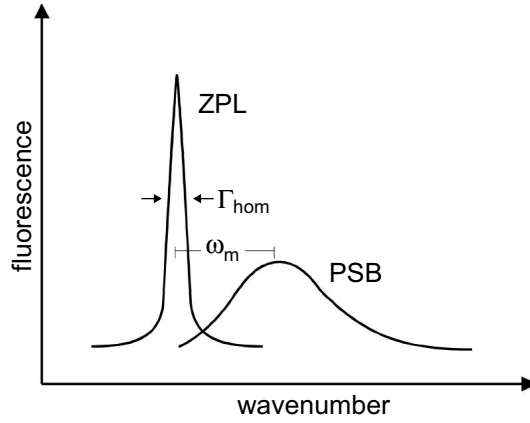


Figure 2.8: Schematic representation of the fluorescence-excitation spectrum of a single molecule at low temperature comprising a narrow zero-phonon line (ZPL) and a broad, blue shifted phonon side-band (PSB). ω_m denotes the mean phonon frequency.

excited state lifetime τ_1 . However, the interaction of the probe molecule with its surrounding causes frequency fluctuations $\delta\nu$ of the absorption whose contributions to the optical line shape depend on the timescale δt of the fluctuations.

In the following only fast fluctuations $\delta\nu \delta t < 1$ such as the coupling of the vibrational motions of the proteins (i.e., phonons) to the electronic transitions of the pigment will be considered. In the case of quadratic electron-phonon coupling [95, 103, 104] these fast fluctuations contribute to a dephasing of the optical transitions within the pure dephasing time τ_2^* . This leads to a temperature dependent homogeneous broadening of the absorption line by phonon scattering

$$\Gamma_{\text{hom}}(T) = \frac{1}{\pi\tau_2(T)} = \frac{1}{2\pi\tau_1} + \frac{1}{\pi\tau_2^*(T)}. \quad (2.4)$$

in which τ_2 denotes the total dephasing time and T the temperature. This line is called zero-phonon line (ZPL) since no net creation or destruction of phonons or other low-frequency excitations takes place. For a linear electron-phonon coupling [95, 103, 104], the homogeneous absorption and emission spectra will also show a contribution due to the simultaneous electronic transition of the pigment and a phonon transition of the protein which is called the phonon side-band (PSB) and is typically separated several 10 cm^{-1} from the maximum of the ZPL as displayed in Fig. 2.8 [95].

The relative intensity of the zero-phonon line (I_{ZPL}) compared to overall spectrum, i.e., the sum of I_{ZPL} and I_{PSB} is described by the Debye-Waller factor mentioned before

$$C_{\text{DW}} = \frac{I_{\text{ZPL}}}{I_{\text{ZPL}} + I_{\text{PSB}}} = \exp(-S(T)) \quad (2.5)$$

which depends exponentially on the temperature T according to the Huang-Rhys factor $S(T)$ [105].

Inhomogeneous broadening and spectral diffusion

The interaction strength between a chromophore and a molecule in its surrounding will follow a distance dependence of R^{-n} with n ranging from about 3–12. Fluctuations in the local environment of the chromophore are represented by distance changes to neighbouring molecules resulting in fluctuations of the absorption frequency of the chromophore.

In contrast to dephasing processes caused by fast fluctuations which lead to *homogeneous* broadening of the absorption line, these slow fluctuations $\delta\nu \delta t > 1$ of the environment — such as structural changes of the proteins — cause spectral diffusion represented by gradual spectral drifts or abrupt jumps of the absorption frequency which results in an *inhomogeneously* broadened absorption. In principle for a spectrally diffusing line the individual frequency jumps could be observed with a sufficiently fast and sensitive detection system.

The best way to follow temporal changes in the local environment of a pigment is by looking at a two-dimensional representation of sequentially taken spectra stacked on top of each other as shown schematically for a single molecule in the identical upper parts of the panels (i)–(iv) in Fig. 2.9. In each scan the molecule absorbs at one specific wavelength as indicated by the black dots and spectral fluctuations of the absorption wavelength of the molecule show up as diffusing “trails” [106] in the time versus wavelength diagram.

For the molecule in this example the absorption wavelength fluctuates between six different values on a fast t_f (small jumps) and a slow T_f (large jumps) timescale. In an experiment in which the detection window of the measurement ranges from the fastest timescale t_m (temporal resolution of the detection) to the slowest timescale T_m (time duration of the experiment) the following situations depending on the timescales of the fluctuations and the measurement can be distinguished [44]:

(i) $T_f \ll t_m$ All fluctuations occur on a faster timescale than the shortest detection window.

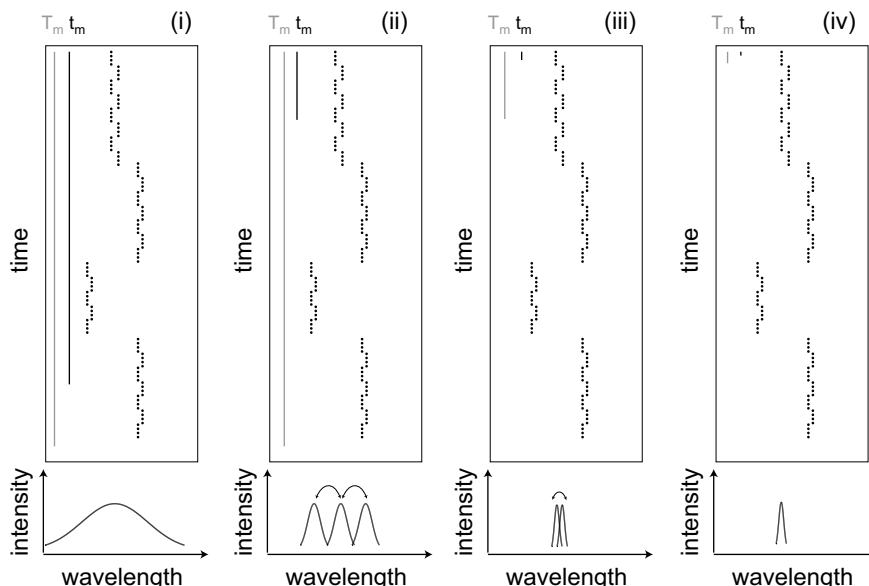


Figure 2.9: Sketch of the spectral diffusion of a molecule featuring two timescales $t_f < T_F$ together with the spectra obtained from four different hypothetical measurements (i)–(iv). In the upper part in each panel the same sequence of consecutively taken spectra is stacked on top of each other whereby the spectral position of the fluorescence is indicated by the black dots. The detection time scales of the four measurements (t_m fastest detection in black, T_m total detection time in grey) are indicated by the solid lines in the panels. The spectra obtained for the four classes are displayed in the lower part of the frames in which the arrows indicate temporal fluctuating spectra.

All molecules would therefore look identical and their spectrum would represent the ensemble spectrum. The system would appear *homogeneous and static*.

(ii) $t_f \ll t_m \ll T_f \ll T_m$ Only slow fluctuations of the system will be detected. Individual molecules would appear statistically equal but their parameters would seem to fluctuate. The system would appear *homogeneous, but fluctuating*.

(iii) $t_f \ll T_m \ll T_f$ The fastest fluctuations can be detected whereas the slower ones are frozen out and are not detectable within the timescale of the measurement. Different molecules sample different parameter spaces which makes the system appear *inhomogeneous and fluctuating*.

(iv) $T_m \ll t_f$ All fluctuations are slower than the largest detection window. No fluctuations are observed and all molecules look different from each other. The system therefore appears to be *inhomogeneous and static*.

The spectra of the single molecule that are recorded in a measurements for the four cases de-

scribed above are shown in the lower parts of the panels in Fig. 2.9 in which arrows above some of the absorptions indicate fluctuating spectra. The detection time scales of the measurement (fastest detection t_m in black and total detection time T_m in grey) are indicated by the lengths of the solid lines on the left in the upper panels. It is obvious that different measurement time windows result in different information that can be obtained from the molecule.

2.2.3 Pigment-pigment interaction

Bacteriochlorophylls do not only interact with their protein and solvent environment but also with neighbouring pigments. The most significant interaction is the Coulomb interaction V_{ij} between two chromophores i and j which can be described by

$$V_{ij} = \frac{1}{4\pi\epsilon\epsilon_0} \sum \frac{q_i q_j}{r_{ij}}, \quad (2.6)$$

where ϵ is the dielectric constant of the medium, ϵ_0 the electric permittivity of free space and r_{ij} the relative distance between electronic or nuclear charges q_i and q_j on the chromophores.

It can be decomposed into the classic Coulomb interaction between the electrons and nuclei and the quantum theoretical exchange interaction caused by the fact that electrons are indistinguishable from each other. If the pigments are not permanently charged and if their relative distance is large compared to their size, the classic Coulombic interactions are much larger than the exchange interactions and the interaction energy can be approximated by the dipole-dipole term in the multipole expansion of the Coulomb interaction [15, 56]

$$V_{ij}^{(D)} = \frac{1}{4\pi\epsilon\epsilon_0} \frac{\mu^2}{r_{ij}^3} \kappa_{ij}, \quad \kappa_{ij} = \frac{1}{\mu^2} \left[(\vec{\mu}_i \cdot \vec{\mu}_j) - 3 \frac{(\vec{\mu}_i \cdot \vec{r}_{ij})(\vec{\mu}_j \cdot \vec{r}_{ij})}{r_{ij}^2} \right]. \quad (2.7)$$

Here, $\vec{\mu}$ is the transition-dipole moment which is a transient dipolar polarisation created by an interaction of electromagnetic radiation with a molecule and describes, to first order, the collective behaviour of all charges of the pigment. The distance between the transition dipoles $\vec{\mu}_i$ and $\vec{\mu}_j$ is given by \vec{r}_{ij} , whereas the orientation factor κ_{ij} covers the mutual orientations of the transition-dipoles by means of normalised vectors. For the B850 ring of LH2 from bacterial photosynthetic light-harvesting complexes the validity of this approximation may be questioned since the distance between pigments is rather small. Therefore, other approaches have been taken as well including the spatial distribution of the transition dipole moment [107,

108], including further multipole terms of the coulomb interaction [109] or taking the exchange interaction into account [110, 111].

Hamilton operator: diagonal and off-diagonal disorder, types of interaction

In the approximation that the structure of the electronic states of each molecule can be described by a two level system the Hamilton operator that describes the electronically excited states of an assembly of N B800 or B850 BChl *a* molecules can be written as [20, 22, 112–114]

$$H = \underbrace{\sum_{n=1}^N E_0 |n\rangle \langle n|}_{\text{energy}} + \underbrace{\sum_{n=1}^N V_0 [|n\rangle \langle n+1| + \text{H.c.}]}_{\text{interaction}}. \quad (2.8)$$

Here E_0 denotes the average excited state energy of an individual pigment, V_0 the average nearest-neighbour interaction and H.c. stands for the Hermitian conjugate of the preceding term.

If energetic and structural disorder are present in the system, the situation changes. The energetic disorder is characterised by diagonal terms in the Hamiltonian δE_n which denote the deviation of the excited state energy of pigment n from the average E_0 and are usually described by a Gaussian distribution with a width of Δ . The structural disorder comprises distance and orientational changes and is therefore reflected by modulations in the interaction energy characterised by off-diagonal terms in the Hamiltonian δV_n . Taking this into account, the Hamilton operator reads [112]

$$H = \underbrace{\sum_{n=1}^N (E_0 + \delta E_n) |n\rangle \langle n|}_{\text{energy}} + \underbrace{\sum_{n=1}^N (V_0 + \delta V_n) [|n\rangle \langle n+1| + \text{H.c.}]}_{\text{interaction}}. \quad (2.9)$$

Two limiting cases can be distinguished for the description of the electronically excited states of such a molecular aggregate. In the limit $V/\Delta \ll 1$ the description of the excited states of the aggregate in terms of excitations localised on the individual molecules is a good approximation. For $V/\Delta \gg 1$ the electronically excited states of the aggregate are described more appropriately as excitations that are coherently delocalised over the molecules.

The B800 and B850 pigment pools of LH2 are representatives of the two types of interaction strengths. The BChl *a* molecules in the B800 ring feature an interaction energy of about 20 cm^{-1} [12, 54, 107] whereas the disorder $\Delta \approx 280 \text{ cm}^{-1}$ and the average difference in site energy

ranges from 10 – 40 cm⁻¹ (see chapter 4). The excitation of the weakly to intermediately coupled chromophores in the B800 ring will therefore be mainly localised on individual chromophores.

In contrast, the BChl *a* molecules in the B850 pool of LH2 feature an interaction energy of about 250 cm⁻¹ and a disorder with $\Delta \approx 250$ cm⁻¹ (see chapter 6). This strong coupling suggests that excitations in the B850 band will be coherently distributed over at least a part of the ring [20, 77, 79, 107, 115].

Pigment-pigment interaction, a dimer model

The most simple example to illustrate the types of interaction between pigments is that of a dimer consisting of two chromophores “1” and “2” as depicted in Fig. 2.10A. It is assumed that the chromophores have a different excited state energy $E_1 > E_2$ with $\delta = E_1 - E_2$ and an interaction energy V . Note the difference between the width of the distribution of site energies Δ and the difference in site energy of neighbouring pigments δ . For the resulting energies and eigenstates of the coupled system denoted by “+” and “-” one finds

$$E_{\pm} = \frac{1}{2}(E_1 + E_2) \pm \frac{1}{2}\sqrt{\delta^2 + 4V^2} \quad (2.10)$$

and

$$\begin{aligned} |\Psi_+\rangle &= \cos \frac{\theta}{2} |1\rangle + \sin \frac{\theta}{2} |2\rangle \\ |\Psi_-\rangle &= -\sin \frac{\theta}{2} |1\rangle + \cos \frac{\theta}{2} |2\rangle, \end{aligned} \quad (2.11)$$

where $\tan \theta = \frac{2V}{\delta}$ and $|i\rangle$ denotes the excited state localised on molecule i . From the two eigenstates one finds for the transition-dipole moments

$$\begin{aligned} \vec{\mu}_+ &= \vec{\mu}_1 \cos \frac{\theta}{2} + \vec{\mu}_2 \sin \frac{\theta}{2} \\ \vec{\mu}_- &= -\vec{\mu}_1 \sin \frac{\theta}{2} + \vec{\mu}_2 \cos \frac{\theta}{2}, \end{aligned} \quad (2.12)$$

where $\vec{\mu}_i$ denotes the transition-dipole moment of an individual chromophore.

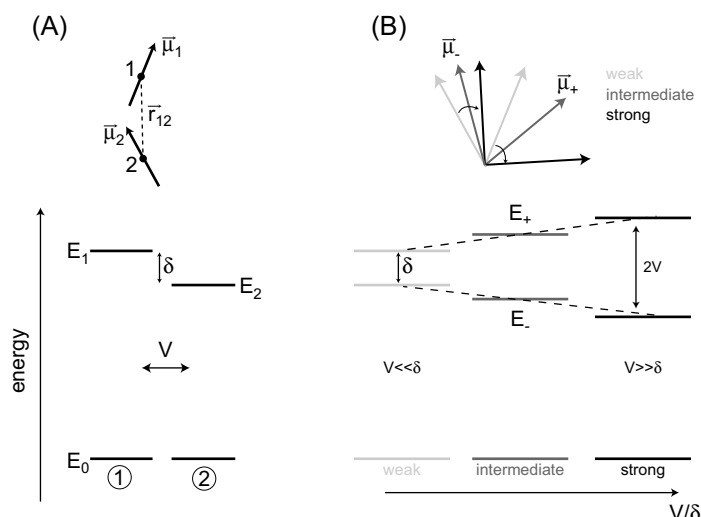


Figure 2.10: Dimeric model of pigment-pigment interaction. (A) Energy diagram of two uncoupled molecules, i.e., $V = 0$ (lower part) together with the orientations of their transition-dipole moments (upper part). (B) Energy diagrams of a coupled dimer for different ratios of interaction strength V over the energetic difference δ between the excited state energies (lower part) together with the orientations of the transition-dipole moments belonging to the coupled states. For more details see text.

Weak interaction, localised excitations

As the interaction energy between the chromophores is increased the splitting of the excited state energies becomes larger and the orientation of the transition-dipole moments changes as is depicted in Fig. 2.10B. Two limiting cases of the dipolar interaction can be distinguished, that of weak and strong coupling. In the case of $V \ll \delta < \Delta$ the coupling between the chromophores will be very weak (left scheme in Fig. 2.10B) and their excited state energies and transition-dipole moments will be similar to the uncoupled case of $V = 0$ in Fig. 2.10A. As a result the excited state wave functions are still mainly localised on the individual chromophores.

In most cases the transfer mechanism between the B800 chromophores has been considered as a Förster type of energy transfer from one donor pigment (D) to the acceptor (A) for which the rate of energy transfer can be written as [116, 117]

$$k_{(D) \rightarrow (A)} = 8.79 \times 10^{-5} J \frac{\kappa^2 \phi_f^{(D)}}{n^4 \tau_1^{(D)} R^6} = \frac{1}{\tau_1^{(D)}} \left(\frac{R_0}{R} \right)^6, \quad (2.13)$$

with the energy overlap integral

$$J = \int_{\lambda} \epsilon^{(A)}(\lambda) f^{(D)}(\lambda) \lambda^4 d\lambda. \quad (2.14)$$

Here, $\phi_f^{(D)}$ denotes the fluorescence quantum yield of the donor, $\tau_1^{(D)}$ the excited state lifetime of the donor with the donor fluorescence rate $k_f^{(D)} = \phi_f^{(D)} / \tau_1^{(D)}$, n the refractive index of the medium, R the distance between donor and acceptor, $\epsilon^{(A)}$ the molecular extinction coefficient of the acceptor, $f^{(D)}$ the normalised emission spectrum of the donor and λ the wavelength of light. The Förster radius R_0 is the distance at which the efficiency of the energy transport is 50%, i.e., half of the donor molecules decay radiatively and half of them transfer their energy to the acceptor. The Förster type of energy transfer that occurs in the weak interaction regime is often referred to as hopping or incoherent energy transfer.

However, the narrow absorption lines are distributed throughout the complete B800 inhomogeneously broadened ensemble absorption and it can be concluded that the spectral overlap of neighbouring B800 pigments is very small (chapter 4). In addition, the rate constants obtained from this model are much slower than the experimental energy transfer rates [72]. Generally the Förster type description is too simple and that other mechanisms (electron-phonon coupling, site energy disorder, carotenoid interaction, etc.) must be taken into account for the energy transfer within the B800 band and from the B800 to the B850 band [75, 118–120].

Strong interaction, Frenkel excitons

The other extreme case, in which $V \gg \Delta > \delta$ holds, is characterised by a very strong excitonic coupling is depicted in the right scheme in Fig. 2.10B [15]. The new eigenfunctions that are given as combinations of the eigenfunctions of the individual chromophores (Eq. 2.11) are delocalised over the pigments and are called Frenkel-excitons [107, 121, 122]. The dipole moments belonging to the new transitions are orthogonally oriented and the oscillator strength of the two exciton levels is determined by the mutual orientation of the transition-dipole moments of the uncoupled chromophores. In an almost perfect head to tail arrangement as is shown in Fig. 2.10A the oscillator strength will be concentrated in the energetically lowest transition. The total spectrum is no longer the sum of the uncoupled chromophore spectra but consists of new absorptions that are separated by a distance $2V$.

Eigenstates of the B850 pigment pool

In the case of the strongly coupled B850 band diagonalisation of the Hamilton operator (Eq. 2.8) leads to the eigenstates, so called the Frenkel excitons [112]

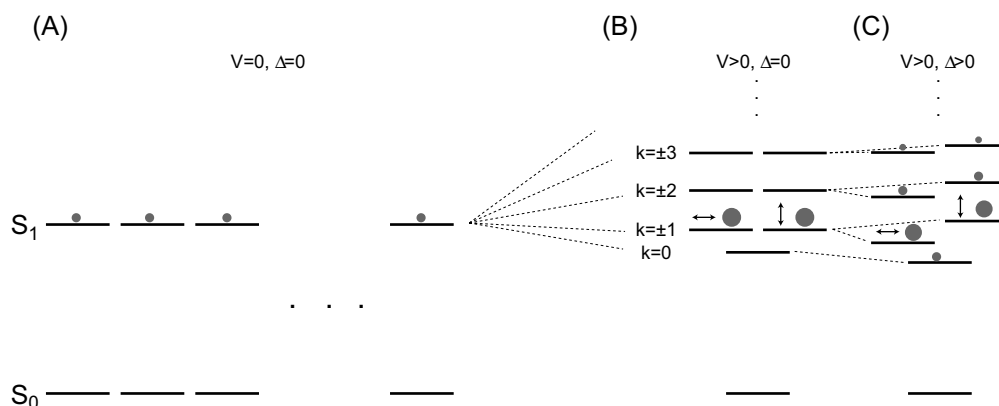


Figure 2.11: Energy diagram of the strongly coupled B850 pigment pool. (A) Energy diagram for the case of no interaction ($V = 0$) between the pigments and no disorder ($\Delta = 0$). (B) Situation for the case of interacting pigments ($V > 0$) but no energetic nor structural heterogeneity ($\Delta = 0$). (C) Exciton states for the case of interacting pigments ($V > 0$) that feature energetic and/or structural disorder $\Delta > 0$). The size of the grey circles reflects the oscillator strength of the transition-dipole moments and the arrows indicate their orientation.

$$|k\rangle = \frac{1}{\sqrt{N}} \sum_{n=1}^N e^{i2\pi k \frac{n}{N}} |n\rangle, \quad (2.15)$$

which are completely delocalised over the whole ring [25]. In contrast to the energy diagram for the uncoupled molecules (Fig. 2.11A) the energy scheme for the strongly coupled system comprises a lowest excited state $k = 0$, eight pairwise degenerate states $k = \pm 1 \dots \pm 4$ and $k = \pm 5 \dots \pm 8$ and on top a single state $k = 9$ for the example of the B850 ring of LH2 from *Rps. acidophila* in which $N = 18$ [112]. However, only the exciton states $k = \pm 1$, which are mutually orthogonal polarised carry significant oscillator strength as for the other states the linear combinations of the individual transition-dipole moments cancel out resulting in a zero net transition dipole moment [112]. The energy scheme for the lowest exciton states is depicted in Fig. 2.11B in which the oscillator strength is indicated by the grey circles.

If energetic and structural disorder are present as described by the Hamiltonian in Eq. 2.9 the degeneracy of the exciton states is lifted and oscillator strength is redistributed from the $k = \pm 1$ states to neighbouring levels as is depicted in Fig. 2.11C [29, 112].

As the emission from the energetically lowest exciton state $k = 0$ is optically forbidden, it has a fluorescence lifetime of about a nanosecond [79].

Materials and methods

3.1 Line narrowing techniques at low temperatures

In the previous chapter it was shown that the static and dynamic distribution of transition energies in an ensemble of pigment-protein complexes due to pigment-protein and pigment-pigment interactions leads to inhomogeneously broadened emission and absorption bands as opposed to the homogeneous absorption and emission lines of single pigments. By looking at the absorption spectrum of LH2 in Fig. 2.4B no significant difference can be seen between the B800 and the B850 band although their electronic properties and coupling mechanisms are totally different. To uncover the parameters determining the homogeneous linewidth from the ensemble bands, special methods can be applied that fall into two categories: those that operate in the frequency domain such as persistent or transient spectral hole-burning as well as single-molecule spectroscopy and those that operate in the time domain such as photon-echo experiments.

3.1.1 Spectral hole-burning

To overcome the limitations of inhomogeneous broadening spectral hole-burning spectroscopy (SHB) [105, 123–126] can be applied which involves the excitation of a group of chromophores

within the sample that absorb within a small wavelength region in the ensemble absorption band. If the decay to the ground state of this group is either blocked (persistent SHB) or delayed (transient SHB) a “spectral hole” appears in the ensemble-absorption spectrum. This process is called hole-burning. However, spectral diffusion processes cause fluctuations in the absorption wavelengths of pigments. Some pigments which have absorbed at a wavelength outside the excitation region prior to the hole-burning process will change their absorption wavelength to a value within the excitation region. Therefore, spectral diffusion processes will lead again to an absorption at the spectral position of the hole. The filling process of the hole can be followed by consecutively taking absorption spectra of the sample, a process called reading of the hole.

Thus, in SHB experiments information about the homogeneous linewidth which is related to the width of the hole as well as information about spectral diffusion processes can be obtained. However, SHB still performs averaging over a subensemble. The group of chromophores burnt does not necessarily represent a structural homogeneous entity but their specific absorption wavelength can have many different causes. Also time averaging during the time between burning and reading the hole limits the information about dynamical processes.

3.1.2 Photon-echo measurements

The photon-echo experiment [124, 127, 128] involves the coherent excitation of the sample with a short laser pulse resulting in a well-defined phase relationship between the oscillating electric dipoles of the excited molecules. At room temperatures this phase relationship is rapidly destroyed by thermally induced scattering processes. However, at low temperatures the scattering is significantly reduced and the temporal development of the relative phases is well-defined even in an inhomogeneously broadened system and despite the variations in resonance frequencies. This temporal development can be reversed by applying a second pulse after a suitable time delay τ_d after which the rephasing of the oscillators proceeds at the same speed as the dephasing before. Thus, the coherent superposition is restored another τ_d after the second pulse which gives rise to an intense burst of coherent radiation, which is known as the photon-echo [127].

The intensity of the two-pulse photon-echo $I_{2\text{PE}} \propto e^{-4\tau_d/\tau_2}$ decays exponentially with increasing time delay and depends on the overall dephasing time τ_2 . Thus the homogeneous linewidth ($\Gamma_{\text{hom}} = 1/\pi\tau_2$) can be obtained by measuring the photon-echo intensity as a function of the time delay between the first and second laser pulse [127].

In two-pulse photon-echo experiments, time averaging can be considered as being absent, since the experiment performs the fastest linewidth measurement that is available [125]. However, due to the spectrally broad laser pulse many molecules within the heterogeneous broadened absorption line will be excited at the same time and ensemble averaging still takes place [127].

3.1.3 Single-molecule spectroscopy

In single-molecule experiments [44–46, 124, 129, 130] the ensemble averaging is completely eliminated. An individual molecule or pigment-protein complex residing in one and only one conformation can be studied. SHB and PE methods can derive information of the homogeneous linewidths of molecules and the rates of spectral diffusion processes. But only using single-molecule spectroscopy (SMS) information on the number of absorption lines that a molecule features and their relative intensities can be obtained. Spectral diffusion processes can not only be monitored in time but also in frequency space because it is possible to determine the spectral jump of an absorption since one can be sure that the absorption appearing at a different wavelength still belongs to the *same* molecule.

However, information can not only be gained about the properties of the molecules but also about their environment by using them as local probes. From the static part of the frequency shifts, information about the conformation of (matrix) molecules around the probe molecule or about proteins in the binding pocket of a chromophore can be obtained whereas from the time dependent part details about the couplings and characteristic times of the motions in the surrounding of the probe can be gained [45]. Studying these dynamics, time averaging has to be taken into account in single-molecule spectroscopy as sufficient photons have to be collected for an appropriate signal-to-noise ratio. However at low temperatures most dynamical processes are slowed down considerably making the time averaging less an issue [12, 52, 131, 132].

3.2 This thesis: single molecule spectroscopy

The purpose of this thesis is to study the static and dynamic properties of pigment-protein and pigment-pigment interactions in photosynthetic light-harvesting complexes. The number of absorption lines of a single complex, their spectral position and their homogeneous linewidths give information about the electronic structure of the different pigment pools and the type of

coupling within as well as about spectral diffusion processes caused by changes in the local environment of the pigments, for instance, due to protein motion. However, even at room temperature the absorptions of single molecules are generally so broad that they would overlap due to homogeneous line broadening. This broadening can be reduced by studying the samples at low temperatures, reducing the dephasing processes [44, 95, 133].

Therefore low-temperature single-molecule spectroscopy was chosen as experimental technique since it is the only method free from ensemble averaging that can distinguish whether absorptions belong to the same or to different molecules. Furthermore, photobleaching processes are strongly reduced at low temperatures allowing to study the complexes for a much longer time than at room temperature. Single pigments in these pigment-protein complexes are excellent candidates for probing the temporal fluctuations in their local environment which are normally hidden in the ensemble spectrum. Although SMS is not free from time averaging, the problem of temporal resolution is lessened by decreasing the temperatures. At low temperatures the dynamics are slowed down and the linewidths of the absorptions are narrowed.

The question may arise about the relevance of cryogenic single-molecule spectroscopy. But at low temperatures very valuable relevant information about the structure and the energy landscape of the molecules studied is still available whereas the dynamics is slowed down to observable time scales. Furthermore, insights into basic interactions and processes of the molecules studied can certainly provide guidance for the interpretation of more complicated room-temperature observations [45, 46].

3.2.1 Prerequisites for single molecule spectroscopy

To obtain as large a signal as possible from a single molecule a number of conditions should be fulfilled: a large absorption cross section, high photostability, short radiative lifetime to ensure a high excitation turnover, low transfer probability into dark states such as triplet states, an operation below the saturation of the molecular absorption and a high fluorescence quantum yield.

Looking at the absorption cross section as defined in Eq. 2.2 τ_2 , C_{FC} and C_{DW} should be as large as possible. At sufficiently low temperatures ($T < 2$ K) most phonon modes are not populated which means that τ_2^* becomes extremely long and therefore τ_2 equals $2\tau_1$ [95] (see also

Eq. 2.4). In addition, electron phonon coupling is weak and the Debye-Waller factor becomes large [44, 105]. For the zero-phonon line of an aromatic molecule the linewidth Γ_{hom} decreases from $\sim 1000 \text{ cm}^{-1}$ at room temperature to $\sim 10^{-3} \text{ cm}^{-1}$ at cryogenic temperatures and is orders of magnitude smaller than that of a typical phonon side band (several 10 cm^{-1}) [95, 133]. Taking into account the higher Debye-Waller factor as well, the peak absorption cross section reaches up to 10^6 \AA^2 at $T < 2 \text{ K}$, 5 orders of magnitude larger than at room temperature and corresponding to about 100 000 times the molecular size [95]. As the lifetime of vibronic levels of large molecules in a matrix is very short (picoseconds) their vibronic ZPLs are very broad compared to those of pure electronic ZPLs (lifetimes of nanoseconds). Therefore in low temperature single molecule excitation spectroscopy experiments only the pure electronic ZPLs show up and their narrow linewidths make detection against the background noise much easier [44, 95].

All together, the number of photons that are emitted from a chlorophyll molecule can be as high as 100 000–1 000 000 per second [24, 101, 102], see section 2.2.1. However, the great difficulty is to separate these photons from all the photons emitted by the other molecules around the chlorophyll. Optical bandpass filters can block most of these background photons at the cost of losing also a significant number of the signal photons. This leads to a typical detection efficiency of a low-temperature single-molecule setup of well below 0.1% which only allows to detect at maximum a few hundred photons of a chlorophyll molecule per second.

3.2.2 Techniques in low temperature single molecule spectroscopy

A short history

In 1989 Moerner and Kador [34] were the first to optically detect a single molecule at low temperatures using a sensitive doubly modulated absorption technique. Soon afterwards, Orrit and Bernard [35] showed that fluorescence-excitation spectra enhanced the SNR dramatically compared to the absorption spectra. Here, a laser excites a small sample volume, in which at most one molecule is present that can absorb at the wavelength of the incident light and only the red-shifted fluorescence is collected from the same volume. This selective fluorescence detection allows to efficiently reduce the residual stray laser photons as well as spectral features due to impurities or Raman scattering of the matrix or the solvent and a signal is observed that arises from a single molecule.

To reduce the background even further, the excitation volume of the sample has to be made as small as possible and the collection efficiency of the fluorescence as large as possible. Various optical schemes have been developed for this purpose. For instance, in the first fluorescence-excitation experiment [35] the sample was glued to the end of an optical single mode fibre limiting the excitation volume to the core diameter of $2\ \mu\text{m}$ of the fibre. Other solutions comprise a small lens [134] or parabolic mirror [135] to focus the laser beam onto the sample, or a pinhole [136] to limit the incident laser beam. The collection of the fluorescence has to be performed over a wide solid angle as it is emitted in all directions. Concave parabolic mirrors [88], objectives [137] or simple lenses [134] were used for this purpose. The excitation volume can be decreased even more by taking advantage of the geometry of the sample and using for instance thin films [132] or nanocrystals [138].

Confocal microscopy

Nowadays, the most commonly used experimental setup for single molecule spectroscopy is the confocal microscope. As depicted in Fig. 3.1, the excitation light is focused onto a pinhole which is subsequently imaged onto the sample by a high numerical aperture objective causing a small focal volume of about $1\ \mu\text{m}^3$ (1 femtolitre). The fluorescence is collected by the same objective, imaged onto a second pinhole — thereby blocking emission light from out of focus regions — and finally focused onto a detector. In this way, the confocal detection scheme ensures that only photons are detected that arise from the sample volume which is confocal with both the excitation as well as the emission pinhole, efficiently suppressing unwanted scattered light and fluorescence from areas outside the focal volume.

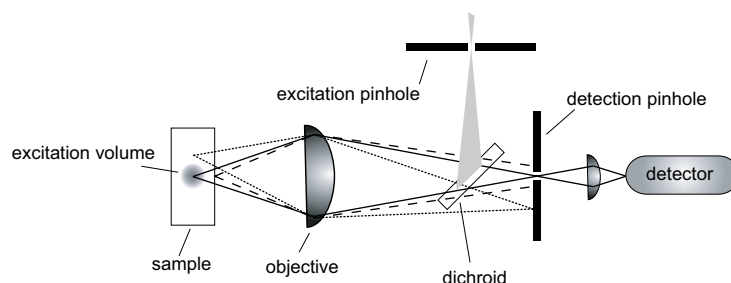


Figure 3.1: Confocal principle. As the sample volume is confocal with both excitation and detection pinhole, only the excitation volume is illuminated and light from out-of-focus regions is efficiently blocked.

3.3 Samples

3.3.1 Sample preparation

LH1, LH1-RC and LH2 complexes of several species of purple non-sulfur bacteria — so called *Rhodospirillaceae* — were investigated in this thesis. Isolation from the bacteria and subsequent purification was carried out by the different collaboration partners and the resulting solutions were diluted in several steps to a concentration of about 1×10^{-11} M. This dilution was performed in detergent buffer to prevent the complexes from aggregation or dissociation; in the last step also 1.8% (wt/wt) polyvinyl alcohol (PVA; M_w 125 000 g/mol) was present.

A drop (10 μ l) of the solution was spin-coated on a Lithium-fluoride (LiF) substrate by spinning it for 15 s at 500 rpm and 60 s at 2000 rpm, producing high quality amorphous polymer films with a thickness of less than 1 μ m in which the pigment-protein complexes are embedded. LiF was chosen as substrate because the inversion symmetry of the alkali halide crystal prevents first-order Raman scattering and the optical resonances are far in the UV. The samples were immediately mounted in a liquid-helium cryostat and cooled to 1.4 K.

3.3.2 List of samples

In the following, a list of all sample types and the buffers in which they were diluted is given together with the cooperation partner who cultivated the bacteria and isolated the complexes and the chapter in which the measurements are discussed.

- Species: *Rhodospirillum (Rs.) molischanum* [139]
 Complex: LH2
 Buffer: 20 mM Tris / 0.1% LDAO / pH = 8.0
 Cooperation partner: H. Michel, MPI of Biophysics, Frankfurt, Germany.
 Discussed in: chapters 4 and 5

- Species: *Rhodopseudomonas (Rps.) acidophila* [2]
 Complex: LH2
 Buffer: 20 mM Tris / 0.1% LDAO / pH = 8.0
 Cooperation partner: R. Cogdell, University of Glasgow, Glasgow, UK.
 Discussed in: chapter 6

- Species: *Rhodopseudomonas (Rps.) acidophila* [140]
 Complex: LH1-RC
 Buffer: 20 mM Tris / 0.1% LDAO / pH = 8.0
 Cooperation partner: R. Cogdell, University of Glasgow, Glasgow, UK.
 Discussed in: chapter 7

- Species: *Rhodobacter (Rb.) sphaeroides* [141]
 Complex: LH1-RC
 Buffer: 0.6% β OG / 0.2% Na-cholate / 50 mM NaGlyGly / pH = 7.8
 Cooperation partner: F. Francia, University of Bologna, Bologna, Italy.
 G. Venturoli, University of Bologna, Bologna, Italy.
 D. Oesterhelt, MPI for Biochemistry, Martinsried, Germany.
 Discussed in: chapters 7 and 8

3.3.3 List of chemicals

trade name	chemical name	company
Tris	Tris-(hydroxymethyl)-aminomethan	Carl Roth GmbH
LDAO	lauryldimethylamine <i>N</i> -oxide	Sigma-Aldrich
β OG	<i>n</i> -Octyl- β -D-glucopyranoside	Sigma-Aldrich
Na-cholate	3 α ,7 α ,12 α -Trihydroxy-5 β -cholan-24-oic acid	Sigma-Aldrich
NaGlyGly	Sodium Glycyl-glycine	Sigma-Aldrich
PVA	polyvinyl alcohol	Sigma-Aldrich

Table 3.1: List of chemicals from Carl Roth GmbH & Co. KG, Karlsruhe, Germany or Sigma-Aldrich, St. Louis MO, USA.

3.3.4 Atomic coordinates

The atomic coordinates of LH2 from *Rhodospirillum molischianum* (identifier code: 1LGH), LH2 from *Rhodopseudomonas acidophila* (identifier code: 1KZU at 2.5 Å, 1NKZ at 2.0 Å) and the RC from *Rhodobacter sphaeroides* (identifier code: 1PSS) were taken from the Protein Data Bank (<http://www.pdb.org/>).

3.4 Experimental setup

To perform fluorescence microscopy and fluorescence-excitation spectroscopy the samples were illuminated with a continuous-wave tunable Titanium-Sapphire (Ti:Sa) laser (3900S, Spectra Physics, Mountain View CA, USA) pumped by a frequency doubled continuous-wave Neodymium-Yttrium-Vanadat (Nd:YVO₄) laser (Millennia Vs, Spectra Physics, Mountain View CA, USA) using a home build microscope that can be operated either in widefield or confocal mode. To obtain a well-defined variation of the wavelength of the Ti:Sa laser the intracavity birefringent filter has been rotated with a motorised micrometer screw (MM4005 and 850f, Newport, Irvine CA, USA). For calibration purposes a wavemeter (Wavemeter jr., EXFO Burleigh Products Group, Victor NY, USA) has been used and an accuracy as well as a reproducibility of 1 cm⁻¹ for the laser frequency have been verified. A fluorescence-excitation spectrum of an individual light-harvesting complex was obtained in two steps. First a widefield image of the sample was taken and a spatially well-isolated complex was chosen. Subsequently a fluorescence-excitation spectrum of this complex was obtained by scanning the laser and simultaneously collecting the fluorescence.

Widefield fluorescence microscopy

A 40 × 40 μm² wide-field image of the sample was taken by exciting the sample through a simple planoconvex lens with a large focal length ($f = 140$ mm) creating a $\sim 100 \times 100$ μm² spot on the film (Fig. 3.2A). Thereby, the excitation wavelength was chosen to coincide with an absorption maximum of the complexes (800 nm for LH2 and 870 nm for LH1-RC) whereas the emitted light was collected by an objective lens (single aspheric lens, $f = 1.45$ mm, NA = 0.55, Thorlabs, Newton NJ, USA) mounted inside the cryostat immersed in liquid helium and focused onto a back-illuminated CCD camera (512 SB, Roper Scientific, Trenton NJ, USA) after passing suitable bandpass filters ($\Delta\lambda \approx 20$ nm, Dr. Hugo Anders, AHF Analysentechnik, Tübingen, Germany) which blocked the residual laser light. The 3D-representation of the fluorescence — as depicted in the lower part of Fig. 3.2A — shows several peaks each representing the diffraction limited airy pattern of individual LH complexes. The lateral resolution was determined to 1 μm corresponding to the theoretical expected resolution using the Rayleigh criterion (e.g., [142]). From this image a spatially well-isolated complex was selected.

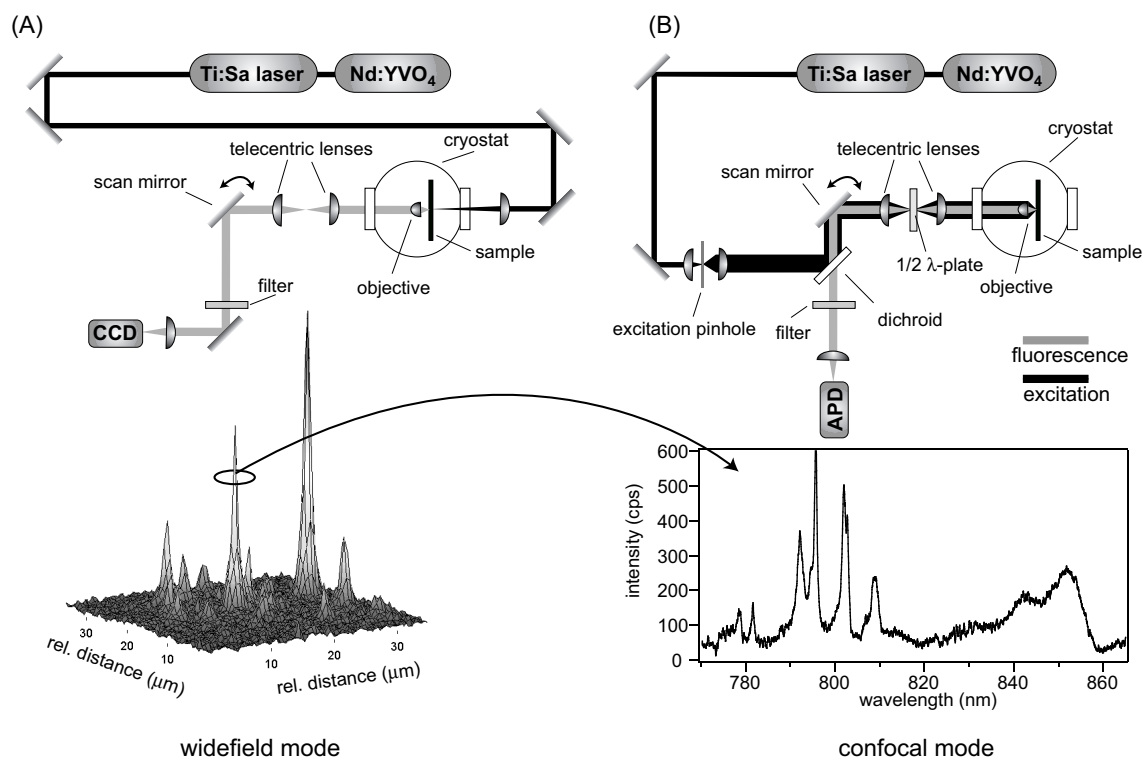


Figure 3.2: Experimental setup for low-temperature single molecule spectroscopy. (A) Widefield arrangement of the microscope. In the lower part a 3D-representation of an example image is shown in which each peak corresponds to the diffraction limited image of an individual LH complex. (B) Confocal mode of the microscope. A typical fluorescence-excitation spectrum of an individual LH2 complex from *Rs. molischianum* is shown in the lower part. See text for more details.

Confocal fluorescence-excitation spectroscopy

A fluorescence-excitation spectrum of this complex was obtained by switching to the confocal mode of the set-up (Fig. 3.2B). In this mode the excitation light was passed through an excitation pinhole and focused onto the sample by the objective lens inside the cryostat creating a diffraction limited excitation volume of less than $1 \mu\text{m}^3$. This confocal volume was made to coincide with the complex by tilting the direction of the excitation beam with the scan mirror. A pair of telecentric lenses ensured a precise and well controlled displacement of the focus on the sample while maintaining alignment with the confocal aperture.

The fluorescence was collected by the same objective lens and focused onto a single-photon counting avalanche photodiode (APD) (SPCM-AQR-16, Perkin Elmer Optoelectronics, Fremont CA, USA) which also fulfilled the role of the detection pinhole. Instead of obtaining a spectrum by slowly scanning the laser once, many spectra were recorded in rapid succession

by scanning repetitively the spectral range of interest and storing the different traces separately. Thereby, not only light-induced fluctuations of the fluorescence intensity on a timescale of seconds could be diminished as reported in [143] but also information about the spectral evolution in time could be gained. With a scan speed of the laser of 3 nm per second ($\approx 50 \text{ cm}^{-1}/\text{s}$) and an acquisition time of 10 ms per data point, this yields a nominal resolution of 0.5 cm^{-1} ensuring that the linewidth is limited by the spectral bandwidth of the laser (1 cm^{-1}). The confocal-detection mode features a superior background suppression that allowed to record fluorescence-excitation spectra with high signal-to-noise ratios as shown for instance in the lower part of Fig. 3.2B [118].

Widefield fluorescence-excitation spectroscopy

Due to the sequential character of the experiment confocal fluorescence-excitation spectroscopy is limited to the investigation of one to two complexes per day. Therefore, it would be advantageous to use a CCD camera instead of the APD in Fig. 3.2B to monitor the fluorescence intensity of many complexes simultaneously while scanning the frequency of the excitation light. Consequently the spectra of as many complexes as can be imaged on the CCD are obtained simultaneously as depicted in Fig. 3.3. Here, the CCD-frame number corresponds to wavelength

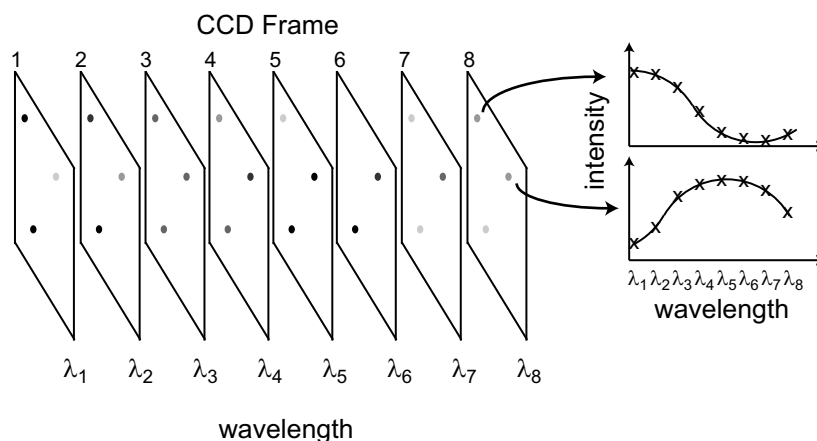


Figure 3.3: Widefield fluorescence-excitation spectroscopy. An EMCCD camera records the fluorescence intensity of a sample containing several individual complexes depicted by the differently bright dots. During the image acquisition, the wavelength of the laser is scanned. The spectra of the complexes can then easily be reconstructed as each frame corresponds to a certain wavelength λ_i and the total fluorescence in this frame is obtained by integration over the image of the individual complexes.

and by integrating the total intensity of the fluorescence image of an individual complex on the CCD as a function of the read-out frame a fluorescence-excitation spectrum can be obtained.

In the past, basically two types of CCDs existed, (i) fast cameras with high read-out noise and (ii) slow cameras with low read-out noise. Fast cameras typically have signal-to-noise ratios (SNR) that is too poor for single LH spectroscopy whereas the slow cameras — as also used for the widefield microscopy — generally have very long read-out times. Nowadays, a new generation of CCD cameras, so called electron multiplying CCDs (EMCCD) exist that eliminate the read-out noise by amplifying the number of counts in a pixel directly on the CCD chip itself. The key feature of such cameras is that they combine high sensitivity and low noise without sacrificing fast read-out.

However, using similar SNR as a target criterion it can be stated that the cycle time (i.e., image acquisition time plus read-out time) of the EMCCD (DV465, Andor, Belfast Ireland) used in this thesis was still about a factor of 50 higher than of the APD in the confocal mode. This is due to the fact that no detection pinhole is present anymore so that the confocal setup is no longer fulfilled and stray light from out-of focus regions is imaged onto the CCD. Also the quantum efficiency of the CCD (15% at 900 nm) is a factor of 3 lower than for the APD (40% at 900 nm). Furthermore, the read-out time of the APD is basically zero whereas the EMCCD still needs 100-150 ms per frame. Nevertheless, the new parallel detection scheme of widefield fluorescence-excitation spectroscopy which was used for the experiments described in chapter 6 enhanced the efficiency of the experimental work by a factor of 50 compared to confocal operation with an APD.

Polarisation dependent spectroscopy

To examine the polarisation dependence of the spectra, a $\frac{1}{2}\lambda$ plate was put in the confocal excitation path. This plate was rotated in steps of 0.9 degrees between two successive scans by which the angle of polarisation of the excitation light changes with twice this value. Limited by the signal noise, this allowed to determine polarisation angles to within 5° accuracy.

The B800 band of LH2 from *Rhodospirillum molischianum*

In this chapter, a study is presented on the B800 absorptions of individual LH2 complexes from *Rhodospirillum molischianum*, which are sensitive to the variations in the electronic coupling between individual BChl *a* molecules. The electronic coupling is determined by the interaction strength V between the pigments and the energetic disorder, characterised by the width Δ of a Gaussian distribution of site energies. For the B800 band the ratio $V/\Delta \ll 1$ is consistent with the picture that the chromophores feature a weak to intermediate coupling and that the excitations are mainly localised on individual chromophores.

The observations are also affected by apparent, temporal variations in the local environment of individual pigments. These can be caused by conformational fluctuations within the protein scaffold. The embedded chromophores react on these fluctuations with changes of their electronic energies which makes them suited to monitor the dynamics of a protein with optical spectroscopy.

The objective is to establish a relationship between spectroscopic observations, the molecular structure, and the statistical variations of the interaction strength and the site energies.

4.1 Structure of the B800 ring

As mentioned in the introduction, the LH2 complex from *Rhodospirillum molischianum* is an octameric hollow cylinder of 90 Å diameter featuring a C_8 -symmetry [3]. It is built up from eight monomer units each comprising two membrane spanning apoproteins (α inside and β outside) binding non covalently three bacteriochlorophyll *a* and presumably one carotenoid molecules, see Fig. 4.1A. In the complex, two distinct BChl *a* assemblies can be distinguished, one comprising eight BChl *a* molecules, named B800 ring owing to its main absorption peak around 800 nm, the other comprising 16 BChl *a* molecules named B850 ring owing to its absorption around 850 nm. The arrangement of the chromophores is shown in Fig. 4.1C together with the orientations of their Q_y absorption dipole moments. From the C_8 symmetry it is evident that the mutual orientations between uncoupled absorption transition-dipole moments equals 0 modulo 45 degrees. Important characteristics of the B800 system are the equivalence of the 8 binding sites, the relatively narrow absorption line widths, and the nearest-neighbour interaction strength V of about 20 cm^{-1} [54].

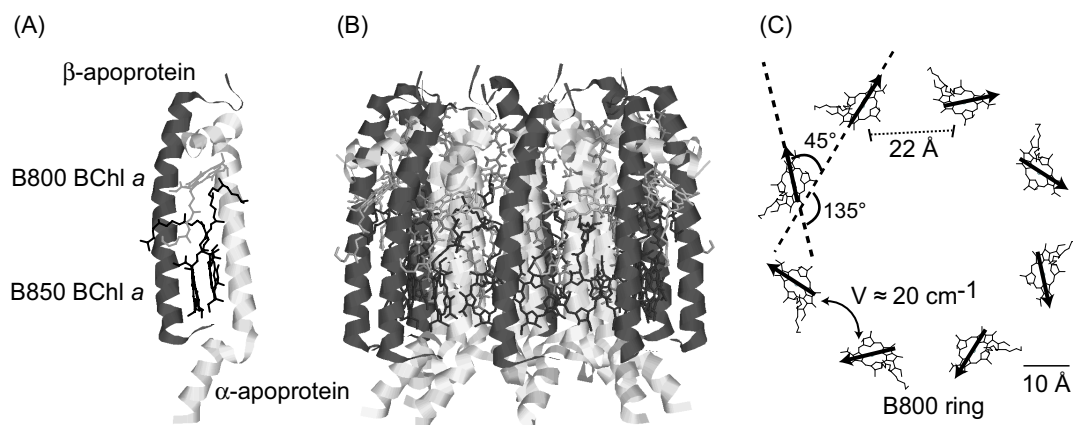


Figure 4.1: Structure of the B800 ring of LH2 from *Rhodospirillum molischianum*. (A) Subunit containing one B800, two B850 bacteriochlorophyll *a* and one carotenoid (not shown) molecules non-covalently bound by two apoproteins. (B) Side view of the LH2 complex. (C) Top view of the B800 ring containing eight B800 BChl *a* molecules arranged in a C_8 symmetry. The arrays indicate the orientations of their Q_y absorption dipole moment.

4.2 Experimental results

Example fluorescence-excitation spectra of the B800 ring of five individual LH2 complexes from *Rs. molischianum* are shown in the lower part of Fig. 4.2. Each spectrum is the result of the summation of six traces recorded with a mutual difference of the incident polarisation vector of the excitation light of 30° , thereby averaging over all possible polarisations. For the individual complexes the spectra typically feature a discrete pattern of 2–6 absorption lines with a spread of several nanometre around the peak absorption of the ensemble value. The variations with respect to the number of lines and the spectral positions of the absorptions will be referred to as spectral heterogeneity in the following. In the top two traces the sum of 24 spectra from individual complexes (solid line) is compared with the B800 spectrum from a large ensemble of pigment protein complexes (bold line). Both spectra are in good agreement and consist of a broad band at 12500 cm^{-1} (800 nm) with a linewidth of 300 cm^{-1} (FWHM).

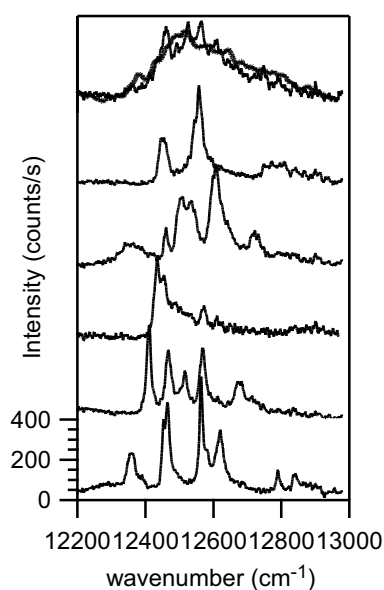


Figure 4.2: Fluorescence-excitation spectra of the B800 band of LH2 complexes from *Rs. molischianum*. The top traces show the comparison between an ensemble spectrum (bold line) and the sum of 24 spectra recorded from individual complexes (solid line). The lower five traces display spectra from single LH2 complexes. Each spectrum has been averaged over all possible excitation polarisations. The vertical scale is valid for the lowest trace, all other traces were offset for clarity. All spectra were recorded at 1.4 K with an excitation intensity of 10 W/cm^2 .

4.2.1 Inter- and intra-complex heterogeneity

Apparently the ensemble B800 band consists of several relatively narrow absorptions and its width reflects contributions to the spectral heterogeneity of two qualitatively different types of energetic disorder: i) intra-complex disorder, also referred to as diagonal disorder or site heterogeneity which results from the differences in site energy of the individual BChl *a* molecules within one complex. ii) inter-complex disorder which reflects the changes in the position of the centre of mass of the whole spectrum for different complexes.

An experimental measure for the inter-complex heterogeneity is given by the distribution of the spectral mean value $\bar{\nu}_i$ of the fluorescence-excitation spectrum of an individual LH2 complex *i*

$$\bar{\nu}_i = \frac{\sum_k I(k)\nu(k)}{\sum_k I(k)}, \quad (4.1)$$

where $I(k)$ denotes the fluorescence intensity at datapoint k , $\nu(k)$ the spectral position corresponding to datapoint k , and the sum runs over all datapoints of the spectrum. Fig. 4.3A shows the histogram of the spectral means from the individual spectra obtained from 43 complexes. It is centred at 12560 cm^{-1} (796 nm) and has a width (FWHM) of 100 cm^{-1} .

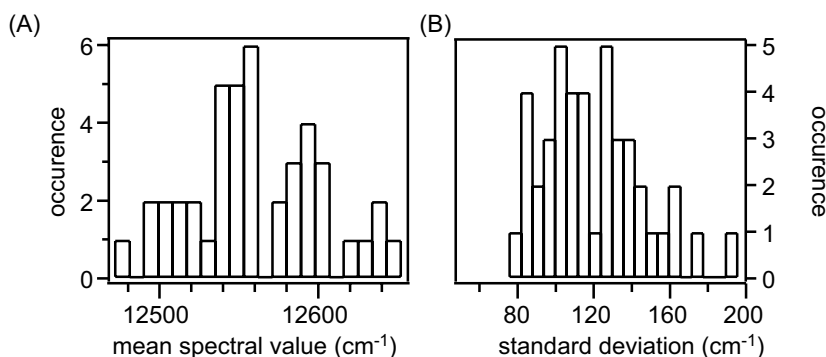


Figure 4.3: Spectral heterogeneity in the B800 band. (A) Distribution of the spectral mean $\bar{\nu}_i$ from 43 LH2 complexes. (B) Distribution of the standard deviations for the spread of absorption lines in the individual fluorescence-excitation spectra for the same 43 LH2 complexes.

The intra-complex heterogeneity can be addressed experimentally by calculating the standard deviations σ_ν of the intensity distributions within the individual spectra

$$\sigma_\nu = \sqrt{\nu^2 - \bar{\nu}^2}, \quad (4.2)$$

where $\overline{\nu^2}$ is given by

$$\overline{\nu^2} = \frac{\sum_k I(k) [\nu(k)]^2}{\sum_k I(k)}. \quad (4.3)$$

The respective histogram for σ_ν , Fig. 4.3B, is centred at a value of about 120 cm^{-1} . Since the diagonal disorder is commonly defined as the full width at half maximum of the distribution of site energies, this value has to be multiplied by 2.36 which yields 280 cm^{-1} (FWHM) for the intra-complex disorder.

4.2.2 Spectral diffusion

Apart from static variations of the absorptions as described in the previous section fluctuations of the B800 fluorescence-excitation spectra in time were also observed. In order to study such effects in more detail the spectra were recorded in rapid succession by scanning the laser repetitively between 770 nm (12987 cm^{-1}) and 820 nm (12195 cm^{-1}) at a scan speed of 3 nm/s ($\approx 50 \text{ cm}^{-1}/\text{s}$) and storing the resulting traces separately. Because the linewidth of the excitation laser is 1 cm^{-1} , this procedure allows to follow the temporal development of the individual B800 absorptions with a time resolution of about 50 ms . Spectral diffusion events that occur on a faster time scale cannot be resolved and contribute to the linewidth of the features observed. In the following, the registered spectra are displayed in a two dimensional representation, where the horizontal axis corresponds to wavenumber, the vertical axis to time and the intensity of the absorptions to the grey scale. Linewidths are always given as the full width at half maximum (FWHM).

Spectral switching of individual absorption lines

For two complexes spectral diffusion patterns could be found which were characterised by the recurrent disappearance of one line and the appearance of one new line at a different spectral position. An example is shown in Fig. 4.4A together with the fluorescence-excitation spectrum that results when the whole sequence of spectra is averaged, Fig. 4.4B. Owing to the sequential data acquisition the intensities of the individual spectral features can be followed as a function of time. The individual absorptions show small temporal shifts ($2\text{--}6 \text{ cm}^{-1}/15 \text{ s}$) in spectral positions which mainly determine the inhomogeneous linewidth of the features in the averaged spectrum. The two absorptions at 12921 cm^{-1} and 12643 cm^{-1} , marked by a and a' respectively, show in

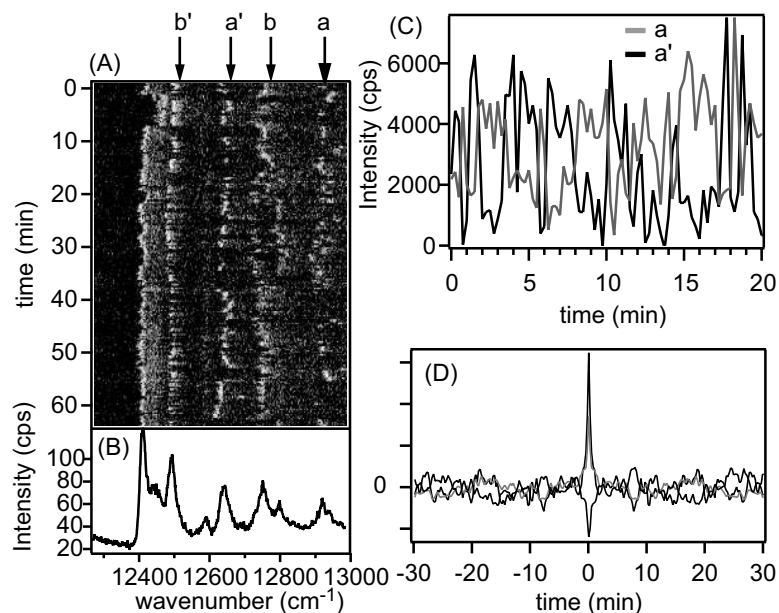


Figure 4.4: Spectral switching of individual absorption lines, Complex nr. 1. (A) Time sequence of 256 fluorescence-excitation spectra recorded at a speed of $50 \text{ cm}^{-1}/\text{s}$ with an excitation intensity of $10 \text{ W}/\text{cm}^2$. The fluorescence intensity is indicated by the grey scale. The average spectrum is depicted in (B). Of the two spectral features labelled a and a' the fluorescence intensity versus time is shown in (C). Their auto-correlation (upper grey, a, and black ,a', lines) and cross-correlation (lower black line) are shown in (D).

addition to the spectral shifts also a strong temporal fluctuation of the intensity. This is shown in more detail in Fig. 4.4C which displays their total emission intensity as a function of time.

Both traces show abrupt changes from several thousand counts per second to the background level which is a typical signature of the single-molecule character of the experiment. From visual inspection of the two traces it seems evident that they are anti-correlated and only one of them can be excited at the same time. Indeed, this conjecture is supported by the auto- and cross-correlations of the two trajectories, Fig. 4.4D. Both auto-correlations (upper black and grey lines) drop within three datapoints corresponding to three scans of 15 s each to an average value of zero, a signature that the observed intensity fluctuations are uncorrelated on the timescale of the experiment. In contrast the cross-correlation (lower black line) features a clear dip around $t = 0$ which unambiguously shows that the two absorption lines, separated by 278 cm^{-1} , are closely associated. The average on-time of line a is 64 s that of line a' 54 s.

The absorptions at 12753 cm^{-1} (b) and 12494 cm^{-1} (b') which are separated by 259 cm^{-1} also show a clear anti-correlation. The average on-times for lines b and b' are 50 s and 46 s respectively. The combinations a–b, a–b', a'–b and a'–b' show no correlation at all.

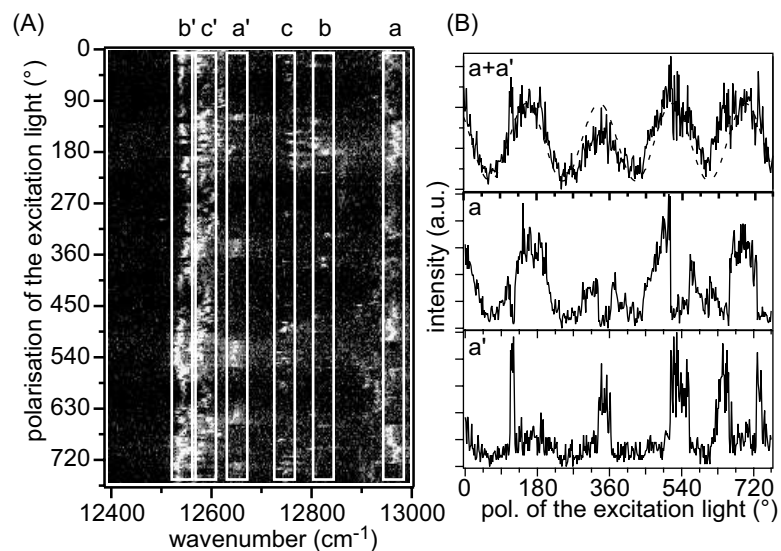


Figure 4.5: Spectral switching of individual absorption lines, Complex nr. 2. (A) Time sequence of 425 fluorescence-excitation spectra recorded at a speed of $50 \text{ cm}^{-1}/\text{s}$ with an excitation intensity of $15 \text{ W}/\text{cm}^2$. The fluorescence intensity is indicated by the grey scale. The polarisation of the excitation light was rotated by 1.8° after each scan. The fluorescence intensity of the two spectral features labelled a and a' as well as the sum is shown in (B). The features shown a clear anti-correlation; their sum can be fitted by a \cos^2 -function (dashed line).

A similar behaviour was found for a second complex which is shown in Fig. 4.5. Again, a sequence of subsequent scans is stacked on top of each other. However, the polarisation of the incident laser light was rotated by a $\frac{1}{2} \lambda$ plate by 1.8° after each scan. In (B), the fluorescence intensities of line a and a' are plotted versus polarisation of the excitation light. It becomes clear that these two lines feature an anti-correlated behaviour as was previously seen for the absorptions in Fig. 4.4. The electrical field vector of the incident excitation light \vec{E} and the transition-dipole moment of the absorber $\vec{\mu}_A$ define the probability for absorption: $P(\theta) = (\vec{\mu}_A \cdot \vec{E})^2$, where θ defines the angle between the electrical field vector and the transition dipole moments. The probability — and with it the observed fluorescence intensity — is therefore proportional to $\cos^2 \theta$. Consequently, the sum of their fluorescence, shown in the upper panel of (B), can be nicely fitted by a \cos^2 -function (dashed line).

Absorption lines b–b' and c–c' are anti-correlated as well, whereas the fluorescence of other combinations (e.g., a–c') shows no correlation.

Spectral diffusion contributing to the homogeneous linewidth

In the two-dimensional representations of sequentially recorded spectra shown in the previous figures it could be seen that the spectral position of the absorption lines changes slightly from scan to scan. The different absorption lines in a spectrum do not shift their spectral position by the same amount, they do not even shift in the same direction. This gives rise to the assumption that the spectral fluctuations reflect an intrinsic property of the complexes studied. Consequently, the fluctuations are assigned to reflect changes of the absorption energy of the chromophores involved in the absorption.

In Fig. 4.6A a stack of 256 sequentially recorded spectra which have been extracted from Fig. 4.4A at the position of line a' at 12643 cm^{-1} is shown in the upper panel as a two-dimensional time versus wavenumber diagram. The spectrum in the lower panel represents the fluorescence intensity of the averaged spectrum of all scans versus wavenumber and has a linewidth

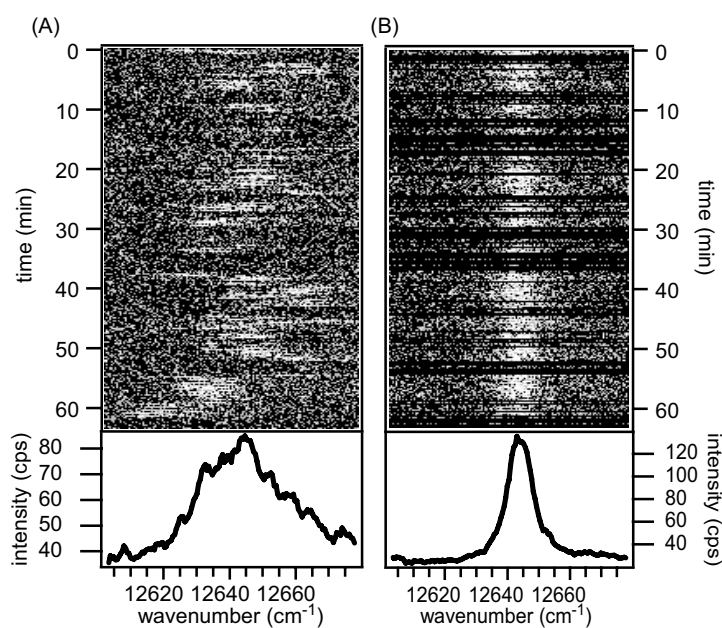


Figure 4.6: Suppressing “slow” spectral diffusion of an absorption line. (A) Stack of 256 fluorescence-excitation spectra recorded at a scan speed of $50\text{ cm}^{-1}/\text{s}$ and an excitation intensity of $10\text{ W}/\text{cm}^2$, taken from Fig. 4.4A at the position of line a' . The fluorescence intensity is indicated by the grey scale. The average of all spectra is shown in the lower panel and has a linewidth of 41.6 cm^{-1} . (B) Stack of 172 fluorescence-excitation spectra that were obtained by fitting the spectra in (A) by a Lorentzian and shifting each scan according to the spectral position of the fit maximum, thereby eliminating the spectral diffusion. During some spectra the absorption was found at position a and could therefore not be fitted at position a' . These 84 spectra were excluded. The absorption line in the lower panel indicates the average of all scans and has a linewidth of 7.5 cm^{-1} .

of 41.6 cm^{-1} . The following technique was applied to eliminate the spectral motion leading to the inhomogeneous broadened averaged absorption line: first the transition in every single scan was fitted with a Lorentzian. This yields that the observed linewidth predominantly results from the accumulation of smaller spectral changes. For this example the peak position changed on average by 4.7 cm^{-1} per scan of 15 s duration. Similar values were observed for the other absorptions from Figs. 4.4 and 4.5 as can be seen from Tab. 4.1. It is worth to note that for the spectra of complex 2 a single scan took 33 s — in contrast to 15 s for complex 1 — without an accompanying increase of the average linewidth of the peak positions.

Then the fitted spectra were spectrally shifted such that the fitted peak positions coincided. Fig. 4.6B shows in the upper panel the spectral sequence of Fig. 4.6A after all spectra were shifted according to the maximum of a Lorentzian fit. During some scans the absorption line was found at position a at 12921 cm^{-1} instead of at position a' at 12643 cm^{-1} . For these scans the related spectrum could not be fitted with a Lorentzian at the spectral position a'. The 84 scans were therefore excluded in the figure. Again, the spectrum in the lower panel represents the average of all scans. Its linewidth is only 7.5 cm^{-1} , about a sixth of the linewidth of the spectrally diffusing absorption line. The same procedure yields for the linewidths of the other absorptions values between $4\text{--}12 \text{ cm}^{-1}$, see Tab. 4.1. Clearly, additional contributions to the linewidth which stem from faster unresolved spectral dynamics while the laser scans through the resonance can not be resolved. However, the observed values cover the same range as those reported for the homogeneous linewidth of the B800 absorptions [24, 72] which restricts additional unresolved contributions to the linewidth to an order of about 1 cm^{-1} . Given the scan speed of the laser the underlying processes have to occur within less than about 200 ms. Spectral diffusion occurring at a faster rate will lead to a broadening of the absorption line, that can not be corrected for by this “fit-and-shift” technique.

In summary, three groups of spectral diffusion can be distinguished: i) large spectral changes spanning several 100 cm^{-1} at a rate of about 10^{-3} s^{-1} ii) moderate spectral changes within several 10 cm^{-1} at a rate of about 0.1 s^{-1} and finally iii) possibly unresolved spectral changes within a few cm^{-1} at a rate of about 10 s^{-1} .

label	spectral position (cm^{-1})	spectral distance (cm^{-1})	rate (s^{-1})	observed linewidth (cm^{-1})	average change/scan (cm^{-1})	processed linewidth (cm^{-1})	scan time (ms)
Complex nr. 1, Figure 4.4							
a	12921	278	1.5×10^{-2}	36.8	3.5	7.4	150
a'	12643		1.9×10^{-2}	41.6	4.7	7.5	180
b	12753	259	2×10^{-2}	28.5	4.5	5.9	130
b'	12494		2.2×10^{-2}	29.1	5.9	11.5	240
Complex nr. 2, Figure 4.5							
a	12928	341	5×10^{-4}	39.1	5.3	11.3	230
a'	12587		2×10^{-3}	21.1	5.4	7	150
b	12754	270	5.5×10^{-3}	11.2	6.8	3.9	80
b'	12484		1×10^{-3}	28.5	3.9	4.7	100
c	12698	180	8.3×10^{-3}	70.3	6	5	100
c'	12518		1.3×10^{-3}	46.7	3.6	5	100

Table 4.1: Properties of the absorptions from complexes 1 and 2 from Figs. 4.4 and 4.5. For each absorption line the following properties are listed: its spectral position, the distance between the line and its anti-correlated partner, the rate at which the absorption energy changes to the energy of the anti-correlated partner, the observed linewidth in the averaged spectrum, the average spectral change of the maximum of the fitted Lorentzian per scan, the linewidth in the averaged spectrum after each scan was shifted according to the maximum of the Lorentzian fit and the time needed for the laser to scan across the processed linewidth.

Simultaneous spectral diffusion of absorption lines

Besides the spectral diffusion of a single line discussed in the previous section it was also observed that several lines changed their spectral positions simultaneously. Fig. 4.7A shows a part of the spectrum from an individual LH2 complex in a two-dimensional representation. In this representation, in total four distinct spectral features labelled a–d can be distinguished. While the absorption d at about 12470 cm^{-1} shows only relative small excursions in frequency space the other absorptions show large spectral jumps to a limited number of spectral positions. This becomes even more evident if a part of the total sequence of consecutive fluorescence-excitation spectra is displayed, Fig. 4.7B. Each spectrum represents the average of the individual traces over the time interval boxed in part (A) of the figure. This procedure clearly uncovers that for this particular complex the B800 spectrum corresponds to the time average of two distinct spectra termed A and B hereafter. The conversion between the two spectra occurs as a reversible sudden spectral jump which is recurrent on a timescale of minutes. A second example is depicted in the same manner in Fig. 4.8. The respective spectra can be characterised by the

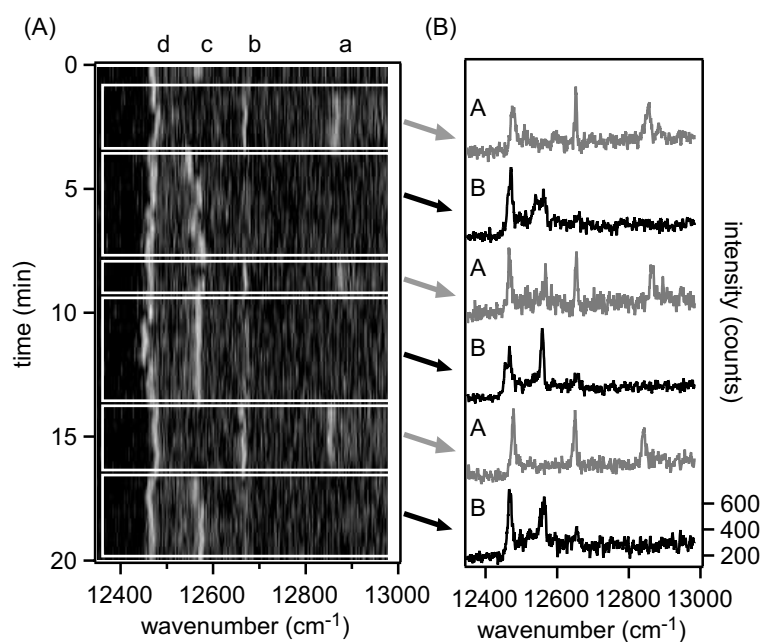


Figure 4.7: Simultaneous spectral diffusion in complex nr. 3. (A) 2D-representation of a sequence of 35 spectra which were recorded subsequently at a speed of about $50\text{ cm}^{-1}/\text{s}$ stacked on top of each other. The horizontal axis corresponds to wavenumber and the vertical axis to time. The fluorescence intensity is given by the grey scale. The excitation intensity was $60\text{ W}/\text{cm}^2$. (B) The panels show the spectra that result when the individual traces are averaged over the indicated time windows.

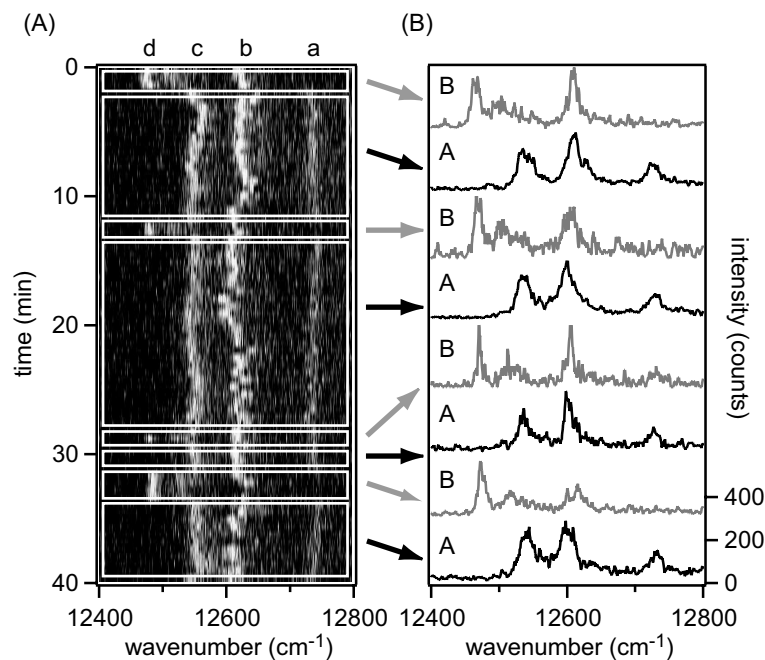


Figure 4.8: Simultaneous spectral diffusion in complex nr. 4. (A) 2D-representation of a sequence of 70 subsequently recorded spectra stacked on top of each other. The horizontal axis corresponds to wavenumber and the vertical axis to time. The fluorescence intensity is given by the grey scale. The excitation intensity is 5 W/cm^2 . (B) The panels show the spectra that result when the individual traces are averaged over the indicated time windows.

position of their absorption lines, their spectral means and intra-complex disorders, which are given in table 4.2. Here, the spectral mean value of the B800 spectrum is defined as in Eq. 4.1. The intra-complex heterogeneity or disorder within a complex is extracted from the data by calculating the standard deviation σ_ν of the intensity distributions in the individual spectra as given in Eq. 4.2.

For complex 3 the spectral mean changes from the A- to the B-type spectrum by 207 cm^{-1} and the intra-complex disorder decreases from 163 cm^{-1} to 63 cm^{-1} . In contrast for complex 4 the spectral mean between the two spectra changes by 61 cm^{-1} while the intra-complex disorder remains nearly unchanged at about 90 cm^{-1} .

Apparently, for these complexes, the B800 band can appear in two possible realisations in each of which it remains during a mean residence time τ . The average time τ_A complex 3 remains in realisation A before switching to realisation B is about 110 s. The average time τ_B complex 3 stays in realisation B is about 250 s. For complex 4, these figures are $\tau_A = 500 \text{ s}$ and $\tau_B = 83 \text{ s}$.

line	ν_A (cm^{-1})	FWHM_A (cm^{-1})	$\bar{\nu}_A$ (cm^{-1})	σ_A (cm^{-1})	τ_A (s) (s)	ν_B (cm^{-1})	FWHM_B (cm^{-1})	$\bar{\nu}_B$ (cm^{-1})	σ_B (cm^{-1})	τ_B (s) (s)
complex nr. 3, Fig. 4.7										
a	12850	37								
b	12651	7	12748	163	110	12654	12	12541	63	250
c						12557	20			
d	12477	11				12468	12			
complex nr. 4, Fig. 4.8										
a	12733	28								
b	12609	35	12639	91	500	12614	32	12578	93	83
c	12541	21				12522	33			
d						12477	10			

Table 4.2: Spectral features for the A- and B-type spectra of complexes 3 and 4 from Fig. 4.7 and Fig. 4.8. ν denotes the spectral position of the absorption lines, FWHM the full spectral width at half of the maximum intensity of the spectral feature. $\bar{\nu}$ denotes the spectral mean, σ the standard deviation of the overall B800 spectrum. The mean residence time τ gives the average time before the complex changes to the other realisation.

Power dependence of spectral diffusion

In the upper panel of Fig. 4.9A, a stack of 225 sequentially recorded scans is shown together with the average spectrum of all traces in the lower panel. The individual scans differ strongly from each other and the five absorption lines which are present in the average spectrum are not present in each individual scan. Increasing the excitation intensity from 0.2 W/cm^2 to 1 W/cm^2 as is shown in (B) not only results in an increase of the fluorescence intensity. The amount of spectral heterogeneity or spectral diffusion also seems to increase if judged by visual inspection. This process continues upon increasing the excitation intensity to 2 W/cm^2 in (C), 5 W/cm^2 in (D), 10 W/cm^2 in (E) and 20 W/cm^2 in (F).

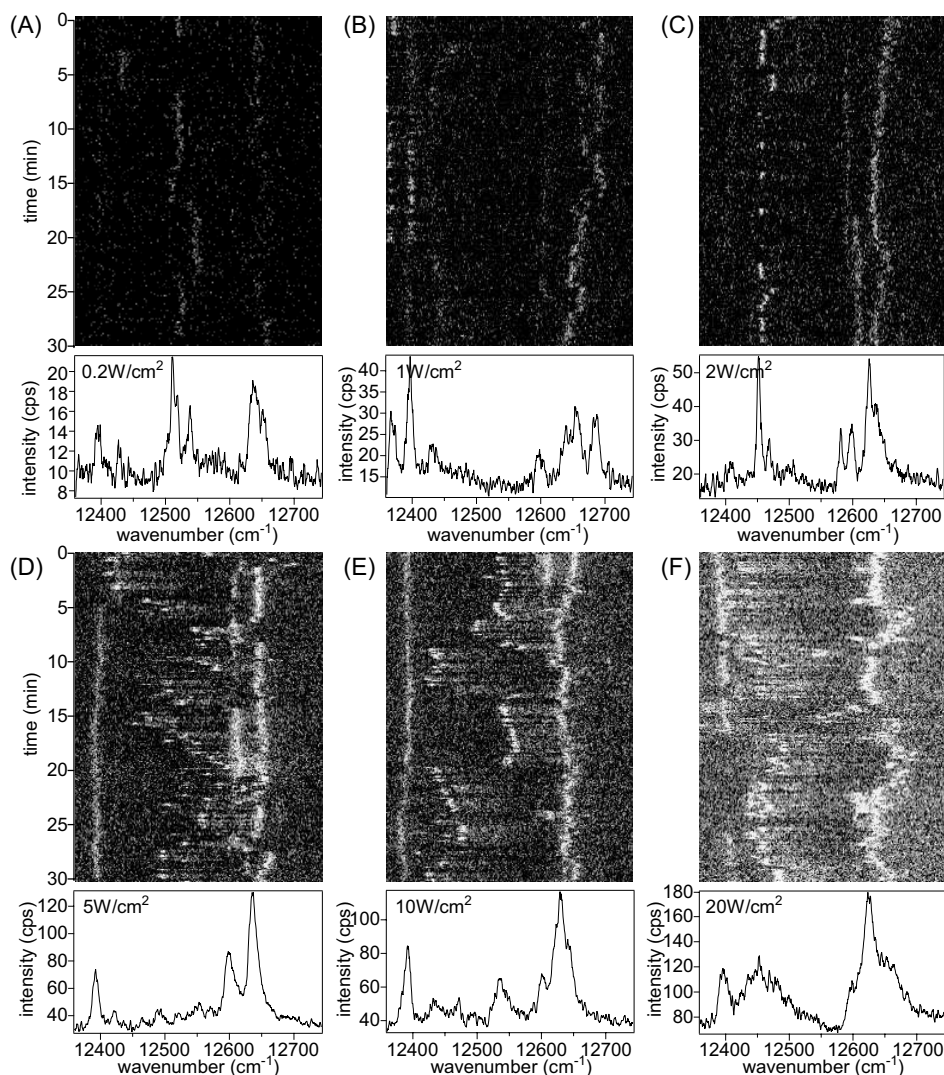


Figure 4.9: Temporal variations of fluorescence-excitation spectra. In all panels a stack of sequentially recorded spectra is shown versus wavelength together with the spectrum that results when all scans are averaged. The fluorescence intensity is given by the grey code. The excitation intensities were (A) 0.2 W/cm^2 (B) 1 W/cm^2 (C) 2 W/cm^2 (D) 5 W/cm^2 (E) 10 W/cm^2 (F) 20 W/cm^2 . Note that the range of the intensity axis differs between the panels.

4.2.3 Electronic couplings in a circular aggregate of molecules

In order to investigate the polarisation dependence of the excitation spectra in more detail, a systematic study was performed in which the focus was set on the mutual angles between the absorption-dipole moments responsible for the narrow absorptions in the B800 band. To this end the laser was swept through the B800 spectral region and a sequence of spectra was recorded while rotating the polarisation of the incident radiation between successive scans.

Mutual angles between absorption-dipole moments

Fig. 4.10A shows a part of the spectrum from an individual LH2 complex. Between successive scans the polarisation of the incident excitation light was rotated by 1.8° . In Fig. 4.10B the fluorescence-excitation spectrum is given that results from the summation of the traces in Fig. 4.10A. In Fig. 4.10C the fluorescence intensity is displayed as a function of the polarisation of the incident radiation for the two absorption lines indicated by the boxed regions in Fig. 4.10A. The observed variation in intensity can be fitted by a \cos^2 -dependence (full and dashed line, respectively). From the difference of the phases in the two traces it was determined that the mutual angle between the transition-dipole moments related to these two absorption lines amounts to 91° . This procedure has been applied to 88 absorption lines from 24 individual LH2 complexes in order to find the distribution of the mutual orientations of the transition-dipole moments within each complex. The values have been obtained either directly from the

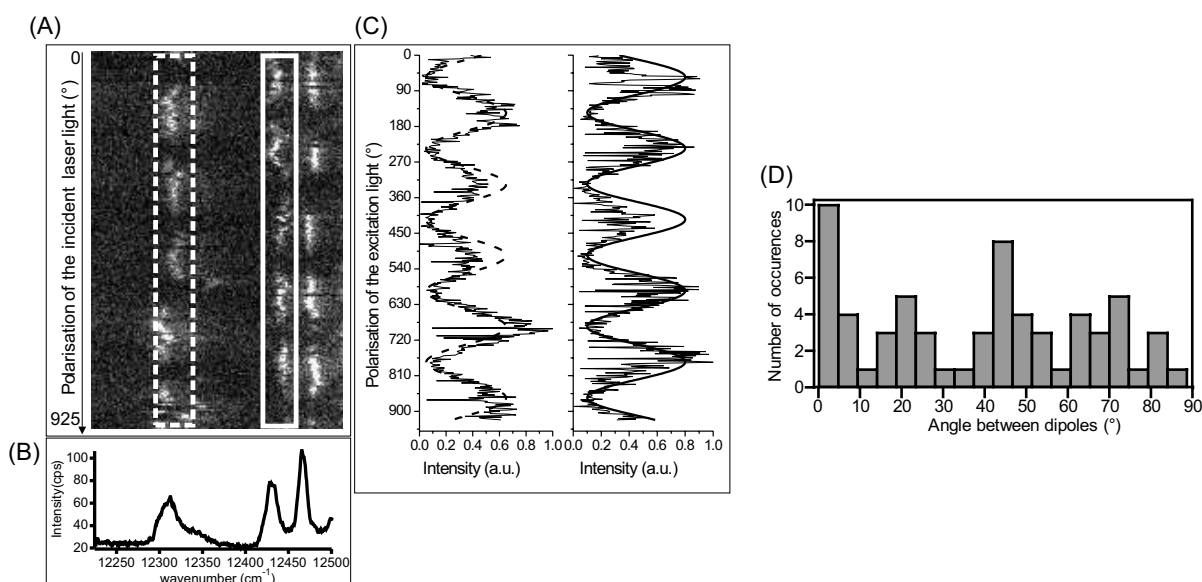


Figure 4.10: (A) Two-dimensional representation of 513 fluorescence-excitation spectra from a part of the B800 band of an individual LH2 complex recorded consecutively at a scan speed of $\approx 50 \text{ cm}^{-1}/\text{s}$ and an excitation intensity of $10 \text{ W}/\text{cm}^2$. The grey scale gives the fluorescence intensity. Between two successive scans the polarisation of the incident radiation has been turned by 1.8° . The horizontal axis corresponds to wavenumber and the vertical axis to polarisation. (B) Average of all 513 spectra. (C) Intensity of the fluorescence for the two absorptions indicated by the boxes in part (A) as a function of the polarisation of the excitation. The full and dashed line correspond to $\cos^2(\alpha(t) + \alpha)$ -type functions fitted to the experimental data with phase angles, α , of 148° and 57° , respectively. (D) Histogram of mutual orientations of the transition-dipole moments from 88 absorption lines from 24 individual complexes.

phase difference $|\alpha_1 - \alpha_2|$ if the result was less than 90° and otherwise from $|\alpha_1 - \alpha_2 - 180^\circ|$ to restrict the scale to the acute angle between the two dipole moments, i.e., to the interval $0^\circ - 90^\circ$. The histogram in Fig. 4.10D shows the result of this study. The distribution covers nearly the whole range between 0° and 90° with slight preferences for the values around 0° , 20° , 45° , and 70° .

Simultaneous temporal fluctuations in the orientation of transition-dipole moments and the absorption energies

For some complexes changes in the spectral position of the individual absorptions were observed as well as in the orientation of the transition-dipole moments during the experiment. An example for such a behaviour is shown in Fig. 4.11. The spectral pattern can be grouped into three distinct sequences labelled A, B and C as indicated by the boxes. In sequence A four absorptions were observed, labelled “1” – “4” with spectral positions 12525.2 cm^{-1} (1), 12489.1 cm^{-1} (2), 12417.9 cm^{-1} (3) and 12367.7 cm^{-1} (4). The respective orientations of the transition-dipole moments with respect to the lab frame were determined to be 70° (1), 4° (2),

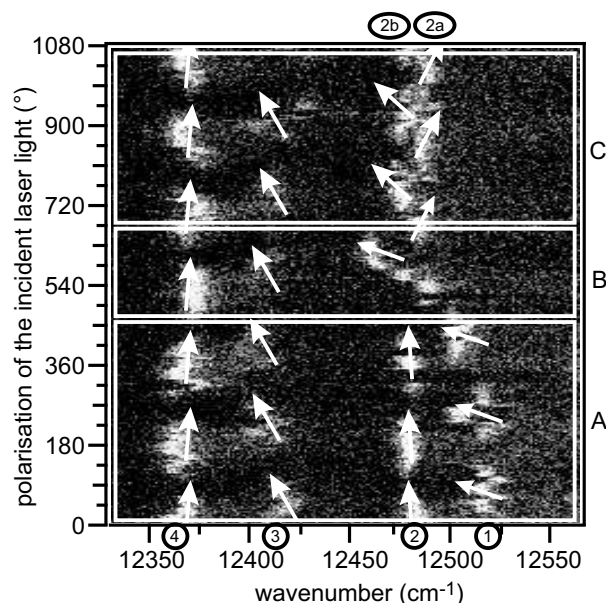


Figure 4.11: Two-dimensional representation of a part of 614 fluorescence-excitation spectra from an individual B800 ring. Between two successive scans the polarisation has been turned by 1.8° . The arrows show the orientation of the transition-dipole moments of the individual absorptions with respect to a laboratory frame. The acquisition times for intervals A, B, and C are 73, 31, and 65 min respectively. Experimental conditions as in Fig. 4.10. For more details see text.

30° (3) and -5° (4) and are visualised by the arrows. During the sequence A absorption “1” creeps continuously in spectral position towards lower energy. None of the absorptions show changes of the phase angle. The creeping of absorption “1” is continued at an increased rate in sequence B, again without any change of the phase angle. This absorption as well as absorption “2” disappear at the end of this sequence. No changes are observed for absorptions “3” and “4”. With the beginning of sequence C new absorptions, “2a” and “2b” appear at spectral positions (phase angles) of 12491.9 cm^{-1} (-26°) and 12481.4 cm^{-1} (41°), respectively. As before absorptions “3” and “4” do not show any changes.

4.3 Discussion

4.3.1 Inter- and intra-complex heterogeneity

In section 4.2.1 the spectral heterogeneity of the B800 band was characterised by two contributions, the inter- and intra-complex disorder. The intra-complex disorder was taken as a measure for the distribution of differences in site energies of the individual BChl *a* molecules whereas the inter-complex disorder reflected the changes for different complexes in the position of the centre of mass of the whole spectrum.

Statistical analysis

In order to describe this issue more quantitatively a statistical analysis of the individual B800 spectra can be performed¹. Therefor the spectral positions of the absorption lines were interpreted as the manifestation of a *single* random variable ν . Information about the distribution of this variable can be obtained from a random sample $\{\nu_{ip}\}$ which corresponds to the set of all absorption frequencies observed where p refers to the N pigments in one complex (indexed by p, q, r) and i refers to the n complexes studied (indexed by i, j, k). In the following $\langle \dots \rangle_p = \frac{1}{N} \sum_{p=1}^N \dots$ and $\langle \dots \rangle_i = \frac{1}{n} \sum_{i=1}^n \dots$ are used as a short notation to express the average over the pigments within one complex or the average over the complexes, respectively. Parameters that can be calculated from a random sample are the expectation value $\bar{\nu}$ and the variance σ^2 of the distribution which are given by

¹Private communication with Michio Matsushita, University of Leiden

$$\bar{\nu} = \frac{1}{nN} \sum_{i=1}^n \sum_{p=1}^N \nu_{ip} = \left\langle \left\langle \nu_{ip} \right\rangle_p \right\rangle_i \quad (4.4)$$

and

$$\sigma^2 = \frac{1}{nN} \sum_{i=1}^n \sum_{p=1}^N (\nu_{ip} - \bar{\nu})^2 = \left\langle \left\langle (\nu_{ip} - \bar{\nu})^2 \right\rangle_p \right\rangle_i = \overline{\nu^2} - \bar{\nu}^2, \quad (4.5)$$

where $\overline{\nu^2} = \left\langle \left\langle \nu_{ip}^2 \right\rangle_p \right\rangle_i$. To decompose the variance into its components resulting from intra- and inter-complex disorder the spectral mean of complex i was defined by

$$\bar{\nu}_i = \frac{1}{N} \sum_{p=1}^N \nu_{ip} = \left\langle \nu_{ip} \right\rangle_p. \quad (4.6)$$

The intra-complex disorder is then given by the distribution of the transition frequencies within a particular complex with respect to its individual spectral mean, which can be expressed as a variance by

$$\sigma_{\text{intra}}^2 = \left\langle \sigma_{\text{intra},i}^2 \right\rangle_i = \left\langle \left\langle (\nu_{ip} - \bar{\nu}_i)^2 \right\rangle_p \right\rangle_i = \overline{\nu^2} - \left\langle \bar{\nu}_i^2 \right\rangle_i. \quad (4.7)$$

For the inter-complex disorder the distribution of the individual spectral means with respect to the total mean $\bar{\nu}$ has to be determined. Thus

$$\sigma_{\text{inter}}^2 = \left\langle (\bar{\nu}_i - \bar{\nu})^2 \right\rangle_i = \left\langle \bar{\nu}_i^2 \right\rangle_i - \bar{\nu}^2. \quad (4.8)$$

It can be verified that the sum of these expressions

$$\sigma_{\text{intra}}^2 + \sigma_{\text{inter}}^2 = \overline{\nu^2} - \bar{\nu}^2 = \sigma^2 \quad (4.9)$$

yields the total variance. To find a relationship between the two types of disorder the term $\left\langle \bar{\nu}_i^2 \right\rangle_i$ has to be analysed.

$$\begin{aligned} \left\langle \bar{\nu}_i^2 \right\rangle_i &= \left\langle \left\langle \nu_{ip} \right\rangle_p \left\langle \nu_{iq} \right\rangle_q \right\rangle_i \\ &= \frac{1}{nN^2} \sum_i^n \sum_p^N \sum_q^N \nu_{ip} \nu_{iq} \end{aligned}$$

$$= \frac{1}{nN^2} \sum_i^n \sum_p^N \nu_{ip}^2 + \frac{1}{nN^2} \sum_i^n \sum_p^N \sum_{q, (p \neq q)}^N \nu_{ip} \nu_{iq}. \quad (4.10)$$

In these equations $\nu_{ip} \nu_{iq}$ for $p \neq q$ denominates two different pigments within the same complex. With the assumption, that there is no correlation between the complexes the average over two pigments from different complexes $\nu_{ip} \nu_{jq}$ will be the same. Therefore

$$\langle \overline{\nu_i^2} \rangle_i = \frac{1}{nN^2} \sum_i^n \sum_p^N \nu_{ip}^2 + \frac{1}{n^2 N^2} \sum_i^n \sum_j^n \sum_p^N \sum_{q, (p \neq q)}^N \nu_{ip} \nu_{jq}. \quad (4.11)$$

The sum $\sum_{p,q;p \neq q}^{N,N}$ contains $N(N-1)$ terms due to the condition $p \neq q$. This yields in case $j \neq i$

$$\sum_p^N \sum_{q, (p \neq q)}^N \nu_{ip} \nu_{jq} = \frac{N(N-1)}{N^2} \sum_p^N \sum_q^N \nu_{ip} \nu_{jq}. \quad (4.12)$$

When i and j are allowed to run freely, only terms in which $i = j$ and $p = q$ hold have to be excluded. This leads to

$$\begin{aligned} \langle \overline{\nu_i^2} \rangle_i &= \frac{1}{nN^2} \sum_i^n \sum_p^N \nu_{ip}^2 + \frac{N(N-1)}{n^2 N^2 N^2} \left(\sum_i^n \sum_j^n \sum_p^N \sum_q^N \nu_{ip} \nu_{jq} - \sum_i^n \sum_p^N \nu_{ip}^2 \right) \\ &= \frac{1}{N} \frac{1}{nN} \sum_i^n \sum_p^N \nu_{ip}^2 + \frac{N-1}{N} \frac{1}{n^2 N^2} \left(\sum_i^n \sum_j^n \sum_p^N \sum_q^N \nu_{ip} \nu_{jq} - \sum_i^n \sum_p^N \nu_{ip}^2 \right) \\ &= \frac{1}{N} \langle \langle \nu_{ip}^2 \rangle_p \rangle_i + \frac{N-1}{N} \langle \langle \nu_{ip} \rangle_p \rangle_i^2 - \frac{N-1}{N} \frac{1}{nN} \langle \langle \nu_{ip}^2 \rangle_p \rangle_i \\ &= \frac{1}{N} \underbrace{\left(1 - \frac{1}{n} \frac{N-1}{N} \right)}_{=1, \text{ for large } n} \langle \langle \nu_{ip}^2 \rangle_p \rangle_i + \frac{N-1}{N} \langle \langle \nu_{ip} \rangle_p \rangle_i^2. \end{aligned} \quad (4.13)$$

Summarising, under the assumption that the disorder among the different complexes is not correlated and that the number of complexes $n \gg 1$, one obtains

$$\langle \overline{\nu_i^2} \rangle_i = \frac{1}{N} \overline{\nu^2} + \frac{N-1}{N} \overline{\nu}^2, \quad (4.14)$$

which yields

$$\begin{aligned} \sigma_{\text{inter}}^2 &= \frac{1}{N} \sigma^2, \\ \sigma_{\text{intra}}^2 &= \frac{N-1}{N} \sigma^2 \end{aligned} \quad (4.15)$$

and finally

$$\frac{\sigma_{\text{inter}}^2}{\sigma_{\text{intra}}^2} = \frac{1}{N - 1} \quad (4.16)$$

for the ratio of inter- to intra-complex disorder.

Comparison between experiment and analysis

The experimental data can be compared with the results from the statistical analysis given above. For the ratio of the inter- and intra-complex disorder contributions a value of 0.36 was observed experimentally which is very close to the value of 0.38 expected from Eq. 4.16 using $N = 8$. Moreover Eqs. 4.15 provide the opportunity to calculate the magnitude of the two disorder components in absolute figures from the observed inhomogeneous ensemble linewidth of 300 cm^{-1} . This yields for the inter-complex contribution $\sqrt{1/8} \cdot 300 \text{ cm}^{-1} \approx 106 \text{ cm}^{-1}$ whereas for the intra-complex contribution $\sqrt{7/8} \cdot 300 \text{ cm}^{-1} \approx 281 \text{ cm}^{-1}$ are predicted. Both values are in excellent agreement with those observed experimentally. Apparently in *Rs. molischianum* the site-energies of the individual B800 BChl *a* pigments are not correlated as the disorder can be explained by using *one* random variable only. Therefore, only one distribution is needed from which the energy sites of all pigments in all complexes can be drawn.

This is in contrast to a previous study described in the literature on the nonameric B800 band from *Rhodopseudomonas acidophila* where it was found that the inter- and intra-complex disorder were 120 cm^{-1} and 130 cm^{-1} , respectively [24]. Applying Eqs. 4.15 yields a ratio of 0.92, whereas from Eq. 4.16 with $N = 9$ a ratio of 0.35 is expected. It seems that for *Rps. acidophila* the B800 site-energy distribution can not be described by one independent random variable only. More than one variable would be necessary if the inter- and intra-complex disorder were independent from each other. The determination of the site energies of the pigments would then require two steps. In a first step the central mean value of each complex is determined by choosing a value from the inter-complex distribution. In the second step the relative site energies within the individual complexes are determined from the intra-complex distribution. The final site energies are then the sum of the relative site energies and the spectral mean. In this procedure the assumption that the average over pigments from the same complex is equal to the average over pigments from different complexes needed for the step from Eq. 4.10 to Eq. 4.11 is no longer fulfilled and the relationship between the two types of disorder as given in Eq. 4.16 does not hold anymore.

4.3.2 Direct observation of distinct tiers in the energy landscape of a protein

The spectroscopic properties of the chromophores embedded in the photosynthetic complexes are determined to a large extent by their mutual spatial arrangement and their interaction with the local environment. However, a protein is not a rigid structure. It consists of a linear chain of amino acids folded into secondary and tertiary structure elements. Due to the relatively weak interactions that stabilise the three dimensional protein structure the lowest energy state of a protein is not unique. The potential energy hypersurface has $3N$ dimensions, where N is the number of atoms (typically > 1000) in the protein, and features a multitude of minima, maxima and saddle points. Commonly, a description in terms of a rugged energy landscape is appropriate where each minimum represents a different conformational substate (CS) of the protein. In order to describe protein dynamics and function a model has been put forward by Frauenfelder and others [31–33] which proposes an arrangement of the protein energy landscape in hierarchical tiers. On each level of the hierarchy the CS are characterised by an average energy barrier between the CS that decreases with descending hierarchy. A consequence of this idea is that structural fluctuations of a protein become hierarchically organised as well, featuring characteristic rate distributions in different tiers. Supporting evidence for this concept has been obtained from experimental work on myoglobin [31, 90, 144–147]. In the context of a rugged protein energy landscape that is organised in tiers, the spectral dynamics observed in the B800 spectra can be interpreted straightforwardly. Since conformational changes of the protein correspond to rearrangements of its atoms, the embedded chromophores are subjected to fluctuations in the electrostatic interactions. The general idea is that the conformational changes are induced by optical excitation of the pigments.

Spectral switching: Chromophores probe the energy landscape

From spectral hole burning experiments on LH2 from *Rhodospseudomonas acidophila* it is known that relative distance changes of $\Delta R/R \approx 10^{-4} - 10^{-2}$ are already sufficient to result in spectral shifts of $1 - 100 \text{ cm}^{-1}$ for the B800 absorptions [148]. Consequently, the observed spectral fluctuations of complexes 1 and 2 (Sec. 4.2.2) are attributed to reflect modulations of the pigment-protein interactions in the vicinity of the chromophore and according to the concept

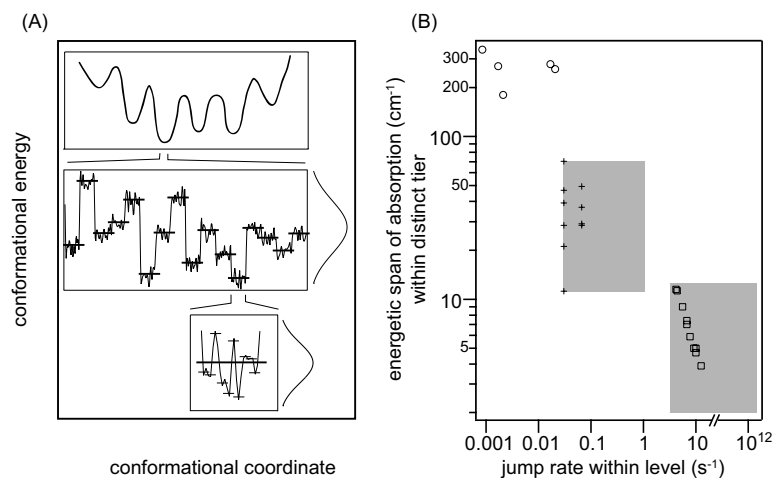


Figure 4.12: Hierarchical tiers in the energy landscape of a protein. (A) Schematic sketch of three subsequent tiers of the potential energy hypersurface of a protein as a function of an arbitrary conformational coordinate. (B) Width of the spectral region that is covered by the spectral fluctuations of the chromophore within a certain time window — termed energetic span — versus the rate of these fluctuations in the three tiers found. Circles correspond to data from large spectral jumps, crosses to data from spectral diffusion, boxes to possibly unresolved small spectral fluctuations, see text for details.

of conformational substates the three observed categories of spectral fluctuations are assigned to the presence of at least three distinct energy tiers in the energy landscape of the protein. In order to address this issue in more detail the term “energetic span” of the chromophore absorption is introduced. This refers to the width of the spectral region that is covered by the spectral fluctuations of the chromophore within a certain time window. In Fig. 4.12 a simplified protein-energy landscape is sketched along an arbitrary conformational coordinate, together with the information that is obtained for the relationship between the energetic spans of the chromophore absorptions and the corresponding timescales. It is assumed that the magnitudes of the observed spectral shifts represent a hierarchy of tiers where the average height of the energy barriers decreases from top to bottom.

The highest tier, Fig. 4.12A top, is thought to represent specific arrangements of the atoms, for example in the protein backbone, and transitions between these levels give rise to spectral shifts of several 100 cm^{-1} in the optical spectrum of the chromophore. Presumably, the spectral shift is indicative for a significant barrier height between the initial and final CS. As the chromophore absorptions sample only few discrete spectral positions the energetic span covered by the pigment absorption at this level of the hierarchy was taken as the energy difference between two anti-correlated lines. The underlying processes in this tier occur at rates of $10^{-2} - 10^{-3}\text{ s}^{-1}$.

However, each energy level in the highest tier is more appropriately described as a rugged energy surface as shown in the centre part of Fig. 4.12A on an enlarged scale. Within this tier the average CS energy is indicated by a bold bar and the distribution of states by the smooth curve to the right. Accordingly, the spectral changes of about 5 cm^{-1} between two successively recorded chromophore spectra are assigned to reflect structural fluctuations of the protein between two CS inside this tier of the energy landscape. Information about the distribution of the CS energies within this level of the hierarchy is provided by the linewidth of about 50 cm^{-1} that is obtained after accumulating hundreds of individual sweeps. Boundaries for the rates of the protein dynamics which result in these spectral fluctuations can be estimated from the repetition rate of the individual laser sweeps ($0.03 - 0.07\text{ s}^{-1}$) and the time required to scan the laser across the accumulated linewidth (1 s^{-1}). The shaded box in the centre of Fig. 4.12B indicates these constraints, the datapoints (crosses) are placed at the repetition rate of the experiments.

Descending further in hierarchy one finally reaches a situation that the protein transitions between the CS are going to cause only minor changes in the chromophore spectra. Certainly, the smallest detectable spectral change corresponds to a broadening rather than a shift of the absorption line. At the bottom of Fig. 4.12A a situation is sketched where the individual CS are already quantised in energy (light bars) and can be characterised by a statistical distribution (smooth curve to the right) around a mean value (bold bar) which represents one of the average CS energies of the next higher tier. Likely causes for the CS within this tier are vibrational and/or librational degrees of freedom of the protein. Within the temporal resolution of the experiment all CS of this tier are sampled. A lower boundary for the rate of the processes that are able to contribute to unresolved spectral dynamics hidden in the residual linewidth of the B800 absorptions is given by the time that is required to scan the laser across this line. Therefore the maximum possible energetic span for the chromophore absorptions and vice versa the smallest possible rate for dynamical processes in the protein can be extracted from the broadest processed linewidth. This fixes the upper left corner of the shaded box at the lower right of Fig. 4.12B. It should be mentioned that an upper boundary for the rate of these processes follows from the Fourier-transform of the linewidth itself which yields about 10^{12} s^{-1} . However, the approach is inappropriate to monitor the ultrafast dynamical processes and focuses on those that occur at low rates. Accordingly, the possible parameter combinations in the lowest observable hierarchical level are restricted to the shaded area at the bottom of Fig. 4.12B. The datapoints (squares) correspond to the processed linewidth versus the reciprocal scantime of the laser.

Certainly, Fig. 4.12B provides only a crude picture. In addition, it should be kept in mind that this method does not permit to distinguish small spectral changes occurring at fast rates from those occurring at slow rates. However, large spectral shifts at fast rates have not been observed and the datapoints in Fig. 4.12B should be read as a boundary for the possible parameter combinations. Only combinations of rates and spectral shifts below the diagonal of the diagram are compatible with the observations.

Simultaneous spectral diffusion: coupling of chromophores

To understand the observations in connection with complexes 3 and 4 in Sec. 4.2.2 one has to consider that the excitations of the B800 BChl *a* molecules can be treated only in first approximation as being localised on individual molecules. In Sec. 4.3.3 it is shown that the ratio of the intermolecular interaction strength, V , and the energy mismatch in site energy, δ , between adjacent BChl *a* molecules is subjected to a distribution. It should be noted that the distribution of differences in site energy δ , of neighbouring BChl *a* molecules as discussed here, can be described by a Gaussian distribution with width Δ . The actual value of V/δ varies between different LH2 complexes and even between different B800 BChl *a* molecules within the same complex. The obtained values cover typically a range of $V/\delta \approx 0.5$ – 2 . Therefore it is very probable that for some LH2 complexes the B800 excitations are slightly delocalised over 2–3 monomer units. This is corroborated by the observation of about 4–6 absorptions in the B800 spectra from individual LH2 complexes rather than 8 absorptions (or 9 for LH2 from *Rhodopseudomonas acidophila* [118]) as should be observable for strictly localised excitations.

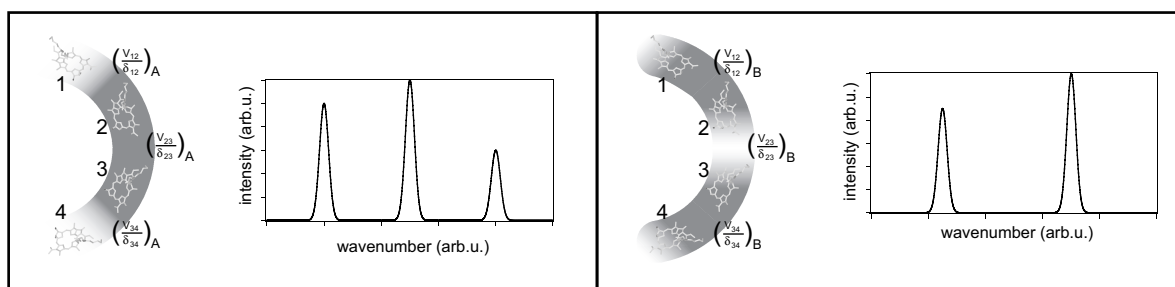


Figure 4.13: Schematic sketch to illustrate the interpretation of the experimental results in connection with complexes 1 and 2. On the left hand side of each figure a part of the B800 assembly is shown. The local intermolecular coupling between the individual B800 molecules i and j is indicated by V_{ij}/δ_{ij} . The right hand side of each figure shows two (arbitrary) fluorescence-excitation spectra for two different sets of coupling parameters, denoted by the suffix A and B.

However, both the difference in site energy, δ , of two pigments and the intermolecular interaction strength, V , depend critically on the mutual orientation and the distance of the pigments. Any change in the protein backbone induces a variation of the local V/δ ratio which is manifested as a change of the optical spectrum. In order to illustrate this interpretation a schematic sketch of a part of the B800 ring is shown in Fig. 4.13. It is emphasised that the figure has only illustrative character and that the actual distribution of the excitation energy in the B800 assembly can not be determined. The coupling strength between adjacent molecules i and j is denoted by V_{ij}/δ_{ij} and it is realistic to assume that its actual value is different for each pair of molecules. In the left part of Fig. 4.13 an arbitrary situation, termed A, is shown where the excitation is localised on molecules 1 and 4 and delocalised between molecules 2 and 3. In the right part of Fig. 4.13 an arbitrary situation, termed B, is shown where the distribution of intermolecular couplings has changed such that the excitation becomes delocalised between molecules 1 and 2 as well as between molecules 3 and 4. Despite the arbitrarily chosen examples for the illustration it is doubtless that such kind of variations in the electronic couplings result in changes of the optical spectrum.

Structural changes in the binding pocket of the BChl *a* molecules

Of course, the intriguing question that arises is whether the observed spectral shifts can be related to structural rearrangements in the binding pocket of the chromophore, which is shown in Fig. 4.14.

It is known from theoretical work that the Q_y transition of BChl *a* is very sensitive to perturbations of the π -conjugation system of the bacteriochlorin macrocycle, and is also affected by the ligands to the central Mg-atom. For instance, an out-of-plane rotation of the C_2 acetyl group with respect to the bacteriochlorin plane yields a blue shift of the pigment transition of up to 500 cm^{-1} [149]. A deviation from planarity of BChl will have similar effects. Density-functional theory calculations comparing LH2 from *Rhodospseudomonas acidophila* and *Rhodospirillum molischanum* showed that the more delocalised π -electron system of *Rhodospirillum molischanum* accounts for a difference of 370 cm^{-1} in its Q_y absorption [150].

It is inferred that the observed spectral variations result from rather local conformational changes that affect the π -conjugation system of the bacteriochlorin macrocycle, e.g., through affecting the planarity of the ring, through a reorientation of side-groups, or through some rearrangement

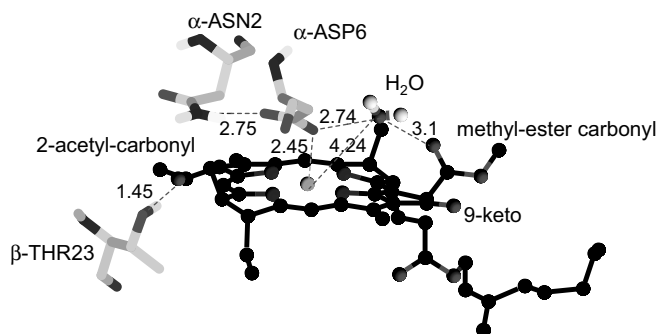


Figure 4.14: Part of the binding pocket for a B800 BChl *a* molecule in *Rs. molischianum*. Dashed lines refer to short distances (in Å) and indicate likely hydrogen and metal bonds.

involving the central-Mg atom and its ligands. In this regard several aspects have to be considered. First, the huge spectral changes might reflect fluctuations in the strength of a hydrogen bond between the β -Thr23 amino acid and the C₂ acetyl group of the BChl *a* molecule [3, 139]. This is evidenced by site-directed mutagenesis on LH2 from *Rhodobacter sphaeroides*. For this species a β -₁₀-Arg amino acid is hydrogen bonded to the C₂ acetyl carbonyl group of the BChl *a* molecule and spectral shifts of 100–200 cm⁻¹ for the B800 absorption maximum are observed if this amino acid is substituted by a non-hydrogen bonding residue [60]. Changes in the protein environment of B850 BChl *a* caused a shift of 154 cm⁻¹ and 342 cm⁻¹ for single and double mutations, respectively [151]. And density-functional theory calculations that examined the ligand-binding of the BChl *a* central Mg-atom to the charged α -Asp6 amino acid in the B800 binding pocket of *Rs. molischianum* estimated a red shift of 190 cm⁻¹ [150] for the site energy of a BChl *a* molecule in the B800 ring.

Second, the polarity of the B800 binding site might be of influence as follows from shifts of up to 300 cm⁻¹ for the spectra from monomeric BChl *a* upon solution in various organic solvents [88]. For *Rs. molischianum* the x-ray structure shows a water molecule in close proximity to the α -Asp6 and the methyl ester carbonyl of the BChl *a* that might cause variations in the electrostatic environment of the pigment [3]. Electrostatic interactions with water molecules or other polar groups at a distance away from the BChl *a* binding pocket will be of no great influence to the spectral characteristics of the chromophore since such interactions depend strongly on distance. Moreover, electrostatic effects depend on the change of the effective dipole moment, $f \cdot \Delta\mu$, upon excitation of BChl *a*, which is only about 1 D.

Finally, also distortions of the bacteriochlorin macrocycle at the position of the C₉-keto group

in the B800 band of LH2 from *Rb. sphaeroides* have been observed to cause spectral shifts of the Q_y absorption of about 80 cm^{-1} [60].

In summary, it appears very reasonable that the observed spectral shifts result from structural fluctuations within the binding pocket of the chromophore. Given the low fluorescence quantum yield of light-harvesting 2 complexes of about 10% *in vitro* [79], it is most likely that the observed conformational changes are light induced at low temperature. For example, van Oijen *et al.* [24] described the observation of light induced spectral diffusion in the B800 band of LH2 from *Rps. acidophila*. Further support comes from the observation that the rate of spectral diffusion in the B800 band increases with excitation intensity in Sec. 4.2.2. A significant fraction of the average absorbed energy is dissipated by radiationless decay and excites nuclear motions of the protein matrix (phonons). If the system is prior to the optical excitation in an initial CS there is finite probability that it will end up in a different CS after the excitation and subsequent relaxation to thermal equilibrium. The dissipated energy exceeds the thermal energy significantly and the space of conformational substates that can be probed is not restricted to the part of the energy landscape that is thermally accessible and provides meaningful information about the energy landscape of the protein.

4.3.3 Electronic couplings in a circular aggregate of molecules

In section 4.2.3 it was shown that the distribution of mutual angles between individual BChl *a* molecules in the B800 ring covered nearly the whole range between 0° and 90° with slight preferences for the values around 0° , 20° , 45° and 70° . For some complexes temporal fluctuations in the spectral position of individual absorptions as well as in the orientation of the transition-dipole moment were observed.

Coupling between neighbouring chromophores

The question is how the observed polarisation of the optical transitions in an individual LH2 complex relates to the structure. The geometrical structure of the B800 ring in the LH2 complex of *Rs. molischianum* yields an inter-chromophore distance of 22 \AA . Assuming that the electronic excitation of the B800 ring is strictly localised on a single BChl *a* chromophore one expects that the mutual angles between the transition-dipole moments of the individual BChl *a*

chromophores will be equal to multiples of 45° , see Fig. 4.1C. However, the coupling between two adjacent molecules will lead to eigenstates different from those of the uncoupled chromophores and consequently to a change in the orientation of the transition-dipole moments. The intra-complex variation in site energy has been measured in Sec. 4.2.1 and yields a broad distribution ranging from $70 - 200 \text{ cm}^{-1}$. From these values it is estimated that the average difference in site energy of two adjacent molecules, δ , is in the order of $10 - 40 \text{ cm}^{-1}$ and that the ratio V/δ between neighbouring molecules varies from about $0.5 - 2$, as the nearest-neighbour interaction strength V is about 20 cm^{-1} [54]. From this ratio it can be concluded that the interaction strengths between the B800 BChl *a* molecules are in the weak to intermediate limit. For the sake of brevity the following discussion is restricted to two adjacent BChl *a* molecules with excitation energies E_1 and E_2 ($E_1 > E_2$). For the resulting energies and eigenstates of the coupled system one finds

$$E_{\pm} = \frac{1}{2}(E_1 + E_2) \pm \frac{1}{2}\sqrt{\delta^2 + 4V^2} \quad (4.17)$$

and

$$\begin{aligned} |\Psi_+ \rangle &= \cos \frac{\theta}{2} |1 \rangle + \sin \frac{\theta}{2} |2 \rangle \\ |\Psi_- \rangle &= -\sin \frac{\theta}{2} |1 \rangle + \cos \frac{\theta}{2} |2 \rangle \end{aligned} \quad (4.18)$$

where $\tan \theta = \frac{2V}{\delta}$, $\delta = E_1 - E_2$, and $|i \rangle$ denotes the excited state localised on molecule i .

From the two eigenstates one finds for the transition-dipole moments

$$\begin{aligned} \vec{\mu}_+ &= \vec{\mu}_1 \cos \frac{\theta}{2} + \vec{\mu}_2 \sin \frac{\theta}{2} \\ \vec{\mu}_- &= -\vec{\mu}_1 \sin \frac{\theta}{2} + \vec{\mu}_2 \cos \frac{\theta}{2} \end{aligned} \quad (4.19)$$

where $\vec{\mu}_i$ denotes the transition-dipole moment of an individual BChl *a* molecule in the B800 ring. From Eq. 4.19 the orientations of the transition-dipole moments of the B800 BChl *a* molecules have been calculated as a function of V/δ , see Fig. 4.15. The orientations of the initial transition-dipole moments, corresponding to $V/\delta = 0$, were set to 0° and 45° . For increasing V/δ the orientations of the transition-dipole moments $\vec{\mu}_+$ and $\vec{\mu}_-$ change gradually with respect to the initial orientations and level off at angles of 22.5° and 112.5° for values of V/δ larger than about 6.

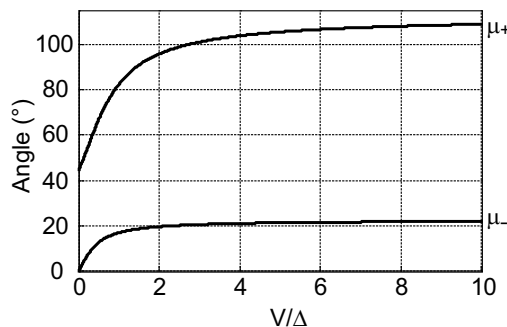


Figure 4.15: Dependence of the orientation of the transition-dipole moments $\vec{\mu}_+$ (upper curve) and $\vec{\mu}_-$ (lower curve) on the ratio V/δ . The orientations of the initial transition moments $\vec{\mu}_1$ and $\vec{\mu}_2$ were set to 0° and 45° and provide the reference frame.

From the range of values estimated for V/δ a distribution of mutual orientations with preferences at 22.5° and 112.5° is expected. With the restriction to acute angles this amounts to observed differences between the angular orientations of 22.5° and 67.5° .

Taking into account BChl *a* molecules that are weakly coupled one expects, in addition, to observe differences between the angular orientations of 45° modulo 45° . In total this results for the mutual orientations of the transition dipole moments in a distribution with preferential values around 0° , 22.5° , 45° , 67.5° , and 90° . Consequently, any observation of mutual orientations of transition-dipole moments different from 0° , 45° and 90° , provides direct evidence for an electronic coupling in the weak to intermediate range between the individual BChl *a* molecules in the B800 assembly. The actual strength of the coupling is subjected to a distribution as a result of the difference in site energies of adjacent molecules.

Temporal fluctuations of the coupling between two chromophores

In addition to spatial fluctuations of the coupling temporal variations were observed as well. When analysing Fig. 4.11, an orientational change of the whole LH2 complex during the experiment can be excluded from the behaviour of absorptions “3” and “4”. Two other absorptions are only visible either during the interval A (absorptions “1” and “2”) or during interval C (absorptions “2a” and “2b”). The two intervals are separated by a period B where absorption “1” shows a drastic change in spectral position and where absorption “2” vanishes. The conjecture is that the absorptions labelled “2a” and “2b” result from two molecules that become electronically coupled during interval B, one of which has initially absorption “2” for the uncoupled situa-

tion. This conclusion is based on the following arguments. Supposing that the transition-dipole moments of the two uncoupled chromophores have initially a mutual orientation of 45° , which is valid for nearest neighbours the local ratio V/δ can be calculated using Eq. 4.19 from the difference of the polarisation angles of absorptions “2a” and “2b”. For the observed $\Delta\alpha = 67^\circ$, a ratio of $V/\delta = 1.07 \pm 0.15$ is obtained. Another way to calculate this ratio follows from (4.17) if E_+ , E_- and one of the unperturbed energies are known. Assigning E_1 to absorption “2” and E_+ and E_- to absorptions “2a” and “2b” yields $V/\delta = 0.95 \pm 0.1$, in agreement with the value obtained from the polarisations. A further independent piece of information is provided by the difference in angle of the transition-dipole moments $\vec{\mu}_1$ and $\vec{\mu}_+$ of the absorptions corresponding to E_1 and E_+ . From Fig. 4.15 a difference of $37^\circ \pm 5^\circ$ is predicted, in reasonable agreement with the observed value of $30^\circ \pm 5^\circ$. So far, our interpretation yields a consistent description for the absorptions “2”, “2a” and “2b”. However, for the absorption strength of the transitions “2a” and “2b” one finds within this approach 1.6 and 0.4 monomer units while the experiment yields about equal intensities for the two transitions. This discrepancy may reflect differences in the energy transfer efficiency from the B800 to the B850 pigment pool, which are not taken into account by the simple dimer approximation. The excited state of a B800 BChl *a* molecule can decay radiatively (rate k_r) or non-radiatively (rate k_{nr}) to the electronic ground state. The total decay rate, k , is given as $k^{-1} = k_r^{-1} + k_{nr}^{-1}$. The most significant contribution to the non-radiative decay rate results from the energy transfer to the B850 pigment pool since its energy transfer time of a few ps is orders of magnitude faster than fluorescence (ns) or intersystem crossing (ISC) to the triplet state (μ s). In these experiments fluorescence-excitation spectroscopy was performed which means that exclusively the fluorescence from the lowest excited state of the B850 manifold at $\lambda = 880$ nm was detected. Therefore, the intensities of the absorptions of the pigments in the B800 ring are determined by the decay to the B850 pigments. This rate depends critically on various parameters such as the separation of the excited state energies or the geometrical distance of the molecules involved. Consequently the two energetically distinct electronically excited states of the coupled chromophores may have different energy-transfer rates to the B850 pigment pool.

Possible explanations for the fluctuations in the electronic coupling are changes in the protein backbone or rearrangements of the BChl *a* molecules in their binding pockets, for example a rotation of the acetyl group or the breakage of hydrogen bonds as discussed extensively in the previous section. Such changes alter the electrostatic environment of the individual chro-

mophores and result in a shift of their absorption energies and consequently in changes of V/δ . The structural perturbations are most probably light induced in these low-temperature measurements, which is corroborated by the low fluorescence quantum yield of the LH2 complexes *in vitro* [79].

4.4 Summary

In this chapter, the spectral properties of the BChl *a* molecules absorbing at around 800 nm in the light-harvesting 2 complex from *Rhodospirillum rubrum* were discussed. Since the geometric structure of the complex is known from x-ray crystallography [3], the spectroscopic observations could be directly linked to its molecular structure. In the complex, eight of these weakly coupled BChl *a* molecules are arranged in a ring — the so called B800 ring — featuring C_8 -symmetry which implies an angle of 45° between the absorption transition-dipole moments of neighbouring BChl *a* molecules.

The spectrum of a B800 ring of an individual LH2 complex generally shows several narrow lines, indicating that the BChl *a* molecules absorb at slightly different excitation energies. This spectral heterogeneity was characterised by the so called intra-complex disorder, reflecting the spread of absorption lines within a complex. Comparing the spectra reveals that they are all different from each other. All spectra consist of 2–6 absorption lines although the exact number and the spectral position of the lines change from complex to complex. This behaviour was quantified by the inter-complex disorder reflecting the difference of the spectral mean value from one complex to the other. The ratio between inter- and intra-complex disorder could be analytically modelled by assuming that the energetic disorder of the site energies of the B800 BChl *a* molecules is described a *single* random variable.

Looking closer at the B800 spectrum of an individual LH2 complex it could be uncovered that the spectrum is not stable in time but undergoes changes that become apparent when recording several spectra in a row. These spectral changes are most probably light induced as the quantum yield of light-harvesting complexes *in vitro* is quite low [79] leading to thermal fluctuations in the sample. The excess energy deposited into the system results in nuclear motion and the induced structural fluctuations probe the space of conformational substates of the proteins in the binding pockets of the BChl *a* molecules. This interpretation is supported by results from

the experiments in Sec. 4.2.2 showing that the rate of spectral diffusion of the B800 absorptions increases with excitation intensity.

A striking observation is the fact that the spectral diffusion in this system is not always a random process. For several complexes, a type of simultaneous spectral diffusion was found for which the fluorescence-excitation spectrum changed between two different realisations. In other cases single absorption lines reversibly switched between two absorption energies separated by several 100 cm^{-1} at a rate of about 10^3 s^{-1} . On a smaller spectral scale all absorption lines showed moderate spectral changes within several 10 cm^{-1} at a rate of about 0.1 s^{-1} leading to a broadening of the absorption line in the time average spectrum of all scans. Even the linewidth of an absorption in a single scan was possibly slightly broadened due to unresolved spectral changes within a few wavenumbers at a rate of about 10 s^{-1} .

These three groups of spectral diffusion could be attributed to the presence of at least three distinct tiers in the hierarchically organised rugged energy landscape of the proteins surrounding the B800 BChl *a* molecules. Each local minimum of the energy landscape corresponds to a conformational substate of the protein, i.e. to a different arrangement of its atoms or equivalently to a different shape of the protein. As several research groups have found spectral shifts of similar orders of magnitudes resulting from structural rearrangements in the binding pocket of the chromophore, it seems reasonable that the observed spectral shifts result indeed from reorientations of the protein which forms the binding pocket of the BChl *a* molecule.

Many of the complexes that were studied featured a more complex temporal development of the spectra due to simultaneous spectral jumps of multiple chromophores. Only for a small fraction of LH2 complexes either the simple “two-state jumps” as for complexes 1 and 2 or the “simultaneous spectral diffusion” behaviour as for complexes 3 and 4 were found. It is one of the intriguing features of single-molecule spectroscopy to isolate such key processes which might become essential for the development of a more general model of protein dynamics.

Another point addressed in this chapter was the possibility to look at the interaction between neighbouring chromophores by applying polarisation dependent spectroscopy. These experiments resulted in the finding that excitations of BChl *a* molecules in the B800 band are mainly localised on individual molecules. However, the observation of mutual orientations of transition-dipole moments different from 0° , 45° or 90° — as predicted by the x-ray structure — provided direct evidence for an electronic coupling in the weak to intermediate range between individual

BChl *a* molecules in the B800 assembly. Also, temporal variations in the coupling strength could be observed.

In summary, using single-molecule spectroscopy it could be shown that the chromophores in the B800 band of LH2 from *Rhodospirillum rubrum* represent a heterogeneous entity. The concept of the hierarchically organised rugged energy landscape of proteins could be confirmed by studying the spectral diffusion of the BChl *a* molecules which is influenced by structural reorientations of their binding pockets. It was also found that the chromophores act as sensitive probes which monitor the local interaction between the individual pigments within the B800 assembly. The interaction strength was found to be subjected to a distribution as well as to temporal fluctuation. These studies demonstrate that single-molecule spectroscopy provides a unique method to reveal details of intermolecular interactions in the weak to intermediate coupling limit that is inaccessible by other experimental methods.

Line shapes of the B800 absorptions

In the previous chapter fluorescence-excitation spectra of the B800 band of LH2 from *Rhodospirillum rubrum* were studied extensively and it was observed that the consecutively recorded spectra differed from spectrum to spectrum. Merely looking at temporal averages will not reveal all information hidden in the spectra and therefore, in this chapter, a pattern recognition approach using multivariate statistical analysis (MSA) was applied to analyse the spectral diffusion patterns of the B800 band.

5.1 Multivariate statistical analysis

5.1.1 The MSA algorithm

Multivariate statistical analysis has been used in a wide area of fields such as the comparison of the amino acid sequence of proteins to discover similarities between proteins from different species [152] or the reconstruction of the three dimensional structure of large biological macromolecules (e.g., proteins) from 2D projections in electron cryo-microscopy ([153, 154] and references therein). In the latter case the sample consists of the protein to be studied in an aqueous solution which has been shock-frozen. The raw images of this sample taken in the

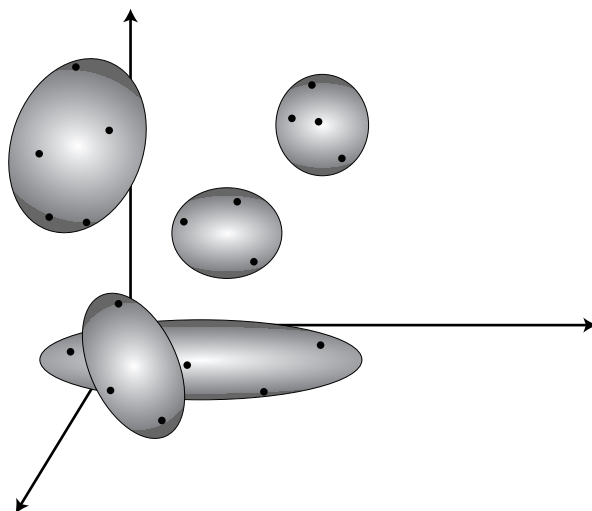


Figure 5.1: Schematic drawing of a n -dimensional vector space spanned by the eigenimages of a set of images. Each image is represented by a point in the space. A pattern recognition approach such as the multivariate statistical analysis groups similar images into classes (depicted by the clouds) thereby minimising the internal variance of the classes and maximising the variance between classes.

electron microscope are 2D projections of the protein in different orientations. The average of all raw images would not improve the signal-to-noise ratio (SNR) of the individual images as it would average over all possible orientations of the protein.

A solution to this problem is given by the MSA approach. Its main purpose is to act as a kind of pattern recognition technique and to group similar looking images into classes. Then the images within a class represent 2D projections from proteins with (nearly) identical orientation and the average of all images within a class significantly improves the SNR ratio. In a last step the relative orientations between the 2D projections of the classes have to be determined in order to fully reconstruct the 3D structure of the protein.

The MSA algorithm considers the raw images as a linear combination of main eigenvectors — in this case eigenimages — of the set. The eigenimages span a n -dimensional vector space and each raw image can be represented by a single point in this space, thereby decreasing the amount of data and facilitating its interpretation. After determining the eigenimages, the raw images are grouped into classes according to their likeness each image becoming a member of one of the classes. The classes can be seen as clouds of points in the n -dimensional vector space as shown schematically in Fig. 5.1. The number of classes can be chosen freely but should be small with respect to the number of images. The classification algorithm is aimed at minimising the internal variance of the classes while at the same time maximising the variance between the

centres of mass of the class averages. Thus the datapoints within each cloud should be as close together as possible whereas the distance between the clouds should be as large as possible. More information can be found in [152, 154].

5.1.2 Using MSA in spectroscopy

In the previous chapter it was described that the narrow absorption lines in the B800 band of LH2 are subjected to spectral diffusion. In some cases it was observed, that individual absorption lines switched reversibly between two distinct spectral positions whereas in other cases a type of simultaneous spectral diffusion was found in which the fluorescence-excitation spectrum of a complex changed between two different realisations. This classification into two realisations of complexes 3 and 4 in Figs. 4.7 and 4.8 was done by eye. By looking at the presence of one of the more prominent absorption lines it was decided whether the particular scan was assigned to realisation A or B. Similarly, the switching behaviour of the absorption lines of complexes 1 and 2 in Figs. 4.4 and 4.5 accidentally stroke the eye when browsing through the spectra. Only then the auto-correlation was calculated which confirmed the initial assumption. However, the method of visual inspection is very susceptible to the objectiveness of the observer. Visual perception is apt to see all kinds of patterns in data with a low signal to noise ratio. Therefore, only very prominent dependencies are reliably detected and weak features can easily be overlooked.

Looking at the spectral diffusion in more detail, smaller spectral jumps were found to contribute to a broadening of the averaged linewidth of an absorption as discussed in section 4.2.2. This type of spectral diffusion was eliminated by fitting the individual spectra with a Lorentzian and shifting each scan according to the fit maximum. However, in doing so detailed information about the line shapes of the individual scans was lost due to averaging of all line shapes. This raises the question whether the analysis of individual scans can be done by a computer, since it is in principle not biased and can handle large amount of data. The task of a computer program would be to classify the sequentially recorded scans into groups of similar spectra.

The IMAGIC-5 image processing system (Image Science, Berlin) is a software package which has been especially developed by van Heel and coworkers for the purpose of classifying images into groups of similar images using the multivariate statistical analyses approach [152–154] which was described in the previous section. In this chapter the IMAGIC-5 software was first

applied for the analysis of the spectral diffusion patterns (i.e., the series of scans) of two complexes which were already analysed by eye in the previous chapter. To process spectra with the IMAGIC-5 software, the sequentially recorded scans were treated as a series of one-dimensional images. This first application of the software was meant as a reference to see whether the software is suitable for the application in spectroscopy. From the analysis of the example spectra it was obvious that the MSA algorithm proved to be useful in analysing spectroscopic data although it was found that a large series of successively recorded spectra is needed to obtain a high enough signal-to-noise ratio to make any quantitative statements on the outcome of the analysis.

Therefore, in the next step, an analysis was carried out on a complex for which as many as 7700 scans were recorded, in this way improving statistics enormously compared to the 35 or even 256 scans for the complexes of the reference analysis. This resulted in detailed information about the line shapes of the individual BChl *a* absorptions in the B800 band which were found to consist of a zero phonon line and a phonon side band. From their ratio, the Huang-Rhys factor could be determined, which is a measure for the strength of the electron-phonon coupling in the B800 ring. The shapes of these lines could neither be resolved in a spectrum obtained from a single scan as the signal-to-noise ratio is too poor nor from the sum of successively recorded scans as the line shape is washed out by the averaging process.

5.2 Pattern recognition on two example spectra

In this section, the IMAGIC-5 software was employed for the analysis of the B800 absorptions of two LH2 complexes from *Rs. molischianum*, complex 1 (Sec. 4.2.2, Fig. 4.4) representing an example for spectral switching and complex 3 (Sec. 4.2.2, Fig. 4.7) representing the simultaneous occurring spectral diffusion.

5.2.1 Application to simultaneous spectral diffusion

Analysis

The first spectral diffusion pattern that was analysed (complex 3 discussed in Sec. 4.2.2) is shown in the left panel of Fig. 5.2A. It was found that the pattern consists of several blocks of

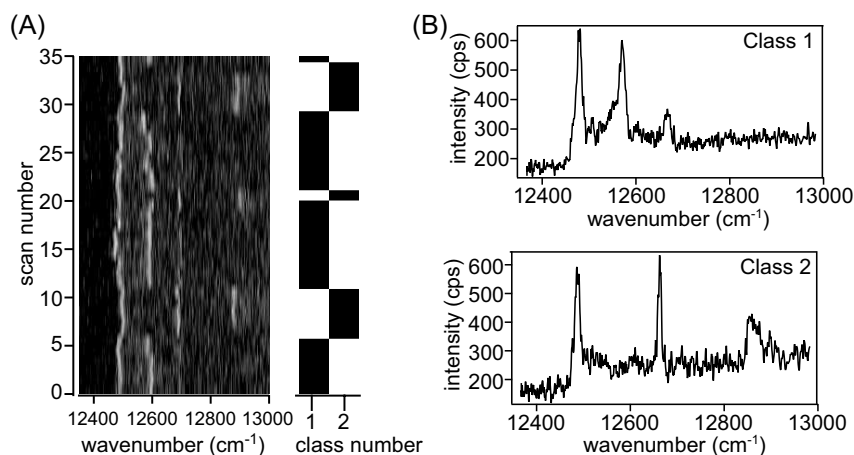


Figure 5.2: Multivariate statistical analyses on complex 3. (A) In the left panel the scans are shown versus wavenumber in a two dimensional representation. The right panel shows scan number versus class number in which a black entry indicates that the specific scan is member of that class. (B) The spectra that result when all scans within each of the two classes are averaged.

similar looking scans. Going from one block to the next the pattern of absorption lines changes as several absorption lines in the B800 band simultaneously change their transition energy. By looking at the average spectra of the blocks it was observed that the fluorescence-excitation spectrum varied recurrently between two different realisations.

The result of the analysis with the IMAGIC-5 software for this complex can be seen in Fig. 5.2 when classifying the spectra into two classes. In the right panel in (A) the scan number is shown versus the class number, in which a black entry means that the specific scan is member of that class. It is clear that each time an absorption is present at the spectral position of about 12600 cm^{-1} the scan is placed in class 1. The small spectral excursions of this absorption during scans 21–28 have no effect on the classification. The spectra in (B) show the average of all scans within each of the two classes.

Discussion

The IMAGIC-5 software was assigned to classify the B800 band fluorescence-excitation spectra of a LH2 complex featuring simultaneous spectral diffusion into two classes (Fig. 5.2A) of which the average spectra are shown in Fig. 5.2B. Comparing these with the spectra of the two realisations of the same complex (Fig. 4.7) which were classified by eye shows clear analogies between realisation A and B and class 2 and 1, respectively. Apparently, the IMAGIC-5 soft-

ware comes up with the same classification as was obtained by visual inspection and proves to be useful in discriminating the spectra of two different realisations of a complex.

5.2.2 Application to spectral switching

Analysis

The second spectral diffusion pattern that was analysed (complex 1 discussed in Sec. 4.2.2) is shown in the left-most panel of Fig. 5.3A in a two-dimensional representation. The pattern is characterised by the recurrent disappearance of one absorption line only together with the appearance of one new line at a different spectral position. For the complex analysed one absorption switched between the spectral positions marked by an a' whereas a second absorption switched between positions b and b' independently from the other absorption.

The result of the spectral pattern analysis of this complex by the IMAGIC-5 software is displayed in Fig. 5.3. Here, in the left and centre panel of (A) the scan number is displayed versus

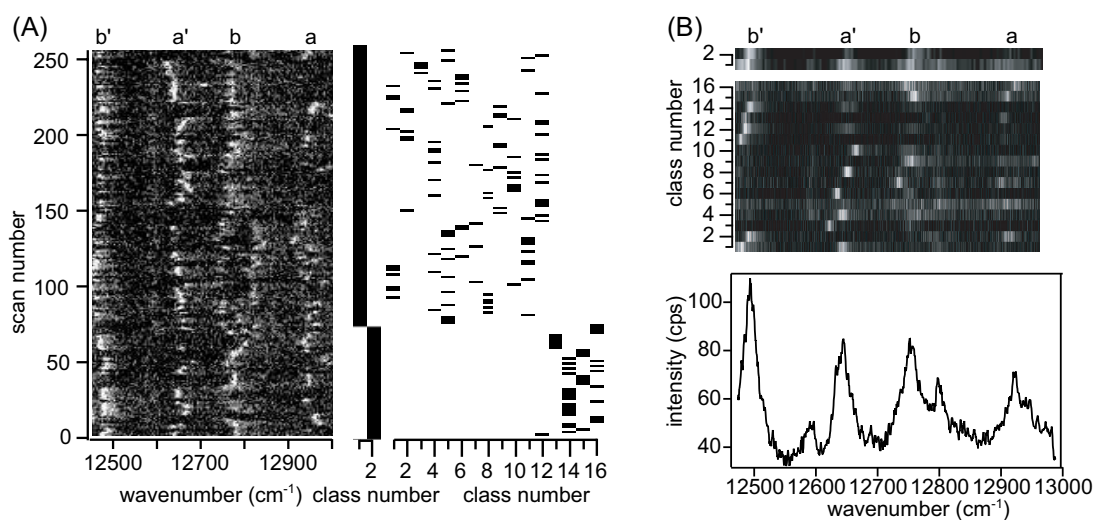


Figure 5.3: Multivariate statistical analyses on complex 1. (A) In the left-most panel the scans are shown versus wavenumber in a two dimensional representation. The centre and right-most panels show scan number versus class number for the classifications into two and 16 classes, respectively. A black entry indicates that the specific scan is member of that class. (B) In the upper and centre panel, the spectra that result when all scans within each of the classes are averaged are versus wavenumber for the classification into two and 16 classes, respectively. The fluorescence intensity is given by the grey code. In the lower panel the fluorescence-excitation spectrum is shown that results when all scans of the measurement are averaged. a , a' , b and b' indicate the absorption lines which were discussed in Sec. 4.2.2.

class number for a classification into two and 16 classes, respectively. Looking at the classification into two classes (centre panel, Fig. 5.3A), it is interesting to observe that the software divides the scans into two halves. The first half ranges from scan 1–74 and the second from scan 75–256. However, a difference between scans from the first half and the second half is not clearly visible by eye. If the spectra are grouped into 16 classes, the distinction between the two halves is maintained by the software as can be seen from the right-most panel in (A). Classes 1–12 only comprise scans from the second half of the spectrum whereas all scans from the first half of the spectrum are assigned to classes 13–16.

The spectra that result when the scans within each class are averaged are depicted in the upper panel of Fig. 5.3B for the case of two classes and in the centre panel for the 16 class classification. In contrast to Fig. 5.2B where the average spectrum of each class is shown as a 2D intensity versus wavelength diagram, here the spectra are shown as 1D plots of the wavelength, in which the averaged fluorescence intensity is given by the grey code. The different spectra are stacked on top of each other which allows to present the average spectra of all 16 classes in a compact way. In the lower panel of (B) the spectrum is shown when all scans of the measurement are averaged as an intensity versus wavenumber diagram.

Discussion

The analysis of a complex featuring spectral switching (complex 1) was chosen such, that the spectra were classified into 2 and 16 classes, respectively, displayed in the upper and centre panel of Fig. 5.3B, respectively. A closer look at the latter classification reveals that the four absorption lines labelled a, a', b and b' do not all occur simultaneously within any of the classes. In Tab. 5.1 the occurrence of an absorption line within a class is indicated by a "*"–symbol. The majority of classes (13) comprises two absorption lines, two classes contain only one absorption line whereas class 2 includes three absorption lines. An interesting observation is the fact that in neither of the classes lines a and a' occur together. Lines b and b' only occur together in class 2 and here line b' is very weak compared the other lines in this class. All other combinations (i.e., a–b, a'–b, a–b' and a'–b') do occur in one or several of the classes.

Based on these findings the classes were grouped into four types: type 1 contains classes in which lines a' and b' occur, type 2 was defined for a and b', type 3 for a'–b and type 4 comprises all classes in which lines a and b are present. The spectra that result when all scans belonging

class	1	2	3	4	5	6	7	8	9	10	11	12	13	14	15	16
line a		*					*		*				*		*	*
line a'	*		*	*		*		*		*				*		
line b		(*)	*	*		*	*	*	*	*					*	*
line b'	*	*									*	*	*	*		
type	1	-	3	3	-	3	4	3	4	3	-	-	2	1	4	4

Table 5.1: Grouping of the 16 classes into four types. The occurrence of an absorption line within a class is indicated by a *-symbol. Type 1 comprises classes in which absorption lines a' and b' occur simultaneously. Type 2 comprises classes in the same way for lines a–b', type 3 for a'–b and type 4 for lines a–b. Classes in which only one line or no absorption lines occur are not assigned to any group.

to the same type are averaged are shown in Fig. 5.4.

In Sec. 4.2.2 it was found that a–a' as well as b–b' are pairs of anti-correlated lines. The emission of a pair probably stems from one absorber which can switch between two different states resulting in unequal absorption energies. However, the intensity fluctuations of a–a' are independent from those of b–b', i.e., the two absorbers switch independently from each other. These results are reflected in the classification scheme resulting from the multivariate statistical analysis of the IMAGIC-5 software. The fact that the combinations a–a' and b–b' do not appear in the classes whereas all other combinations do occur shows that the software could detect the correlation within and the absence of correlation between the pairs of absorption lines.

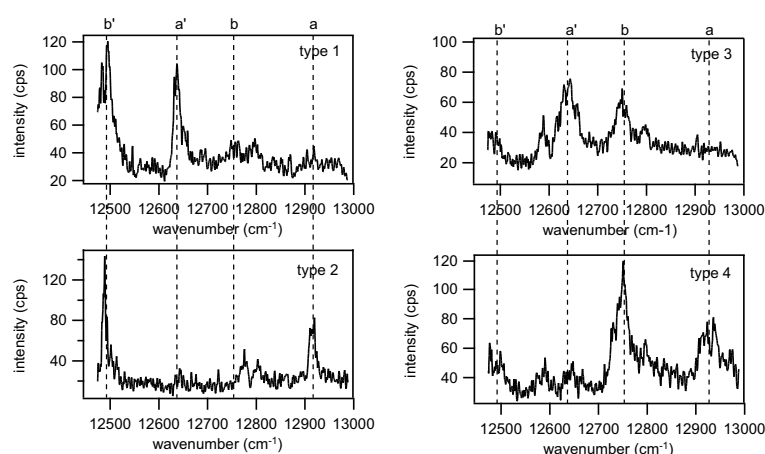


Figure 5.4: Spectra of the B800 band of complex 1 that result when the scans of all classes within each of the four types are averaged. The lines a–a' and b–b' do not occur simultaneously in any type.

5.3 The shape of the absorption lines in the B800 band

From the results of the previous section it is evident that the MSA algorithm provides useful information on spectroscopic data. Using several tens or several hundreds of spectra, spectral diffusion processes could be followed in time. However, the number of spectra per class was rather low resulting in a low SNR for the average class-spectrum. This made it difficult to group the classes of the example on spectral switching into distinctly different types. In order to obtain more detailed information about the B800 absorptions statistics needs to be improved.

In addition most of the complexes studied exhibited a more complex temporal development of the spectra due to simultaneous spectral jumps of multiple chromophores. This prohibits unambiguous assignment of spectral features at different time intervals as belonging to one particular BChl *a* molecule by eye. Only for a relatively small fraction of the complexes simple "two-state" jumps of individual absorptions have been observed, facilitating a clear assignment of the "jumping partners". Such spectral diffusion patterns should be analysed by a computer with the help of especially developed software tools.

Therefore, in this section the IMAGIC-5 software was used to analyse the spectral diffusion pattern of the B800 ring of a single LH2 complex from *Rhodospirillum molischianum* consisting of several thousand scans. By applying the MSA algorithm to such a large number of scans detailed information about the line shape of the individual B800 absorptions could be gained. A zero-phonon line together with a phonon side band could be identified. The resulting Huang-Rhys factor of about 0.4 implies a weak electron-phonon coupling for the chromophores in the B800 ring.

5.3.1 Experimental

To obtain a statistically significant number of spectra a single LH2 complex from *Rhodospirillum molischianum* was studied for 35 hours in total, measuring subsequently at 4 days in a row. As the bath cryostat can only be kept at 1.4 K for about 12–14 hours before the helium is used up the measurement had to be stopped every evening. By the morning of the next day, the sample inside the cryostat had reached a temperature of about 50–100 K and the cryostat was refilled and cooled down again to 1.4 K. A wide-field image of the sample was taken which

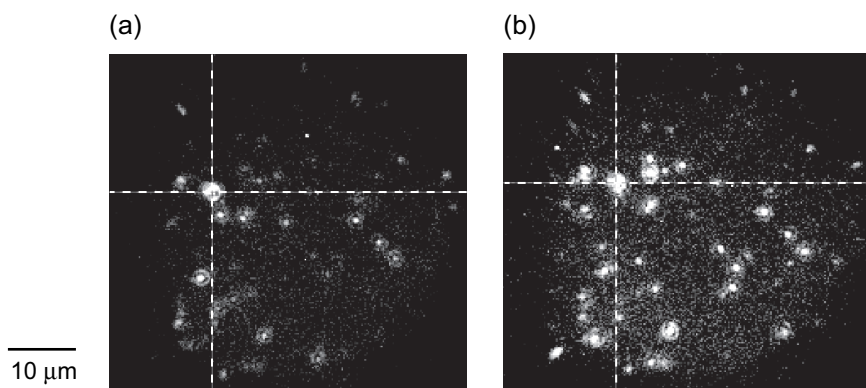


Figure 5.5: Widefield image of a sample of LH2 complexes from *Rs. molischianum* taken on two successive days. The same complex, indicated by the cursor cross, can clearly be identified on both images.

presents a characteristic assembly of bright dots and the same complex that was studied the day before could be identified within this assembly, see Fig. 5.5. In total 7700 consecutive scans were recorded whereby after each scan the polarisation of the incident laser light was rotated by 1.8° . The number of scans taken on day 1, 2, 3 and 4 were 1600, 2000, 2100 and 2000, respectively.

5.3.2 Analysis

In Fig. 5.6A the sequence of 7700 scans is shown. The average of all scans is given in the lowest trace of part (B). The end of a day's measurement is indicated by arrows on the right side of the spectral diffusion pattern. Between the end of day 1 and the beginning of day 2, the spectral diffusion pattern does not seem to change. Between days 2–3 and 3–4 the spectrum does change, although the overall appearance of the diffusion pattern, especially the absorption at about 12050 cm^{-1} is still similar to that of the preceding days, a clear indication that the spectral diffusion pattern — and hence the complex itself — is not disturbed by the recurrent heating and cooling.

The IMAGIC-5 software was set to classify the scans into 50 classes, resulting in about 150 scans per class, which is about the normal number of scans for a whole measurement on one complex in chapter 4. For each class, a class-spectrum was calculated by averaging all scans in the class. As an example, the average of all scans within a class is shown for four classes in the upper four traces of Fig. 5.6B. Each class-spectrum consists of one or more narrow lines and some less intense broad features. To get an indication for the high signal-to-noise ratio of these

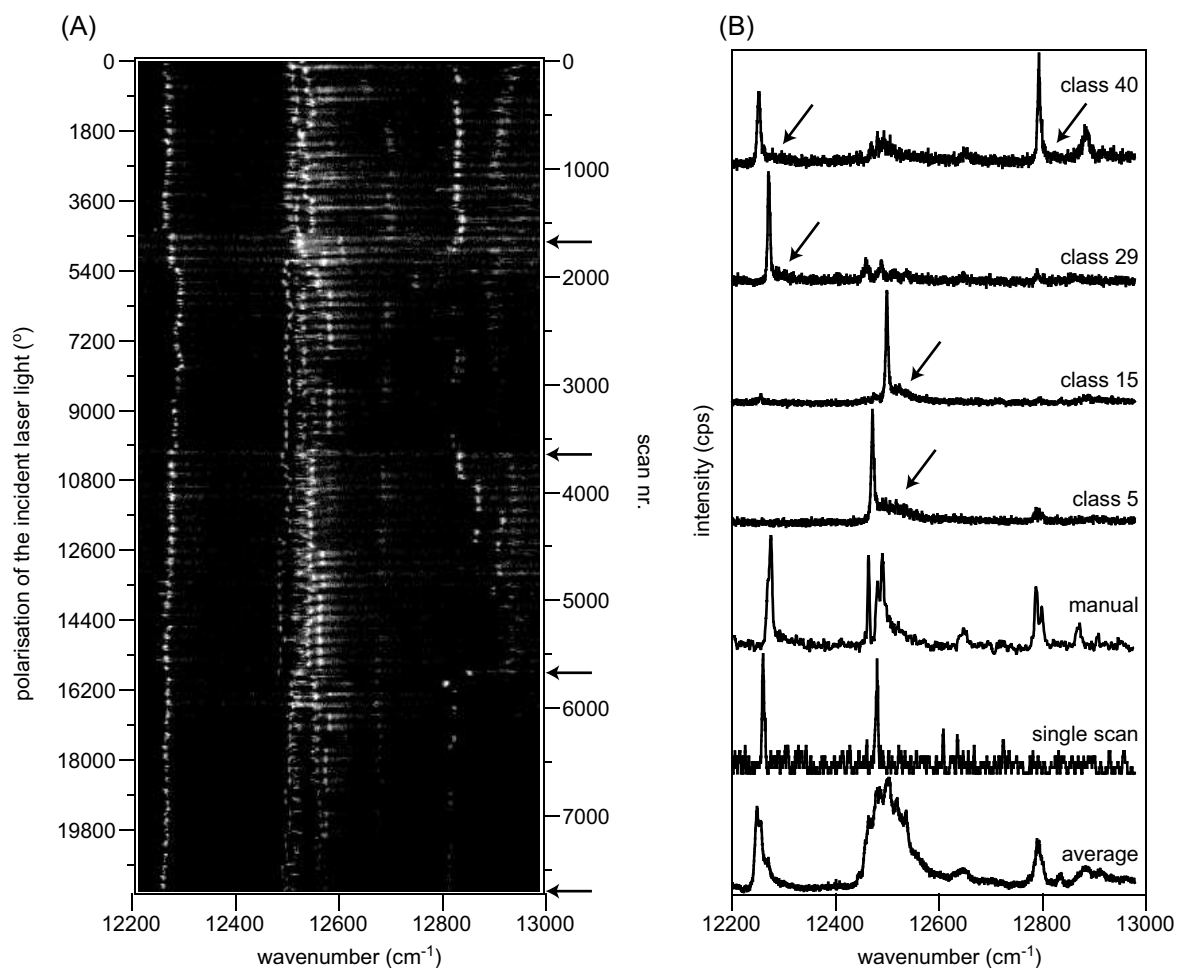


Figure 5.6: Multivariate statistical analysis on a complex of which the spectra were measured for 35 hours. (A) Sequence of 7700 consecutively recorded spectra in a two-dimensional representation displaying polarisation of the incident laser light versus wavenumber. The fluorescence intensity is given by the grey scale. The arrows indicate the end of the measurement on each day. (B) The lowest trace represents the average of all 7700 scans, the one but lowest trace shows a spectrum resulting from a single scan, the second but lowest trace a spectrum that was derived by manually averaging a sequence of 120 similar looking scans and the upper four traces display examples of the averaged spectra of four out of 50 classes.

class-averages the spectrum derived from a single scan is given in the one but lowest trace in the right panel. Only two narrow lines are visible, other less intense features are hidden in the background noise.

When looking closer at the line shape of the individual B800 absorptions an asymmetry is found. A small side band – indicated by the arrows in the spectra in Fig. 5.6B — is present at the high-energy side for all lines in the averaged class spectra. This side band can not be found in the average spectrum of all scans (lowest trace in Fig. 5.6B) as it is merged with the

inhomogeneously broadened absorptions, whereas for the spectrum of a single scan (one but lowest trace in Fig. 5.6B) it is not visible due to the low SNR. If a sequence of 120 similar looking scans at around scan number 2500 is averaged (second but lowest trace in Fig. 5.6B), a weak broad sideband can be anticipated for the left-most narrow absorption. However, for the absorptions at around 12450 cm^{-1} the broad sidebands are not visible as the absorptions overlap spectrally. Also, in the case where residual spectral diffusion of an absorption line was removed by fitting each scan with a Lorentzian and shifting the scan such that the maxima coincided (Fig. 4.6) no asymmetry in the line shape was observed. The reason might be that the methods still involves an averaging process over all the different line shapes obtained during the measurement. And going through the B800 band spectra in chapter 4 which each comprise about 35–400 scans yields that these side bands are not visible.

5.3.3 Discussion

It was found that in the average spectrum of all scans the absorption lines are broadened due to spectral diffusion processes and the exact line shape of the individual B800 absorptions can not be extracted from the spectra. In contrast, the IMAGIC-5 software groups those spectra into the same class for which the line shapes of the absorptions are similar thereby eliminating much of the spectral diffusion and unravelling a line shape of a B800 absorption that consists of a narrow peak accompanied by a weak broader feature at the high energy side.

The small side band is indeed a real part of the line shape of an absorption as can be seen

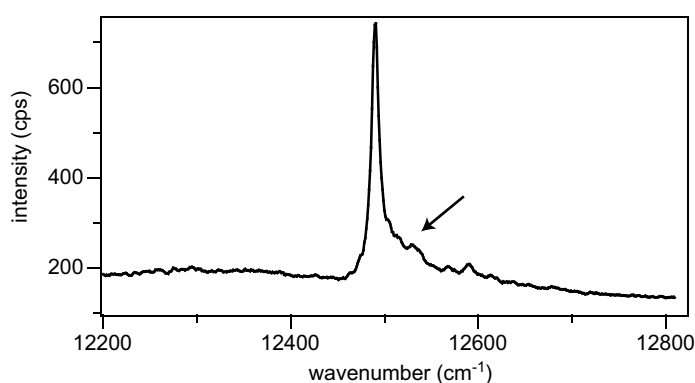


Figure 5.7: Fluorescence-excitation spectrum of the B800 band of an individual LH2 complex from *Rhodospseudomonas acidophila* at 1.4 K. The spectrum features only one narrow absorption line together with a well resolved broad side band marked by the arrow. Adapted from [143].

from a spectrum of a B800 band of LH2 from *Rhodospseudomonas acidophila* recorded by van Oijen *et. al* [143], Fig. 5.7. In this spectrum only one absorption line was found. Therefore, the authors assumed that the variation in site energy of the BChl *a* molecules in this complex was very small, at least smaller than the dipolar interaction strength. As a result, the excitation might have been coherently delocalised over a substantial number of BChl *a* molecules of the B800 ring. This assumption is supported by the high count rate of the absorption. Owing to the concentration of the oscillator strength of all BChl *a* molecules in the B800 ring into one absorption the signal-to-noise of this absorption is very high and a pronounced side band at the larger wavenumber edge marked by the arrow is visible.

The question arises how these narrow lines and broad bands can be interpreted. In this concern it is helpful to look at a theory from Jang and Silbey [155, 156] that describes the line shapes in a multichromophoric macromolecule, i.e., a macromolecule with multiple centres of excitation.

Line shapes of a multichromophoric macromolecule

In a multichromophoric macromolecule (MCMM), interaction between the chromophores can lead to a coupling of their excited states forming an exciton manifold. The absorption and emission line shapes of this manifold will be affected by intramolecular motions and fluctuations in the environment. Fast dephasing and relaxation dynamics of the excitonic states will cause homogeneous broadening of the lines whereas structural and energetic fluctuations much slower than the lifetime of the excited state result in inhomogeneous broadened lines as discussed in section 2.2.2. In ensemble spectroscopy these slow fluctuations may not be noticeable if their distribution is narrower than that of the static disorder in the system. However, in single molecule spectroscopy (SMS) fluctuations can accumulate during the timescale of the experiment thereby substantially affecting the observed line shape.

Although many experiments have been performed using single-molecule spectroscopy only few have considered the information retained in the experimental line shapes [157–160]. In [155] Jang and Silbey have developed a theory that accounts for the two major line broadening contributions. They introduce the concept of an “ideal line shape” (ILS) of a MCMM. For this concept they categorise the degrees of freedom in the system into two categories depending on the timescale at which they occur. The microscopic degrees of freedom that are slower than the lifetime of the excited state but much faster than the measurement time are characterised by a

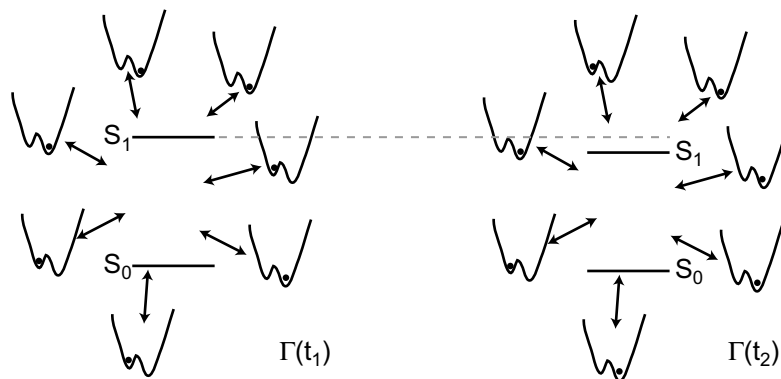


Figure 5.8: Schematic sketch of the interaction (indicated by the arrows) of a chromophore with its environment. The microscopic degrees of freedom of the environment $\Gamma(t)$ are indicated by two level systems for two times $t_1 < t_2$ and the ground and excited state energies of the chromophore are indicated by S_0 and S_1 , respectively. The occupation of the two level systems fluctuates in time which is reflected by a change in the excited state energy of the chromophore.

value called $\Gamma(t)$. All other slow degrees of freedom are assumed to contribute as time dependent fluctuations of the parameters entering the system Hamiltonian. The ILS is the line shape resulting from the hypothetical situation in which an experiment can be conducted on a single MCMM with a fixed value of $\Gamma(t)$. In Fig. 5.8 a hypothetical situation is sketched in which the degrees of freedom in the environment of a chromophore are indicated by two level systems (TLS) for two different times, $t_1 < t_2$. The fluctuations in the environment between t_1 and t_2 are indicated by different occupations of the TLSs and are reflected in the change of the transition energy of the chromophore. Single-molecule spectroscopy involves multiple excitations over a long measurement time during which $\Gamma(t)$ fluctuates. It is clear that an accumulation of such changes of the excited-state energy results in a broadening of the absorption line shape of the chromophore and. Consequently, the measured line shape will appear broader than that of the ILS.

The line shape extracted by the MSA algorithm

In summary, Jang and Silbey clearly showed that the line shape of an absorption of a multi-chromophoric macromolecule (MCMM) derived from single-molecule spectroscopy is different from its ideal line shape, which is the line shape in the absence of slow structural and energetic fluctuations, i.e., without any inhomogeneous broadening effects.

The question that arises is whether the pattern recognition approach using the MSA algorithm

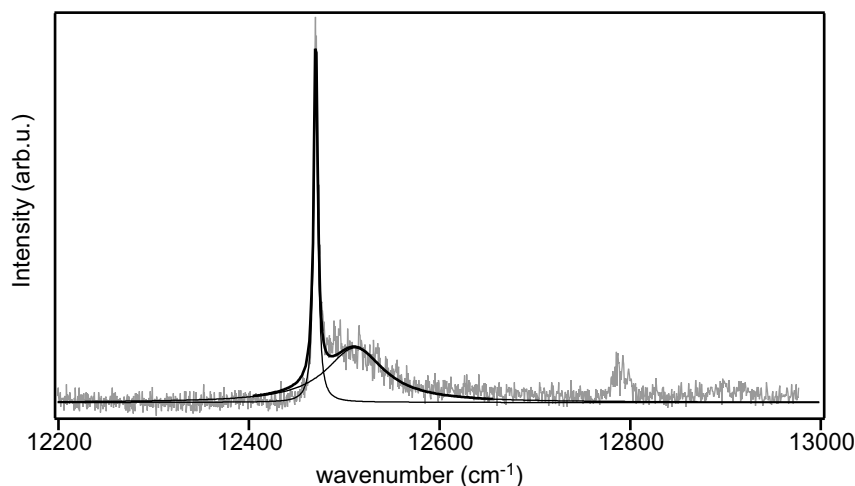


Figure 5.9: Fit of the class average spectrum of class nr. 5 with a two-fold Lorentzian. The experimental data is shown in grey, whereas the fitted data is shown in black. The bold black curve indicates the two-fold Lorentzian and the slim black lines the individual Lorentzian curves.

has extracted the ideal line shape from the series of SMS spectra. As a large number of spectra was recorded, the environment of the complex will have been in the same configuration (i.e., have had the same Γ) for some of the spectra. This group of spectra do not show any type of spectral diffusion and the average of the spectra that have been recorded at different times would comprise the ideal line shapes of the B800 absorptions. By looking at Fig. 5.8 it becomes immediately clear that the transition energies of the chromophores depend on Γ . For equal values of Γ , the transition energies will be equal and the fluorescence-excitation spectra will look alike. The IMAGIC-5 software groups similar looking spectra together and the interpretation is that each class comprises spectra that have been recorded at times during which the system featured similar values of Γ . Then, the average class-spectrum would consist of or get close to the ideal line shapes of the B800 absorptions for a specific configuration of the complex and its environment.

Thus, the narrow peak and the small side band in the B800 absorptions are attributed to closely resemble the ideal line shape of a B800 chromophore absorption. The small broad band is thought to represent a phonon side-band (PSB) of the narrow and intense absorption which itself is assigned to represent the zero-phonon line (ZPL) as described in Sec. 2.2.2. The full widths at half maximum, intensities, and spectral distance could be determined for the ZPL and PSB (see Tab. 5.2), from the absorption lines indicated with an arrow in Fig. 5.6B by fitting the absorptions with a two-fold Lorentzian, see for an example Fig. 5.9.

Parameter	<i>Rs. molischianum</i> (this work)	<i>Rps. acidophila</i> [75] (literature)	LH complexes [161] (literature)
FWHM of ZPL	4–8.4 cm ⁻¹	≈ 5 cm ⁻¹	
FWHM of PSB	21–73 cm ⁻¹		30–40 cm ⁻¹
ω_m	22–56 cm ⁻¹	20–30 cm ⁻¹	≈ 20 cm ⁻¹
C_{DW}	0.43–0.81	0.74	0.6
S	0.21–0.84	0.3	0.5

Table 5.2: Parameters of the ZPLs and PSBs of LH2 complexes from *Rs. molischianum* (Fig. 5.6B) at 1.4 K, *Rps. acidophila* at 4.2 K [75] and average values for several light-harvesting complexes at 4.2 K [161]. ω_m denotes the mean phonon frequency, i.e., the distance between the ZPL and the PSB, C_{DW} the Debye-Waller factor and S the Huang-Rhys factor as defined in Eq. 2.5.

The assumption, that the narrow line and the broad side band are a zero-phonon line and a phonon side-band leads to the conclusion that the electron-phonon coupling is very weak in the B800 ring of the LH2 complex from *Rs. molischianum*. This finding is corroborated by persistent spectral hole burning measurements that were used to study electronic structure and energy relaxation in a large number of antenna complexes [110, 161]. In all cases the electron-phonon coupling for the Q_y states was found to be weak even when the complex possesses a structural unit containing several strongly exciton-coupled BChl molecules such as the LH1 and the B850 ring in the LH2 complexes [162, 163]. The Huang-Rhys factor was on average 0.5 and the distance between the ZPL and the PSB 20 cm⁻¹ [161]. Because the electron-phonon coupling is weak in the antenna complexes, the PSBs were dominated by the one-phonon profile.

Comparing the measured data on *Rs. molischianum* with the hole-burning data on *Rps. acidophila* in the literature it can be seen that the mean phonon frequency and the width of the phonon distribution is slightly larger for *Rs. molischianum*, Tab. 5.2. Whether this is significant or not is not clear and deserves further investigation. In contrast the Huang-Rhys factor is in agreement with the data from literature.

5.4 Summary

The IMAGIC-5 software was applied to the analysis of several LH2 complexes. By multivariate statistical analysis, the consecutively recorded scans were grouped into classes of similar scans.

First, the software was tested for its applicability on spectroscopic data on two previously analysed complexes featuring different types of spectral diffusion. In the case of simultaneous spectral diffusion where a complex can change between two different realisations featuring two distinct fluorescence-excitation spectra the software classified the spectra belonging to the same realisations into the same group. In the case of spectral switching where two absorbers switched independently from each other between two different absorption frequencies the software could detect the correlation within and the absence of correlation between the pairs of absorption lines. Thus, the software proved to be useful in analysing spectroscopic data from single-molecule experiments.

In the second step, a complex for which a huge numbers of scans had been recorded was analysed. The IMAGIC-5 software could extract details about the line shape of individual absorptions by eliminating inhomogeneous broadening due to spectral diffusion within a small wavenumber region. The line shapes extracted by the software were thought to represent the ideal line shapes (ILS) of a B800 BChl *a* absorption in the LH2 complex from *Rs. molischianum* according to the theory of Jang and Silbey [155]. A broad side band was found at the larger wavenumber side of the absorptions which was interpreted as a phonon side band. From the relative intensities of the ZPL and the PSB, the Huang-Rhys factor was found to range from 0.21–0.84 indicating that the B800 band is dominated by very weak electron-phonon coupling.

An application for the IMAGIC software might also lie in the analysis of the B850 band of LH2. For this band normally two broad absorption bands are observed in the fluorescence-excitation spectrum whose line shapes appear identical in low temperature single-molecule experiments. However, the ideal line shape theory from Jang and Silbey predicts that the linewidths of the two bands should be different [155, 156]. It would be interesting whether an analysis of the B850 band of LH2 with the IMAGIC-5 software could reveal this difference.

The B850 band of LH2 from *Rhodopseudomonas acidophila*

In the B800 ring of LH2 it was observed that the distance between the chromophores was about 20 Å leading to an interaction strength between the chromophores of $V \approx 20 \text{ cm}^{-1}$. The width Δ of the Gaussian distribution of site energies (i.e., the intra complex disorder) was determined as 280 cm^{-1} . This width Δ should not be confused with the average difference in site energy of two adjacent molecules δ . The ratio $V/\Delta \ll 1$ is consistent with the picture that the chromophores in the B800 ring feature a weak to intermediate coupling and that the excitations are mainly localised on individual chromophores.

For the B850 ring in the LH2 complexes the situation is completely different. The small chromophore-chromophore distance of less than 10 Å leads to an interaction strength of $V \approx 250 \text{ cm}^{-1}$, whereas the amount of diagonal disorder in the B850 band $\Delta \approx 250 \text{ cm}^{-1}$ is similar to that of the B800 band [25, 26]. Therefore, the ratio V/Δ is about 1, which is consistent with the interpretation that the excitations are completely delocalised over the pigments in the B850 ring. The observed fluorescence-excitation spectra are dominated by two broad absorption bands featuring a mutual orthogonal polarisation dependence, which result from the circular $k = \pm 1$ exciton states of such a coupled system.

In a series of papers [25, 26, 112] these absorptions in the B850 band of individual LH2 complexes from *Rps. acidophila* were analysed in view of their energetic separation, their intensity ratio and the mutual orientation of the related transition-dipole moments. From the distributions of these parameters the amount of energetic and structural disorder in the LH2 complexes was estimated and it was suggested that the LH2 complexes might be significantly elliptically deformed. However, the conclusions were drawn on the basis of 24 LH2 complexes. The statistical significance of the distributions might therefore be questioned and more detailed statements about the random and correlated disorder in the B850 band could not be made.

In this chapter measurements on the B850 band of LH2 complexes from *Rps. acidophila* were conducted using a novel experimental technique allowing to measure as many as 146 complexes in several days as opposed to weeks needed for the 24 complexes in the experiments described in the literature. The results agree with the outcome of the previous experiments, but the new approach allows to extract much more detailed information at a higher statistical significance.

6.1 Geometric structure of the B850 ring

The light-harvesting 2 complex from *Rps. acidophila* consists of — similar to the LH2 complex from *Rs. molischianum* which was discussed in Sec. 2.1.2 — $\alpha\beta$ -heterodimers which non-covalently bind one B800 and two B850 BChl *a* molecules as well as two carotenoids. The main difference is the nine-fold symmetry of *Rps. acidophila* in contrast to the eight-fold symmetry of *Rs. molischianum* [2, 4]. The arrangement of the chromophores in the B850 ring is shown in detail in Fig. 6.1 together with the orientations of their Q_y absorption dipole moments. The Mg- α -B850 to Mg- β -B850 distance is 9.6 Å within a dimer and 8.9 Å between dimers.

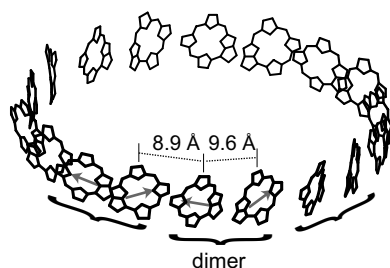


Figure 6.1: Detailed view on the spatial arrangement of the B850 BChl *a* pigments from *Rhodospseudomonas acidophila*. The phytol chains are omitted for clarity. The numbers indicate the inter- and intra-dimer centre to centre distances of the pigments. The arrows indicate the orientation of their Q_y transition-dipole moments.

6.2 Electronic structure of the B850 ring

The numerical derivation of the spectrum of an aggregate of closely interaction pigments was discussed in Sec. 2.2.3 and it was shown that random and correlated disorder in the site energies as well as in the interactions influence the appearance of the spectra. In previous work by van Oijen *et al.* [25], Ketelaars *et al.* [26] and Matsushita *et al.* [112] it was concluded that a correlated C₂-type of disorder had to be present in the system. This was introduced through a modulation of the interactions, which led to the assumption that the ring was structurally deformed into an ellipse with an deformation amplitude $\delta r/r_0 \approx 7\text{--}8.5\%$, where r_0 is the radius of the unperturbed ring and the long and short axes of the ellipse deviate from r_0 by δr [25, 26, 112]. The C₂-type perturbation was expressed as a $\cos(2\theta)$ modulation of both the nearest- and second-neighbour interaction energies, where θ gives the angular position of the pigment in the ring.

In general, the C₂-type perturbation can be introduced into the off-diagonal elements of the Hamiltonian (i.e., the interaction) as done in the literature as well as through a $\cos(2\theta)$ modulation of the diagonal elements (i.e., the excited state energies). The Hamiltonian including the random diagonal and correlated diagonal and off-diagonal disorder reads:

$$\begin{aligned}
 H &= \sum_{n=1}^{18} \{E_{0,n} + E_{\text{mod}} \cos(2\phi n) + \delta E_n\} |n\rangle \langle n| \\
 &+ \sum_{n=1}^{18} \left\{ V_{0,n} + V_{\text{mod}} \cos \left[2\phi \left(n + \frac{1}{2} \right) \right] \right\} [|n\rangle \langle n+1| + \text{H.c.}] \\
 &+ \sum_{n=1}^{18} \{W_{0,n} + W_{\text{mod}} \cos [2\phi(n+1)]\} [|n\rangle \langle n+2| + \text{H.c.}], \quad (6.1)
 \end{aligned}$$

where $E_{0,n}$ denotes the site-energy of the individual pigment, $V_{0,n}$ and $W_{0,n}$ are the nearest- and second-neighbour interactions, respectively, E_{mod} , V_{mod} and W_{mod} are the amplitudes of the modulation of the energies, the nearest- and second-neighbour interaction, respectively, $\phi = 2\pi/N$, with $N = 18$ the number of pigments in the ring and H.c. stands for the Hermitian conjugate of the preceding term. The amplitude W_{mod} was taken to be 12% of V_{mod} based on the assumption that V_{mod} and W_{mod} scale similarly as $V_{0,n}$ and $W_{0,n}$. In this work, the inter-pigment interactions are taken into account up to second neighbours. Each $\alpha\beta$ -heterodimer binds two B850 chromophores which is taken into account by introducing a dimerisation into

the ring and assigning different site-energies to the α - and β -bound pigments [26]. As a dimer, the $\alpha\beta$ unit with the tail-tail configuration of the Q_y transition-dipole moments was chosen.

The $\cos(2\theta)$, or C_2 -type of perturbation couples only excited states that have a difference of their quantum number $\Delta k = \pm 2$. The dominant effect of the modulation is the coupling between the $k = \pm 1$ states. Their degeneracy is lifted and the oscillator strength is redistributed among the exciton states. Obeying the $\Delta k = \pm 2$ selection rule, only the energetically close $k = \pm 3$ states gain significant oscillator strength, whereas the C_2 perturbation does not give rise to an extra oscillator strength of the $k = 0$ state. Its oscillator strength results from the presence of random disorder only.

The energy transfer among the B850 chromophores is about 100 fs [76–78], and consequently the states are assigned a homogeneous linewidth of 100 cm^{-1} . The lowest exciton state has a relative long fluorescent lifetime of approximately 1 ns [79]. However, as the experimentally observed linewidth is determined by the spectral resolution of the measurement it is assigned a linewidth of 1 cm^{-1} .

In the previous work mentioned before [25, 26, 112] it was found that fluorescence-excitation spectra of the B850 band of individual LH2 complexes are dominated by few broad absorptions (see also Fig. 6.3). The gross spectral features were compatible with the exciton model of a circular aggregate of nine dimers as described in Sec. 2.2.3 and the two lowest energetic absorptions were assigned to the low energy $k = \pm 1$ exciton states. This assignment was done on the basis of the observation that the transition-dipole moments are orthogonal and lie in the plane of the ring. Further support for the model came from the observation of a narrow absorption line at the red edge of the lowest energetic of the $k = \pm 1$ bands in some of the spectra. Additional broad absorption bands at higher energies were attributed to higher exciton states. The lifting of the degeneracy of the $k = \pm 1$ states and the appreciable oscillator strength of the $k = 0$ and the higher exciton levels was ascribed to random disorder in the excited state energies together with a perturbation of the circular symmetry of the LH2 complexes from which it was inferred that the LH2 complexes were subjected to an elliptical deformation.

For most spectra, the narrow $k = 0$ absorption line was not observed. It was found that this line undergoes fast spectral diffusion processes and it was assumed it could be “smeared out” in the underlying broad absorption band which prevents it from being observed in the spectra. However, its oscillator strength still adds to the observed intensity of the red-most absorption

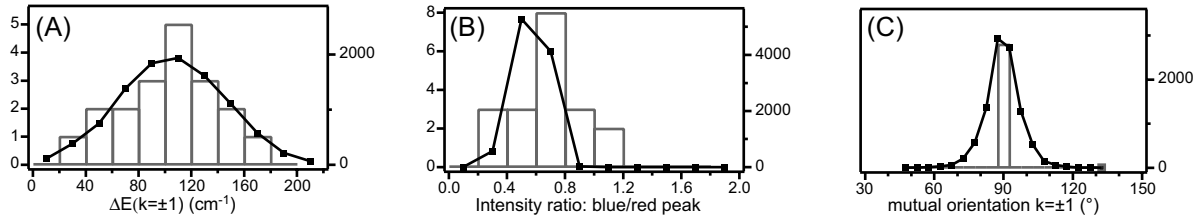


Figure 6.2: Comparison between the experimental distributions (histograms) and numerical simulations (solid squares), adapted from [25, 26, 112]. The experimental data refer to the left vertical scale, whereas the simulations refer to the right vertical scale. The details of the simulations are given in the text. (A) Energy separation of the two $k = \pm 1$ transitions. (B) Intensity ratio blue peak/red peak ($I_{k=-1}/I_{k=0,+1}$) of the two $k = \pm 1$ transitions. (C) Mutual angle between the $k = \pm 1$ transition dipole moments.

band. Therefore, when looking at the intensity ratio between the two lowest energetic band, always $(I_{k=0} + I_{k=+1})/I_{k=-1} = I_{k=0,+1}/I_{k=-1}$ is considered.

The experimental distributions (histograms) together with numerical simulations (solid squares) of several parameters derived from the 24 complexes measured previously using confocal fluorescence-excitation spectroscopy [25, 26, 112] are shown in Fig. 6.2. Quantitative details on the parameters can be found in Tab. 6.1. The energy separation between the $k = \pm 1$ transitions ($\Delta E_{k=\pm 1} = 105 \pm 38 \text{ cm}^{-1}$) is shown in (A), the intensity ratio of the blue (i.e., the higher energetic) band and the red (i.e., the lower energetic) band $I_{k=-1}/I_{k=0,+1} = 0.7 \pm 0.2$ in (B) and the mutual angle $\Delta \alpha_{k=\pm 1} = 90 \pm 0^\circ$ between the $k = \pm 1$ transition dipole moments is shown in Fig. 6.2C. Due to the low angular resolution of $\approx 30^\circ$, no distribution of the mutual angles around 90° was observable. For their simulations, of the B850 band of the LH2 complex from *Rps. acidophila*, a site energy of the α -bound pigments of $E_{0,\alpha} = 12300 \text{ cm}^{-1}$ and a site of the β -bound pigments of $E_{0,\beta} = 12060 \text{ cm}^{-1}$ represented a reasonable set of parameters for the energies [25, 26, 112]. Using the point-dipole approximation (Sec. 2.2.3) the interactions between the pigments can be calculated and are given for a perfect circular ring: intra-dimer interaction $V_i = 254 \text{ cm}^{-1}$, inter-dimer interaction $V_e = 226 \text{ cm}^{-1}$, second neighbour interaction between α -bound pigments $W_i = -35 \text{ cm}^{-1}$ and second neighbour interaction between β -bound pigments $W_e = -25 \text{ cm}^{-1}$. The authors assumed a Gaussian distribution of the site energies of a width $\Delta = 250 \text{ cm}^{-1}$ and a modulation amplitude in the interactions of $V_{\text{mod}} \approx 63 \text{ cm}^{-1}$ (25%) which they ascribed to an elliptical deformation of the complex with an deformation amplitude of $\delta r/r_0 = 8.5\%$ [26, 112].

The results of the numerical simulations of the single LH2 spectra were confirmed by an ana-

lytical analysis of the data by Mostovoy and Knoester [20]. If the parameters the authors used are translated to the notation used in this thesis, they found the best accordance for a random energetic disorder with a width $\Delta = 235 \text{ cm}^{-1}$ and an elliptical deformation of the complexes with a deformation amplitude $\delta r/r_0 = 7.5\%$. These numbers agree very well with the numbers derived from the numerical simulations.

6.3 Experimental results

In the top trace of Fig. 6.3A (grey) the spectrum of the B850 band from a large ensemble of LH2 complexes from *Rhodospseudomonas acidophila* is shown which features a single broad band

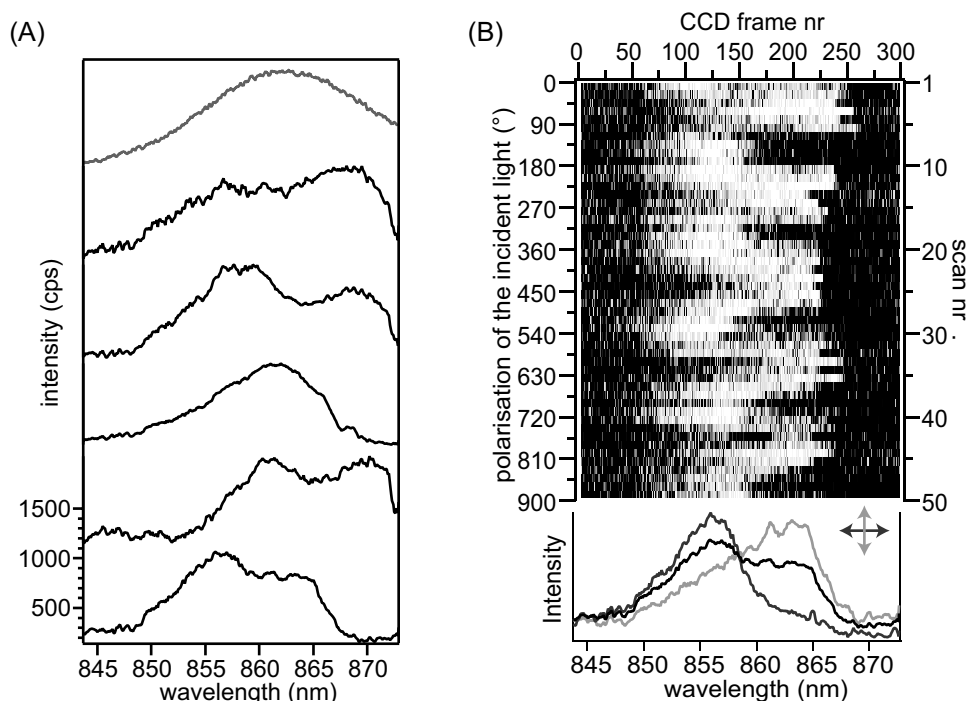


Figure 6.3: Fluorescence-excitation spectra of the B850 band of LH2 complexes from *Rps. acidophila*. (A) The top trace shows an ensemble spectrum (grey), whereas the lower five traces display spectra from single LH2 complexes (black). Each spectrum has been averaged over all possible excitation polarisations. The vertical scale is valid for the lowest trace, all other traces are offset for clarity. All spectra were recorded at 1.4 K with an excitation intensity of 30 W/cm^2 . (B) Spectral diffusion pattern of the B850 band of an individual LH2 complex from *Rps. acidophila*. In the upper panel a time sequence of 50 spectra obtained by widefield fluorescence-excitation spectroscopy is shown. The horizontal axis corresponds to CCD-frame number as well as wavelength of the excitation light. After each scan the polarisation of the incident laser light was rotated by 18° . The average spectrum of all scans (black) together with two spectra with mutually orthogonal polarisation (dark and light grey) as indicated by the arrows is given in the lower panel.

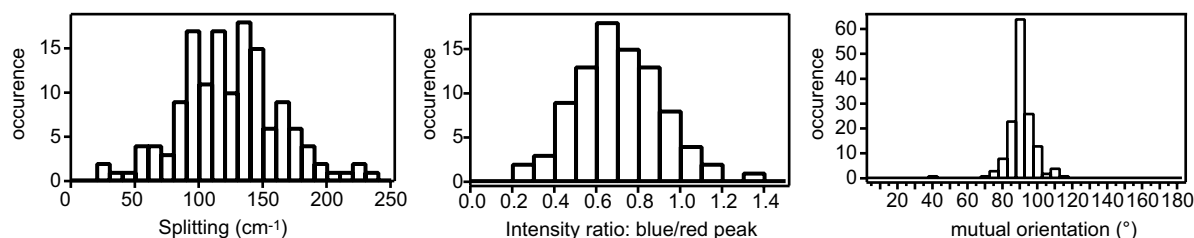


Figure 6.4: Histograms of some parameters concerning the B850 band of LH2 from *Rps. acidophila*. (A) Energy separation of the two lowest energetic transitions. (B) Intensity ratio blue peak/red peak of the two transitions. (C) Mutual angle between the related transition dipole moments.

at around 860 nm. Example fluorescence-excitation spectra of the B850 ring of five individual LH2 complexes (black) are shown in the lower part. The spectra were measured using widefield fluorescence-excitation spectroscopy (Sec. 3.4). The fluorescence of typically 40–60 complexes was measured simultaneously with an EMCCD camera while at the same time consecutively scanning the wavelength of the excitation laser. Consequently, the CCD-frame number corresponds to wavelength and by integrating the total intensity of an individual complex on the CCD as a function of read-out frame a fluorescence-excitation spectrum was obtained. This procedure was repeated three times and yielded in total 146 B850 spectra. In most of the spectra from the single complexes 2–3 broad absorption lines at around 860 nm are observed.

An example of the spectral diffusion pattern of the B850 band of a single LH2 complex is shown in Fig. 6.3B. The laser was scanned 50 times between 843 and 873 nm at a speed of about 0.16 nm/s. It could not be scanned to larger wavelengths due to the combination of optical excitation and emission filters. The excitation intensity was 30 W/cm². While scanning the laser the CCD acquired about 300 images of 260×250 pixels at a speed of 620 ms per image (500 ms accumulation time of the fluorescence and 120 ms read-out time). This yields a nominal spectral resolution of 0.1 nm. After each scan the polarisation of the incident laser light was rotated by 18°. The whole series of 50 scans corresponds to five complete turns of the polarisation which allowed to determine polarisation angles to within about 10° accuracy.

From the spectral diffusion patterns, the energetic difference between the two red-most broad peaks, their intensity ratio and the mutual angle of polarisation were determined. In Fig. 6.4 the histograms of these values are depicted for all measured complexes. The average energy separation between the two bands amounts to 126 ± 43 cm⁻¹, the intensity ratio of the blue peak and the red peak to 0.73 ± 0.23 and the mutual orientation of the transition dipole moments is distributed around $91 \pm 8.0^\circ$. If the histograms from literature (Fig. 6.2) are compared with

the distributions derived in this work using widefield fluorescence-excitation spectroscopy as depicted in Fig. 6.4 it becomes obvious the newly developed technique has a clear advantage concerning the statistical significance of the data.

6.4 Discussion

This chapter focuses on the two lowest energetic absorptions in the B850 band of individual LH2 complexes from *Rps. acidophila* which are assigned to the low energy $k = \pm 1$ exciton states in accordance with previous observations [25, 26, 112]. In this work, a narrow line, arising from the lowest exciton state $k = 0$ was never observed as opposed to the previous measurements described in Sec. 6.2 which is probably due to the experimental method used for this work. For a comparable signal-to-noise ratio the acquisition time in the widefield method (≈ 500 ms) has to be much longer than for the confocal method (≈ 10 ms). If the spectral resolutions are kept comparable (0.1 nm for the widefield versus 0.07 nm for the confocal method) the scan speed at which the spectra are recorded has to be much slower for the widefield approach (0.16 nm/s) compared to the confocal method (3 nm/s). This prohibits to resolve narrow absorption lines that undergo fast spectral diffusion processes such as those measured for the B800 band in chapter 4 or the $k = 0$ transition in the B850 band [25, 26, 112].

However, for the broad (50–250 cm^{-1}) absorption bands of the $k = \pm 1$ transitions in the exciton manifold of the B850 band of LH2 the widefield method is by far superior as has been shown by the comparison of the experimental distributions in Figs. 6.2 and 6.4. This is due to the large parallelisation in the recording of the data. Using an electron-multiplying CCD camera the spectra of 40–60 individual complexes can be recorded at the same time in the widefield-setup whereas in the confocal system the complexes have to be measured one by one with an avalanche photodiode. In comparison to confocal fluorescence-excitation spectroscopy the widefield approach allows to speed up the measurement time by a factor of about 50.

To analyse the observations, at first the influence of random disorder on the properties of the $k = \pm 1$ exciton levels of the unperturbed ring of B850 BChl *a* pigments is considered. The only fitting parameter in this configuration is the width of the distribution of site energies which is used to fit the average energetic splitting of the $k = \pm 1$ states. The simulations are based on a Monte Carlo calculation averaged over 5 000 iterations, each with a pseudo-random choice

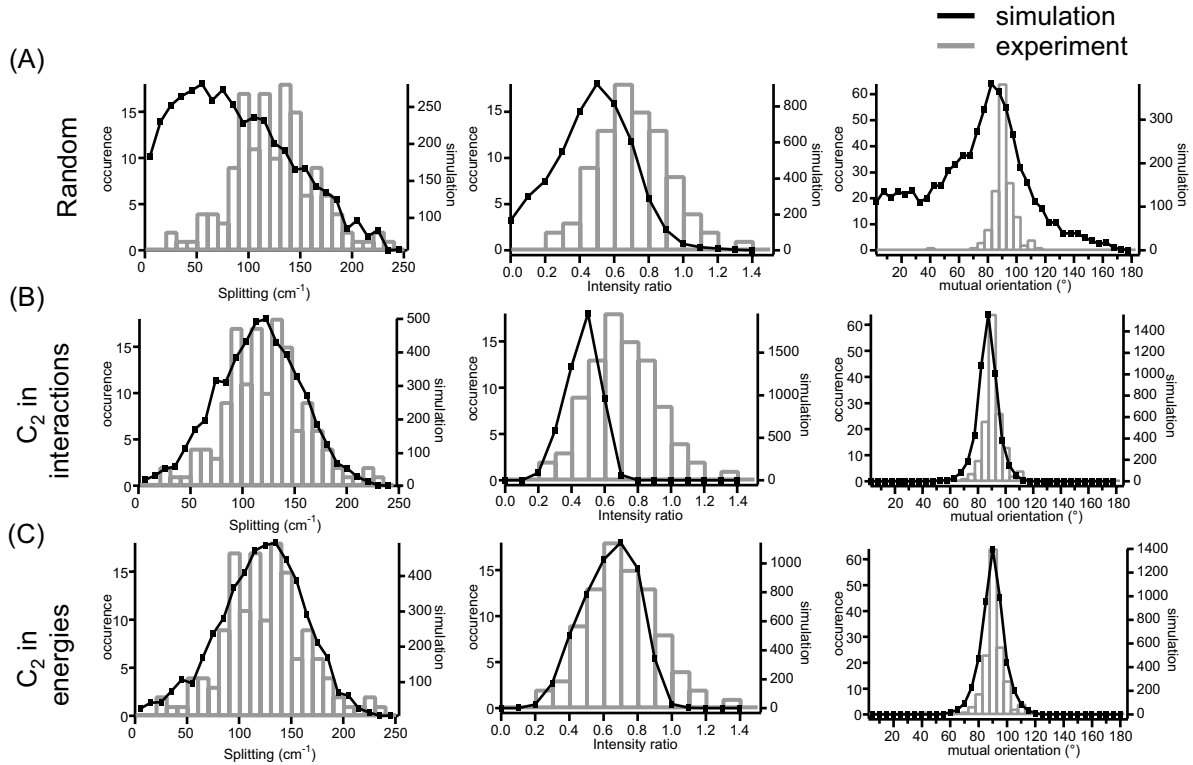


Figure 6.5: Comparison between the experimental distributions (histograms) from Fig. 6.4 and numerical simulations (solid squares) of different types of disorder. The experimental data refer to the left vertical scale, whereas the simulations refer to the right vertical scale. For details on the simulations see text and Tab. 6.1. For each type of disorder, the left panel displays the energy separation of the two $k = \pm 1$ transitions, the middle panel the intensity ratio blue peak/red peak ($I_{k=-1}/I_{k=0,+1}$) of the two $k = \pm 1$ transitions and the right panel the mutual angle between the $k = \pm 1$ transition-dipole moments. (A) In the simulation only random disorder in the energies is taken into account. (B) Apart from random disorder in the energies a C_2 -type modulation of the interactions is included in the simulation. (C) Random disorder in the energies as well as an additional C_2 -type modulation in the excited state energies is accounted for in the simulations.

of site energies from a Gaussian distribution of width Δ . To obtain the observed splitting of 126 cm^{-1} for the $k = \pm 1$ states a random disorder with $\Delta = 950 \text{ cm}^{-1}$ has to be used in the simulations. In Fig. 6.5A the results of the simulations are shown (black line) together with the experimental data (grey histograms). A summary of all relevant parameters is given in Tab. 6.1 in the column labelled “random”.

The large disorder of $\Delta = 950 \text{ cm}^{-1}$ implies a strongly broadened exciton manifold which should be reflected by the spectral width of the ensemble spectrum. As the observed width is only about 300 cm^{-1} , the assumption of the simulation is in total contradiction to the observations. This contradiction is continued if the outcome of the simulations for the different parameters is compared to the observed distributions. Although the average energetic splitting

parameter	experiment	simulation			literature	
		random	C_2 in int.	C_2 in energy	experiment	C_2 in int.
$\Delta E_{k=\pm 1}$ (cm ⁻¹)	126 ± 43	122 ± 89	122 ± 41	126 ± 42	105 ± 38	103 ± 39
$I_{k=-1}/I_{k=0,+1}$	0.73 ± 0.23	0.53 ± 0.22	0.52 ± 0.10	0.69 ± 0.16	0.7 ± 0.2	0.57 ± 0.10
$\Delta\alpha_{k=\pm 1}$ (°)	91 ± 8.0	73 ± 35	89 ± 7.9	90 ± 8.9	90 ± 0	89 ± 8.1
Δ (cm ⁻¹)		950	250	250		250
E_{mod} (cm ⁻¹)		0	0	180 (1.5%)		0
V_{mod} (cm ⁻¹)		0	75 (30%)	0		63 (25%)
$\delta r/r_0$ (%)		0	10	0		8.5

Table 6.1: Comparison between the experimentally and numerically obtained values of the energy separation of the two $k = \pm 1$ transitions $\Delta E_{k=\pm 1}$, the intensity ratio blue peak/red peak of the two $k = \pm 1$ transitions $I_{k=-1}/I_{k=0,+1}$ and the mutual angle between the $k = \pm 1$ transition dipole moments $\Delta\alpha_{k=\pm 1}$. Listed are the values derived by widefield fluorescence-excitation spectroscopy in this work (experimental), by a simulation including only random disorder (random), a simulation including random disorder and a modulation in the interaction strengths (C_2 in int.) and a simulation including random disorder and a modulation in the site energies (C_2 in energy). For comparison, the experimental values (experiment) as well as the parameters for the simulation including random disorder and a modulation in the site energies (C_2 in int.) of the confocal fluorescence-excitation spectroscopy measurement from [25, 26, 112] are given in the “literature” labelled columns. The parameters that were used in the simulations are the width of the Gaussian distribution of site energies Δ , the correlated modulation in site energies E_{mod} and the correlated modulation of the interaction strengths V_{mod} which is possibly induced by an elliptical deformation of the circular ring with a deformation amplitude $\delta r/r_0$, see also Eq. 6.1.

of the $k = \pm 1$ states in the simulation is equal to that of the experimental distribution as can be seen in Tab. 6.1 its maximum peak and its width differ significantly, Fig. 6.5. The average intensity ratio derived by the simulation is too low, although the shape is comparable to that of the experimental distribution. Note that introduction of random disorder does not change the intensity ratio $I_{k=+1}/I_{k=-1} = 1$ of the undisturbed system but only causes a lifting of the degeneracy of the $k = \pm 1$ states. Because the $k = 0$ absorption line is “smeared out” by spectral diffusion processes in the underlying $k = +1$ absorption band the intensity ratio of the blue and red band are always observed as $I_{k=-1}/I_{k=0,+1}$ which is less than 1. Consequently, also in the numerical simulations the intensity ratio of $I_{k=-1}/I_{k=0,+1}$ is considered. In the case of the mutual orientations between the transition-dipole moments the simulation can not reproduce the experimentally derived distribution.

Because of the statistical significance of the distributions in this work it is reasonable to conclude solely on the basis of the $k = \pm 1$ transitions that an alternative explanation for the ob-

served features of the $k = \pm 1$ states has to be found. In the previous work discussed in Sec. 6.2 the spectral properties of higher exciton levels were also studied and it was found consistently that random disorder alone is not sufficient to explain the optical features of the experimentally obtained spectra.

In the next step, a C_2 -type modulation of the interactions between adjacent BChl *a* molecules was introduced in addition to random energetic disorder as proposed in the literature [25, 26, 112]. The fitting parameters in this situation are the modulation amplitude of the nearest-neighbour interaction V_{mod} and the width of the distribution of site energies which are used to fit the average energetic splitting of the $k = \pm 1$ states and the width of the distribution of splittings. To obtain the observed splitting of $126 \pm 43 \text{ cm}^{-1}$ random disorder with $\Delta = 250 \text{ cm}^{-1}$ and a modulation amplitude of $V_{\text{mod}} \approx 75 \text{ cm}^{-1}$, i.e., $V_{\text{mod}}/V_0 \approx 30\%$ are required in the simulation. In Fig. 6.5B the results of the simulations are shown (black line) together with the experimental data (grey histograms). A summary of all relevant parameters is given in Tab. 6.1 in the column labelled “ C_2 in int.”.

This model explains the major spectral features of the $k = \pm 1$ transitions, i.e., their energetic splitting $\Delta E_{k=\pm 1} \approx 122 \pm 41 \text{ cm}^{-1}$ and the mutual orientation of the $k = \pm 1$ transition-dipole moments $\Delta \alpha_{k=\pm 1} \approx 89 \pm 8^\circ$. However, the outcome of the simulations where $I_{k=-1}/I_{k=0,+1} = 0.52 \pm 0.10$ is not compatible with the observed distribution of the intensity ratio of the peaks $I_{k=-1}/I_{k=0,+1} = 0.73 \pm 0.23$. The calculated average value is too low and the width too small. The origin of the modulation of the interactions might be attributed to a structural C_2 -type deformation of the complex. C_2 is the lowest symmetry component of an ellipse and therefore, the modulation of the interactions of $V_{\text{mod}} = 75 \text{ cm}^{-1}$ could be ascribed to an elliptical deformation with $\delta r/r_0 = 10\%$. However, the reduced symmetry of the LH2 complexes due to the elliptical deformation contravenes the nine-fold symmetry of LH2 in crystalline form.

Alternatively a C_2 -type modulation was introduced in the excited state energies in addition to random energetic disorder. The fitting parameters in this situation are the modulation amplitude of the energies E_{mod} and the width of the distribution of site energies which are again used to fit the average energetic splitting of the $k = \pm 1$ states and the width of the distribution of splittings. Here, random disorder with $\Delta = 250 \text{ cm}^{-1}$ and a modulation amplitude of $E_{\text{mod}} \approx 180 \text{ cm}^{-1}$, i.e., $E_{\text{mod}}/E_0 = 1.5\%$ are required in the simulations to obtain the observed splitting of $126 \pm 43 \text{ cm}^{-1}$. In Fig. 6.5C the results of the simulations are shown (black line) together with

the experimental data (grey histograms). A summary of all relevant parameters is given in Tab. 6.1 in the column labelled “C₂ in energy”.

This model explains all observed spectral features of the $k = \pm 1$ transitions very well as can be seen in Tab. 6.1. The energetic splitting of the $k = \pm 1$ states of $\Delta E_{k=\pm 1} \approx 126 \pm 42$, the intensity ratio $I_{k=-1}/I_{k=0,+1} = 0.69 \pm 0.16$ and the mutual orientation of the $k = \pm 1$ transition-dipole moments $\Delta\alpha_{k=\pm 1} \approx 90 \pm 9^\circ$ reproduce the experimental observations in all details.

The distinction between a correlated disorder in the interactions or the energies was made upon the fit of the simulation to the experimentally derived distribution of the intensity ratio between the two $k = \pm 1$ absorption bands. Using the histograms from literature, a distinction between the two different types of correlated disorder could not have been made, as the distribution of the intensity ratios contained too few data points. The question that arises is how the modulation in the excited state energies can be explained. In Sec. 4.3.2 it was discussed that conformational fluctuations of the proteins in the binding pocket of the BChl *a* molecules lead to changes in the pigment-protein interaction and therefore to fluctuations in the site energies of the individual BChl *a* chromophores. A structural deformation of the complex will most certainly cause a conformational rearrangement in the binding pockets and result in a perturbation of the site energies of the BChl *a* molecules. Therefore, the coexistence of correlated structural as well as correlated energetic disorder can not be excluded and is, moreover, the most likely situation.

If it is assumed that the modulation in the site energies follows the structural deformation, the C₂-type modulation of the site energies could very well be explained by an elliptical deformation of the complexes in analogy to the situation discussed above. The perturbation of the site energies following an imposed elliptical deformation will require a less pronounced deformation amplitude due to the interplay of the two types of modulations. A small structural deformation would not be resolvable in x-ray crystallography and the model of the correlated disorder coexisting in both site energies as well as in the interactions would be compatible with the observation of circular structures of LH2 in crystalline form.

6.5 Summary

In this chapter two experimental methods to study single molecules were compared in the investigation of the structure of the electronically excited states of the B850 ring of LH2 complexes from *Rhodospseudomonas acidophila*: widefield fluorescence-excitation spectroscopy (data derived in this work) and confocal fluorescence-excitation spectroscopy (data from previous work [25, 26, 112]). The results presented in this chapter show that widefield fluorescence-excitation spectroscopy can be applied successfully to elucidate the electronic structure of photosynthetic pigment-protein complexes. It can be concluded that the B850 assembly of BChl *a* pigments in LH2 represents a strongly coupled system of which the low energy $k = \pm 1$ exciton states could be resolved. The experimental distributions of the energy separation $\Delta E_{k=\pm 1}$ and the intensity ratio $I_{k=-1}/I_{k=0,+1}$ of the two $k = \pm 1$ transitions as well as the mutual angle $\Delta\alpha_{k=\pm 1}$ between the $k = \pm 1$ transition-dipole moments could all be determined with a high statistical significance.

In line with previous work [25, 26, 112] a distribution of the site energies (random diagonal disorder) with a FWHM of 250 cm^{-1} as well as a correlated C_2 -type of disorder had to be assumed to account for the relative intensities and spectral positions of the exciton transitions. In the aforementioned references the experimental distributions were explained by introducing the correlated disorder through a modulation of the interactions of $V_{\text{mod}} = 63\text{ cm}^{-1}$. This modulation was ascribed to arise from an elliptical deformation of the LH2 complexes with a deformation amplitude of $\delta r/r_0 = 8.5\%$. Due to the statistical significance of the data in this work it was found that a C_2 -type modulation in the interactions alone is not sufficient to explain all observed parameters. Based on the results of chapter 4 it was assumed that a small structural deformation of the complex will lead to conformational changes in the binding pockets of the BChl *a* molecules that affect their site energies. By assuming a C_2 modulation in the site energies the observed parameters could be described more accurately than in the case of a modulation in the interactions. Therefore, a combination of a small structural deformation together with a modulation of the site energies will probably reflect the situation in the complexes most appropriately. A small geometrical perturbation instead of the deformation amplitude of 7–10% is also more compatible with the circular structure observed in x-ray crystallography.

The core complex: LH1-RC

In contrast to the peripheral light-harvesting 2 (LH2) complex which is a closed circular array comprising eight or nine $\alpha\beta$ -heterodimers, the x-ray structure of the central light-harvesting 1 (LH1) complex has not been determined as yet and the exact three-dimensional arrangement of its subunits remains to be ascertained. As discussed in Sec. 2.1.2, pigment analysis, the homology of protein subunits and several electron-microscopy experiments lead to the assumption that the LH1 complex is also composed of a circular array of $\alpha\beta$ -heterodimers and that the main difference between LH2 and LH1 is the size of the ring.

Therefore, it would be very attractive to carry out experiments similar to those on LH2 on individual LH1-reaction centre (LH1-RC) complexes, which are also termed core complexes. The idea is that the optically excited states of the LH1 complex are characterised by excitonic interactions — like for the B850 band of LH2 — and that its spectroscopic features reveal details about the spatial organisation of the subunits in the LH1 ring. For example, the presence of an open ring structure as discussed by Cogdell *et al.* [11] or a dimeric structure as discussed by Francia *et al.* [164] will have implications on the manifold of excited states.

This chapter presents a study on LH1-RC complexes from two different species. First experiments were carried out on LH1-RC complexes from *Rhodospseudomonas acidophila* which

showed that structural heterogeneity significantly influences the spectroscopic properties of the complexes. The conclusion was that the LH1 rings of many LH1-RC complexes studied were not intact closed circular structures.

In a second series of measurements three different types of core complexes from *Rhodobacter sphaeroides* were investigated. For each type of these complexes a different structural model of the spatial arrangement of their subunits has been proposed in literature which allowed a more systematic approach to the investigation of the relationship between geometric structure and optical spectrum. It was the aim of this work to perform pilot experiments to demonstrate that spectroscopy can contribute to the discussion on the structure of light-harvesting complexes. The experimental observations proved to be compatible with the hypothetical structural models although other models could not be ruled out.

7.1 Structural models for LH1

Following the electron density map of *Rs. rubrum* [6] depicted in Fig. 2.5A a closed-ring model of the LH1 complex can be established comprising 16 $\alpha\beta$ -subunits, as depicted schematically in Fig. 7.1A. Each of the subunits is believed to contain only two coupled pigments contributing to its absorption band around 870 nm in contrast to three pigments for LH2 [80]. However, various reasons can be found to question the closed ring model. Firstly, pigment analysis showed that for

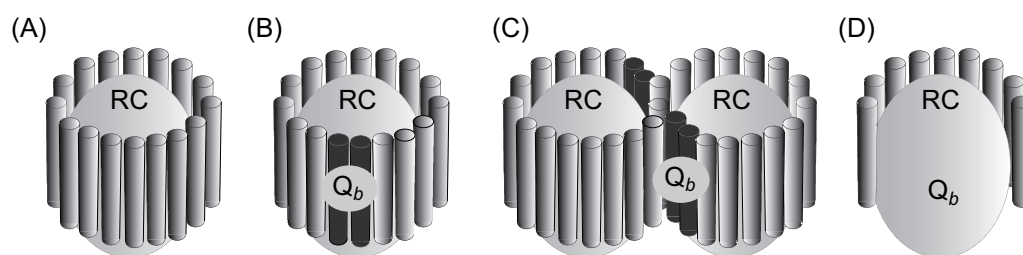


Figure 7.1: Four hypothetical structural models for LH1-RC complexes. The $\alpha\beta$ -subunits are displayed as light grey cylinders, the PufX protein is indicated by the dark grey cylinders, Q_b represents the ubiquinone site of the RC. (A) A closed-ring model in which the LH1 ring, comprising 16 $\alpha\beta$ -subunits, completely surrounds the RC. The Q_b site is effectively blocked. (B) A LH1 model where a small transmembrane protein PufX is incorporated in the ring, replacing 2 subunits. PufX might facilitate ubiquinone flow from the Q_b site. (C) S-shaped model composed of two LH1 rings with an incorporated PufX protein enclosing two RCs. (D) An open-ring model comprising eight $\alpha\beta$ -subunits. The Q_b site is exposed and the ubiquinone can leave the RC. Adapted from [11].

many strains the number of pigments per RC is less than 32. If they were closed ring aggregates of pigments only, they would be too small to incorporate a RC. Secondly, the representativity of the two 2-D projection maps of LH1 from *Rb. sphaeroides* and *Rs. rubrum* (see Sec. 2.1.2) showing a closed ring structure can be questioned. The complexes from *Rs. rubrum* [6] were reconstituted from $\alpha\beta$ -subunits obtained by detergent treatment of the native complexes and for the experiments on *Rb. sphaeroides* [7] a genetically modified species was used lacking the gene *pufX* which codes for the protein PufX. Without this protein the bacterium is incapable of photosynthetic growth.

In addition, non-circular structures of LH1-RC complexes have been reported as well. A projection map of LH1 complexes from *Rb. sphaeroides* derived by Jungas *et al.* [8] revealed a S-shaped structure composed of two incomplete antenna rings, each containing a RC, suggesting a dimeric LH1-RC complex, Fig. 2.5B. And LH1-RC complexes from *Rs. rubrum* revealed an almost square structure [165]. For the latter complex a small protein, the Ω -peptide was found which could not be resolved in the 2-D map. Scheuring *et al.* showed that the LH1 subunits of *Rhodospseudomonas viridis* in native membranes form a closed hexadecameric elliptic assembly with a high degree of flexibility [10] using high-resolution AFM. And also the core complex of *Chromatium purpuratum* featured an elliptical arrangement in the x-ray structure¹.

The small transmembrane proteins, PufX in *Rb. sphaeroides* and *Rb. capsulatus* and the Ω -peptide in *Rs. rubrum* are thought to be an integral part of the LH1 ring [8, 11, 164, 166, 167]. For *Rb. sphaeroides* it is known that PufX is compulsory for photosynthetic growth [168, 169]. However, in the absence of LH1 or if the LH1 complexes are reduced in size, photosynthetic growths is possible without PufX [86]. Apparently PufX is only required if the LH1 antenna system is present and if its macromolecular structure which encloses the RC is intact. These observations led to the proposal that PufX facilitates the ubiquinone/ubiquinol flow between the RC and the cytochrome *bc*₁ complex by acting as a gate in the LH1 ring [86, 170, 171].

In the absence of PufX the LH1 ring is larger by 1–2 subunits (i.e., comprising about 18 subunits) compared to wild type LH1 and the dimeric structure discussed above comprises about 1.7 times the number of pigments (i.e., 27 subunits) present in wild type monomeric complexes [164]. In Fig. 7.1B a model of a LH1-RC complex is depicted in which two subunits are substituted by a PufX protein. In other species which do not express PufX other proteins, like the

¹Private communication with R. Cogdell, University of Glasgow.

Ω -peptide in *Rs. rubrum*, might have a similar function. In (C) a model of an open S-shaped dimer is shown in analogy to the projection map of *Rb. sphaeroides* in Fig. 2.5B. Tentatively, the protein PufX is drawn in the gaps of the incomplete rings, although no evidence for this structural arrangement has been found. Linear dichroism measurements on oriented membranes of *Rb. sphaeroides* indicated that PufX plays a role in the orientation of the RC in the LH1 ring as well as in the formation of long-range regular arrays of LH1-RC complexes [166]. This supports the assumption that PufX acts as a gate in the LH1 ring.

However there is no direct evidence that any of the small proteins forms indeed part of the LH1 ring. For species for which no such small protein has been found it might also be possible that the LH1 ring is open and features a gap in the subunit circumference around the RC. Also in this model photosynthetic growth would not be blocked as can be concluded from the experiments on *Rb. sphaeroides*. The quinone site in the RC is exposed and the ubiquinone could leave the RC through the gap. In Fig. 7.1D such a model is depicted.

It should be stressed, that the models presented in Fig. 7.1 have been proposed in the absence of detailed structural knowledge from, for example, a high resolved x-ray structure. Nevertheless, the experimental indications of an open-ring or even dimeric structure suggest that the LH1 complexes are subjected to much more spatial and compositional variation than LH2, at least *in vitro*. In this chapter this variability is termed structural heterogeneity. However, the results will depend strongly on the specific species under investigation and also mutations of the genetic code and the (biochemical) history of the sample will influence the experimental outcome. The motivation of studying individual LH1-RC complexes by means of optical spectroscopy is to contribute to the discussion about the structural heterogeneity by correlating electronic structure derived from optical spectra with spatial arrangement of the pigments in the LH1 complex.

7.2 Simulation of the optical spectra

In order to understand the shape of the observed spectra several aspects that determine the optical properties have to be considered such as site heterogeneity, structural heterogeneity and the orientation of the complexes in the polymer film. As the primary donor (P) of the RC is separated by about 43 Å [13] from the pigments of the LH1 ring, the RC is not thought to influence the electronic structure of the LH1 significantly. However, the RC may act as a mould

for the LH1 ring and it is therefore not unlikely that it will induce structural distortions. As the RC has a twofold symmetry, it could induce a twofold structural deformation on the LH1 ring, which could affect its electronic structure [112].

Therefore, further insight into the effects of site and structural disorder on the optical spectra of light-harvesting complexes can be gained by numerical simulations of the electronic states. Applying Frenkel exciton theory to perfectly circular aggregates results in an excited state manifold as described in the introduction in Sec. 2.2.3. The most prominent features are the lowest degenerate excited states labelled $k = \pm 1$ of which the related transition-dipole moments are mutually orthogonal and which possess most of the oscillator strength.

7.2.1 Methods

To simulate optical spectra, as a starting point it was used assuming that the LH1-RC complexes consist of a closed ring structure comprising 16 $\alpha\beta$ -subunits each binding two BChl *a* molecules [6]. The distances between the pigments and their mutual orientations were taken identical as in LH2 [2]. It was assumed that the complexes are oriented with the plane of the ring parallel to the plane of the spin-coated sample, i.e., perpendicular to the propagation vector of the excitation light. The electronic structure of LH1 was approximated using only the lowest (Q_y) excited states of the individual BChl *a* molecules. Owing to the orientation of the complexes, only the projections of the transition-dipole moments in the plane of the ring were taken into account as the contributions from transition-dipole moments perpendicular to the ring are not accessible by the experimental procedure.

The interaction between the pigments was determined up to second neighbours using a point-dipole approximation [107] resulting in a nearest neighbour interaction of 253 cm^{-1} and 229 cm^{-1} for intra- and inter-dimer interaction, respectively. The excited state energy of the β -bound pigments was taken as $11\,800\text{ cm}^{-1}$, whereas the site energy of the α -bound pigments was taken 240 cm^{-1} higher due to slightly different local environments [26]. The energy transfer among the B870 chromophores is about 100 fs [54, 67, 87], and consequently the states are assigned a homogeneous linewidth of 100 cm^{-1} . The lowest exciton state has a relative long fluorescent lifetime of approximately 1 ns [79]. However, as the experimentally observed linewidth is determined by the spectral resolution of the measurement it is assigned a linewidth of 1 cm^{-1} .

7.2.2 Structural heterogeneity

To study the implications of different spatial arrangements, four types of oligomeric structures of LH1 complexes were investigated. For closed-ring LH1 complexes a ring size of 16 subunits was assumed, each binding two BChl *a* molecules. For open-ring LH1 complexes, an individual subunit was removed from the ring whereas a half-ring complex comprised only eight subunits. A dimeric shaped LH1-RC complex was modelled to comprise 1.7 times as many BChl *a* molecules (27 subunits) as closed ring LH1 complexes. The subunits in the dimer were placed in an S-shaped form following the electron projection map [164], Fig. 2.5B.

The optical spectra that have been calculated for four different oligomeric structures of LH1 in the absence of site heterogeneity are shown in Fig. 7.2 and will be discussed below.

Model A: complete ring of 16 subunits

The optical spectrum is clearly dominated by two broad bands ($k = \pm 1$) that are mutually orthogonal and carry almost all oscillator strength. As no site heterogeneity was incorporated the degeneracy of the two states remains. The lowest excited state ($k = 0$) is optically forbidden and carries no oscillator strength.

Model B: ring with one subunit (i.e., 2 pigments) missing

Due to the removal of one $\alpha\beta$ -subunit the symmetry of the structure is broken. This lifts the pairwise degeneracy of the exciton states. In this model the lowest state is no longer labelled $k = 0$ but $k^{\text{lin}} = 1$ similar to a linear aggregate. Consequently, the second lowest state is labelled $k^{\text{lin}} = 2$, etc. As the $k^{\text{lin}} = 1$ state is no longer optically forbidden it carries oscillator strength and a narrow absorption line originating from the long-lived lowest excited state appears at the red end of the spectrum. The $k^{\text{lin}} = 2$ state carries approximately the same oscillator strength as the $k = \pm 1$ states in model A whereas the $k^{\text{lin}} = 3$ carries less. Compared to the closed ring structure the exciton levels are all shifted slightly to higher energies. This blue shift with decreasing size of the oligomer structure has previously been observed [172].

Model C: S-shaped dimeric structure comprising 27 subunits

Surprisingly the optical spectrum of the dimeric LH1 structure is very similar to the spectrum of the open ring structure. The positions and relative oscillator strengths of their

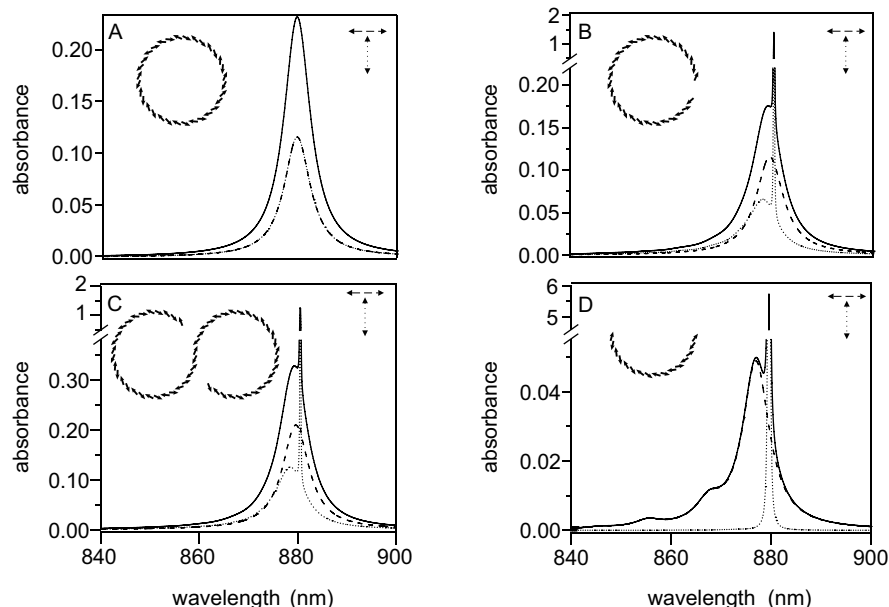


Figure 7.2: Simulation of the absorption spectrum of an individual LHI complex, which forms a complete ring of 16 $\alpha\beta$ -subunits (model A), a ring with one $\alpha\beta$ -subunit missing (model B), a S-shaped structure comprising 27 $\alpha\beta$ -subunits (model C) and a partial ring consisting of 8 $\alpha\beta$ -subunits (model D). The overall absorption spectrum in the xy plane of the complex is plotted (solid line) together with the absorption spectrum along the x -axis (dashed line) and the y -axis (dotted line). The absorbance is given in units of the monomer absorbance. The x -axis is chosen along the transition-dipole moment of one of the $k = \pm 1$ states in the case of model A and along the $k^{\text{lin}} = 2$ in models B–D. The insets sketch the arrangement of the subunits in the xy plane, showing the Q_y transition-dipole moments (arrows). The lowest energetic state of the exciton manifold is assigned a homogeneous linewidth of 1 cm^{-1} , all other states 100 cm^{-1} .

three most prominent states $k^{\text{lin}} = 1-3$ are almost identical. From the huge oligomer size a significantly red shift would have been expected but apparently only the size of one of the monomer units of the dimer determines the energy positions of the exciton states whereas twice the number of pigments is reflected by an absolute oscillator strength of the $k^{\text{lin}} = 2, 3$ states which is twice as high as in model B. The transition-dipole moments related to the two broad absorption bands are not oriented fully orthogonal anymore although they still show a mutual angle of about 80° .

Model D: half-ring structure with 8 subunits

Compared to the open ring structures the $k^{\text{lin}} = 1$ state gains even more oscillator strength, whereas the $k^{\text{lin}} = 2$ state carries less and the $k^{\text{lin}} = 3$ almost no oscillator strength. The transition-dipole moments related to the states with almost all oscillator

strength (i.e., $k^{\text{lin}} = 1, 2$) are mutually orthogonal. The exciton levels are still further blue shifted compared to models B and C.

7.2.3 Site heterogeneity

Upon introducing site heterogeneity, the exciton levels are mixed and the oscillator strength is redistributed to neighbouring levels. For a closed ring aggregate (model A) a narrow absorption line appears at the red-most end of the spectrum as the long-lived lowest excited state ($k = 0$) gains oscillator strength. The degeneracy of the lowest excited state levels is lifted but their mutual orthogonality remains with a narrow distribution around 90° whose width depends on the magnitude of site heterogeneity [26, 111].

The redistribution of the oscillator strength depends on both the extent of site heterogeneity as well as the energy separation of the exciton levels. All levels of the exciton manifolds lie within the same energetic width of about 4 times the average interaction strength V_{avg} . Thus, the density of states scales linearly with the number of pigments in such a complex. Consequently, the density for a dimeric LH1 complex is about twice as high as for a monomeric LH1 complex

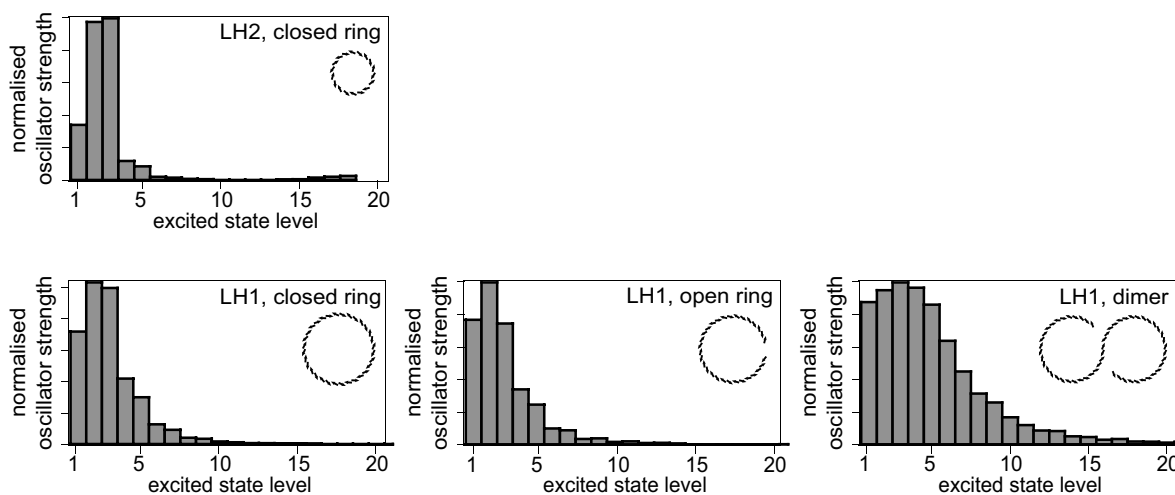


Figure 7.3: Simulation of the excited state energies of LH2 and several oligomer forms of LH1. For LH1, only the 20 lowest levels of the exciton manifold are depicted. The transition probabilities from the ground state to the various excited states of the exciton manifold are depicted by the lengths of the grey bars. The exciton levels are ordered according to their excitation energy. In the presence of site heterogeneity averaging over 1 000 complexes was performed. The oscillator strength was normalised to the highest value. The insets sketch the arrangement of the subunits in the xy plane, showing the Q_y transition-dipole moments (arrows).

which is nearly twice as high as for a LH2 complex. The smaller separation of the exciton states causes a stronger mixing of the exciton levels as can be seen in Fig. 7.3. For different light-harvesting complexes the oscillator strength is depicted versus the individual exciton levels. For all complexes the ratio of interaction strength to disorder V_{avg}/Δ is the same, where Δ is defined as the full width at half maximum of a Gaussian distribution of site energies within a complex. Each histogram represents the average over 1 000 complexes.

For a closed-ring LH2 complex comprising 9 subunits, most of the oscillator strength is concentrated in the $k = \pm 1$ states and the $k = 0$ carries only little oscillator strength as can be seen in the upper left panel. The closed- and open-ring LH1 complexes — shown in the lower left and lower centre panel, respectively — feature a similar distribution in which the higher exciton states as well as the lowest $k = 0$ state clearly carry more oscillator strength. The dimer features the broadest distribution where also higher exciton levels carry significant oscillator strength as depicted in the lower right panel in Fig. 7.3.

For these calculation it was assumed that the heterogeneity for LH1 and LH2 complexes is similar. This assumption is supported by the high degree of homology in the protein subunits and is in line with hole-burning experiments [126] which showed that the energy distribution of the lowest non-degenerate state $k = 0$ of the exciton manifold of LH1 and LH2 was found to have the same width within 20%. The difference in the optical spectra therefore stems mainly from the different densities of states leading to a different distribution of oscillator strength over the exciton levels. For the LH1 complexes the transition-dipole moment of the $k = 0$ state should be much stronger than for LH2 and therefore have an higher probability to appear in the spectra. In addition, more broad bands should appear in the spectra owing to the enhanced mixing with radiative states. Compared to the normal LH1 complexes, the dimer LH1 complexes are expected to show even more broad bands of comparable intensity which will tend to overlap strongly.

7.2.4 Orientation of the complexes

The observed polarisation dependence of a transition also depends on the orientation of the complex with respect to the plane of polarisation of the excitation light. In the experimental setup used for this thesis, only the projection of the transition-dipole moments onto the plane of the substrate can be measured.

For individual LH2 complexes the mutual angle between the $k = \pm 1$ states was found to lie within a narrow distribution around 90° , implying that the complexes are oriented with their symmetry axis perpendicular to the surface of the substrate (chapter 6, [26]). This preferred orientation might be the result of electrostatic interactions between the complex and the substrate together with a laminar flow induced by the spin-coating process during sample preparation.

For LH1-RC complexes Cogdell *et al.* proposed a model in which the RC sticks out on the N terminus site of the LH1 ring by 20 \AA [11, 13]. A LH1-RC complex with the protruding RC facing towards the substrate could therefore be slightly tilted. As a result the mutual angle between the transition-dipole moments related to the broad absorptions will be less than 90° in the projection onto the plane parallel to the sample surface. In the extreme situation of a sideways lying complex (i.e., like a tyre on the road) the projections of the transition-dipole moments could be even parallel to each other. However, such an extreme orientation is very unlikely as the diameter of light-harvesting complexes is about a factor of two bigger than their height.

For structures that are no longer complete rings like the half-ring structure of model C, the orientation of the complex with respect to the substrate is probably completely different and could vary strongly between complexes.

7.2.5 Discussion of the simulations

Numerical simulations show that structural and site heterogeneity greatly influence the optical spectrum. The structural differences are mainly responsible for the increase in oscillator strength of the lowest excited state when removing subunits from the ring whereas the site heterogeneity causes a mixing of the exciton states and a concomitant redistribution of oscillator strength resulting in an increase of the number of broad bands in the spectrum. Degeneracy of the states is lifted by both types of disorder. The spectra of all oligomer structures are dominated by two broad bands whose related transition-dipole moments are more or less orthogonal oriented whereas the dimeric structure contains further broad bands of similar intensity. However, this orthogonality might not be found back in the experimental measurement if the plane of the ring of the complex is not perpendicular with respect to the plane of polarisation of the excitation light. Variations in the polarisation dependency of the intensity of absorption bands could therefore well be caused by variations in the orientation of the complexes on the substrate.

7.3 LH1-RC from *Rhodopseudomonas acidophila*

7.3.1 Experimental results

In Fig. 7.4 the fluorescence-excitation spectrum of an ensemble of LH1-RC complexes from *Rhodopseudomonas acidophila* in a PVA film (dotted line) at 1.4 K is shown. Its maximum absorption occurs at about 891 nm and the fluorescence was detected at 910 nm with a detection bandwidth of 20 nm. The dashed line indicates the transmission characteristic of this emission filter. The sum spectrum that results when the fluorescence-excitation spectra of all measured LH1-RC complexes are added (solid line) is slightly blue shifted compared to the ensemble spectrum and also the blue wings of the two bands are not fully identical.

Example fluorescence-excitation spectra of six out of the 24 measured individual LH1-RC complexes are depicted in Fig. 7.5. All spectra are averages of all possible polarisations of the excitation light. It is clearly visible that they largely differ by the number of bands, bandwidths and intensities. However, common features are the positions of the broad absorption bands around 860 to 890 nm and their width ranging from 150 to 200 cm^{-1} indicating dephasing times of the electronically excited state of several ten femtoseconds. In some spectra the bands are very close to each other and in others bands coincide with the transmission of the emission filter which makes it difficult to determine the exact number of bands.

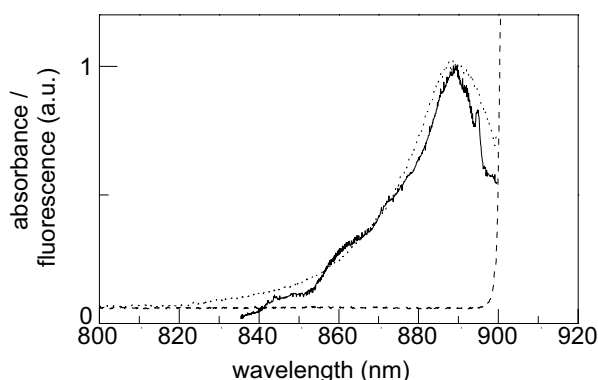


Figure 7.4: Ensemble spectra of LH1-RC complexes from *Rhodopseudomonas acidophila*. The dotted line represents the fluorescence-excitation spectrum at 1.4 K. The solid line is the sum of 24 fluorescence-excitation spectra of individual complexes at 1.4 K recorded at an intensity of 2–10 W/cm^2 and the dashed line indicates the transmission of the emission path filters used in the low temperature measurements.

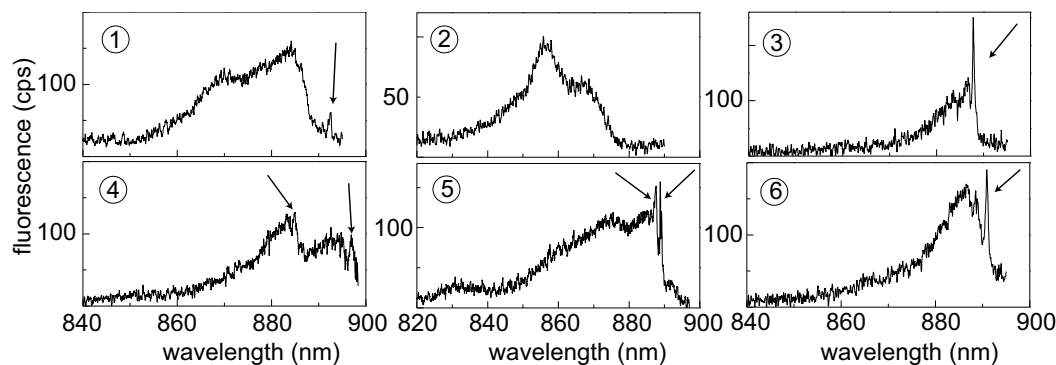


Figure 7.5: Six example spectra of individual LH1-RC complexes from *Rps. acidophila* recorded at an intensity of 2–10 W/cm² at 1.4 K. The arrows indicate narrow absorption lines present in some of the spectra.

Apart from the broad bands 80% of the spectra also show narrow absorption lines like those in spectra 1,3 and 4–6 in Fig. 7.5. These narrow lines were always found on the red wing of a broad absorption band. Although their intensity varied from spectrum to spectrum the signal-to-noise ratio was normally sufficient to determine the width within one scan of the laser, thereby minimising a broadening of the line due to spectral diffusion. The widths range from 1–3 cm⁻¹ and are mainly determined by the width of the excitation laser (1 cm⁻¹). For some complexes even two narrow lines appeared in the spectrum (spectrum 4 and 5; Fig. 7.5) both of which were on the red wing of broad absorptions.

The 24 observed individual LH1-RC spectra can be divided roughly into four groups on the basis of polarisation behaviour and other spectral features. In the following the characteristics of the different groups will be described; an example spectrum of each group is depicted in Fig. 7.6.

Group I: 30% (7 out of 24) of the complexes featured spectra that are dominated by 2 broad bands around 870–890 nm which are mutually orthogonal polarised within 6°. Their energetic splitting amounts to 116 ± 77 cm⁻¹. Occasionally the spectra show a narrow absorption line at the red-end side of the spectrum which is much more pronounced for LH1-RC complexes than for the LH2 complexes and was detected more often, i.e., in five out of seven cases as opposed to 3 out of 24 cases [25, 26].

Group II: 17% (4 out of 24) of the complexes featured two broad absorption bands whose mutual angles of polarisation ranged from 30–64°, i.e., significantly less than 90°. Two complexes in this group featured a narrow line at the low-energy side in their spectra.

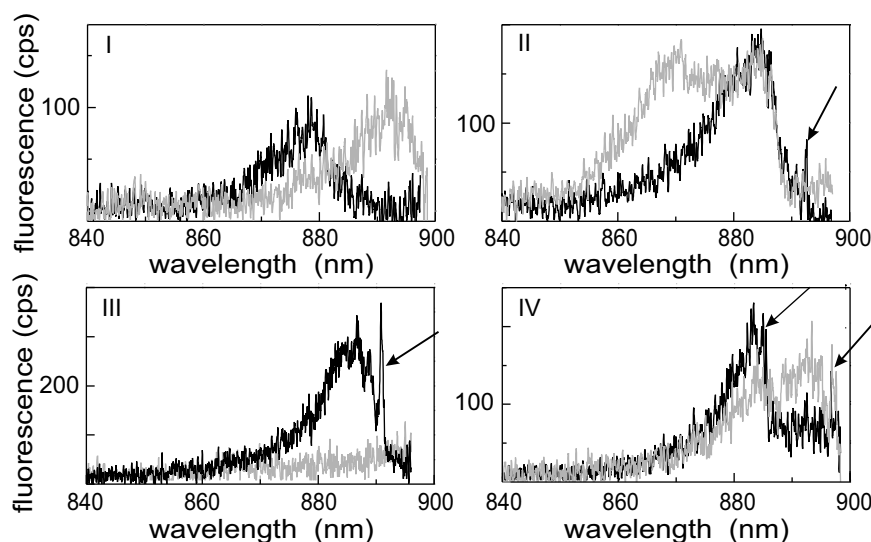


Figure 7.6: Four different types of polarisation behaviour and spectral features of LH1-RC complexes from *Rps. acidophila*. For each group I-IV a typical example spectrum is given that consists of two spectra recorded for different polarisations of the incident laser light. In (I) two orthogonally polarised broad bands are observed. In (II) two broad bands are present with a mutual angle of polarisation of less than 90° . In (III) one broad band is observed with no absorption at the perpendicular polarisation. In (IV) multiple narrow lines are observed. The arrows point towards the narrow absorption lines present in some of the spectra. Experimental conditions were as in Fig. 7.5.

Group III: 17% (4 out of 24) of the complexes showed no detectable absorption for a specific angle of polarisation. This becomes obvious by looking at the example spectrum of this group in the lower left panel in Fig. 7.6 for which two spectra of mutual orthogonal polarisation are displayed. One of these spectra only features background noise whereas the other clearly shows a typical LH1-RC spectrum. For two complexes a narrow line was found in the red edge of a broad band, with the same polarisation as the broad band.

Group IV: 36% (9 out of 24) of the complexes featured two narrow absorption lines or one narrow absorption line in the centre of the spectrum together with a broad absorption band extending into the detection window, thereby possibly masking a second narrow line. The narrow lines always occurred on the red edge of a broad absorption band.

7.3.2 Discussion

At first thought it might be surprising to observe fluorescence from LH1 complexes in which the reaction centre is present. However, in these type of experiments the quenching of the

fluorescence by the RC does not play a great role. At low temperatures the lowest energy level of a significant fraction of the LH1 complexes is thought to be shifted to lower energies with respect to the primary donor (P) of the RC [173, 174] reducing its trapping efficiency. In addition, electron transfer from the primary quinone acceptor Q_A to Q_B is, in fact, blocked below 150 K [175, 176] and once Q_A has been reduced following the first photon, no further chemistry and concomitant quenching of the fluorescence can occur. See Sec. 2.1.2 for details of the electron transfer in the RC.

The most pronounced features that were observed in the fluorescence-excitation spectra of LH1-RC complexes from *Rps. acidophila* are the limited number of broad bands with a characteristic polarisation behaviour and a large variation in their appearance. The spectra featured in general three to four broad bands and even if the shoulders were counted as separate bands no more than six bands could be distinguished. These spectral features can be best described in terms of a collective excitation of the complete ring. In this model, the optical properties are described in terms of circular Frenkel excitons (see Sec. 2.2.3). The variation in appearance manifests itself in the different number of bands and their polarisation behaviour, their bandwidths and spectral positions. It was not always possible to resolve all bands because most of the observed bands are broad.

The spectra that were observed for the LH1-RC complexes from *Rhodopseudomonas acidophila* were categorised into four groups. Below, the optical properties of the different types of spectra are compared with the outcome of numerical simulations of the electronic structure of aggregates featuring different oligomer structures and site heterogeneity. In addition, the influence of the orientation of a complex with respect to substrate is taken into account.

Group I: In this group the spectra were dominated by two broad absorption bands around 870–890 nm featuring mutual orthogonal polarisation. They resemble the spectra observed for the B850 band of LH2 from *Rps. acidophila* [25, 26] and tentatively the broad bands are assigned to represent the lowest degenerate states of a circular exciton and are consequently denoted $k = \pm 1$. The degeneracy of these two states is lifted due to energetic disorder and their energetic splitting $\delta E_{\pm 1}$ is roughly the same for LH1-RC ($116 \pm 77 \text{ cm}^{-1}$) and LH2 ($126 \pm 43 \text{ cm}^{-1}$). In contrast, the average energy separation $\delta E_{1|k|}$ between the spectral mean of the $k = \pm 1$ states and the band at higher energy is much larger for LH1-RC ($418 \pm 129 \text{ cm}^{-1}$) than for the LH2 spectra ($285 \pm 35 \text{ cm}^{-1}$) [26].

As their mutual polarisation was only distributed by 6° around perfect orthogonality it is assumed that their orientation was parallel to the surface of the substrate. In several spectra, a narrow absorption line was found at the red end of the $k = \pm 1$ states which was attributed to the long-lived emitting $k = 0$ state like in the case of LH2 [26]. This line was observed more often than for the LH2 complexes which is explained by the stronger mixing of the exciton states because of the reduced energy separation (Fig. 7.3).

However an open ring configuration with one or two subunits missing is also compatible with the observations. Then the broad bands have to be assigned to the $k^{\text{lin}} = 2, 3$ states.

Group II: The spectra in this group were also dominated by two broad absorption bands with a mutual polarisation ranging from $30\text{-}64^\circ$. Although the mutual polarisation of the two absorption bands is not orthogonal they were still thought to represent the two lowest degenerate states of a circular exciton and were therefore also assigned $k = \pm 1$. The deviation from orthogonality could well be explained by a non-perpendicular orientation of the complex with respect to the plane of polarisation of the excitation light. For these complexes the side where the RC protrudes from the LH1 ring could have faced towards the substrate, inducing a tilt of the complexes.

Like for group I), an open ring configuration with one or two subunits missing is also compatible with the observations in this group. In that case, then the broad bands would have to be assigned to the $k^{\text{lin}} = 2, 3$ states.

Group III: This group comprised spectra showing no detectable absorption for a specific angle of polarisation of the exciting laser. This behaviour could in principle be explained by a closed ring structure oriented perpendicular to the substrate (i.e., lying on its side) together with a specific orientation of the transition-dipole moments of the $k = \pm 1$ states, i.e., one must lie parallel and the other perpendicular to the exciting laser. This is a very unlikely case. Even a half-ring structure lying flat on the substrate cannot explain the observations as it should also feature two orthogonally polarised absorption bands. A possible explanation would be a half-ring structure tilted within the PVA film. Such a configuration is much more likely than a sideways oriented ring structure.

Group IV: Spectra in this group were characterised by two narrow absorption lines which indicates the presence of at least two weakly coupled aggregates. There are two possibilities

for such a behaviour. First, the two aggregates could both be LH1-RC monomers. However one of the monomers would have to comprise less than 16 $\alpha\beta$ -subunits to explain the spectral position of the blue-most narrow line and subsequent lower energetic broad bands. Dimerisation of the LH1-RC structure is reported by Francia *et al.* for LH1-RC complexes (PMC4_{WT}) from *Rb. sphaeroides* [164] which are also studied in this chapter. They found that the dimeric structure existing in native conditions is converted into a monomeric structure by increasing the detergent concentration. Since a high detergent concentration was used in the preparation procedure of the LH1-RC complexes from *Rps. acidophila* the formation of dimeric LH1-RC structures is very unlikely.

A second explanation of the spectral features could be the presence of more or less isolated domains of pigment arrays whose oligomer size is much smaller than that of a LH1 complex to account for the blue shift. These domains must be isolated from the LH1 ring by either defects in the ring or by additional proteins that form part of the LH1 structure but do not participate in the transfer of energy.

7.4 LH1-RC from *Rhodobacter sphaeroides*

For the second set of experiments LH1-RC complexes from *Rhodobacter sphaeroides* were used that were prepared as described by Francia *et al.* [164]. For wild type (WT) samples of *Rb. sphaeroides* they identified two photosynthetic membrane complexes (PMC), PMC3_{WT} and PMC4_{WT}. The PMC3_{WT} complexes contained 16.4 ± 0.7 $\alpha\beta$ -subunits, one RC and one PufX-His₆ molecule and were thought to correspond to monomeric LH1-RC complex in which the PufX protein forms an integral part of the LH1 ring. The PMC4_{WT} comprised 26.8 ± 2.3 $\alpha\beta$ -subunits, two RCs and two PufX-His₆ molecules. Its electron projection map [8] indicated an S-shaped form and consequently the PMC4_{WT} were thought to represent dimeric LH1-RC complexes. The dimeric complexes were only stable in a narrow range of detergent concentration. Upon increasing or decreasing this concentration PMC4_{WT} was converted into PMC3_{WT}. Another type of LH1-RC complex (PMC3 _{Δ X}) was obtained by deleting the *pufX* gene (Δ X) which codes for the expression of the protein PufX. The resulting bacteria produced complexes with an increased BChl/RC stoichiometry. PMC3 _{Δ X} complexes contained 17.8 ± 1.3 $\alpha\beta$ -subunits per RC and are expected to form a closed ring.

7.4.1 Experimental results

In Fig. 7.7 the low-temperature fluorescence-excitation spectra of ensembles of the three LH1-RC complex types from *Rhodobacter sphaeroides* in a PVA film are shown. The maximum absorption of the wild type samples containing the protein PufX lies at around 875 nm and is clearly blue shifted by about 4 nm compared to the mutant which is not capable of expressing PufX. The fluorescence was detected at 917 nm with a detection bandwidth of about 20 nm. A similar red shift (4–5 nm) of the mutant spectrum with respect to the wild type spectrum is observed in room temperature absorption spectra [177].

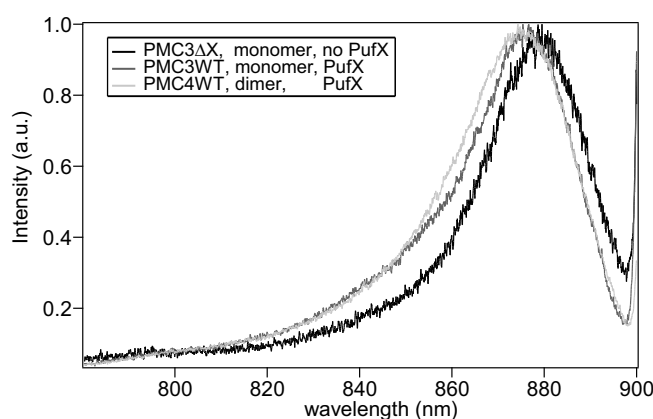


Figure 7.7: Ensemble fluorescence-excitation spectra of wild type monomeric ($PMC3_{WT}$, dark grey), wild type dimeric ($PMC4_{WT}$, light grey) and mutant monomeric ($PMC3_{\Delta X}$, black) LH1-RC complexes from *Rhodobacter sphaeroides* at 1.4 K. No background was subtracted and therefore the transmission of the detection window is visible in the red edge of the spectrum.

In the following the results of the single-molecule measurements will be summarised for each sample type.

$PMC3_{\Delta X}$: Mutant LH1-RC monomer; without PufX.

In total 11 complexes were studied. The spectra featured 2–5 broad absorption bands, mostly dominated by two broad bands around 860–890 nm. The energetic splitting of the two bands amounts to $180 \pm 80 \text{ cm}^{-1}$, which is much larger than for the LH1-RC complexes from *Rps. acidophila*. The mutual angles of polarisation between the bands ranged from 50–90°. In none of the spectra a narrow line could be observed.

The spectra resemble those observed for LH1-RC complexes from *Rps. acidophila* in groups I and II. A histogram of the mutual angles of polarisation and energetic splittings

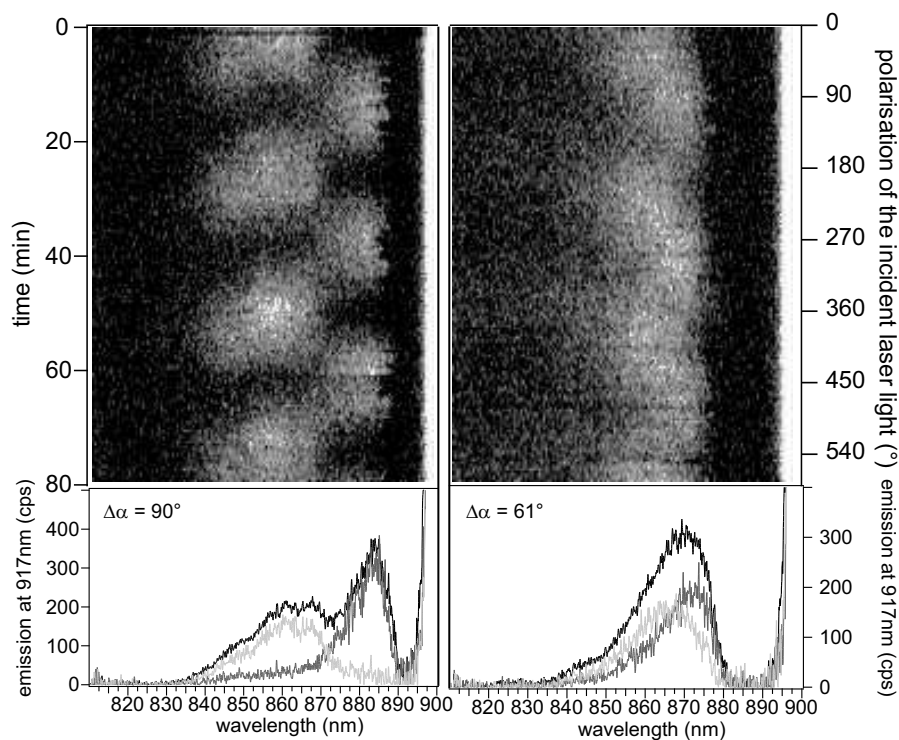


Figure 7.8: Two example spectra of the mutant monomeric LH1-RC complexes ($PMC3_{\Delta X}$) from *Rb. sphaeroides*. The upper panels show a stack of sequentially recorded fluorescence-excitation scans. After each scan the polarisation was rotated by 3.6° . The fluorescence intensity is given by the grey code. In the lower panels two spectra of a specific polarisation of the incident laser light are shown for each complexes and their mutual polarisation is indicated. No background was subtracted and therefore the transmission of the detection window is visible in the red edge of the spectrum.

between the two lowest energetic bands of all complexes can be found in the left two panels of Fig. 7.9. Two example spectra, typical for this sample are depicted in Fig. 7.8

$PMC3_{WT}$: Wild type LH1-RC monomer; with PufX.

In total 10 complexes were studied and their spectra featured 2–4 broad absorption bands. Again most of the spectra are dominated by two broad absorption bands at about 855–900 nm. The energetic splitting amounts to $190 \pm 100 \text{ cm}^{-1}$, similar to the mutant monomers. The mutual angles of polarisation of the two bands ranged from 70 – 90° . For six complexes a narrow absorption line was observed. This line was always detected on the red edge of a broad band. Interestingly, only for three complexes it was found red of the energetically lowest broad band whereas for three complexes it was found on the energetically next but lowest broad band.

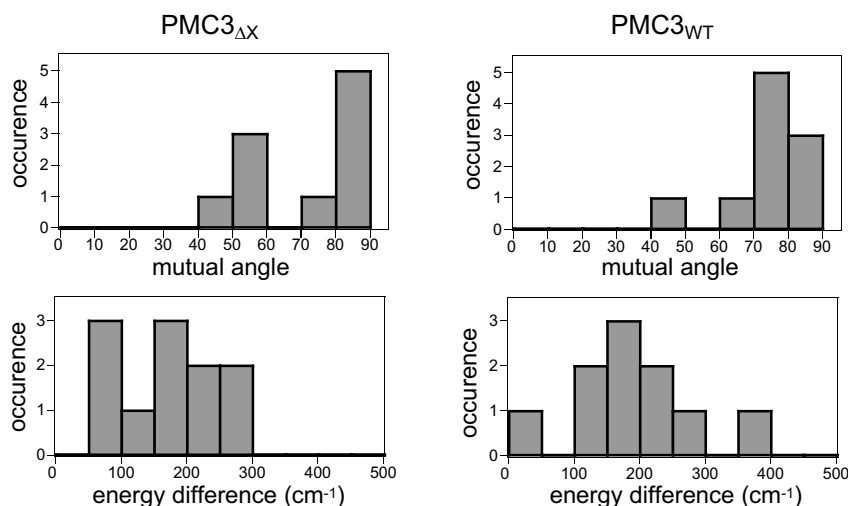


Figure 7.9: Histograms of the mutual angles of polarisation and energy splittings between the dominant broad bands of the wild type (PMC3_{WT}) and mutant (PMC3 Δ X) monomer LH1-RC complexes from *Rb. sphaeroides*.

These spectra resemble those observed for LH1-RC complexes from *Rps. acidophila* in groups I and II as well. A histogram of the mutual angles of polarisation and energetic splittings between the two bands of all complexes can be found in the right two panels of Fig. 7.9. Two typical example spectra are depicted in Fig. 7.10.

PMC4_{WT}: Wild type LH1-RC dimer; with PufX.

In total 9 complexes were studied and their spectra featured 2–4 broad absorption bands. Most of the spectra were dominated by three or four broad bands of similar intensity around 860–890 nm. Due to the small spectral separation the lines are not well resolved. Three spectra featured one narrow absorption line and two spectra featured two narrow lines, each on the red edge of a broad band. These five spectra resemble those observed for LH1-RC complexes from *Rps. acidophila* in group IV, whereas the spectra without narrow features cannot be compared to any of the groups. Two example spectra, typical for this sample are depicted in Fig. 7.11.

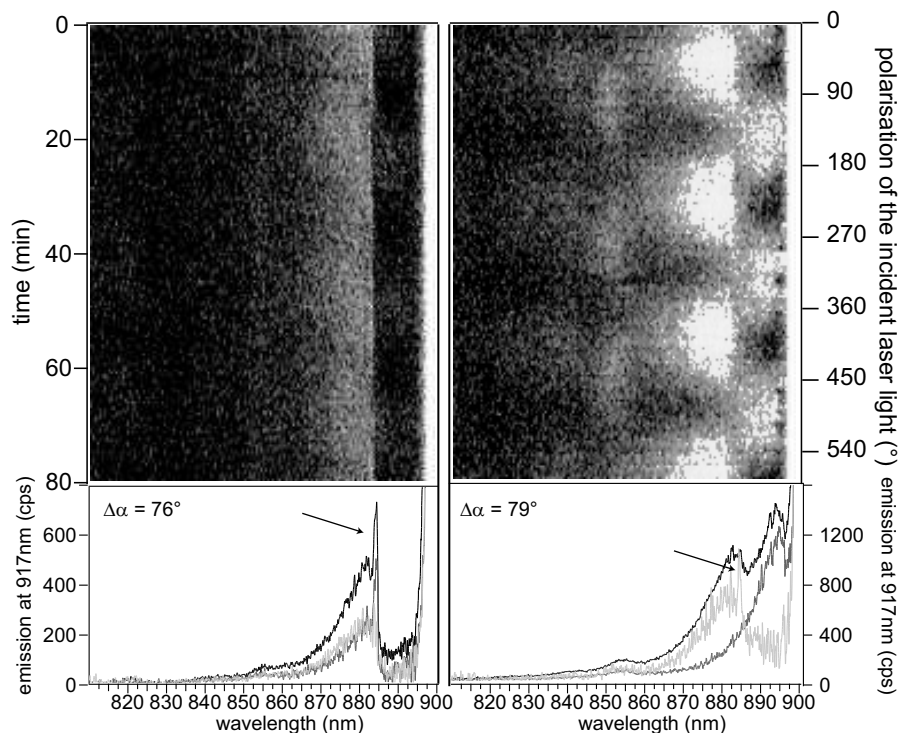


Figure 7.10: Two example spectra of the wild type LH1-RC monomeric LH1-RC complexes ($PMC3_{WT}$) from *Rb. sphaeroides*. The representation is as in Fig. 7.8, the arrows point towards narrow lines observed in the spectra.

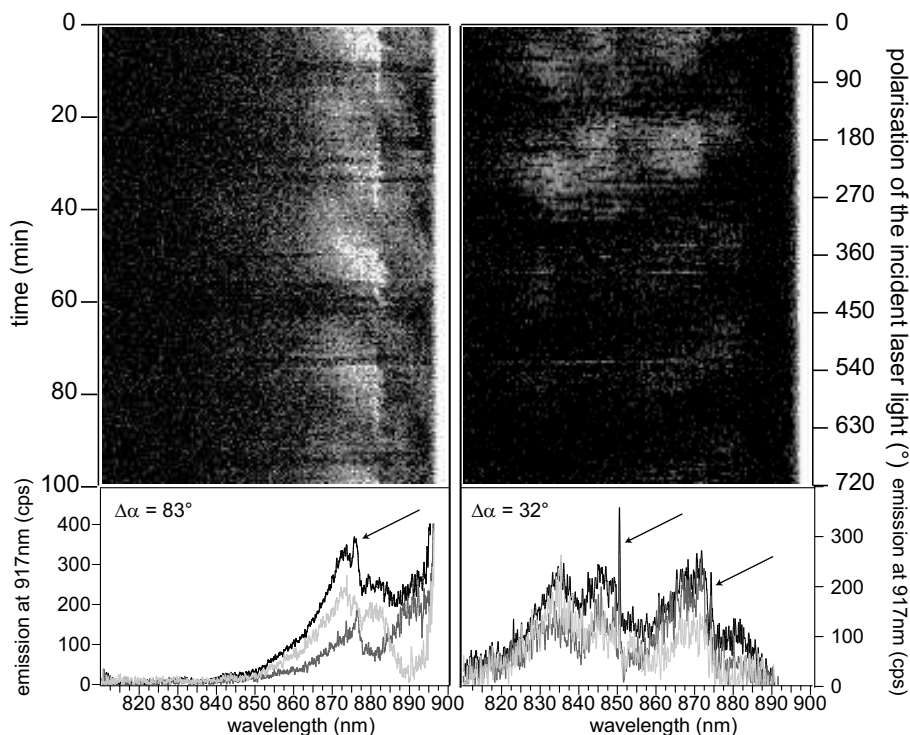


Figure 7.11: Two example spectra of the wild type LH1-RC dimeric LH1-RC complexes ($PMC4_{WT}$) from *Rb. sphaeroides*. The representation is as in Fig. 7.8, the arrows point towards narrow lines observed in the spectra.

7.4.2 Discussion

Like for *Rps. acidophila* the most pronounced features that were observed in the fluorescence-excitation spectra of LH1-RC complexes from *Rb. sphaeroides* are the limited number of broad bands with a characteristic polarisation behaviour and a large variation in their appearance. In general, three to four broad bands were observed whose optical properties can best be described in terms of collective excitations of the complete ring, so called Frenkel excitons (see Sec. 2.2.3). It was not always possible to resolve all bands due to their spectrally overlap.

From *Rb. sphaeroides*, three different types of LH1-RC complexes were studied. The wild type PMC3_{WT} complexes were thought to correspond to monomeric LH1-RC complex comprising 16 $\alpha\beta$ -subunits and a PufX protein forming an integral part of the LH1 ring. The wild type PMC4_{WT} were thought to correspond to dimeric LH1-RC complexes, comprised about 27 $\alpha\beta$ -subunits in a S-shaped structure and two PufX molecules.

A mutant sample of PMC3 _{Δ X} complexes lacked the *pufX* gene coding for the expression of the protein PufX. The complexes were thought to correspond to monomeric LH1-RC complexes comprising about 18 $\alpha\beta$ -subunits that enclose the RC.

In the ensemble spectrum the maximum absorption of the wild type complexes was shifted by about 4 nm to the blue compared to the mutant sample. This can be explained by the different oligomer sizes of the LH1 rings. Simulations showed that the maximum absorption is blue shifted with decreasing oligomer size [172].

The results of the single molecule measurements for the different sample types will be discussed below.

PMC3 _{Δ X}: Mutant LH1-RC monomer; without PufX.

The spectra of this sample type are characterised by two broad absorption bands around 860–890 nm with mutual polarisations ranging from 50–90°. These observations are very well compatible with a circular exciton and consequently, the broad bands are assigned to the $k = \pm 1$ states for which the degeneracy is lifted due to energetic disorder. The site heterogeneity is much larger than for the LH1-RC complexes from *Rps. acidophila* as can be seen from the large energy splitting of the $k = \pm 1$ states.

The absence of any narrow line in the spectra is only a weak evidence for a closed ring

structure as the oscillator strength of the $k = 0$ line is just little less for a closed (18%) than for an open ring (21%) in the presence of random energetic disorder, Fig. 7.3. The $k = 0$ absorption is most probable subjected to spectral diffusion as can be deduced from the large site heterogeneity. The absorption could be hidden in the underlying broad band such that it is no longer detectable [25]. However also an open ring configuration with one or two subunits missing is compatible with the observations as the spectral features are similar to those of a closed ring. Then the broad bands have to be assigned to the $k^{\text{lin}} = 2, 3$ states.

The histogram of mutual polarisations of the broad bands, Fig 7.9, indicates that most of the complexes lie flat on the surface whereas some might be slightly tilted.

PMC3_{WT}: Wild type LH1-RC monomer; with PufX.

The spectra of this sample type were characterised by two broad absorption bands around 855–900 nm with mutual polarisations ranging from 70–90°. The main difference with the mutant sample (*PMC3_{ΔX}*) is the observation of narrow lines in six of the spectra.

The spectra without a narrow line and those with a narrow line occurring at the red end of the spectra are compatible with both the open and closed ring model. However, the probability of detecting a narrow line increases with the number of subunits removed from the ring, see Fig. 7.2. Therefore, the observation of a narrow line is more likely for an open ring.

In contrast, the spectra that featured a narrow line in the centre of their spectrum can not be explained by a closed ring model. An explanation for these spectral features could be trap states due to an isolated oligomer unit caused by a defect in the LH1 ring or additional proteins that form part of the LH1 structure but do not participate in the transfer of energy.

PMC4_{WT}: Wild type LH1-RC dimer; with PufX.

Two spectra of complexes from this sample comprised two narrow absorption lines and five spectra featured a single narrow line. These spectra resembled the LH1-RC spectra of group IV from *Rps. acidophila*.

The other spectra were dominated by three or four broad absorption bands around 860–890 nm. These features fit very well in the picture of a dimeric LH1-RC aggregate as the small energy separations between its exciton levels leads to a strong mixing of the

states. As can be seen from Fig. 7.3, also higher exciton states possess significant oscillator strength.

7.5 Summary of the experiments on core complexes

It can be concluded that the LH1 assembly of BChl *a* pigments at low temperature represents a strongly coupled system whose excited states can be described as collective excitations, so called Frenkel excitons. Indications that support this description are the limited number of observed bands (3–4), the large linewidths of 150–200 cm⁻¹ and the polarisation behaviour of the two energetically lowest absorptions which indicated a mutual orientation of the transition-dipole moments related to these absorptions for most of the complexes.

The number of bands, bandwidths and their polarisation behaviour varied strongly for the different complexes. This variation was attributed to structural heterogeneity as LH2 complexes from *Rps. acidophila*— whose optical properties are dominated by site heterogeneity — do not show such a variation [26].

The study on individual LH1-RC complexes presented in this chapter was carried out in two steps. In a first set of experiments individual core (LH1-RC) complexes from *Rps. acidophila* were studied. Only 30% of the complexes featured optical spectra compatible with the structural model of a closed ring. The optical spectra of the other complexes were probably affected by structural heterogeneity in combination with various orientations of the complexes in the PVA film.

It was not clear whether these structural variations are a native property of the complexes or whether they are induced by isolation, purification and deposition of the sample. Maybe the different structures represent snapshots of a possible dynamic equilibrium in the photosynthetic membrane between complete rings and complexes in the process of being built.

In a second step, further research was conducted on complexes with a more defined structural variation. For this purpose three different types of LH1-RC complexes from *Rb. sphaeroides* were used. This species was chosen because a small protein PufX has been found which is thought to form an integral part of the LH1 ring [8, 11, 164, 166, 167]. For the wild type sample (PMC3_{WT}) this implies a model of an open ring in which one or two subunits are replaced by PufX. The expression of this protein can be switched off by genetic manipulation

and consequently the mutant (PMC3_{ΔX}) sample should contain closed ring LH1-RC complexes. A third sample (PMC4_{WT}) was investigated that showed a dimeric arrangement in electron-microscopy pictures [8]. The observed spectra of most complexes resembled those of *Rps. acidophila* although some of the PMC4_{WT} type could not be compared to any spectrum of *Rps. acidophila*.

The experimental observations agreed with the proposed structural models. However, this accordance is not an absolute proof for the correctness of the models because other structural arrangements are also compatible with the observations. Nevertheless the experimental approach is a good starting point to show that single-molecule spectroscopy can provide valuable information regarding to question about the structural arrangement of light-harvesting complexes. In future experiments, a native environment could be mimicked by incorporating the core complexes into lipid bilayers, thereby hopefully reducing the amount of structural heterogeneity. This would also lead to a more defined orientation of the complexes. Also, an increase of the number of spectra is required before any definitive statement can be made.

Self-aggregation of the photosynthetic unit (LH2-LH1-RC)

In most purple bacteria, the photosynthetic unit (PSU) present in the membrane, contains besides the reaction centre (RC) two types of photosynthetic membrane complexes (PMCs), the light-harvesting complex 1 (LH1) and the peripheral light-harvesting complex 2 (LH2) [11]. Depending on the growth conditions of the bacterium some species express another peripheral complex, LH3, which is a spectroscopic variant of LH2. LH1 and the RC are closely associated and form the so-called core complex, whereas LH2 is not in direct contact with the RC but transfers the energy to the RC via the LH1 complex [12].

From the knowledge of the X-ray structure of the LH2 complex, along with the lower-resolution structural information for LH1 and theoretical modelling a scheme of the arrangement of the pigment-protein complexes within the PSU has been proposed in which the core complex is surrounded by several LH2 complexes in a two-dimensional structure [13, 14]. Interestingly, the pigments show a hierarchical arrangement where pigments absorbing at higher energies are placed further away from the RC. It seems that the whole structure is highly optimised to capture light energy and, depending on the illumination conditions, either to funnel the excitation energy to the RC or to act as a reservoir to store the energy in order to avoid overexposure and damage

of the RC. A more detailed description of the PSU and its building blocks can be found in sections 2.1.1 and 2.1.2.

In the following, two experiments are presented in which the energy transfer from LH2 to the core complex within single self-aggregated photosynthetic units could be measured. In the first experiment, a sample of LH1-RC complexes was studied which contained only a low concentration of LH2 after purification. The rare events of occasionally self-aggregated PSUs could never have been found in conventional bulk measurements since the concentration of LH2 “impurities” is below the detection limit of ensemble spectroscopy. In a second experiment the self-aggregation capabilities of PMCs were examined in a more defined way by mixing a solution of LH2 complexes with a solution of LH1-RC complexes. The findings suggest that the building blocks of the PSU form stable, functional aggregates in a detergent suspension.

8.1 Experimental

8.1.1 LH1-RC sample with low concentration of LH2 impurities

In the first experiment a polymer film doped with isolated LH1-RC complexes from *Rhodobacter sphaeroides* in detergent buffer solution was studied that contained only a very low residual concentration of LH2 impurities after purification. In Fig. 8.1A a series of wide-field images from a sample of LH1-RC complexes from *Rhodobacter sphaeroides* is shown as a function of the excitation wavelength. Each bright dot represents the diffraction-limited image of an individual core complex. In order to obtain these images the excitation wavelength has been switched between 800 nm, 835 nm and 870 nm while for all images the detection wavelength has been fixed to 917 nm, i.e., the maximum of the LH1 emission. Exciting the sample at 870 nm the wide-field fluorescence image (Fig. 8.1A, right), shows several individual LH1-RC complexes from *Rhodobacter sphaeroides*. After changing the excitation to 800 or to 835 nm (Fig. 8.1A, left and centre, respectively), one of the features detected previously is still able to emit light at 917 nm although LH1-RC complexes do not absorb significantly at 800 or 835 nm.

In order to investigate this finding in more detail the fluorescence-excitation spectrum of this particular feature has been recorded, Fig. 8.1B. It consists of several narrow absorptions at 800 nm and two broad bands at about 830 nm and 870 nm which feature further substructure.

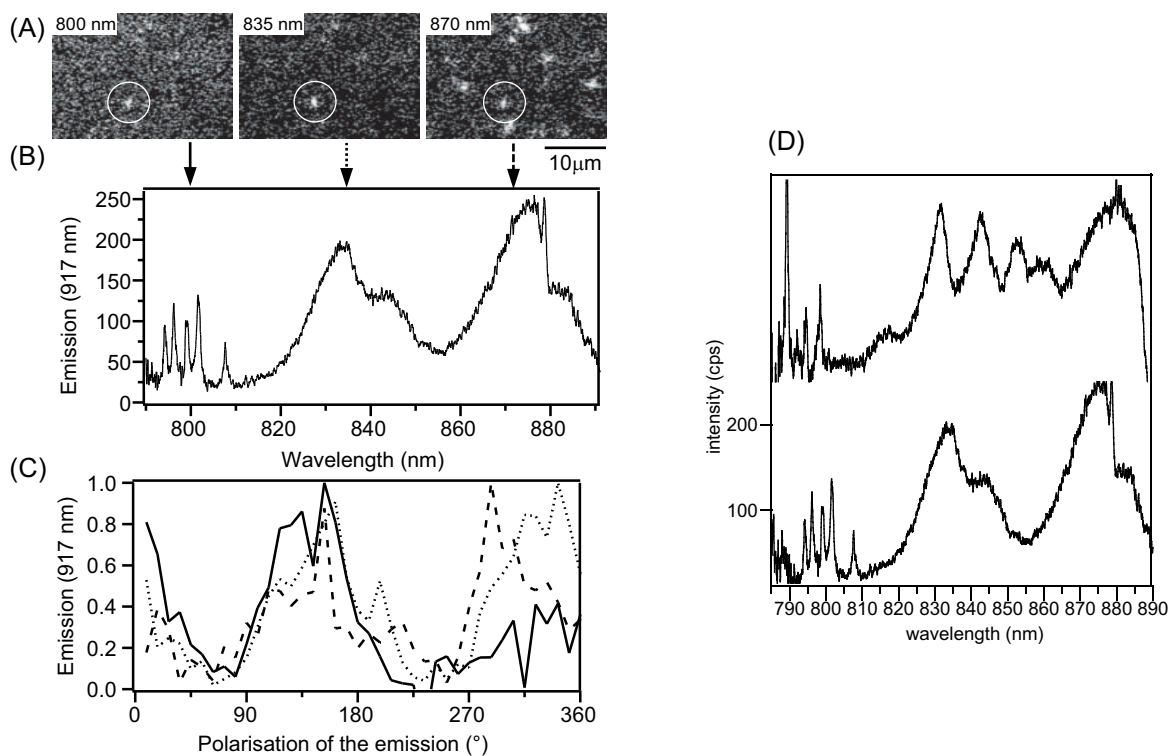


Figure 8.1: Fluorescence-imaging and fluorescence-excitation spectroscopy of a single photosynthetic unit from *Rhodobacter sphaeroides*. (A) Wide-field fluorescence images ($20 \times 25 \mu\text{m}^2$) from LHI-RC dissolved in a polymer film at 1.4 K. From left to right the excitation wavelengths were 800, 835 and 870 nm respectively at an intensity of 250 W/cm^2 . The fluorescence was detected at 917 nm. (B) Fluorescence-excitation spectrum of the feature encircled in (A). The sample has been excited at an illumination intensity of 20 W/cm^2 . (C) Intensity of the LHI fluorescence as a function of the polarisation of the emission for the feature encircled in (A). The three traces correspond to excitation wavelengths of 800 nm (solid), 835 nm (dotted) and 870 nm (dashed) as indicated by the arrows in (A). (D) Fluorescence-excitation spectra of the feature in (A) together with the second feature that showed narrow absorption lines at around 800 nm and broad bands in the 830/850 nm and 870 nm region.

Fig. 8.1C displays the relative fluorescence intensity at 917 nm as a function of the polarisation of the emission for excitation wavelengths at 800 nm, 835 nm and 870 nm as indicated by the arrows in part (B).

These data were obtained by introducing a polariser plate in front of the CCD camera. While rapidly taking fluorescence images the polariser was rotated in steps of 9° between successive images. By integrating the total intensity of the fluorescence image of an individual complex on the CCD as a function of the read-out frame number the dependence of the emitted light on the angular position of the polariser was reconstructed. Within the experimental accuracy no difference in the orientation of the emitting transition-dipole moment is observable.

Studying this sample a second “dot” showed similar spectral behaviour and its fluorescence-excitation spectrum is shown together with that of the feature described above in Fig. 8.1D.

8.1.2 Mixing of LH1-RC and LH2 solutions

In a second series of experiments, two suspensions, one containing isolated purified LH2 and the other isolated purified LH1-RC complexes, both from *Rhodospseudomonas acidophila* were mixed together in a ratio of roughly 2 LH2 complexes per LH1-RC complex before diluting the mixture in detergent buffer and spin-coating a polymer film onto a substrate as described in section 3.3. From an area of this sample a widefield image was taken by exciting the LH1 absorption at 870 nm and monitoring the LH1 fluorescence at 917 nm showing about 12 bright dots (Fig. 8.2A). A second widefield image of the same area was taken by exciting the LH2 absorption at 800 nm while recording the LH1 fluorescence at 917 nm showing about 4 bright dots. The emission from the LH1 complex is much weaker when the PSU is illuminated at 800 nm as opposed to an excitation at 870 nm. Therefore, the signal-to-background contrast is

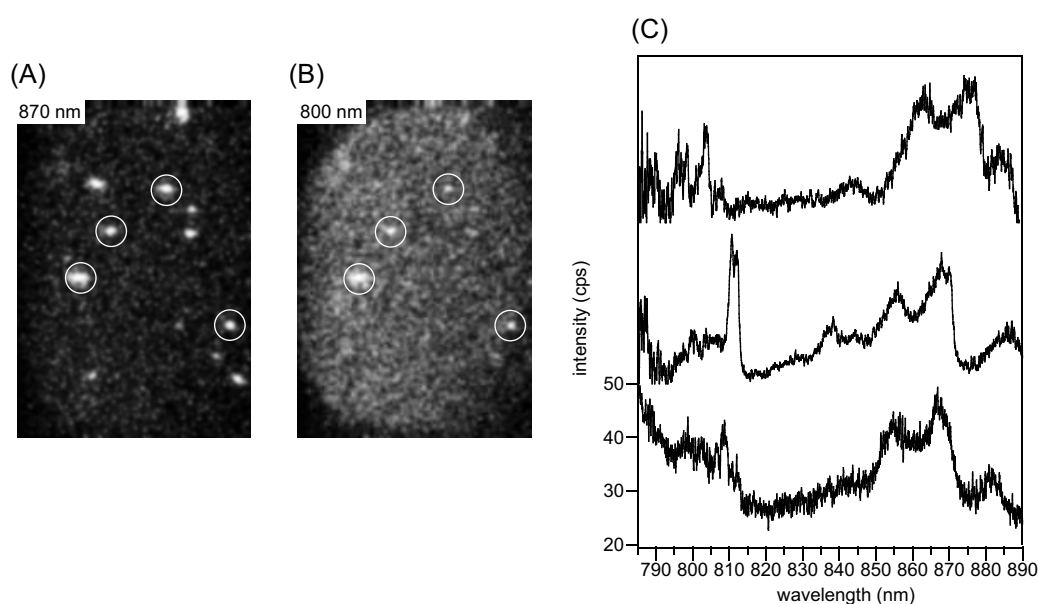


Figure 8.2: Widefield fluorescence images and fluorescence-excitation spectra from a sample for which isolated LH2 complexes from *Rps. acidophila* were mixed with LH1-RC complexes from the same species. (A) Widefield image taken by exciting at the LH1 absorption of 870 nm and detecting the LH1 emission at 917 nm. (B) Widefield image taken by exciting at the LH2 absorption of 800 nm and detecting the LH1 emission at 917 nm. The encircled “dots” appear at the same position as in image (A). (C) Fluorescence-excitation spectra that shown narrow features at around 800 nm and broad band in the 850 nm and 870 nm region.

worse when exciting at 800 nm. The dots in the image derived with an excitation at 800 nm are at positions where also at the 870 nm excitation bright dots had been visible (Fig. 8.2B). Of three spectral features that were visible at both excitation wavelengths, a confocal fluorescence-excitation spectrum was taken. The spectra show narrow features in the 800 nm region and broad features in the 850 and 870 nm regions, Fig. 8.2C.

8.2 Discussion

From these results it was concluded that the excitation-energy transfer in a single photosynthetic unit (LH2-LH1-RC) had been observed, as sketched in Fig. 8.3. This interpretation is supported by inspecting fluorescence-excitation spectra from individual, isolated LH2 and LH1-RC complexes, Fig. 8.4. The upper traces show the low temperature fluorescence-excitation spectra from isolated LH2 (*Rhodospseudomonas acidophila*) [25] and isolated LH1-RC (*Rhodobacter sphaeroides*) recorded from a large ensemble of proteins while the lower traces show the respective fluorescence-excitation spectra of an individual light-harvesting complex.

When comparing the data presented so far two discrepancies between the spectra shown in Figs. 8.1D and 8.4 become apparent. First, the spectra in Fig. 8.1D show broad bands at about 830 nm rather than a band at 850 nm and second in the lower spectrum in Fig. 8.1D a sharp peak is visible in the band at 870 nm which does not appear in the displayed isolated LH1-RC spectrum. Due to the lack of single-molecule spectra of isolated LH2 from *Rhodobacter sphaeroides* in Fig. 8.4A spectra from individual LH2 complexes from *Rhodospseudomonas acidophila* have been displayed. However, it is known that at low temperatures the B850 band

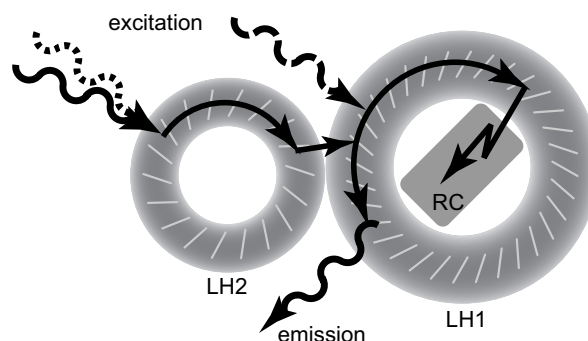


Figure 8.3: Schematic sketch of the supramolecular arrangement of a photosynthetic unit adapted from [70]. The arrows indicate the excitation, emission and energy transfer pathways.

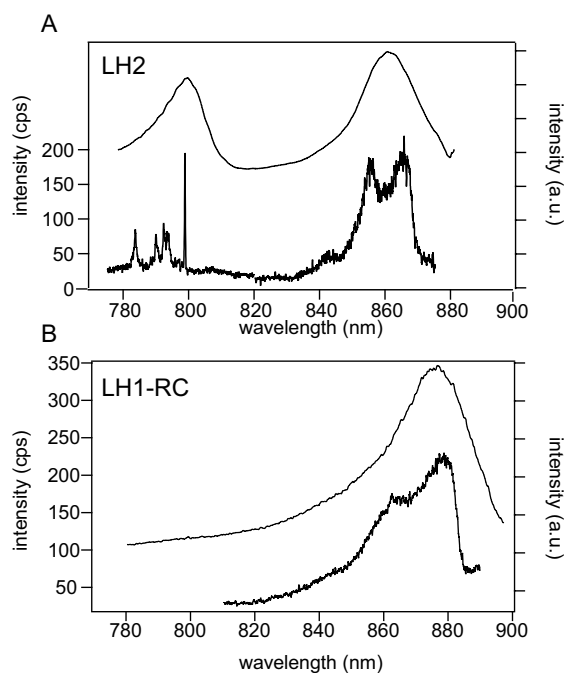


Figure 8.4: Comparison of various fluorescence-excitation spectra from light-harvesting complexes recorded at 1.4 K. (A) LH2 from *Rhodospseudomonas acidophila*. The upper trace has been recorded from a large ensemble of complexes and the lower trace shows the respective spectrum from an individual complex. For both spectra the LH2 emission has been detected at 890 nm. The left vertical scale is valid for the lower trace (Adapted from [25]). B: LH1-RC from *Rhodobacter sphaeroides*. The upper trace has been recorded from a large ensemble of complexes and the lower trace shows the respective spectrum from an individual complex. For both spectra the LH1 emission has been detected at 917 nm. The left vertical scale is valid for the lower trace.

of LH2 from *Rb. sphaeroides* is shifted 18 nm to the blue with respect to the B850 band of LH2 from *Rps. acidophila* [113]. The sharp feature in the fluorescence-excitation spectra of individual light-harvesting complexes has been observed previously for both LH2 and LH1. It can be explained to result from the emission of the lowest excited state of the exciton manifold ($k = 0$) which has a long fluorescence lifetime of about 1 ns [25] or by the presence of a trap state in the ring of chromophores [28]. Whether it can be detected depends on the details of the electronically excited states of the particular pigment-protein complex under study. As the LH complexes in the mixed sample are from *Rps. acidophila* their B850 band is at the same spectral position as in the spectrum in Fig. 8.4A. However, the B850 and B870 bands tend to overlap as can be seen in Fig. 8.2C and can not be distinguished as well as for *Rb. sphaeroides*. Taking these arguments into account it can be stated that the spectra shown in Figs. 8.1 and 8.2 resemble a superposition of a spectrum of an individual LH2 and an individual LH1-RC complex.

In Fig. 8.1C the trace that corresponds to an excitation wavelength of 800 nm shows beyond a polarisation angle of 270° a significant decrease in intensity with respect to the other two traces. If the narrow features at about 800 nm in Fig. 8.1B are assigned to the B800 absorptions of an individual LH2 complex this can be explained straightforwardly. In chapter 4 it has been found that the pigment-protein complexes are susceptible to light induced spectral fluctuations resulting in slight changes of the spectral positions of the individual absorptions during the experiment. This is of minor influence for the broad B850 and B870 spectral features but the relatively narrow absorption lines of the B800 band might get shifted out of resonance with the excitation laser during data acquisition.

From the relative intensity of the LH2 bands with respect to the LH1 bands in Figs. 8.1 and 8.2 it has to be concluded that the transfer of excitation energy occurs very efficiently even in a non-membrane environment. Although the signal-to-noise ratio is worse for the mixed sample in Fig. 8.2C compared to the LH1-RC sample in Fig. 8.1D the ratio of the intensities of the LH2 bands to the LH1 bands is comparable. Due to chromatic aberrations in the low-temperature microscope the effective excitation intensity (photon energy / time \times area) is lower at 800 nm as compared with the intensity at 870 nm. As a consequence of this, the efficiency of the LH2-LH1 energy transfer is even underestimated by the above mentioned criterion.

In summary, the data indicate clearly an energy transfer from the peripheral LH2 to a LH1-RC complex in single supramolecular LH2-LH1-RC aggregates. The observation of narrow lines in the B800 region of the fluorescence-excitation spectrum suggests that one or, at most two LH2 are attached to the LH1-RC complex. A larger number of LH2 complexes would result in a significant change of the spectral shape of the B800 absorption due to “ensemble” averaging. The detection of the fluorescence features of the LH1-RC sample presented in Fig. 8.1, testifying energy transfer within an individual PSU, was a relatively rare event that could be observed only for 2 out of 32 complexes studied.

This can be understood because the concentration of LH2 complexes in the LH1-RC preparations is very low, i.e., below the detection limit of a conventional ensemble absorption spectrum [164]. In the case of the “mixing” experiment, 4 out of 12 dots emitted light at both excitation wavelengths, i.e., one third of LH1-RC complexes was bound to one to two LH2 complexes. As the concentration of LH2 was twice as high as the LH1-RC concentration it can be stated that about 10–30% of the LH2 complexes in the sample were attached to LH1. This suggests that

the interaction between the peripheral and core antenna complex is strong enough to withstand partly detergent exposure during the purification procedure.

Previously, excitation-energy transfer from LH2 to LH1-RC has been observed at a reduced rate for assemblies reconstituted into liposomes [178]. The work presented in this chapter shows the formation of functional PSUs even in a non-membrane environment. Finally, given the relatively low probability of LH2 binding to the core complex in detergent PMC suspensions, ensemble studies of the purified system are severely hampered. In contrast, the results show that the single-molecule approach allows the investigation of energy transfer and protein-protein interactions in spontaneously reconstituted PSUs.

8.3 Summary

In this chapter the energy transfer from a peripheral LH2 complex to a core LH1-RC complex was observed in a minimal photosynthetic unit comprising one or at most two LH2 complexes attached to a single LH1-RC complex. In a first set of experiments that was conducted on a sample of LH1-RC complexes from *Rb. sphaeroides* containing a low concentration of LH2 impurities of which about 10–30% were attached to LH1. In a second series of experiments two independent solutions were mixed which contained either isolated LH2 or isolated LH1-RC complexes from *Rps. acidophila*. This resulted in fluorescence-excitation spectra similar to those observed for *Rb. sphaeroides* suggesting that LH2-LH1-RC complexes can be formed in a non-membrane environment.

In summary, these experiments suggest that the interaction between the peripheral and core antenna complex is strong enough to withstand partly detergent exposure during the purification procedure and to form photosynthetic units even in a non-membrane environment.

Summary and outlook

In this thesis, individual light-harvesting (LH) complexes that are involved in the first steps of photosynthesis in purple bacteria were studied. The steps consist of the absorption of a photon, for instance by the B800 pigment pool in the peripheral LH2 complex (chapters 4 and 5) followed by a rapid transfer of the excitation energy via the B850 pool of LH2 (chapter 6) and the B870 assembly of LH1 (chapter 7) to the reaction centre, where a charge separation occurs leading to the protonation of a ubiquinone. This hydroquinone leaves the RC and fuels further biochemical processes (chapter 7). The whole sequence of energy transfer steps occurs in the so called photosynthetic unit which is a supramolecular assembly of these pigment-protein complexes (chapter 8). In the following the results derived in this thesis will be summarised.

In one series of experiments the focus lay on the spectral properties of the bacteriochlorophyll (BChl) *a* molecules within the light-harvesting complexes. By applying polarisation dependent spectroscopy, detailed information about the interactions between the pigments was obtained and the structure of the excited states could be unravelled for all three types of pigment pools.

For the B800 band, these experiments resulted in the finding that excitations of BChl *a* molecules are mainly localised on individual molecules. However, the observation of mutual orientations of transition-dipole moments different from 0° , 45° or 90° — as predicted by the x-ray struc-

ture — provided direct evidence for an electronic coupling in the weak to intermediate range between individual BChl *a* molecules in the B800 assembly. Also, temporal variations in the coupling strength could be observed.

The electronic structure of the B850 band was analysed using a novel technique — widefield fluorescence-excitation spectroscopy — which was shown to speed up the measurement time by a factor of 50 compared to conventional confocal fluorescence-excitation spectroscopy. It was confirmed that the B850 assembly of BChl *a* pigments in LH2 represents a strongly coupled system whose excited states at low temperature can be described as collective excitations, so called Frenkel excitons. The low energy $k = \pm 1$ exciton states could be resolved. On the basis of Monte-Carlo simulations a distribution of the site energies (random diagonal disorder) and a C_2 -type modulation of the site energies and the interactions (correlated diagonal and off-diagonal disorder) had to be assumed to account for the relative intensities and spectral positions of the $k = \pm 1$ exciton transitions. The modulation of the site energies was thought to be imposed by a small elliptical deformation of the complex which induces conformational changes in the local proteins environment of the BChl *a* molecule and influences their site energies. Such a small geometrical perturbation instead of an elliptical deformation of 7–8.5% as proposed in literature is more compatible with the circular structure observed in x-ray crystallography.

From measurements on LH1 it was concluded that the B870 assembly of BChl *a* pigments also represents a strongly coupled system. The experimental observations proved to be distinctly different from those of the B850 band of LH2. The evidence for a circular exciton was less pronounced as the spectra showed a large variation concerning the number of absorption bands and their polarisation behaviour which was attributed to a pronounced structural disorder on the basis of theoretical considerations as well as Monte-Carlo simulations. For LH1 complexes from *Rhodopseudomonas acidophila* it was not clear whether these structural variations are a native property of the complexes or whether they are induced by isolation, purification and deposition of the sample. In contrast three different types of LH1 complexes from *Rhodobacter sphaeroides* were looked at for which a structural model exists in literature. The optical properties of the measured spectra were in accordance with the suggested models. However, the observations did not completely rule out other structural arrangements.

A second point of interest lay in spectral diffusion processes in the weakly coupled assembly of B800 pigments. Here, the chromophores were used as local probes to monitor the heterogeneity

in their local environment. In general, the spectrum of a B800 ring of an individual LH2 complex from *Rs. molischianum* showed several narrow lines, indicating that the BChl *a* molecules absorb at slightly different excitation energies. This spectral heterogeneity could be attributed to intra- and inter-complex disorder, reflecting the differences in excitation energy of the B800 chromophores within and between complexes and their ratio could be analytically modelled by assuming that the energetic disorder of the site energies of the B800 BChl *a* molecules is described by a *single* random variable.

Apart from static disorder, also temporal spectral changes in the B800 spectrum were observed which were attributed to conformational changes of the proteins in the vicinity of the chromophores as the BChl *a* molecules react on changes of the pigment-protein interaction with changes of their excited state energy. It was found that the spectral diffusion was not always a random process but that for some complexes the absorptions changed their spectral position in a correlated way. With respect to the energy separation of correlated diffusing absorption lines and the related timescales three different groups of spectral diffusion were found. These groups could be attributed to the presence of at least three distinct tiers in the hierarchically organised rugged energy landscape of the proteins in the binding pocket of the B800 BChl *a* molecules.

To automatise and simplify the analysis of a large number of consecutively recorded spectra a pattern recognition approach using multivariate statistical analysis was applied which groups similar looking spectra into classes. As the transition energy of the BChl *a* chromophores depends on their environment each class comprises spectra that were recorded at times during which the chromophores featured very similar environments, thus eliminating spectral diffusion. The approach was first tested for its applicability on spectroscopic data on two previously analysed complexes featuring different types of spectral diffusion and it was found that the software proved to be useful in analysing spectroscopic data from single-molecule experiments. In the second step, a complex for which a huge number of spectra had been recorded was analysed. This revealed that the B800 absorptions consist of a narrow zero-phonon line accompanied by a broad less intense phonon side-band. The related Huang–Rhys factor of 0.21–0.84 is indicative for a very weak electron-phonon coupling in the B800 band.

A final experiment was performed on a sample of LH1 complexes from *Rhodobacter sphaeroides* containing a low concentration of LH2 impurities. In some spectra a clear indication was found for an energy transfer from a peripheral LH2 to a core LH1-RC complex in a single supramolec-

ular LH2-LH1-RC aggregate. The observation of narrow lines in the B800 region of the fluorescence excitation spectrum suggested that one or, at most two LH2 were attached to a LH1-RC complex. These findings were supported by further experiments in which two independent solutions were mixed which contained either isolated LH2 or isolated LH1-RC complexes from *Rhodospseudomonas acidophila*. This resulted in fluorescence-excitation spectra similar to those observed for *Rhodobacter sphaeroides*, suggesting that the interaction between the peripheral and core antenna complex is strong enough to withstand partly detergent exposure during the purification procedure and to form photosynthetic units even in a non-membrane environment.

All experiments in this thesis were conducted on light-harvesting complexes embedded in a polymer matrix, which is far off from the natural environment and it was argued that some of the observed properties, especially the large structural heterogeneity, might be induced by the polymer environment. Therefore, it would be interesting to study the complexes in their biological surrounding. In future experiments, a native environment could be mimicked by incorporating the complexes into lipid bilayers, which would also lead to a more defined orientation of the complexes with respect to the substrate.

A further goal would be the application of the multivariate statistical analysis to the B850 band of LH2, where the broad $k = \pm 1$ absorptions appear to have identical line shapes. However, theory predicts that the linewidths of the two bands should be different and only appear identical in the measurements due to spectral diffusion processes. It would be interesting whether the pattern recognition approach could eliminate the spectral diffusion and reveal this difference.

The development of technological products is a continuous process which has led, for instance, in the case of the electron-multiplied CCD camera to an enormous improvement of its sensitivity and read-out speed during the work on this thesis. Also optical techniques have improved and it is now possible to employ total internal reflection microscopy inside the cryostat used for this thesis, increasing the signal-to-noise ratio. This progress has opened the possibility to investigate the narrow spectrally diffusing absorptions in the B800 band of LH2 with widefield fluorescence-excitation microscopy, which would allow to gain equally detailed information on the observed phenomena but at a much higher statistical significance.

In conclusion, this thesis demonstrated that low-temperature single-molecule spectroscopy provides a unique method to reveal details of pigment-pigment interactions in the weak to intermediate as well as strong coupling limit that are inaccessible by other experimental methods.

Bibliography

- [1] DEISENHOFER, J., O. EPP, K. MIKI, R. HUBER, AND H. MICHEL, “X-ray structure analysis of a membrane protein complex. Electron density map at 3 Å resolution and a model of the chromophores of the photosynthetic reaction center from *Rhodospseudomonas viridis*.” *J. Mol. Biol.* **180** 385–398 (1984).
- [2] MCDERMOTT, G., S. PRINCE, A. FREER, A. HAWTHORNTHWAIT-LAWLESS, M. PAPIZ, R. COGDELL, AND N. ISAACS, “Crystal structure of an integral membrane light-harvesting complex from photosynthetic bacteria.” *Nature* **374** 517–521 (1995).
- [3] KOEPKE, J., X. HU, C. MUENKE, K. SCHULTEN, AND H. MICHEL, “The crystal structure of the light-harvesting complex II (B800-850) from *Rhodospirillum molischianum*”. *Structure* **4** 581–597 (1996).
- [4] PAPIZ, M., S. PRINCE, T. HOWARD, R. COGDELL, AND N. ISAACS, “The structure and thermal motion of the B800-850 LH2 complex from *Rps. acidophila* at 2.0 Å resolution and 100 K: New structural features and functionally relevant motions”. *J. Mol. Biol.* **326** 1523–1538 (2003).
- [5] MCLUSKEY, K., S. PRINCE, R. COGDELL, AND N. ISAACS, “The Crystallographic Structure of the B800-820 LH3 Light-Harvesting Complex from the Purple Bacteria *Rhodospseudomonas acidophila* strain 7050”. *Biochemistry* **40** 8783–8789 (2001).
- [6] KARRASCH, S., P. BULLOUGH, AND R. GHOSH, “The 8.5 Å projection map of the light-harvesting complex 1 from *Rhodospirillum rubrum* reveals a ring composed of 16 subunits”. *EMBO J.* **14** 631–638 (1995).
- [7] WALZ, T., S. JAMIESON, C. BOWERS, P. BULLOUGH, AND C. HUNTER, “Projection Structures of Three Photosynthetic Complexes from *Rhodobacter sphaeroides*: LH2 at 6 Å, LH1 and RC-LH1 at 25 Å”. *J. Mol. Biol.* **282** 833–845 (1998).
- [8] JUNGAS, C., J. RANCK, J. RIGAUD, P. JOLIOT, AND A. VERMEGLIO, “Supramolecular organization of the photosynthetic apparatus of *Rhodobacter sphaeroides*”. *EMBO J.* **18** 534–542 (1999).
- [9] JAMIESON, S., P. WANG, P. QIAN, J. KIRKLAND, M. CONROY, C. HUNTER, AND P. BULLOUGH, “Projection structure of the photosynthetic reaction centre-antenna complex of *Rhodospirillum rubrum* at 8.5 Å resolution”. *EMBO J.* **21** 3927–3935 (2002).
- [10] SCHEURING, S., J. SEGUIN, S. MARCO, D. LÉVY, B. ROBERT, AND J. RIGAUD, “Nanodissection and high-resolution imaging of the photosynthetic core complex in native membranes of *Rhodospseudomonas viridis* by atomic force microscopy”. *Proc. Natl. Acad. Sci. USA* **100** 1690–1693 (2003).

- [11] COGDELL, R., P. FYFE, S. BARRETT, S. PRINCE, A. FREER, N. ISAACS, P. MCGLYNN, AND C. HUNTER, "The purple bacterial photosynthetic unit". *Photosynth. Res.* **48** 55–63 (1996).
- [12] SUNDSTRÖM, V., T. PULLERITS, AND R. VAN GRONDELLE, "Photosynthetic Light-Harvesting: Reconciling Dynamics and Structure of Purple Bacterial LH2 Reveals Function of Photosynthetic Unit". *J. Phys. Chem. B* **103** 2327–2346 (1999).
- [13] PAPIZ, M., S. PRINCE, A. HAWTHORNTHWAIT-LAWLESS, G. MCDERMOTT, A. FREER, N. ISAACS, AND R. COGDELL, "A model for the photosynthetic apparatus of purple bacteria". *Trends Plant Sci.* **1** 198–206 (1996).
- [14] HU, S. AND K. SCHULTEN, "How nature harvests sunlight". *Physics Today* **50** 28–34 (1997).
- [15] VAN AMERONGEN, H., L. VALKUNAS, AND R. VAN GRONDELLE, *Photosynthetic Excitons* (World Scientific Publishing Co. Pte. Ltd., Singapore, New Jersey, London, Hong Kong 2000).
- [16] FIDDER, H., J. KNOESTER, AND D. WIERSMA, "Optical properties of disordered molecular aggregates: A numerical study". *J. Chem. Phys.* **95** 7880–7890 (1991).
- [17] JUZELUNAS, G. AND P. REINEKER, "Influence of exciton-exciton interaction on one-to-two exciton transitions in molecular aggregates with linear and circular geometries". *J. Chem. Phys.* **107** 9801–9806 (1997).
- [18] CORY, M., M. ZERNER, X. HU, AND K. SCHULTEN, "Electronic Excitations in Aggregates of Bacteriochlorophylls". *J. Phys. Chem. B* **102** 7640–7650 (1998).
- [19] DE ROSSI, U., S. DÄHNE, U. GOMEZ, AND H. PORT, "Evidence for incoherent energy transfer processes in J-aggregates with Davydov splitting". *Chem. Phys. Lett.* **287** 395–402 (1998).
- [20] MOSTOVOY, M. AND J. KNOESTER, "Statistics of Optical Spectra from Single-Ring Aggregates and Its Application to LH2." *J. Phys. Chem. B* **104** 12355–12364 (2000).
- [21] SCHEBLYKIN, I., O. SLIUSARENKO, L. LEPNEV, A. VITUKHNOVSKY, AND M. VAN DER AUWERAER, "Strong Nonmonotonous Temperature Dependence of Exciton Migration Rate in J Aggregates at Temperatures from 5 to 300 K". *J. Phys. Chem. B* **104** 10949–10951 (2000).
- [22] DEMPSTER, S., S. JANG, AND R. SILBEY, "Single molecule spectroscopy of disordered circular aggregates: A perturbation analysis". *J. Chem. Phys.* **114** 10015–10023 (2001).
- [23] VACHA, M., M. SAEKI, O. ISOBE, K. HASHIZUME, AND T. TANI, "Mapping the orientation of exciton transition dipoles along individual nanostructures of molecular J-aggregates". *J. Chem. Phys.* **115** 4973–4976 (2001).
- [24] VAN OIJEN, A., M. KETELAARS, J. KÖHLER, T. AARTSMA, AND J. SCHMIDT, "Spectroscopy of individual light-harvesting 2 complexes of *Rhodospseudomonas acidophila*: diagonal disorder, intercomplex heterogeneity, spectral diffusion, and energy transfer in the B800 band". *Biophys. J.* **78** 1570–1577 (2000).
- [25] VAN OIJEN, A., M. KETELAARS, J. KÖHLER, T. AARTSMA, AND J. SCHMIDT, "Unraveling the electronic structure of individual photosynthetic pigment-protein complexes". *Science* **285** 400–402 (1999).
- [26] KETELAARS, M., A. VAN OIJEN, M. MATSUSHITA, J. KÖHLER, J. SCHMIDT, AND T. AARTSMA, "Spectroscopy on the B850 Band of Individual Light-Harvesting 2 Complexes of *Rhodospseudomonas acidophila* I. Experiments and Monte Carlo Simulations". *Biophys. J.* **80** 1591–1603 (2001).

- [27] TIETZ, C., O. CHEKHLOV, A. DRÄBENSTEDT, J. SCHUSTER, AND J. WRACHTRUP, "Spectroscopy on single light-harvesting complexes at low temperature". *J. Phys. Chem. B* **103** 6328–6333 (1999).
- [28] GERKEN, U., F. JELEZKO, B. GÖTZE, M. BRANSCHÄDEL, C. TIETZ, R. GHOSH, AND J. WRACHTRUP, "Membrane Environment Reduces the Accessible Conformational Space Available to an Integral Membrane Protein". *J. Phys. Chem. B* **107** 338–343 (2003).
- [29] HU, X., T. RITZ, A. DAMJANOVIC, F. AUTENRIETH, AND K. SCHULTEN, "Photosynthetic Apparatus of Purple Bacteria". *Q. Rev. Biophys.* **35** 1–62 (2002).
- [30] AUSTIN, R., R. BEESON, L. EISENSTEIN, H. FRAUENFELDER, AND I. GUNSALUS, "Dynamics of Ligand Binding to Myoglobin". *Biochemistry* **14** 5355–5373 (1975).
- [31] FRAUENFELDER, H., S. SLIGAR, AND P. WOLYNES, "The energy landscapes and motions of proteins". *Science* **254** 1598–1603 (1991).
- [32] NIENHAUS, G. AND R. YOUNG, "Protein Dynamics". In G. TRIGG AND E. IMMERGUT, eds., "Encyclopedia of Applied Physics Volume 15: Power Electronics to Raman Scattering", volume 15 of *Encyclopedia of Applied Physics*, pages 163–184 (Wiley VCH, New York 1996).
- [33] FRAUENFELDER, H., G. NIENHAUS, AND R. YOUNG, "Relaxation and Disorder in Proteins". In R. RICHERT, ed., "Disorder effects in relaxational processes", pages 591–614 (Springer Verlag Berlin, Berlin 1994).
- [34] MOERNER, W. AND L. KADOR, "Optical detection and spectroscopy of single molecules in a solid". *Phys. Rev. Lett.* **62** 2535–2538 (1989).
- [35] ORRIT, M. AND J. BERNARD, "Single pentacene molecules detected by fluorescence excitation in a *p*-terphenyl crystal". *Phys. Rev. Lett.* **65** 2716–2719 (1990).
- [36] STRICK, T., J.-F. ALLEMAND, V. CROQUETTE, AND D. BENSIMON, "Twisting and stretching single DNA molecules". *Prog. Biophys. Mol. Biol.* **74** 115–140 (2000).
- [37] HARMS, G., L. COGNET, P. LOMMERSE, G. BLAB, AND T. SCHMIDT, "Autofluorescent Proteins in Single-Molecule Research: Applications to Live Cell Imaging Microscopy". *Biophys. J.* **80** 2396–2408 (2001).
- [38] HUGEL, T., N. HOLLAND, A. CATTANI, L. MORODER, M. SEITZ, AND H. GAUB, "Single-Molecule Optomechanical Cycle". *Science* **296** 1103–1106 (2002).
- [39] SAUER, M., B. ANGERER, W. ANKENBAUER, Z. FÖLDES-PAPP, F. GÖBEL, K.-T. HAN, R. RIGLER, A. SCHULZ, J. WOLFRUM, AND C. ZANDER, "Single molecule DNA sequencing in submicrometer channels: state of the art and future prospects". *J. Biotechnol.* **86** 181–201 (2001).
- [40] ALI, M., S. UEMURA, K. ADACHI, H. ITOH, K. KINOSITA, AND S. ISHIWATA, "Myosin V is a left-handed spiral motor on the right-handed actin helix." *Nat. Struct. Biol.* **9** 464–467 (2002).
- [41] YASUDA, R., T. MASAIKE, K. ADACHI, H. NOJI, H. ITOH, AND K. KINOSITA, "The ATP-waiting conformation of rotating F1-ATPase revealed by single-pair fluorescence resonance energy transfer". *Proc. Natl. Acad. Sci. USA* **100** 9314–9316 (2003).
- [42] SEISENBERGER, G., M. RIED, T. ENDRESS, H. BUNING, M. HALLEK, AND C. BRÄUCHLE, "Real-time single-molecule imaging of the infection pathway of an adeno-associated virus". *Science* **294** 1929–1932 (2001).

- [43] LOUNIS, B. AND W. MOERNER, "Single photons on demand from a single molecule at room temperature". *Nature* **407** 491–493 (2000).
- [44] TAMARAT, P., A. MAALI, B. LOUNIS, AND M. ORRIT, "Ten years of Single-Molecule Spectroscopy". *J. Phys. Chem. A* **104** 1–16 (2000).
- [45] ORRIT, M., "Single-molecule spectroscopy: The road ahead". *J. Chem. Phys.* **117** 10938–10946 (2002).
- [46] MOERNER, W., "A Dozen Years of Single-Molecule Spectroscopy in Physics, Chemistry, and Biophysics". *J. Phys. Chem. B* **106** 910–927 (2002).
- [47] KÖHLER, J., J. DISSELHORST, M. DONCKERS, E. GROENEN, J. SCHMIDT, AND W. MOERNER, "Magnetic resonance of a single molecular spin". *Nature* **363** 242–244 (1993).
- [48] WRACHTRUP, J., C. VON BORCZYKOWSKI, J. BERNARD, M. ORRIT, AND R. BROWN, "Optical detection of magnetic resonance in a single molecule". *Nature* **363** 244–245 (1993).
- [49] BLANKENSHIP, R., *Molecular mechanisms of Photosynthesis* (Blackwell Science, Malden, MA 2002).
- [50] STRASBURGER, E., *Lehrbuch der Botanik* (Gustav Fischer Verlag, Stuttgart, Jena, New York 1991), 33 edition.
- [51] HU, X., A. DAMJANOVIC, T. RITZ, AND K. SCHULTEN, "Architecture and mechanism of the light-harvesting apparatus of purple bacteria". *Proc. Natl. Acad. Sci. USA* **95** 5935–5941 (1998).
- [52] MCMAHON, B., J. MÜLLER, C. WRAIGHT, AND G. NIENHAUS, "Electron Transfer and Protein Dynamics in the Photosynthetic Reaction Center". *Biophys. J.* **74** 2567–2587 (1998).
- [53] STRYER, L., *Biochemistry* (W. H. Freeman and Company, New York 2000), fourth edition.
- [54] VAN GRONDELLE, R., J. DEKKER, T. GILLBRO, AND V. SUNDSTRÖM, "Review: Energy transfer and trapping in photosynthesis". *Biochim. Biophys. Acta* **1187** 1–65 (1994).
- [55] COGDELL, R., N. ISAACS, T. HOWARD, K. MCLUSKEY, N. FRASER, AND S. PRINCE, "How Photosynthetic Bacteria Harvest Solar Energy". *J. Bacteriol.* **181** 3869–3879 (1999).
- [56] RÖDER, B., *Einführung in die molekulare Photobiophysik* (Teubner, Stuttgart; Leipzig 1999).
- [57] FISCHER, F., *Die Chemie der Pyrrole* (Academ. Verlagsges., Berlin 1940).
- [58] SCHEER, H., *Chlorophylls* (CRC Press, Boca Raton, Florida 1991).
- [59] GOUTERMAN, M., "Spectra of porphyrins". *J. Molec. Spectroscopy* **6** 138–163 (1961).
- [60] GALL, A., G. FOWLER, C. HUNTER, AND B. ROBERT, "Influence of the Protein Binding Site on the Absorption Properties of the Monomeric Bacteriochlorophyll in *Rhodobacter sphaeroides* LH2 Complex". *Biochemistry* **36** 16282–16287 (1997).
- [61] KOYAMA, Y., M. KUKI, P. ANDERSSON, AND T. GILLBRO, "Singlet excited states and the light-harvesting function of carotenoids in bacterial photosynthesis". *Photochem. Photobiol.* **63** 243–256 (1996).
- [62] COGDELL, R., "Carotenoids in photosynthesis". *Pure Applied Chem.* **57** 723–728 (1985).

- [63] COGDELL, R., N. ISAACS, A. FREER, J. ARRELANO, T. HOWARD, M. PAPIZ, A. HAWTHORNTWHAITE-LAWLESS, AND S. PRINCE, "The structure and function of the LH2 (B800-850) complex from the purple photosynthetic bacterium *Rhodospseudomonas acidophila* strain 10050 [published erratum appears in *Prog Biophys Mol Biol* 1998;70(3):I-V]". *Prog. Biophys. Mol. Biol.* **68** 1–27 (1997).
- [64] HORN, R. AND H. PAULSEN, "Folding *In vitro* of Light-harvesting Chlorophyll *a/b* Protein is Coupled with Pigment Binding". *J. Mol. Biol.* **318** 547–556 (2002).
- [65] MAUZERALL, D. AND N. GREENBAUM, "The absolute size of a photosynthetic unit". *Biochim. Biophys. Acta* **974** 119–140 (1989).
- [66] VAN GRONDELLE, R. AND V. SUNDSTRÖM, *Photosynthetic light harvesting systems* (Walter de Gruyter & Co., Berlin, New York 1988).
- [67] HU, X., T. RITZ, A. DAMJANOVIC, AND K. SCHULTEN, "Pigment Organization and Transfer of Electronic Excitation in the Photosynthetic Unit of Purple Bacteria". *J. Phys. Chem. B* **101** 3854–3871 (1997).
- [68] PULLERITS, T. AND V. SUNDSTRÖM, "Photosynthetic Light-Harvesting Pigment-Protein Complexes: Toward Understanding How and Why". *Acc. Chem. Res.* **29** 381–389 (1996).
- [69] ZUBER, H., "Structure and function of light-harvesting complexes and their polypeptides". *Photochem. Photobiol.* **42** 821–844 (1985).
- [70] KÜHLBRANDT, W., "Many wheels make light work". *Nature* **374** 497–498 (1995).
- [71] BERNHARDT, K. AND H.-W. TRISSL, "Theories for kinetics and yields of fluorescence and photochemistry: how, if at all, can different models of antenna organization be distinguished experimentally?" *Biochim. Biophys. Acta* **1409** 125–142 (1999).
- [72] DE CARO, C., R. VISSCHERS, R. VAN GRONDELLE, AND S. VÖLKER, "Inter- and Intraband Energy Transfer in LH2-Antenna Complexes of Purple Bacteria. A Fluorescence Line-Narrowing and Hole-Burning Study". *J. Phys. Chem.* **98** 10584–10590 (1994).
- [73] KENNIS, J., A. STRELTSOV, H. PERMENTLER, T. AARTSMA, AND J. AMESZ, "Exciton Coherence and Energy Transfer in the LH2 Antenna Complex of *Rhodospseudomonas acidophila* at Low Temperature". *J. Phys. Chem. B* **101** 8369–8374 (1997).
- [74] WENDLING, M., F. VAN MOURIK, I. VAN STOKKUM, J. SALVERDA, H. MICHEL, AND R. VAN GRONDELLE, "Low-Intensity Pump-Probe Measurements on the B800 Band of *Rhodospirillum molischianum*". *Biophys. J.* **84** 440–449 (2003).
- [75] WU, H.-M., S. SAVIKHIN, N. REDDY, R. JANKOWIAK, R. COGDELL, W. STRUVE, AND G. SMALL, "Femtosecond and hole-burning studies of the B800's excitation energy relaxation dynamics in the LH2 antenna complex of *Rhodospseudomonas acidophila* (Strain 10050)". *J. Phys. Chem.* **100** 12022–12033 (1996).
- [76] CHACHISVILIS, M., O. KÜHN, T. PULLERITS, AND V. SUNDSTRÖM, "Excitons in photosynthetic purple bacteria: wavelike motion or incoherent hopping?" *J. Phys. Chem. B* **101** 7275–7283 (1997).
- [77] JIMENEZ, R., S. DIKSHIT, S. BRADFORTH, AND G. FLEMING, "Electronic excitation transfer in the LH2 complex of *Rhodobacter sphaeroides*". *J. Phys. Chem.* **100** 6825–6834 (1996).

- [78] VULTO, S., J. KENNIS, A. STRELTSOV, J. AMESZ, AND T. AARTSMA, "Energy relaxation within the B850 absorption band of the isolated light-harvesting complex LH2 from *Rhodospseudomonas acidophila* at low temperature". *J. Phys. Chem. B* **103** 878–883 (1999).
- [79] MONSHOUWER, R., M. ABRAHAMSSON, F. VAN MOURIK, AND R. VAN GRONDELLE, "Superradiance and Exciton Delocalization in Bacterial Photosynthetic Light-Harvesting Systems". *J. Phys. Chem. B* **101** 7241–7248 (1997).
- [80] VISSCHERS, R., C. CHANG, F. VAN MOURIK, P. PARKES-LOACH, A. HELLER, P. LOACH, AND R. VAN GRONDELLE, "Fluorescence polarization and low-temperature absorption spectroscopy of a subunit form of light harvesting complex I from purple bacteria". *Biochemistry* **30** 5734–5742 (1991).
- [81] GALL, A., *Purification, characterisation and crystallisation from a range of Rhodospirillineae pigment-protein complexes*. PhD thesis, University of Glasgow, U.K. (1995).
- [82] PARKES-LOACH, P., C. LAW, P. RECCHIA, J. KEHOE, S. NEHRLICH, J. CHEN, AND P. LOACH, "Role of the core region of the PufX protein in inhibition of reconstitution of the core light-harvesting complexes of *Rhodobacter sphaeroides* and *Rhodobacter capsulatus*". *Biochemistry* **40** 5593–5601 (2001).
- [83] QIAN, P., T. AGURA, Y. OYAMA, AND R. COGDELL, "Isolation and purification of the reaction center (RC) and the core (RC-LH1) complex from *Rhodobium marinum*: the LH1 ring of the detergent-solubilized core complex contains 32 bacteriochlorophylls". *Plant Cell Physiol.* **41** 1347–1353 (2000).
- [84] ALLEN, J., G. FEHER, T. YEATES, D. REES, J. DEISENHOFER, AND H. MICHEL, "Structural homology of the reaction centers from *Rb. sphaeroides* and *Rp. viridis* as determined by X-ray diffraction." *Proc. Natl. Acad. Sci. USA* **83** 8589–8593 (1986).
- [85] ROBERT, B., "Resonance Raman studies of bacterial reaction centers". *Biochim. Biophys. Acta* **1017** 99–111 (1990).
- [86] MCGLYNN, P., C. HUNTER, AND M. JONES, "The *Rhodobacter sphaeroides* PufX protein is not required for photosynthetic competence in the absence of a light harvesting system". *FEBS Lett.* **349** 349–353 (1994).
- [87] FLEMING, G. AND R. VAN GRONDELLE, "Femtosecond spectroscopy of photosynthetic light-harvesting systems". *Curr. Opin. Struct. Biol.* **7** 738–748 (1997).
- [88] LIMANTARA, L., S. SAKAMOTO, Y. KOYAMA, AND H. NAGAE, "Effects of Nonpolar and Polar Solvents on the Q_x , and Q_y , Energies of Bacteriochlorophyll a and Bacteriopheophytin a". *Photochem. Photobiol.* **65** 330–337 (1997).
- [89] FRAUENFELDER, H. AND P. WOLYNES, "Biomolecules: where the physics of complexity and simplicity meet". *Physics Today* **1994** 58–64 (1994).
- [90] FRAUENFELDER, H. AND B. MCMAHON, "The energy landscape". In R. RIGLER, M. ORRIT, AND T. BASCHÉ, eds., "Single molecule spectroscopy, Nobel conference lectures", pages 257–276 (Springer Verlag, Berlin 2001).
- [91] TRETIK, S., C. MIDDLETON, V. CHERNYAK, AND S. MUKAMEL, "Bacteriochlorophyll and Carotenoid Excitonic Couplings in the LH2 System of Purple Bacteria". *J. Phys. Chem. B* **104** 9540–9553 (2000).

- [92] BRÜGGEMANN, B., J. HEREK, V. SUNDSTRÖM, T. PULLERITS, AND V. MAY, "Microscopic Theory of Exciton Annihilation: Application to the LH2 Antenna System". *J. Phys. Chem. B* **105** 11391–11394 (2001).
- [93] KASHA, M., "Characterization of electronic transitions in complex molecules". *Discuss. Faraday Soc.* **9** 14–19 (1950).
- [94] REBANE, K., "Zero-phonon line as the foundation stone of high-resolution matrix spectroscopy, persistent hole burning, single molecule spectroscopy". *Chem. Phys.* **189** 139–148 (1994).
- [95] BASCHÉ, T., S. KUMMER, AND C. BRÄUCHLE, "Excitation and Emission Spectroscopy and Quantum Optical Measurements". In T. BASCHÉ, W. MOERNER, M. ORRIT, AND U. WILD, eds., "Single-Molecule Optical Detection, Imaging and Spectroscopy", (VCH, Weinheim 1996).
- [96] COGDELL, R. AND H. FRANK, "How carotenoids function in photosynthetic bacteria". *Biochim. Biophys. Acta* **895** 63–79 (1987).
- [97] MONGER, T., R. COGDELL, AND W. PARSON, "Triplet states of bacteriochlorophyll and carotenoids in chromatophores of photosynthetic bacteria". *Biochim. Biophys. Acta* **449** 136–153 (1976).
- [98] MONGER, T. AND W. PARSON, "Singlet-triplet fusion in *Rhodospseudomonas sphaeroides* chromatophores. A probe of the organization of the photosynthetic apparatus". *Biochim. Biophys. Acta* **460** 393–407 (1977).
- [99] COGDELL, R., M. HIPKINS, W. MACDONALD, AND T. TRUSCOTT, "Energy transfer between the carotenoid and the bacteriochlorophyll within the B-800-850 light-harvesting pigment-protein complex of *Rhodospseudomonas sphaeroides*". *Biochim. Biophys. Acta* **634** 191–202 (1981).
- [100] ANGERHOFER, A., F. BORNHÄUSER, A. GALL, AND R. COGDELL, "Optical and optically detected magnetic-resonance investigation on purple photosynthetic bacterial antenna complexes". *Chem. Phys.* **194** 259–274 (1995).
- [101] BOPP, M., Y. JIA, L. LI, R. COGDELL, AND R. HOCHSTRASSER, "Fluorescence and photobleaching dynamics of single light-harvesting complexes". *Proc. Natl. Acad. Sci. USA* **94** 10630–10635 (1997).
- [102] KETELAARS, M., *Spectroscopy on single light harvesting complexes of photosynthetic bacteria*. PhD thesis, Leiden University, Netherlands (2002).
- [103] HSU, D. AND J. SKINNER, "Nonperturbative theory of temperature-dependent optical dephasing in crystals. I. Acoustic or optical phonons". *J. Chem. Phys.* **81** 5471–5479 (1984).
- [104] TOUTOUTNJI, M., G. SMALL, AND S. MUKAMEL, "Optical response functions for condensed systems with linear and quadratic electron-vibration coupling". *J. Chem. Phys.* **109** 7949–7960 (1998).
- [105] ORRIT, M., J. BERNARD, AND R. PERSONOV, "High-Resolution Spectroscopy of Organic Molecules in Solids: From Fluorescence Line Narrowing and Hole Burning to Single Molecule Spectroscopy". *J. Chem. Phys.* **97** 10256–10268 (1993).
- [106] BOIRON, A.-M., P. TAMARAT, B. LOUNIS, R. BROWN, AND M. ORRIT, "Are the spectral trails of single molecules consistent with the standard two-level system model of glasses at low temperatures?" *Chem. Phys.* **247** 119–132 (1999).

- [107] SAUER, K., R. COGDELL, S. PRINCE, A. FREER, N. ISAACS, AND H. SCHEER, "Structure-based calculations of the optical spectra of the LH2 bacteriochlorophyll-protein complex from *Rhodospseudomonas acidophila*". *Photochem. Photobiol.* **64** 564–576 (1996).
- [108] KRUEGER, B., G. SCHOLES, AND G. FLEMING, "Calculation of Couplings and Energy-Transfer Pathways between the Pigments of LH2 by the *ab Initio* Transition Density Cube Method". *J. Phys. Chem. B* **102** 5378–5386 (1998).
- [109] MUKAI, K., S. ABE, AND H. SUMI, "Theory of excitation-energy transfer processes involving optically forbidden exciton states in antenna systems of photosynthesis". *Int. J. Mod. Phys. B* **15** 3637–3640 (2001).
- [110] SCHOLES, G., I. GOULD, R. COGDELL, AND G. FLEMING, "*Ab Initio* Molecular Orbital Calculations of Electronic Couplings in the LH2 Bacterial Light-Harvesting Complex of *Rps. Acidophila*". *J. Phys. Chem. B* **103** 2543–2553 (1999).
- [111] ALDEN, R., E. JOHNSON, V. NAGARAJAN, W. PARSON, C. LAW, AND R. COGDELL, "Calculations of Spectroscopic Properties of the LH2 Bacteriochlorophyll-Protein Antenna Complex from *Rhodospseudomonas acidophila*". *J. Phys. Chem. B* **101** 4667–4680 (1997).
- [112] MATSUSHITA, M., M. KETELAARS, A. VAN OIJEN, J. KÖHLER, T. AARTSMA, AND J. SCHMIDT, "Spectroscopy on the B850 Band of Individual Light-Harvesting 2 Complexes of *Rhodospseudomonas acidophila* II. Exciton States of an Elliptically Deformed Ring Aggregate". *Biophys. J.* **80** 1604–1614 (2001).
- [113] WU, H.-M., M. RATSEP, R. COGDELL, AND G. SMALL, "Exciton Level Structure and Energy Disorder of the B850 Ring of the LH2 Antenna Complex". *J. Phys. Chem. B* **101** 7654–7663 (1997).
- [114] KOOLHAAS, M., G. ZWAN, AND R. VAN GRONDELLE, "Local and Nonlocal Contributions to the Linear Spectroscopy of Light-Harvesting Antenna Systems". *J. Phys. Chem. B* **104** 4489–4502 (2000).
- [115] PULLERITS, T., M. CHACHISVILIS, AND V. SUNDSTRÖM, "Exciton Delocalization Length in the B850 Antenna of *Rhodobacter sphaeroides*". *J. Phys. Chem.* **100** 10787–10792 (1996).
- [116] FÖRSTER, T., "Delocalized excitation and energy transfer". In O. SINANOGLU, ed., "Modern Quantum Chemistry Istanbul Lectures", volume 3, pages 93–137 (Academic Press, New York 1965).
- [117] CANTOR, C. AND P. SCHIMMEL, *Biophysical Chemistry Part II. Techniques for the Study of Biological Structure and Function* (W. H. Freeman, San Francisco 1980).
- [118] VAN OIJEN, A., M. KETELAARS, J. KÖHLER, T. AARTSMA, AND J. SCHMIDT, "Spectroscopy of individual LH2 complexes of *Rhodospseudomonas acidophila*: localized excitations in the B800 band". *Chem. Phys.* **247** 53–60 (1999).
- [119] MATSUZAKI, S., V. ZAZUBOVICH, N. FRASER, R. COGDELL, AND G. SMALL, "Energy Transfer Dynamics in LH2 Complexes of *Rhodospseudomonas acidophila* Containing Only One B800 Molecule". *J. Phys. Chem. B* **105** 7049–7056 (2001).
- [120] IHALAINEN, J., J. LINNANTO, P. MYLLYPERKIÖ, I. STOKKUM, B. ÜCKER, H. SCHEER, AND J. KORPPI-TÖMMOLA, "Energy Transfer in LH2 of *Rhodospirillum Molischianum*, Studied by Subpicosecond Spectroscopy and Configuration Interaction Exciton Calculations". *J. Phys. Chem. B* **105** 9849–9856 (2001).

- [121] FRENKEL, J., "On the transformation of light into heat in solids". *Phys. Rev.* **37** 17–44 (1931).
- [122] HU, X. AND K. SCHULTEN, "Model for the light-harvesting Complex I (B875) of *Rhodobacter sphaeroides*". *Biophys. J.* **75** 683–694 (1998).
- [123] REDDY, N. AND G. SMALL, "Spectral hole burning: Methods and Applications to photosynthesis". In J. AMESZ AND A. HOFF, eds., "Biophysical Techniques in Photosynthesis", volume 3 of *Advances in Photosynthesis*, pages 123–136 (Kluwer Academic Publishers, Dordrecht, Boston, London 1996).
- [124] ZILKER, S., L. KADOR, J. FRIEBEL, Y. VAINER, M. KOL'CHENKO, AND R. PERSONOV, "Comparison of photon echo, hole burning, and single molecule spectroscopy data on low-temperature dynamics of organic amorphous solids". *J. Chem. Phys.* **109** 6780–6790 (1998).
- [125] BERG, M., C. WALSH, L. NARASIMHAN, K. LITAU, AND M. FAYER, "Dynamics in low temperature glasses: Theory and experiments on optical dephasing, spectral diffusion, and hydrogen tunneling". *J. Chem. Phys.* **88** 1564–1687 (2003).
- [126] WU, H.-M., M. RATSEP, R. JANKOWIAK, R. COGDELL, AND G. SMALL, "Hole-Burning and Absorption Studies of the LH1 Antenna Complex of Purple Bacteria: Effects of Pressure and Temperature". *J. Phys. Chem. B* **102** 4023–4034 (1998).
- [127] AARTSMA, T., R. LOUWE, AND P. SCHELLENBERG, "Accumulated Photon Echo Measurements of Excited State Dynamics in Pigment-Protein Complexes". In J. AMESZ AND A. HOFF, eds., "Biophysical Techniques in Photosynthesis", volume 3 of *Advances in Photosynthesis*, pages 109–122 (Kluwer Academic Publishers, Dordrecht, Boston, London 1996).
- [128] VAINER, Y., M. KOL'CHENKO, A. NAUMOV, R. PERSONOV, AND S. ZILKER, "Photon echoes in doped organic amorphous systems over a wide (0.35–50 K) temperature range". *J. Lumin.* **86** 265–272 (2000).
- [129] MOERNER, W. AND T. BASCHÉ, "Optische Spektroskopie von einzelnen Dotierungsmolekülen in Festkörpern". *Angewandte Chemie* **105** 537–557 (1993).
- [130] NIE, S. AND R. ZARE, "Optical Detection of Single Molecules". *Annu. Rev. Biophys. Biomol. Struct.* **26** 567–596 (1997).
- [131] KRUPYANSKII, Y. AND V. GOLDANSKII, "Dynamical properties and energy landscape of simple globular proteins". *Physics-Uspokhi* **45** 1131–1151 (2002).
- [132] FRAUENFELDER, H., P. WOLYNES, AND R. AUSTIN, "Biological Physics". *Rev. Mod. Phys.* **71** 419–430 (1999).
- [133] MOERNER, W. AND M. ORRIT, "Illuminating Single Molecules in Condensed Matter". *Science* **283** 1670–1676 (1999).
- [134] AMBROSE, W., T. BASCHÉ, AND W. MOERNER, "Detection and spectroscopy of single pentacene molecules in a para-terphenyl crystal by means of fluorescence excitation". *J. Chem. Phys.* **95** 7150–7163 (1991).
- [135] FLEURY, L., P. TAMARAT, B. LOUNIS, J. BERNARD, AND M. ORRIT, "Fluorescence-spectra of single pentacene molecules in *p*-terphenyl at 1.7 K". *Chem. Phys. Lett.* **236** 87–95 (1995).
- [136] WILD, U., F. GÜTTLER, M. PIROTTA, AND A. RENN, "Single Molecule Spectroscopy - Stark-Effect of Pentacene in para-Terphenyl". *Chem. Phys. Lett.* **193** 451–455 (1992).

- [137] NIE, S., D. CHIU, AND R. ZARE, "Probing Individual Molecules with Confocal Microscopy". *Science* **266** 1018–1021 (1994).
- [138] MICHAELIS, J., C. HETTICH, J. MLYNEK, AND V. SANDOGHDAR, "Optical microscopy using a single-molecule light source". *Nature* **405** 325–328 (2000).
- [139] GERMEROOTH, L., F. LOTTSPREICH, B. ROBERT, AND H. MICHEL, "Unexpected similarities of the B800-850 light-harvesting complex from *Rhodospirillum rubrum* to the B870 light-harvesting complexes from other purple photosynthetic bacteria". *Biochemistry* **32** 5615–5621 (1993).
- [140] LAW, C. PhD thesis, University of Glasgow, U.K. (1998).
- [141] RITZ, T., X. HU, A. DAMJANOVIC, AND K. SCHULTEN, "Excitons and excitation transfer in the photosynthetic unit of purple bacteria". *J. Lumin.* **76, 77** 310–321 (1998).
- [142] ALONSO, M. AND E. FINN, *Physics* (Addison-Wesley, Harlow, U.K. 1992), revised edition edition.
- [143] VAN OIJEN, A., M. KETELAARS, J. KÖHLER, T. AARTSMA, AND J. SCHMIDT, "Spectroscopy of Single Light-Harvesting Complexes from Purple Photosynthetic Bacteria at 1.2 K". *J. Phys. Chem. B* **102** 9363–9366 (1998).
- [144] FRAUENFELDER, H., B. MCMAHON, R. AUSTIN, K. CHU, AND J. GROVES, "The role of structure, energy landscape, dynamics, and allostery in the enzymatic function of myoglobin". *Proc. Natl. Acad. Sci. USA* **98** 2370–2374 (2001).
- [145] LEESON, D., D. WIERSMA, K. FRITSCH, AND J. FRIEDRICH, "The Energy Landscape of Myoglobin: An Optical Study". *J. Phys. Chem. B* **101** 6331–6340 (1997).
- [146] FRITSCH, K., J. FRIEDRICH, F. PARAK, AND J. SKINNER, "Spectral diffusion and the energy landscape of a protein". *Proc. Natl. Acad. Sci. USA* **93** 15141–15145 (1996).
- [147] PARAK, F. AND G. NIENHAUS, "Myoglobin, a Paradigm in the Study of Protein Dynamics". *ChemPhysChem* **3** 249–254 (2002).
- [148] ZAZUBOVICH, V., R. JANKOWIAK, AND G. SMALL, "A High-Pressure Spectral Hole Burning Study of Correlation between Energy Disorder and Excitonic Couplings in the LH2 Complex from *Rhodospseudomonas Acidophila*". *J. Phys. Chem. B* **106** 6802–6814 (2002).
- [149] GUDOWSKA-NOVAK, E., M. NEWTON, AND J. FAJER, "Conformational and Environmental Effects on Bacteriochlorophyll Optical Spectra: Correlations of Calculated Spectra with Structural Results". *J. Phys. Chem.* **94** 5795–5801 (1990).
- [150] HE, Z., V. SUNDSTRÖM, AND T. PULLERITS, "Influence of the Protein Binding Site on the Excited States of Bacteriochlorophyll: DFT Calculations of B800 in LH2". *J. Phys. Chem. B* **106** 11606–11612 (2002).
- [151] FOWLER, G., R. VISSCHERS, G. GRIEF, R. VAN GRONDELLE, AND C. HUNTER, "Genetically modified photosynthetic antenna complexes with blueshifted absorbance bands". *Nature* **355** 848–850 (1992).
- [152] VAN HEEL, M., "A new family of powerful multivariate statistical sequence analysis techniques". *J. Mol. Biol.* **220** 87–887 (1991).
- [153] VAN HEEL, M., B. GOWEN, R. MATADEEN, E. ORLOVA, R. FINN, T. PAPE, D. COHEN, H. STARK, R. SCHMIDT, M. SCHATZ, AND A. PATWARDHAN, "Single-particle electron cryo-microscopy : towards atomic resolution". *Q. Rev. Biophys.* **33** 307–369 (2000).

- [154] VAN HEEL, M., G. HARAUZ, E. ORLOVA, R. SCHMIDT, AND M. SCHATZ, "A New Generation of the IMAGIC Image Processing System". *J. Struct. Biol.* **116** 17–24 (1996).
- [155] JANG, S. AND R. SILBEY, "Theory of single molecule line shapes of multichromophoric macromolecules". *J. Chem. Phys.* **118** 9312–9323 (2003).
- [156] JANG, S. AND R. SILBEY, "Single complex line shapes of the B850 band of LH2". *J. Chem. Phys.* **118** 9324–9336 (2003).
- [157] SKINNER, J. AND W. MOERNER, "Structure and Dynamics in Solids as Probed by Optical Spectroscopy". *J. Phys. Chem.* **100** 13251–13262 (1996).
- [158] SKINNER, J., "Theoretical Model for the Spectral Dynamics of Individual Molecules in Solids". In T. BASCHÉ, W. MOERNER, M. ORRIT, AND U. WILD, eds., "Single-Molecule Optical Detection, Imaging and Spectroscopy", (VCH, Weinheim 1996).
- [159] PLAKHOTNIK, T., "Spectral line shapes of single molecules beyond the sudden jump model". *J. Chem. Phys.* **114** 5631–5636 (2001).
- [160] VAINER, Y., T. PLAKHOTNIK, AND R. PERSONOV, "Dephasing and diffusional linewidths in spectra of doped amorphous solids: comparison of photon echo and single molecule spectroscopy data for terylene in polyethylene". *Chem. Phys.* **209** 101–110 (1996).
- [161] SMALL, G., "On the validity of the standard model for primary charge separation in the bacterial reaction center". *Chem. Phys.* **197** 239–257 (1995).
- [162] REDDY, N., G. SMALL, M. SEIBERT, AND R. PICOREL, "Energy transfer dynamics of the B800–B850 antenna complex of *Rhodobacter sphaeroides*: a hole burning study". *Chem. Phys. Lett.* **181** 391–399 (1991).
- [163] REDDY, N., R. PICOREL, AND G. SMALL, "B896 and B870 Components of the *Rhodobacter sphaeroides* Antenna: A Hole Burning Study". *J. Phys. Chem.* **96** 6458–6464 (1992).
- [164] FRANCIA, F., J. WANG, G. VENTUROLI, B. MELANDRI, W. BARZ, AND D. OESTERHELT, "The reaction center-LHI antenna complex of *Rhodobacter sphaeroides* contains one PufX molecule which is involved in dimerization of this complex". *Biochemistry* **38** 6834–6845 (1999).
- [165] STAHLBERG, H., J. DUBOCHET, H. VOGEL, AND R. GHOSH, "The reaction centre of the photounit of *Rhodospirillum rubrum* is anchored to the light-harvesting complex with four-fold rotational disorder". *Photosynth. Res.* **55** 363–368 (1998).
- [166] FRESE, R., J. OLSEN, R. BRANVALL, W. WESTERHUIS, C. HUNTER, AND R. VAN GRONDELLE, "The long-range supraorganization of the bacterial photosynthetic unit: A key role for PufX". *Proc. Natl. Acad. Sci. USA* **97** 5197–5202 (2000).
- [167] LOACH, P., "Supramolecular complexes in photosynthetic bacteria". *Proc. Natl. Acad. Sci. USA* **97** 5016–5018 (2000).
- [168] FARCHAUS, J., W. BARZ, H. GRÜNBERG, AND D. OESTERHELT, "Studies on the expression of the pufX polypeptide and its requirement for photoheterotrophic growth in *Rhodobacter sphaeroides*." *EMBO J.* **11** 2777–2788 (1992).
- [169] LILBURN, T., C. HAITH, R. PRINCE, AND J. BEATTY, "Pleiotropic effects of pufX gene deletion on the structure and function of the photosynthetic apparatus of *Rhodobacter capsulatus*." *Biochim. Biophys. Acta* **1100** 160–170 (1992).

- [170] BARZ, W., F. FRANCA, G. VENTUROLI, B. MELANDRI, A. VERMEGLIO, AND D. OESTERHELT, "Role of PufX protein in photosynthetic growth of *Rhodobacter sphaeroides*. 1. PufX is required for efficient light-driven electron transfer and photophosphorylation under anaerobic conditions." *Biochemistry* **34** 15235–15247 (1995).
- [171] BARZ, W., A. VERMEGLIO, F. FRANCA, G. VENTUROLI, B. MELANDRI, AND D. OESTERHELT, "Role of the PufX protein in photosynthetic growth of *Rhodobacter sphaeroides*. 2. PufX is required for efficient ubiquinone/ubiquinol exchange between the reaction center Q_B site and the cytochrome bc_1 complex." *Biochemistry* **34** 15248–15258 (1995).
- [172] WESTERHUIS, W., C. HUNTER, R. VAN GRONDELLE, AND R. NIEDERMAN, "Modeling of Oligomeric-State Dependent Spectral Heterogeneity in the B875 Light-Harvesting Complex of *Rhodobacter sphaeroides* by Numerical Simulation". *J. Phys. Chem. B* **103** 7733–7742 (1999).
- [173] SOMSEN, O., F. VAN MOURIK, R. VAN GRONDELLE, AND L. VALKUNAS, "Energy migration and trapping in a spectrally and spatially inhomogeneous light-harvesting antenna". *Biophys. J.* **66** 1580–1596 (1994).
- [174] VALKUNAS, L., F. VAN MOURIK, AND R. VAN GRONDELLE, "On the role of spectral and spatial antenna inhomogeneity in the process of excitation energy trapping in photosynthesis". *J. Photochem. Photobiol. B* **15** 159–170 (1992).
- [175] KLEINFELD, D., M. OKAMURA, AND G. FEHER, "Electron-transfer kinetics in photosynthetic reaction centers cooled to cryogenic temperatures in the charge-separated state: evidence for light-induced structural changes". *Biochemistry* **23** 5780–5786 (1984).
- [176] XU, Q. AND M. GUNNER, "Trapping conformational intermediate states in the reaction center protein from photosynthetic bacteria". *Biochemistry* **40** 3232–3241 (2001).
- [177] WESTERHUIS, W., J. FARCHAUS, AND R. NIEDERMAN, "Altered special properties of the B875 light-harvesting pigment-protein complex in a *Rhodobacter sphaeroides* mutant lacking pufX". *Photochem. Photobiol.* **58** 460–463 (1993).
- [178] MOSKALENKO, A., O. TOROPYGINA, V. GODIK, K. TIMPMANN, AND A. FREIBERG, "Investigation of spatial relationships and energy transfer between complexes B800-850 and B890-RC from *Chromatium minutissimum* reconstituted into liposomes". *FEBS Lett.* **308** 133–136 (1992).

Deutsche Zusammenfassung

In dieser Arbeit wurden so genannte Lichtsammelkomplexe (light-harvesting complexes, LH) aus dem Photosyntheseapparat von Purpurbakterien untersucht. Die bakterielle Photosynthese ist in verschiedene Schritte gegliedert und beginnt mit der Absorption eines Photons von, zum Beispiel, eine Gruppe von B800 Bacteriochlorophyll (BChl) *a* Molekülen im peripheren LH2 Komplex (Kapitel 4 und 5). Dieser folgen rasche Energieüberträge auf die B850 Pigmentgruppe von LH2 (Kapitel 6), weiter auf die B870 Pigmentgruppe im zentralen LH1 Komplex (Kapitel 7) und letztendlich zum Reaktionszentrum (reaction centre, RC), wo eine Ladungstrennung stattfindet, die ihrerseits eine Protonierung eines Chinons zur Folge hat. Die Namen der Pigmentgruppen beziehen sich dabei auf deren Absorptionsmaximum im nahen Infrarot. Das protonierte Chinon verläßt das RC, um weitere biochemische Prozesse in der Membran anzutreiben. Die vollständige Abfolge der Energieüberträge findet in der sogenannten photosynthetischen Einheit (photosynthetic unit, PSU) statt, welche ein supramolekulares Aggregat aus Antennenkomplexen darstellt (Kapitel 8). Im Folgenden werden die Resultate dieser Arbeit zusammengefaßt.

In einer Reihe von Experimenten lag das Hauptaugenmerk auf den spektralen Eigenschaften der in den Lichtsammelkomplexen eingebetteten BChl *a* Moleküle. Mittels polarisationsabhängiger Spektroskopie konnten für alle Pigmentgruppen detaillierte Erkenntnisse bezüglich der Wechselwirkung zwischen den Pigmenten gewonnen und der Charakter der angeregten Zustände aufgeklärt werden.

Die B800 Pigmentgruppe zeichnet sich dadurch aus, daß die Anregungen der BChl *a* Pigmente hauptsächlich auf einzelnen Molekülen lokalisiert sind. Die Beobachtung, daß sich die relativen

Orientierungen der Übergangsdipolmomente von 0° , 45° oder 90° — wie von der Röntgenkristallstruktur vorhergesagt — unterscheiden ist jedoch ein direkter Hinweis auf eine schwache bis mittelstarke elektronische Kopplung zwischen den einzelnen BChl *a* Molekülen.

Die elektronische Struktur der B850 Bande wurde mit einer neu entwickelten Technik untersucht, der Weitefeld-Fluoreszenzanregungsspektroskopie, welche die Messungen um einen Faktor 50 im Vergleich zur herkömmlichen konfokalen Fluoreszenzanregungsspektroskopie beschleunigen konnte. Es konnte bestätigt werden, daß die B850 Pigmentgruppe ein stark gekoppeltes System darstellt dessen angeregte Zustände bei tiefen Temperaturen als kollektive Anregungen, so genannte Frenkel-Exzitonen, beschrieben werden können. Dabei wurden die energetisch niedrigsten $k = \pm 1$ Exzitonzustände identifiziert. Um die experimentell beobachteten relativen Intensitäten und spektralen Positionen der $k = \pm 1$ Exzitonübergänge in Monte-Carlo Simulationen reproduzieren zu können, mußte eine Streuung der Übergangsenergien (willkürliche diagonale Unordnung) sowie eine C_2 -artige Modulation der Übergangsenergien und der Wechselwirkungen (korrelierte diagonale und außerdiagonale Unordnung) angenommen werden. Es wurde vermutet, daß die Modulation der Übergangsenergien durch eine kleine elliptische Deformierung des Komplexes hervorgerufen wird. Dies ist durchaus denkbar, da eine strukturelle Deformierung Konformationsänderungen in der lokalen Proteinumgebung der BChl *a* Moleküle hervorruft, welche deren Übergangsenergien beeinflusst. Eine solch kleine geometrische Störung statt einer elliptischen Deformierung von 7–8.5%, wie in der Literatur vorgeschlagen, ist auch besser im Einklang mit der zirkularen Symmetrie, die in der Röntgenstruktur beobachtet wurde.

Auf Grund von Messungen an LH1 wurde gefolgert, daß die B870 Pigmentgruppe ebenfalls einen stark gekoppelten Verbund darstellt. Die experimentellen Beobachtungen unterschieden sich jedoch eindeutig von jenen an der B850 Bande von LH2. Die LH1 Spektren weisen starke Schwankungen in Bezug auf die Anzahl der Absorptionsbanden und deren Polarisationsverhalten auf wodurch die Indizien für ein zirkulares Exziton weitaus weniger ausgeprägt sind. Theoretische Betrachtungen und der Vergleich mit Monte-Carlo Simulationen ließen strukturelle Unordnung als Ursache in Betracht kommen. Bei den LH1 Komplexen von *Rps. acidophila* war nicht klar, ob die strukturellen Schwankungen eine native Eigenschaft der Komplexe sind, oder ob sie durch Trennen, Reinigen und Aufbringen der Komplexe auf dem Probenträger verursacht wurden. Im Gegensatz dazu wurden drei unterschiedliche Typen LH1 von *Rb. sphaeroides* vermessen, für die in der Literatur Strukturmodelle existieren. Die optischen Eigenschaften der gemessenen Spektren stehen im Einklang mit den hypothetischen Modellen, schließen jedoch

andere strukturelle Zuordnungen nicht vollständig aus.

Ein zweiter Interessenpunkt lag in spektralen Diffusionsprozessen die im schwach gekoppelten B800 Verbund auftreten. In diesem Fall wurden die Chromophore als lokale Sonden benutzt, um neue Erkenntnisse über ihre lokale Umgebung und die Wechselwirkungen mit dem Protein-gerüst zu gewinnen. Das Spektrum eines B800 Rings eines einzelnen LH2 Komplexes von *R. molischianum* besteht im Allgemeinen aus mehreren schmalen Linien, was ein Zeichen dafür ist, daß die BChl *a* Moleküle bei leicht unterschiedlichen Energien absorbieren. Diese spektrale Heterogenität konnte Inter- und Intra-Unordnung zugewiesen werden welche Unterschiede in Anregungsenergien der B800 BChl *a* Moleküle innerhalb, beziehungsweise zwischen den Komplexen beschreiben. Ihr relativen Beitrag zur Gesamtunordnung konnte unter der Annahme, daß die energetische Unordnung der Anregungsenergien der B800 BChl *a* Moleküle mittels *einer* unabhängigen Variablen beschrieben werden kann analytisch modelliert werden .

Neben der statischen Unordnung wurden auch zeitliche spektrale Änderungen im B800 Spektrum beobachtet, welche auf Konformationsänderungen der Proteine in der Nähe der Chromophore zurückgeführt wurden, da die BChl *a* Moleküle auf Veränderungen der Pigment-Protein Wechselwirkung mit einer Änderung der Energie ihres angeregten Zustandes reagieren. Es wurde beobachtet, daß solche spektralen Änderungen längst nicht immer ein willkürlicher Prozeß sind, sondern, daß bei manchen Komplexen die Absorptionen in einer korrelierten Art und Weise ihre spektrale Positionen änderten. In Bezug auf den energetischen Abstand der korreliert diffundierenden Linien und die zugehörigen Zeitskalen wurden drei verschiedene Arten von spektraler Diffusion beobachtet, die dem Vorhandensein von mindestens drei eindeutig ausgeprägten Stufen in der hierarchisch organisierten Energielandschaft der Proteine in den Bindungstaschen der B800 BChl *a* Moleküle zugeschrieben wurden.

Um die Auswertung einer großen Anzahl von sequentiell aufgenommenen Spektren zu vereinfachen und zu automatisieren, wurde eine Vorgehensweise mittels Mustererkennung eingeführt, welche mit Hilfe der multivariaten statistischen Analyse Gruppen von ähnlichen Spektren in Klassen sortiert. Da die Übergangsenergie der BChl *a* Moleküle und damit das Aussehen des Spektrums von ihrer lokalen Umgebung abhängt, wird jede Klasse solche Spektren beinhalten, die zu Zeiten aufgenommen wurden in denen sich die Chromophore in gleichartiger Umgebung befanden mit dem Resultat, daß das gemittelte Spektrum einer jeden Klasse praktisch frei ist von spektraler Diffusion. Diese Vorgehensweise wurde zuerst anhand von zwei bereits manuell

ausgewerteten Komplexen auf ihre Anwendungsfähigkeit auf spektroskopischer Daten getestet. Dieser Test verlief erfolgreich und bestätigte der Methode einen sinnvollen Einsatz in der Auswertung spektroskopischer Daten von Einzelmolekülexperimenten. In einem zweiten Schritt wurde ein Komplex analysiert von welchem eine sehr große Anzahl an Spektren gemessen worden war. Dies offenbarte, daß die B800 Absorptionen aus einer schmalen Nullphononenlinie bestehen, die von einer breiten, weniger intensiven Phononseitenbande begleitet wird. Der damit zusammenhängende Huang-Rhys Faktor beträgt 0.21–0.84, welches auf eine sehr schwache Elektron-Phonon-Kopplung hinweist.

Eine letzte Beobachtung betraf eine Probe von LH1 Komplexen von *Rhodobacter sphaeroides*, in welcher sich eine geringe Konzentration an LH2 Verunreinigung befand. Dabei wurde in machen Spektren ein klares Indiz für den Energieübertrag von einem peripheren LH2 Komplex auf einen zentralen LH1 Komplex in einem einzelnen supramolekularen LH2-LH1-RC Aggregat gefunden. Die Beobachtung von schmalen Linien in der B800 Umgebung des Fluoreszenzanregungsspektrums deutete darauf hin, daß ein, oder höchstens zwei LH2 Komplexe an einen LH1 Komplex gebunden waren. Diese Resultate wurden durch weitere Experimente untermauert in welchen zwei unabhängige Lösungen, einerseits mit isolierten LH2 Komplexen von *Rps. acidophila* und andererseits mit LH1-RC Komplexen der gleichen Spezies, gemischt wurden. Dies mündete in der Beobachtung von ähnlichen Fluoreszenzanregungsspektren wie bei *Rb. sphaeroides* und deutete auf eine hinreichend starke Wechselwirkung zwischen peripherem und zentralem Antennenkomplex hin, wodurch eine Kopplung der beiden Komplexe auch bei Aussetzung an Detergens während der Proteinreinigung bestehen bleiben kann.

Alle Experimente der vorliegenden Arbeit wurden an Lichtsammelkomplexen, die in einem Polymerfilm eingebettet waren durchgeführt, was nicht im Entferntesten ihrer natürlichen Umgebung entspricht. Es wäre denkbar, daß einige der beobachteten spektralen Eigenschaften, vor allem die strukturelle Inhomogenität, durch die Polymerumgebung induziert wurden. Daher wäre es von Interesse, die Komplexe in ihrer biologischen Umgebung zu untersuchen. In zukünftigen Experimenten könnte man eine native Umgebung nachahmen, indem man die Komplexe in eine Doppellipidschicht integriert. Diese Art der Einbettung würde auch eine definiertere Orientierung bezüglich des Substrates als in den Polymerfilmen versprechen.

Ein weiteres Ziel wäre die Anwendung der multivariaten statistischen Analyse auf die B850 Bande von LH2. Die $k = \pm 1$ Absorptionsbanden scheinen in den im Rahmen dieser Arbeit

durchgeführten Messungen die gleiche Linienform aufzuweisen. Theoretische Betrachtungen sagen jedoch unterschiedliche Linienformen vorher und machen spektrale Diffusion für die Angleichung der Linienformen an einander verantwortlich. Es wäre interessant, ob die Vorgehensweise mittels Mustererkennung die spektrale Diffusion eliminieren könnte und unterschiedliche Linienformen preisgäbe.

Die Entwicklung technischer Produkte ist ein kontinuierlicher Prozeß der während der Durchführung dieser Arbeit zum Beispiel bei der Elektronmultiplizierenden-CCD Kamera zu einem enormen Zuwachs der Empfindlichkeit und Auslesegeschwindigkeit geführt hat. Optische Techniken haben sich ebenfalls weiterentwickelt und es ist heutzutage möglich, Tieftemperaturspektroskopie mittels totaler interner Reflexion durchzuführen und damit das Signal-zu-Rausch Verhältnis der Spektren zu erhöhen. Diese Fortschritte haben die Möglichkeit eröffnet, die schmalen spektral diffundierenden Absorptionslinien der B800 Bande von LH2 mittels Weitfeld-Fluoreszenzanregungsspektroskopie zu untersuchen und somit die statistische Signifikanz der beobachteten Phänomene drastisch zu verbessern.

Zusammenfassend konnte in dieser Arbeit gezeigt werden, daß die Tieftemperatureinzelmolekülspektroskopie eine einzigartige Methode darstellt, um wichtige Details der Pigment-Pigment Wechselwirkungen im Bereich der schwachen, mittleren sowie starke Kopplung zu untersuchen, die für andere experimentelle Methoden unzugänglich sind.

Acknowledgements

Nachdem ich im September 1999 in München bei Prof. Dr. Jürgen Köhler als Doktorand angefangen hatte, bekam Jürgen Köhler schon im darauf folgenden Jahr einen Ruf an die Universität Bayreuth, dem er alsbald folgte. Die anschließende Zeit meiner Doktorarbeit war sicherlich ganz entscheidend geprägt von den ständigen Wechseln zwischen den Universitäten in München und Bayreuth. Von meinem Doppelleben zeugten auch die im Zweierpack vorkommenden Adressen auf Homepage und Visitenkarte, welches die meisten Vertreter etwas in Verwirrung brachte.

In den viereinhalb Jahren meiner Doktorarbeit habe ich an beiden Universitäten viele Diplomanden und Postdocs kommen und auch wieder gehen sehen, doch zum Glück Doktoranden nur entweder gehen oder kommen sehen. Viele von ihnen haben dabei direkt oder indirekt zum guten Gelingen dieser Arbeit beigetragen und sollten deshalb nicht unerwähnt bleiben.

Als erstes möchte ich mich aber bei Prof. Dr. Jürgen Köhler ganz ausdrücklich für die phantastische Betreuung meiner Doktorarbeit bedanken. Als Doktorvater hast Du mich auf dem Weg in die Wissenschaft begleitet und mir die schönen Seiten aber auch die Tücken der Forschung und des akademischen Lebens gezeigt. Jederzeit hattest Du ein offenes Ohr für meine Fragen und konntest mir auch im Labor mit den entscheidenden Tips und Tricks weiterhelfen. Für Dein Verständnis für meinen Wunsch in München zu bleiben und nicht mit nach Bayreuth zu gehen — obwohl ich mich vor Ort sicherlich mehr in den Lehrstuhl hätte einbringen können als von München aus — möchte ich Dir nochmals danken. Du hast es immer geschafft, daß die räumliche Distanz der Betreuungsqualität keinen Abbruch getan hat.

Bei Martin Richter möchte ich mich für so vieles bedanken, daß ich damit spielend ein ganzes Buch vollschreiben könnte. Immer wenn ich Dich anrief und fragte ob ich mal wieder übernachten könne bekam ich als Antwort ein freudiges: „ja klar, gerne“. Wir waren ein richtig eingespieltes Team in Deiner Wohnung, fast so als wären wir schon einige Jahrzehnte verheiratet. Doch nicht nur die Übernachtungsfrage war kein Problem, sondern auch die gemütliche Auskleidung der Feierabende. Du wußtest immer genau wann es wo welchen Cocktail oder welches Nudelgericht zum halben Preis gab. Und war in der einen Kneipe die Happy-hour vorbei, zogen wir einfach in die nächste weiter. Ich bin sicher, daß ich in Bayreuth mehr Kneipen besucht habe als in München. Und wenn mal keine Kneipe auf dem Programm stand dann gab es immer noch die Caipi- und Feuerzangenbowleabende bei Dir.

Für das körperliche und geistige Training in Bayreuth war Erwin Lang zuständig. Das wöchentlichen Hallenfußballereignis, das Du organisiertest ließ zwar Tanja immer verzweifeln vor lauter blauen Flecken und Schürfwunden doch meine Kondition nahm rapide zu. Und bei unseren Programmier-Sessions fing mein Hirn zu rauchen an, beim Versuch, Deinen komplizierten Meßaufbau mit den zig Meßarten zu durchschauen.

Karin Baier und Evelyn Hülsmann möchte danken, daß Sie mir soviel administrative Arbeit abgenommen haben, mir ein Zimmer in Bayreuth vermittelt haben und immer eine motivierende Bemerkung parat hatten. So habe ich immer noch daran zu knabbern, daß mir Evelyn im Frühjahr 2003 sagte, daß ich eine akademische Karriere vergessen könne, wenn ich nicht bis zum Sommer fertig würde. Es hat bei mir bis zum Frühjahr 2004 gedauert.... Vergib mir Evelyn, daß ich trotzdem eine Postdocstelle angenommen habe.

Michael Heimler und Renate Liebsch-Hofmann möchte ich für die gute Unterstützung beim

Aufbau des Meßplatzes in Bayreuth danken. Nochmals vielen Dank Michel, daß Du mich den einen Morgen nach Wallenfels mit meiner leichten Magenverstimmung zum Bahnhof nach Bayreuth mitgenommen hast. Werner Reichstein möchte ich für die Organisation des Fahrrades danken, das ich in Bayreuth immer benutzt habe. Waltraud Joy für die Unterstützung im Chemielabor.

Außer den schon Erwähnten möchte ich auch Jürgen Baier, Richard Hildner, Renate Müller, Frank Pöhner, Dr. Wolfgang Richter, den Mitgliedern der Gruppen von Dr. Dagmar Klostermeier, Prof. Dr. Werner Köhler, Dr. Lothar Kador und Prof. Dr. D. Haarer für das phantastische Arbeitsklima am Lehrstuhl EP IV danken. Die unzähligen Kuchen, die ich gegessen und leider oft auch verpaßt habe und die unglaubliche Hilfsbereitschaft untereinander, die von einem fest verankerten Miteinander zeugte, habe ich in der Form noch nicht erlebt.

Prof. Dr. Jochen Feldmann möchte ich ganz herzlich für die Aufnahme am Lehrstuhl in München danken. Als Jürgen Köhler im Herbst 2000 an die Universität Bayreuth wechselte, erklärtest Du Dich ohne Probleme damit einverstanden, den Meßplatz noch eine Weile in München zu lassen. Dadurch konnte ich mit Tanja zusammen wohnen bleiben und auch ohne Verzögerung mit meinen Experimenten fortfahren. Auch nach dem Umzug des Meßplatzes Anfang 2002 nach Bayreuth konnte ich meinen Schreibtisch am Lehrstuhl in München behalten und mich als Dauergast einnisten. Bei den Umzügen in den Turmbau und wieder zurück in die frisch renovierte Amalienstraße wurde immer an mich gedacht und ein Platz in einem Zimmer für mich reserviert. Diese absolut nicht selbstverständliche Gastfreundschaft hat das Pendeln zwischen Bayreuth und München auf ein Minimum reduziert und mir eine wunderschöne Zeit mit Tanja in München ermöglicht. Auch im Namen von Tanja nochmals ein herzliches Dankeschön!

John Lupton und Florian Schindler haben mir gezeigt, daß man auch mit normalen Polymeren und nicht nur mit Biopolymeren interessante Einzelmolekülphysik machen kann. Für die vielen Diskussionen und interessanten Einblicke ein großes Dankeschön.

Dr. Carsten Sönnichsen, Gunnar Raschke und Thomas Franzl möchte ich für die Hilfestellung bei Computerproblemen danken. Sogar das mir treue iBook wurde ins neue Windowsnetz aufgenommen.

Wer lange promoviert hat, hatte auch viele Zimmergenossen. Jana Crewett, Robert Köppe, Andreas Biebersdorf, Stefan Kowarik, Dr. Alexei Platonov, Dr. Jürgen Müller, Moritz Ringle, und Robert Kraus möchte ich für die nette Atmosphäre, die lebendigen Gespräche und die Hilfsbereitschaft bei Problemen jedweder Art danken. Außer den eben Genannten hat der Rest der Münchner Truppe, angefangen bei den Altdoktoranden Dr. Christoph Link, Dr. Michael Breit, Dr. Carsten Sönnichsen und Dr. Stephan Riechel hin zu den Neudoktoranden Eric Dulkeith, Martin Reufer, Joseph Müller, Florian Schindler, Thomas Franzl, Gunnar Raschke und den vielen Diplomanden und Postdocs zu der netten Arbeitsatmosphäre am Lehrstuhl beigetragen. Dabei wurde die Arbeit immer wieder durch den ein oder anderen Biergartenbesuch und die Lehrstuhlausflüge aufgelockert.

Den Münchner Technikern" Werner Stadler, Christian Holopirek und Stefan Niedermaier möchte ich für die schnelle und unkomplizierte Hilfe bei technischen Problemen aller Art danken. Werner und Stefan vor allem für ihre große Hilfe beim Aufbau meines Meßplatzes (Werner, nie werde ich unsere Hartlöt-Sessions mit Vakuumcheck im Waschbecken vergessen) und Christian für die Entwicklung der Schrittmotorsteuerung. Den Münchner Sekretärinnen I. Krella, G. Adam, I. Beier möchte ich für die problemlose Überwindung bürokratischer Schwierigkeiten danken, M. Bochner für die Literaturbesorgungen.

Prof. Dr. M. Schwoerer und Prof. Dr. J. Friedrich möchte ich ganz herzlich für die Übernahme der weiteren Gutachten danken.

Martijn Ketelaars wil ik bedanken voor de toegang tot de single-molecule setup. Samen met jouw heb ik een paar maanden in München gezwoegd totdat we eindelijk het eerste single-molecule signaal hadden. Bovendien heb jij ervoor gezorgd dat mijn Nederlands niet helemaal is ingeroest.

Dr. Thijs Aartsma wil ik bedanken voor de vele constructive discussies en hulp bij het interpreteren van mijn metingen.

Dr. Michio Matsushita taught me about the theoretical background of excitations and excitons. I'm still sorry that you had to miss the church tour at the VW meeting in Kloster Banz because you had to explain the Hamilton operator and Frenkel excitons to me.

I would like to thank Prof. Dr. Marin van Heel and Dr. Michael Schatz for providing me with the IMAGIC-5 software and for their support.

If a physicist studies biological samples he is rather helpless without specialist cooperation partners. Therefore I want to express my deepest gratitude to Prof. Dr. H. Michel, Prof. Dr. Richard Cogdell, Prof. Dr. H. Scheer, Dr. Leszek Fiedor, Prof. Dr. D. Oesterhelt, Prof. Dr. G. Venturoli, Dr. Francesco Francia and Dr. Thijs J. Aartsma for supplying me with all the samples I wanted.

I would like to thank Dr. Francesco Francia for showing me the secrets of liposomes with (for a physicist) unspeakable names, for the help with the sephadex column and vesicle generation and of course for the nice two weeks of Italian flair during your visit in Bayreuth.

Vor allem aber möchte ich Dir, Tanja, danken für alles, was Du für mich getan hast. Du hast mir in den entscheidenden Phasen immer den Rücken frei gehalten und mich, wo immer Du nur konntest, unterstützt. Und wenn wir uns weiterhin so gut ergänzen und gegenseitig stärken, werden wir immer so glücklich bleiben, wie wir es in München gewesen sind.

Curriculum Vitae

Dipl.-Phys. ir. Clemens Hofmann, MSc.

Born 11 January 1974 in Hamburg (D)

Married to Tanja Hofmann (née Seitz)

Education

- since 09/2002 Universität Bayreuth (D): Continuation of work towards the Dr.rer.nat.
- 09/1999–08/2002 Ludwig-Maximilians-Universität München (D): Dr.rer.nat. (Ph.D.) candidate in physics.
- 10/1998–08/1999 University of Exeter (UK): Master of Science in Medical Physics. Dissertation entitled *Development of an Optical Coherence Microscopy System*.
- 09/1992–09/1998 Delft University of Technology (NL): ingenieur technische natuurkunde (MSc. in applied physics). Eberhard-Karls-Universität Tübingen (D): Diplom-Physiker (MSc. in Physics). Dissertation entitled *Light intensity distribution beneath artificial vessels, a model for Anigoscotomata*.
- 09/1986–06/1992 Praedinius Gymnasium Groningen (NL): Eindexamen (secondary education).

Awards and Scholarships

- 08/1999 University of Exeter: Graduation with distinction.
- 09/1998 Eberhard-Karls-Universität Tübingen: Graduation “mit Auszeichnung” (with distinction).
- 02/1997–08/1999 Studienstiftung des deutschen Volkes (German National Academic Foundation): national scholarship, postgraduate scholarship at foreign university and Ph.D. scholarship.
- 07/2000–09/2002
- 06/1992 Praedinius Gymnasium Groningen: Best “Eindexamen” in science related courses.

